

Suitability of the Yucca Mountain Site to Accommodate a permanent  
Repository for High-Level Radioactive Waste  
and Spent Nuclear Fuel: an Independent Assessment

Part Three

Mineralogical and Geochemical Diagnosis:  
Long-Term Behavior of the Hydrologic System at Yucca Mountain  
as It Is Expressed in the Geologic Record

by

Y.V. Dublyansky,

J.S. Szymanski,

S.Z. Smirnov,

S.E. Pashenko,

and

G.P. Palianova

## Acknowledgments

Most of the research on mineralogy, fluid inclusions and stable isotope geochemistry of the Yucca Mountain secondary minerals discussed in this report was funded by the State of Nevada through Agency for Nuclear Projects – Nuclear Waste Project Office (Carson City, NV).

Office of the Attorney General, State of Nevada has played crucial role in initiation of the research on secondary minerals from the ESF in 1998. Institute for Energy and Environmental Research (Washington, DC) has funded part of the fluid inclusion research (1998) and was instrumental in organizing the process of verification of the results.

Dr. Robert Bodnar has kindly provided facilities and equipment for fluid inclusion studies at Virginia Tech (Blacksburg, VA). Drs. Zachary Sharp, Viorel Atudorei and Jean Selverstone of the University of New Mexico (Albuquerque, NM) have helped greatly with coupled stable isotope – fluid inclusion studies.

Through the course of the research and during the preparation of this report we enjoyed incessant support and encouragement from Mr. Harry Swainston, who served as our contact with the Office of the Attorney General of the State of Nevada.

## Table of contents

Introduction	3-6
Chapter 3-1. Epigenetic alteration of the tuffs at Yucca Mountain: Geochemical and mineralogical constraints – <i>By J.S. Szymanski, S.Z. Smirnov, and Y.V. Dublyansky</i>	7-108
Chapter 3-2. Thermodynamic modeling of rhyolite – meteoric water interaction at Yucca Mountain – <i>By G.P. Palyanova, S.Z. Smirnov, and Y.V. Dublyansky</i>	109-126
Chapter 3-3. Calcite-silica deposits at the topographic surface – <i>By J.S. Szymanski and Y.V. Dublyansky</i>	127-177
Chapter 3-4. Mineralogy and geochemistry of the open-space secondary deposits from fractures and lithophysal cavities in the ESF – <i>By S.Z. Smirnov and Y.V. Dublyansky</i>	178-275
Chapter 3-5. Stable isotope geochemistry of calcites from the Yucca Mountain vadose zone – <i>By Y.V. Dublyansky and J.S. Szymanski</i>	276-297
Chapter 3-6. Fluid inclusion studies – <i>By Y.V. Dublyansky</i>	298-351
Chapter 3-7. Geochemistry of U and Pb in secondary minerals from Yucca Mountain and interpretation of the results of the U-Pb dating – <i>By S.E. Pashenko and Y.V. Dublyansky</i>	352-462
Chapter 3-8. Thermal history of Yucca Mountain – <i>By Y.V. Dublyansky and J.S. Szymanski</i>	463-481

## Introduction

Volcanic tuffs in the Yucca Mountain area host a variety of epigenetic (or secondary) authigenic minerals. The term epigenetic is used here as a broad catch all definition of minerals that were formed after the emplacement and solidification of the bedrock tuffs, including those that were formed through late devitrification of volcanic glass. It is to be noted, however, that other researchers define part of the minerals (mostly zeolites and clays) present in the Yucca Mountain tuffs as diagenetic minerals (e.g., Broxton et al. 1987). We prefer to avoid the usage of this term, since its definition is vague (e.g., Glossary of Geology, 1972) and different researchers may understand it differently.

The appearance of epigenetic minerals is tightly controlled by the character of the host tuffs; it ranges from pervasive alteration mineralization in the porous non-welded and ash-fall tuffs to coarse fracture- and void fillings and linings in the competent welded tuff units. Fractures and cavities entirely filled with secondary minerals are characteristic of the saturated or phreatic zone (below the static water level). Above, in the vadose zone, minerals typically occur as linings and coatings on the walls of openings (although completely filled voids also exist, e.g., cements of mosaic breccias). Mineral deposits also occur on the topographic surface or in the near-surface position (down to a depth of approximately 30 m). The characteristic forms of the surface deposits are micritic veins in the faults and fractures, and slope-parallel layered carbonaceous deposits ("calcretes") mantling the bedrock exposures and cementing alluvial and colluvial deposits and soils. Types of the epigenetic mineralization at Yucca Mountain are schematically shown in Figure 3-1.

All epigenetic minerals at Yucca Mountain are hydrogenic, in the sense that they were deposited from or by the action of aqueous solutions. As such, these epigenetic minerals provide a record of the past migration of water in Yucca Mountain. In subsequent chapters of Part III we will discuss these mineral deposits in a systematic manner, with the purpose of reconstructing the past hydrologic regimes.

Presently, there exists a general consensus regarding the origin of mineralization occurring below the regional water table. Zeolites, illite-smectite clays, calcite, and opals from the phreatic zone are thought to have formed during the so-called Timber Mountain Caldera hydrothermal episode. By that time, a granitic magma body emplaced beneath the Timber Mountain–Oasis Valley caldera complex had triggered a hydro-tectonic instability, which expressed itself as a convective circulation system in the water-saturated rocks adjacent to the magma body. Prolonged (0.5 to 1.0 Ma) circulation of heated waters caused pervasive devitrification of volcanic glass and deposition of alteration minerals in the affected rock mass. Results of the radiometric dating of clays (K-Ar) and opals (U-Pb) have constrained the age of this activity to 10.5-11.0 Ma ago (Bish and Aronson, 1993; Neymark et al. 1998-a).

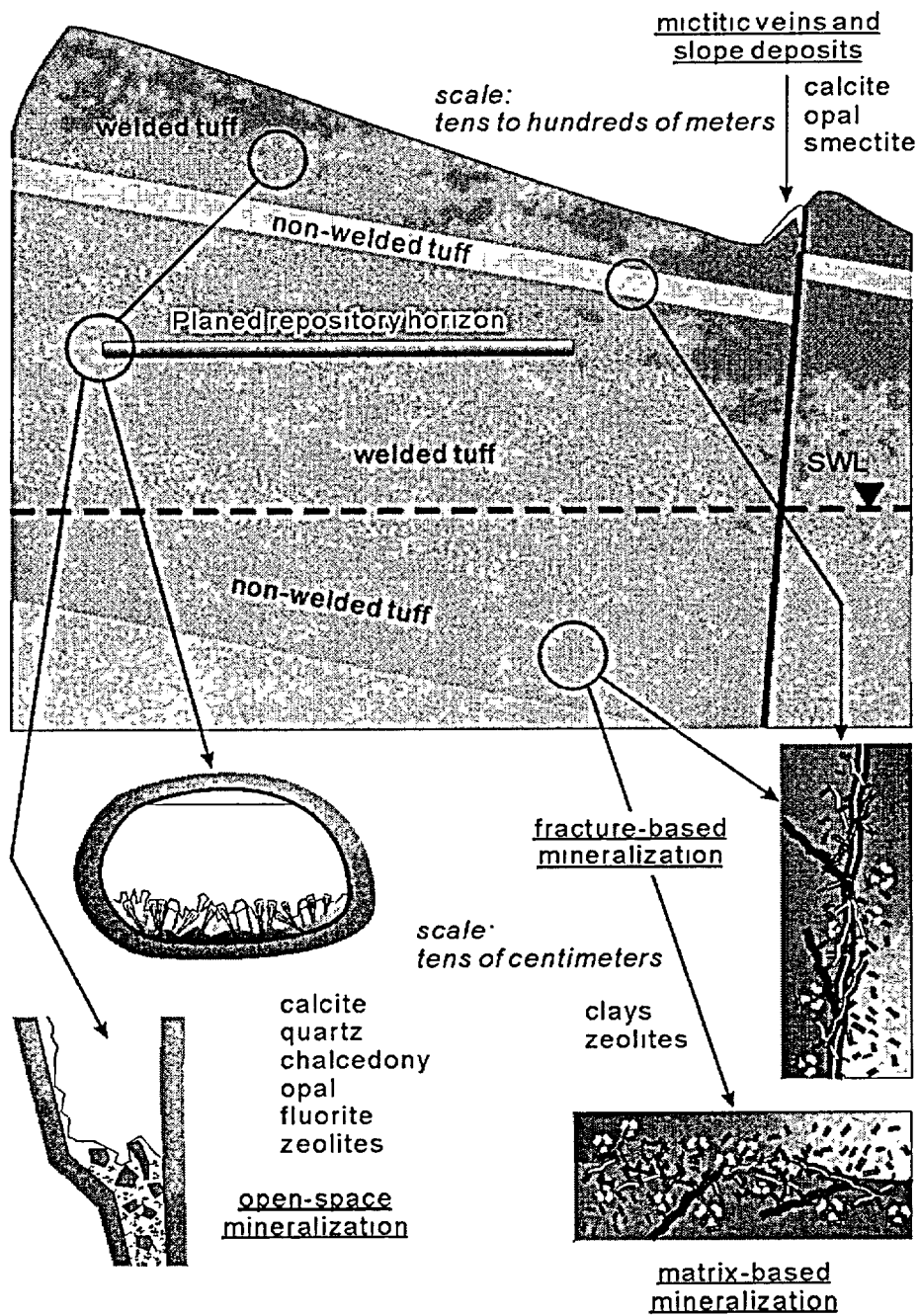


Figure 3-1. Schematic presentation of types of mineralization in the Yucca Mountain subsurface discussed in Part III. Major minerals and most important accessory minerals are listed in blue. See text for details.

As for the origin of secondary minerals in the vadose zone of Yucca Mountain and at its surface, there are two competing conceptual models. The concept advanced by the Yucca Mountain Project scientists is that the secondary minerals in the vadose zone were formed from infiltrating rainwater reacting, over the past 8-9 Ma, first with the calcareous soils and then with the silicic (acidic) bedrock tuffs. For simplicity, we will call it the “rainwater concept”. This concept assigns the secondary minerals a supergene origin. The recommendation of the Yucca Mountain site to the President for development as a repository by the Secretary of Energy and the subsequent approval by the President and his recommendation of the site to the Congress necessarily regards this concept as a settled proposition.

The competing concept, set forth in the preceding two parts of this book characterizes Yucca Mountain as being unsuitable for development as a repository. It regards the epigenetic minerals in the vadose zone as having a hypogene origin deriving their existence from hydro-tectonic processes. The character of the energy sources which fueled the hydro-tectonic instabilities distinguishes them from the deeper minerals formed in the course of the Timber Mountain Caldera hydrothermal metamorphism. In contrast to the earlier Timber Mountain instabilities, which were fueled by a "strong" heat source (a magma chamber), the subsequent instabilities have been fueled by "weak" sources. For simplicity, this will be called the “hydrothermal upwelling concept” in the discussion that follows.

Our understanding of the long-term behavior of the hydrologic system at Yucca Mountain has caused us to reject three notions generally accepted by the Yucca Mountain Project scientists. The first is based on an observation that the controversial minerals in the vadose zone display a set of characteristics, including isotope and trace element signatures, which are similar to those that characterize the calcite-silica deposits at the ground surface. We take this observation to mean only that both of the deposits have a common origin. We reject the notion that this observation necessarily means that both of the deposits were formed by infiltrating rainwater.

The second notion is based on an observation that the controversial minerals in the vadose zone display a set of characteristics, including isotope and trace element signatures, which distinguish them from the Timber Mountain hydrothermal minerals. We take this observation to mean only that different hydrologic processes, operating during different time spans, must have been involved in forming both of the mineral sets. Thus, we reject the notion that this observation necessarily means that the controversial minerals could not have been formed from geothermal solutions.

The third notion is based on the observation that some, but not all, of the controversial minerals display characteristics, which suggest a downward flow of parental solutions (e.g., Vaniman et al. 1999 and Hanks et al. 1999). We take this observation to mean only that downward moving solutions could have been involved in producing these characteristics. Although infiltrating rainwater is included among

such solutions, it is by no means the only one. Thus, we reject the notion that the characteristics observed mean that the controversial minerals could not have been formed from geothermal solutions.

The extensive mineralogical database established from characterization studies of Yucca Mountain permits an examination of the temporal and spatial distribution of epigenetic minerals, both at the surface and in the interior of the mountain. This four-dimensional distribution provides for an accurate analysis of the geologic record, which has been written into the tuffs in response to long-term behavior of the hydrologic system.

The discussions presented below are broadly subdivided into two parts. The first deals with chemical and mineralogical alteration of the tuffs, based on a variety of laboratory analyses of rock cores extracted from the interior of Yucca Mountain down to a depth of approximately 2.0 km. The second part is devoted to the calcite-silica deposits, which occur at the ground surface, in the vadose zone, and in the phreatic zone. Here, the origin of these deposits is considered based on their stable and radiogenic isotope signatures, the data on fluid inclusions, the trace element signatures, and the results of thermodynamic modeling. In the second part, the hydrothermal origin of the calcite-silica deposits is firmly established and the proposed conceptual model of hydrothermal upwelling water is validated.

## Chapter 3-1. Epigenetic alteration of the tuffs at Yucca Mountain: Geochemical and Mineralogical Constraints

*By J.S. Szymanski, S.Z. Smirnov, and Y.V. Dublyansky*

### Table of contents

<b>Chapter 3-1. Epigenetic alteration of the tuffs at Yucca Mountain: Geochemical and Mineralogical constraints</b>	<b>8</b>
3.1.1. Pervious Investigations	11
3.1.2. Major Element Geochemistry of the Whole-Rock Tuffs	19
3.1.2.1. Chemical Composition of the Glass and of the Altered Tuff	21
3.1.2.2. Suggested Mobility of Ti, Fe, and Al	27
3.1.2.3. Spatial Distribution of the Alteration	30
3.1.2.4. K, Ca, and Mg Alteration in the Northern Sector	35
3.1.2.5. Is the Presumption of a Supergene Epigenetic Alteration Feasible?	37
3.1.2.6. Concluding Remarks	38
3.1.3. Montmorillonite Alteration of the Tuffs	40
3.1.3.1. Geothermometry and Geochronology by smectite series: Background	42
3.1.3.2. Spatial Distribution of the Montmorillonite Alteration Species	44
3.1.3.3. Age and Significance of the Smectite Alteration Species	45
Concluding Remarks	48
3.1.4. Zeolite Alteration of the Tuffs	50
3.1.4.1. Background	50
3.1.4.2. Database	56
3.1.4.3. Spatial Distribution of the Glass in Relation to the Present-day Water Table	58
3.1.4.4. Vertical Zonation	59
3.1.4.5. Age Relationship between the Zeolite Alteration and the Deuteric Alteration	61
3.1.4.6. Fracture-Based Zeolite Species	63
3.1.4.7. Multiple Episodes of the Zeolite Alteration and Mineralization	64
3.1.4.8. Geologic Ages of the Potassic and Calcic Zeolite Species	65
3.1.4.9. Origin of the Calcic Zeolite Species	68
3.1.4.10. Concluding Remarks	79
3.1.5. K/Ar Ages of the Alkali and Alkaline-Earth Zeolite Species	82
3.1.5.1. Sample Preparation and Analytical Methods	83
3.1.5.2. Reliability of K/Ar Ages	84
3.1.5.3. K/Ar Database	88
3.1.5.4. The K/Ar Clinoptilolite Ages as a Function of Depth	97
3.1.5.5. The Problem with Clinoptilolite Dehydration	99
3.1.5.6. What Does the Apparent K/Ar Age vs. Depth Gradient Express?	101
3.1.5.7. Major Cation Composition as a Function of the Apparent K/Ar Ages	104
3.1.5.8. Concluding Remarks	107

## Chapter 3-1. Epigenetic alteration of the tuffs at Yucca Mountain: Geochemical and Mineralogical Constraints

*By J.S. Szymanski, S.Z. Smirnov, and Y.V. Dublyansky*

The volcanic deposits, which form Yucca Mountain, consist of a complex sequence of layered tuffs, varying greatly in mineralogy, texture, and chemical composition. The emplacement mechanisms are either air-fall or ash-flow depositions. The primary (deuteric) and secondary (epigenetic) processes of alteration and mineralization principally control the variability encountered in these deposits. The primary processes are those that operated during cooling and solidification of the tuffs. These processes include welding, which produced significant variability in density and porosity of the ash-flow tuffs, and the primary devitrification, which caused a breakdown of the glass to cristobalite and alkali feldspar under sub-solidus temperatures. They also include the precipitation of vapor-phase minerals (tridymite with minor iron and titanium oxides) during degassing of the ash-flow sheets.

The secondary alteration is principally confined to those tuffs, which are non-welded to moderately welded. This alteration generally reflects exchange reactions of vitric phases, such as pumice and glass fragments, with ionic aqueous solutions. The resulting minerals primarily include montmorillonite (smectite) and kaolinite clays, micas, zeolites, silica polymorphs, and authigenic alkali feldspars and plagioclases. The secondary alteration is typically absent in the densely welded tuffs, except for thin and inconspicuous fracture-based alteration aureoles. However, in places, the welded tuffs host abundant secondary minerals in the form of crystalline in-fillings of faults and fractures, lithophysal cavities, dilatatory openings, etc. The precipitation of these minerals involved ionic and possibly colloidal aqueous solutions that must have occupied the openings some time during the past 12.7 Ma. The abundance and chemical composition of the open-space secondary minerals vary significantly both with depth and laterally across Yucca Mountain. The most abundant minerals include silica polymorphs (quartz, chalcedony, opal), calcite, zeolites (stellerite, heulandite, mordenite, clinoptilolite, erionite, phillipsite), and Mn-oxides (lithiophorite and rancieite), with trace amounts of fluorite, smectite, Fe-oxides, apatite, and gypsum. This open-space epigenetic mineralization will be discussed in detail in Chapter 3-4.

The secondary alteration could be expressing either supergene or hypogene epigenetic processes. The essential condition for supergene processes involves the placement of a vitric rock in an aqueous environment where silica activity, the pH, temperature, and the cation abundance together are sufficiently

high to support the chemical reactions and precipitation of minerals. Saline-alkaline lake, sub-sea beds, and deep burial in subsiding basins are environments that promote diagenetic-type reactions. The same type of alteration can be promoted by a number of other supergene environments characterized by chemical and physical weathering of rocks (formation of weathering crusts), the reaction of hot air-fall volcanic ash with meteoric water (zeolitization) as well as a variety of other environments. In contrast, the hypogene reactions are those wherein the solution chemistry and the temperature are both a result of the flow of thermally unstable fluid, which means that they are a result of Rayleigh-Bernard instabilities. An important threshold question, then, that needs to be answered is: Are the minerals at Yucca Mountain primarily of a supergene origin, or are they of a hypogene origin?

Epigenetic alteration and mineralization of silicic tuffs by hydrothermal solutions naturally resemble those, which develop in the tuffs altered by surficial meteoric waters. The distinguishing feature between the two processes is geothermal, specifically the intensity and character of the heat flow. The supergene minerals are produced under normal conductive heat flow of less than, say,  $80 \text{ mW m}^{-2}$  in an environment resulting from either the burial or the chemistry of the aqueous solutions. By contrast, hypogene epigenetic minerals are produced under conditions of enhanced heat flow, whose intensity exceeds, say,  $80 \text{ mW}\cdot\text{m}^{-2}$ , so that the  $R_c/R_a$  attains an appropriately low value. The combined interpretations, presented in Part I and Part II of this book, imply that the potential for thermal instability of aquifer fluids and the resulting occasional enhancement of the total heat flow, are the permanent features at Yucca Mountain. Initially, some 10-11 Ma ago, the solidifying granite massif beneath the Timber Mountain Caldera fueled the hydrodynamic instability. It has been inferred that this instability was relatively shallow, involved mainly solutions enriched in alkalis, and produced an enhancement of the heat flow which persisted for a long period of time, in the order of 1 Ma (Bish and Aronson, 1993).

With the eventual solidification of the batholith, the situation must have changed. This does not mean, however, that hydrothermal processes ceased to be active all together. The increasingly more intense conductive heating of the crust by the mantle effectively increased the temperature in the crust, so that renewed hydrothermal activity was possible. Basaltic volcanoes and lava flows occurring throughout the Yucca Mountain region and vicinity indicate that the mantle heat source has affected the area over a 14 Ma – 70 Ka time span. Thus, the question is whether the secondary minerals indicate that such activity took place at Yucca Mountain during the past 8-9 Ma. If such were the case, then, assuming the static water table was as deep as it is today, the hydrothermal processes would be expected to take the form of short-lived plumes. Tectonic events such as fault ruptures and volcanic intrusions would trigger the ascent, and the plumes would involve aqueous and gas-charged solutions of juvenile origin from deep-seated aquifers.

The preceding possibility may be tested by the means of establishing whether the tuffs at Yucca Mountain host two distinct sets of alteration minerals, which differ from each other in terms of age and chemistry. The older set would include both the smectite and the alkali zeolite alteration series. The minerals from both of these alteration series should carry the same radiometric ages, ranging between 10 and 11 Ma (the age of the Timber Mountain Caldera hydrothermal activity). They would be developed in the form of a spatially extensive and pervasive alteration aureole. By contrast, the younger set would be much less pervasive and primarily confined to aureoles that surround faults and fractures in the vitric ash-flow tuffs and the porous ash-fall units. This set would include zeolite species from the alkaline-earth series as well as randomly interstratified (R0) smectite. The orderly-interstratified smectite clays would be absent, which would reflect the alkaline-earth character of the altering solutions as well as the relatively short-lived circulation of these solutions. The alkaline-earth alteration minerals would carry radiometric ages younger than 8-9 Ma.

The preceding expectations are sufficiently explicit, so that their presence or absence may readily be tested in the altered tuffs at Yucca Mountain. In our evaluation we will rely on the database from the published literature, or data released in the form of open-file reports or other official documents.

### 3.1.1. Pervious Investigations

Chemical and mineralogical alteration of the Tertiary tuffs, at the Nevada Test Site, has been studied for several decades. Hoover (1968) was the first researcher who considered the origin of the alteration. He concluded that “...*crystalite, quartz, feldspar, and clay minerals were deposited by groundwater that leached vitric volcanic rocks in the unsaturated zone and reacted with similar vitric rocks just above permeability barriers where the rocks are nearly saturated.*” As far as the spatial character is concerned, he stated: “...*Ca and Mg are concentrated in the uppermost part of the zeolitized rocks, K in the middle part, and Na in the lowermost part.*” This general chemical stratification is similar to the large-scale chemical stratification, which has been found later in the northern and western parts of Yucca Mountain by Caporuscio et al. (1982) and Broxton et al. (1986).

The underlying premise for Hoover's conclusion is that zeolite minerals form in a variety of geologic environments. They include a vadose environment, which is invariably associated with low temperature, and with solutions having a low ionic strength and a low abundance of dissolved cations. Hoover (1968) believed that zeolitization and the associated chemical alteration could form in response to four processes. These are: “...*hydrothermal alteration, burial metamorphism, reaction of glass and water in a saturated system (below a water table), and leaching and deposition in an unsaturated system (above a water table).*” Discussing the alteration of tuffs in the Nevada Test Site area, Hoover noted: “*Relative changes in calcium and magnesium during hydration of glass are the largest changes of any of the constituents, but the source of the calcium and magnesium to account for the increase is not known.*” He further stated: “*Although 10 to 20 percent changes in  $Al_2O_3$  were noted in matched pairs of vitric and zeolitized rock, new data indicate that such changes are local and are probably caused by special conditions of pH and permeability*”

Hoover (1968) neither addressed the source of calcium nor the conspicuous mobility of aluminum, which requires a pH of less than 4.5 or more than 10 at a temperature of 25 °C, as given in Wedepohl (1971). Hoover dismissed hydrothermal metamorphism with the statement: “*Temperature in the zeolitized rocks measured in drill holes are 25 to 60 °C and there is no evidence for higher temperature during zeolitization...Thus, a hydrothermal and burial metamorphic origin is unlikely.*” Evidently, it did not occur to him that the zeolite minerals could be regarded as evidence for a higher temperature and fluid salinity in the past.

By rejecting elevated temperatures and groundwater levels during zeolitization of the tuffs, Hoover (1968) arrived at the conclusion that this alteration must have been formed in a vadose zone at

temperatures comparable to present-day temperatures. However, this conclusion is burdened with two obvious flaws. First, the hydrothermal metamorphism and the alteration in a phreatic zone were both rejected without a valid justification. Second, Hoover's major premise (formation of zeolites is possible in a vadose zone) illogically becomes his conclusion.

An extensive study of the alteration of the tuffs at Yucca Mountain was undertaken by Broxton, et al. (1986), at a time when the concept of the disposal of radioactive waste in the vadose zone had been proposed by Winograd and Szabo (1988). The following quotation sums up the authors' conclusion: *"The non-welded tuffs... were highly susceptible to alteration because of the instability of glass in the presence of groundwater. During diagenesis, glass was replaced primarily by the zeolites clinoptilolite, heulandite, and mordenite. Analcime and authigenic feldspars replace clinoptilolite and mordenite in the deeper parts of the volcanic sequence. These authigenic minerals form four diagenetic zones that become progressively less hydrous with depth. These mineralogic zones are similar to those described by Iijima (1975, 1978, and 1980) for burial diagenesis of volcanic ash beds in thick sedimentary sequences."*

The phrase *"thick sedimentary sequences"*, as intended by Iijima, refers to marine sequences whose thickness is sufficient to attain temperature, which would allow for the crystallization of authigenic albite. This temperature is between about 65 °C, for a Na-abundance of  $10^5$  ppm, and 140 °C, for the Na-abundance of  $10^4$  ppm, as given in Smyth and Caporuscio (1981). To assure the absence of convection in a 1-km thick sedimentary sequence with permeability as low as  $10^{-14}$  m<sup>2</sup> (see Figure 1-30), it is necessary to presume a value of the geothermal gradient of less than 35 °C km<sup>-1</sup>. This assumption, in turn, leads to a conclusion that *"thick sedimentary sequences"* refers to formations with a thickness of more than 1.7-3.9 km, depending upon the abundance of dissolved sodium. Although the lower thickness is comparable to the depth at which authigenic albite occurs at Yucca Mountain, the assumption of a comparable abundance of sodium ( $10^5$  ppm) for Yucca Mountain is unfounded and, therefore, begs the question: How is it possible to regard the alteration as diagenetic, rather than epigenetic?

Broxton et al. (1986) distinguished the following four zones of alteration at Yucca Mountain (refer to Table 3-1-1 depicting the stratigraphy of the volcanic sequence at Yucca Mountain):

Zone I, the shallowest zone, is characterized by tuffs that contain substantial unaltered volcanic glass. Smectite, opal, heulandite, and calcic clinoptilolite are minor alteration phases and concentrate in fractures and in thin discontinuous zones parallel to bedding. Two notable occurrences of zeolites in Zone I include a) thin but widespread accumulations of smectites, calcic clinoptilolites, and heulandite at the top of the basal vitrophyre of the Topopah Spring Member and b) a 130-m-thick sequence of smectite- and calcic clinoptilolite-rich tuffs in the Yucca Mountain, Pah Canyon, and upper Topopah

Spring Members in drill hole USW G-2. Despite their different stratigraphic and lithologic settings, both zeolite occurrences are similar in mineralogy and chemistry.

Zone II is characterized by complete replacement of volcanic glass by clinoptilolite +/- mordenite, with minor opal, quartz, potassium feldspar, and smectite. Clinoptilolite is the most abundant zeolite in this zone and commonly makes up to 50-75 % of the tuffs. These zeolite-rich tuffs occur at well-defined intervals including a) the interval extending from the base of the Topopah Spring Member, through the tuff of Calico Hills, and into the top of the Prow Pass Member; b) the interval at the base of the Prow Pass Member and top of the Bullfrog Member; and c) the interval at the base of the Bullfrog Member and top of the Tram Member...There are no significant mineralogic and chemical changes in authigenic minerals across stratigraphic contacts within these intervals, suggesting that lithology rather than stratigraphy controls sites of zeolite alteration. Individual zeolitized beds range in thickness from 10 to 150 m....

Diagenetic Zones III and IV are confined to the deeper structural levels of Yucca Mountain. Zone III is characterized by the progressive replacement of clinoptilolite and mordenite by analcime, potassium feldspar, quartz, and minor calcite and smectite. Zone IV, the deepest diagenetic zone penetrated by drill holes, is characterized by the replacement of analcime by authigenic albite.

It is evident from the description that alteration of the volcanic glass, characterized by zonation, is independent of the stratigraphic framework. The observed sequence of smectite → clinoptilolite, mordenite → analcime → albite express an increasing degree of dehydration and alkalinity of aluminosilicates and indicates an increasing temperature with depth of the alteration and/or an increasing alkali concentration, sodium, in particular. Sheppard (1971) proposed that similar zonation can be produced during an alteration by meteoric waters. The increasing alkalinity of percolating water allows the crystallization of zeolitic assemblages in the following order: fresh glass+montmorillonite → zeolites → analcime → feldspar. However Gottardi and Galli (1985) noted that this zonation is almost identical to the zoning characteristic of burial diagenesis or metamorphism. Similar mineralogical features would also be produced in epigenetic hydrothermal environments.

The zonation alone therefore cannot be used to distinguish one alteration environment from the other. What is certain, however, is that the development of zonation post-dates the sequential emplacement, devitrification, and deuteritic cooling of each stratigraphic member of the volcanic sequence at Yucca Mountain. Therefore, the U.S. DOE (1998) assertion "... examination of the volcanic rocks at Yucca Mountain shows that most zeolite alteration occurred at the same time as tuff emplacement" (p. 2-66) is grossly misleading.

Broxton et al. (1986) made repeated references to the terms "*diagenesis*", "*diagenetically altered tuffs*", and "*diagenetic zone*". However, nowhere in their writing is the meaning of these terms defined. In "Glossary of Geology" by Bates and Jackson (1980), the term "*diagenesis*" is defined as: "*all the chemical, physical, and biological changes undergone by a sediment after its initial deposition, and during and after its lithification, exclusive of surficial alteration (weathering) and metamorphism.*" This definition implies that Broxton et al. (1986) used the term "diagenetic" to express the viewpoint that the tuff alteration is not a product of hydrothermal metamorphism occurring after lithification of the host tuffs. Such a viewpoint would, indeed, be a very important conclusion. However, no evidence has been offered in support of it.

The presence of alkaline-earth zeolites in the area of eastern Yucca Mountain, as compared to alkali zeolites in the western part, has led Broxton et al. (1986) to conclude that this alteration expresses the upwelling of fluids from a greater depth. However, the authors considered that this conclusion applies only to the tuffs below the present-day water table. Nevertheless, Broxton et al. (1986) did recognize many occurrences of alkaline-earth zeolites in units that comprise the present-day vadose zone. To account for these occurrences they ambiguously stated: "*Alteration of volcanic glass to clinoptilolite-group minerals occurred in an open chemical system, resulting in significant rearrangement of mobile cations in the host tuff.*" However, neither the source of the allogenic cations was specified nor an environment, which would allow for the "*open chemical system*" alteration, was identified.

The conclusions by Peterman et al. (1993) are, similarly, ambiguous. Referring to the tuffs at Yucca Mountain, they concluded: "*In agreement with earlier studies, zeolitization is shown to have occurred under whole open-system conditions. Calcium was increased by up to two to three times the baseline values and strontium up to twenty times.*" This quotation sums up a comparison of chemistry of stratigraphically equivalent tuffs, but at two different locations. The altered tuffs are from drill hole UE-25 a/b#1, in the eastern Yucca Mountain area, whereas the baseline tuffs are from Raven Canyon, which is located 16 km to the south-southwest from this drill hole. Peterman et al. (1993) did not address the obvious question of why there is such a large difference in the abundance of the clearly allogenic elements within the same ash-flow sheet.

Following Broxton et al. (1986), Peterman et al. (1993) further concluded: "Much of the section of non-welded to partially welded tuffs in the unsaturated zone, including the rhyolite of Calico Hills and part of the Prow Pass and Bullfrog Members of the Crater Flat Tuff, was extensively altered to clinoptilolite and mordenite during regional diagenesis... However, K/Ar dating of zeolites, which are less retentive for Ar than illite, yields a wide spectrum of ages suggesting that the rock has continued to be susceptible to low-temperature alteration long after the main episode of diagenesis."

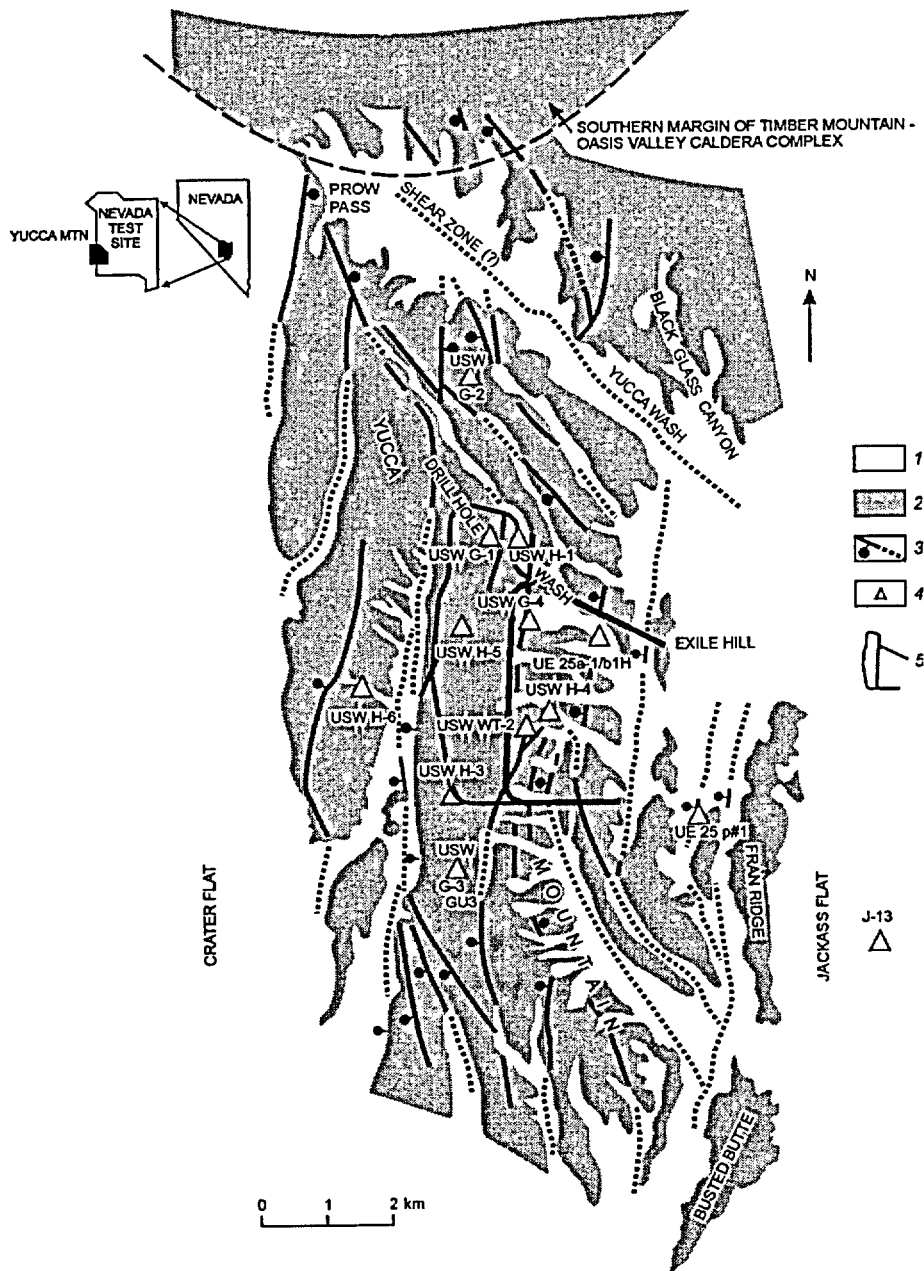


Figure 3-1-1. Generalized geologic map of Yucca Mountain, showing location of drill holes discussed in the text. 1 – Quaternary alluvium and colluvium; 2 – Miocene-Pliocene silicic tuffs; 3 – normal faults, bar and ball on downthrown side, dotted line shows concealed part of fault; 4 – drill hole location and ID; 5 – Exploratory studies facility (ESF) with proposed repository outline.

Peterman et al. (1993) did not make direct references to the meaning of terms "*regional diagenesis*" and "*low-temperature alteration*". Thus, they left it to the reader to decide to what extent these terms are used to denote a non-hydrothermal alteration, which resulted from rainwater that descended from the topographic surface into the unsaturated tuffs. Presumably, the rainwater would have added as dissolved

components, the alkaline-earth elements (Ca and Sr) from windblown dust, which was being re-worked and incorporated into the soil horizons by pedogenic processes.

Weiss (1990) was much more forthcoming in his assessment of the origin of the tuff alteration. Based on a non-destructive examination of cores, which were extracted from the interior of Yucca Mountain, he drew the conclusion, which is summed up by the following statement: *"In general, most of the visibly altered rocks contain alteration mineral assemblages (calcite, zeolite, montmorillonitic clay, chlorite (?), magnetite, pyrite) characteristic of propylitic alteration... The presence of extensive and pervasive propylitic alteration +/- fluorite, in otherwise fresh tuffs of Miocene age, clearly implies the existence of a large fossil hydrothermal system in Yucca Mountain, and supports our earlier contention that zeolitic alteration may not be entirely of a diagenetic or deuteritic origin as is commonly believed."*

This point of view was restated more emphatically by Weiss et al. (1996): "Ample well-documented textural and mineralogic evidence exists for at least one episode of widespread alteration of volcanic rocks deep within Yucca Mountain based on detailed studies of core and cuttings from deep drill holes (e.g. Broxton et al., 1982; Caporusio et al., 1982; Scott and Castellanos, 1984; Vaniman et al., 1984; Warren et al., 1984; Bish, 1987; Bish and Aronson, 1993)." One is hard pressed to disagree with this conclusion, which is supported by geological observations from many modern geothermal systems worldwide.

Researchers at the Los Alamos National Laboratory began to recognize the possible involvement of hydrothermal solutions in the late 1980's and early 1990's. In this regard, Bish (1989) examined clay mineralogy of the altered tuffs from drill holes USW G-1, G-2, and G-3 (Figure 3-1-1) to a depth of between 1500 to 1828 m, using X-ray powder diffraction. Alteration temperatures were inferred, based on the observed clay mineralogy and the homogenization temperature of two-phase fluid inclusions, which were found within the associated gangue calcite. Bish reported:

The clay minerals in Yucca Mountain tuffs are predominantly interstratified illite/smectites, with minor amounts of chlorite, kaolinite, and interstratified chlorite/smectite at depth in USW G-1 and G-2...With depths, the illite/smectites transform from random interstratification (R=0) through ordered intermediates (R=1) to illite in USW G-2 and to Kalkberg (R greater than or equal to 3) interstratifications in USW G-1. The illite/smectites in USW G-3 have not significantly transformed. It appears that the illites in deeper rock result from hydrothermal and diagenetic reactions of earlier-formed smectites. These data demonstrate that the rocks at depth in the northern end of Yucca Mountain were significantly altered about 11 Ma ago. Both clay mineralogy and fluid inclusions suggest that the rocks at depth in USW G-2 have been subjected to post-depositional temperatures of at

least 275 °C, those in USW G-1 have reached 200 °C, and USW G-3 rocks probably have not exceeded 100 °C.

The hydrothermally altered tuffs, however, do not appear to be confined to deeper parts of the vadose zone. The tuffs, which have been altered by hydrothermal solutions, are extensively exposed in outcrops at Prow Pass in the northern part of Yucca Mountain. They belong to the Tuff of Calico Hills. Broxton (1992) examined them in detail:

The zeolitic tuffs at Prow Pass are significantly more calcic (mean 2.07%) and less sodic (mean 1.11%) than the vitric tuffs at Busted Butte or the zeolitic tuffs in the western part of central Yucca Mountain. Potassium concentrations in the tuffs at Prow Pass are highly variable, ranging from 3.44% to 8.75% K<sub>2</sub>O but tend to be greater (mean 5.47%) than the vitric or zeolitic tuffs to the south... There is no consistent pattern of major-element variation with respect to vertical stratigraphic position in the measured sections. Alkali- and alkaline-earth contents in these sections vary by up to 1 wt. % from sample to sample. K<sub>2</sub>O contents have an antithetic relationship with Na<sub>2</sub>O and CaO... Sr is more abundant in the southern part of the outcrop. Sr concentrations are particularly elevated in the uppermost part of the southern outcrops where concentrations are as high as 742 ppm... The zeolitized tuffs at Prow Pass have many of the same chemical and mineralogic characteristics as the tuffs at Calico Hills. Therefore, it seems probable that these tuffs also underwent hydrothermal alteration, but at lower temperatures. Lower temperature hydrothermal alteration is suggested by the greater abundance of clinoptilolite, which is stable only at relatively low temperatures, and by the lower abundance of authigenic feldspar in the tuffs at Prow Pass. The lower K<sub>2</sub>O content of tuffs at Prow Pass probably indicates that hydrothermal fluids were less potassic than those at Calico Hills. The northward increase in K contents in tuffs at Prow Pass suggest that the focus of hydrothermal alteration was located to the north, perhaps near the ring fracture systems of the Timber Mountain or Claim Canyon Calderas.

Because the transformation of smectite into kalkberg and illite is facilitated by the K-abundance, it seems reasonable to associate the alteration at Prow Pass with that, which Bish (1989) found in drill holes USW G-1 and G-2. Thus, the Timber Mountain hydrothermal metamorphism seems to have been in the form of an extensive and pervasive alteration aureole. To the north of Yucca Mountain, parts of this aureole seem to be exposed at the ground surface. How is it possible, then, for researchers to continue to insist that the tuffs, which occur beneath the repository block in the vadose zone some 10 – 15 km away from Timber Mountain–Oasis Valley caldera (see Figure 3-1-1), remained unaffected by hydrothermal solutions from the Timber Mountain hydrothermal system?

In an attempt to resolve the ambiguities and the lingering contradictions, Szymanski (1992) reviewed the database concerning the tuff alteration at Yucca Mountain:

The earliest hydrothermal episode produced alkali-earth metasomatism (Ca+Mg ~10-25 %), which is pervasive in the lower part of the stratigraphic section. Associated alteration minerals include clinoptilolites with K/Ar ages ranging from 9.5 to 10.5, contemporaneous with hydrothermal stages of activity of the Timber Mountain Caldera... Hydrothermal activity subsequent to the Timber Mountain episode differs spatially, chemically, isotopically, and in duration. The more recent metasomatism observed higher in the stratigraphic section is less pervasive, and appears to be confined to aureoles typically associated with faults and fractures. The whole-rock Ca+Mg substitution is greater, ranging above 50 %. Clinoptilolites have (mixed) K/Ar ages ranging from 2 to 8.5 Ma... In contrast to the prolonged (1 million years) Timber Mountain metasomatism, hydrothermal flow over the past 8.5 Ma has been intermittent, has span a much greater depth range, and has been associated with faults and fractures.

Szymanski (1992) regarded the post-Timber Mountain hydrothermal alteration as a mineralogical and hydrologic expression of the high input of heat from the upper mantle: *"In the Great Basin, the flow of terrestrial heat through the crust is affected in part by the flow of fluids (magma, aqueous solutions, and gases). At Yucca Mountain, the role of fluids in crustal heat transport is manifested at the surface by youthful calcretes, sinters, bedrock veins, hydrothermal eruption breccias, and hydrothermal alteration "*

### *3.1.2. Major Element Geochemistry of the Whole-Rock Tuffs*

The interior of Yucca Mountain has been explored to a depth of ~ 2.0 km with a number of drill holes. Chemical analyses of samples from miles of drill hole cores are available to establish in such cores the extent and degree of alteration of the original elemental composition of the tuffs, by circulating groundwater, over the past 12.7 Ma. By combining this information with data relative to the mineralogical alteration of the tuffs, the intent is to develop a framework for the subsequent considerations of the history of long-term behavior of the hydrologic system at Yucca Mountain. The chemical database, which is used herein, is as reported in appendices to the report by Broxton et al. (1986). This database consists of 112 electron microprobe analyses (EMPA) of glass from the vitric tuff and of 63 X-ray fluorescence (XRF) whole-rock analyses of the altered tuffs.

Except for 13 samples collected from the surface exposures at Prow Pass, located to the northwest of the proposed repository footprint, all of the samples were taken from cores extracted from drill holes, the locations of which are shown in Figure 3-1-1. These samples represent the 2.0-km thick volcanic sequence. The stratigraphy and lithology of the sequence is summarized in Table 3-1-1.

The data consists of three lithologically and stratigraphically distinct sets shown in Table 3-1-2. The first set consists only of samples of the glass phase, which represent the uppermost units Tiva Canyon (Tpc), Yucca Mountain member (Tpy) and Bedded Tuff (Tb). The second set consists of mixed samples of glass and altered phases, which represent the underlying Pah Canyon and Topopah Spring Members (Tpp and Tpt), the Tuff of Calico Hills (Tac), and the Prow Pass Member of the Crater Flat Tuff (Tcp). The third set consists of samples of only the altered phase, which represent the older members of the Crater Flat Tuff (Tcb and Tct) as well as the underlying lava's, flow breccia, and tuffs (Tfb, Tlr, Tb and Tot).

Although the number of the analyzed samples is large (175), it can be seen from Table 3-1-2 that the coverage is sparse and spotty with respect to both the drill holes and the stratigraphic units. The most completely covered units are the Topopah Spring Member (Tpt), the Tuff of Calico Hills (Tac), and the Prow Pass Member (Tcp). The glass has been preserved only in these younger units. The underlying units have been intensely altered; so that most of the glass has been destroyed. The unavailability of samples of the older glass is one shortcoming of the database.

Table 3-1

Generalized stratigraphy of volcanic units at Yucca Mountain  
(from Broxton et al. 1986 and Slate et al. 1999)

Stratigraphic Unit	Unit Symbol	Thickness (m)	Lithology
Tiva canyon member	Tpc	45-120	Ash-flow tuff; compound cooling unit, nonwelded vitric base; moderately to densely welded, devitrified interior with some vapor-phase crystallization. Two compositional units, an upper crystal-rich densely welded trachyte with about 14 percent phenocrysts, consisting of sanidine, plagioclase, less than 1 percent each of biotite and clinopyroxene, and a lower crystal-poor, densely welded rhyolite with phenocrysts, consisting of sanidine and traces of clinopyroxene, plagioclase, sphene, biotite, hornblende, and quartz.
Yucca Mountain Member	Tpy	0-30	High-silica rhyolite ash-flow tuff nonwelded vitric top and base; partially welded devitrified interior with some vapor-phase crystallization, present under northern half of Yucca Mountain.
Pah Canyon Member	Tpp	0-80	Crystal-poor, nonwelded to moderately welded, low-silica rhyolite ash-flow tuff, vitric throughout, present under northern half of Yucca Mountain
Topopah Spring Member	Tpt	240-365	Rhyolitic ash-flow tuff A compound cooling unit that is compositionally zoned from an upper trachyte with phenocrysts, consisting of sanidine, plagioclase, and less than 1 percent each of biotite, clinopyroxene, and quartz, to a lower high-silica rhyolite with phenocrysts, consisting of less than percent each of plagioclase, sanidine, quartz, and biotite. Nonwelded zones at top and base and moderately to densely welded, devitrified interior with zones of vapor-phase crystallization, vitrophyres at top and base of unit Zeolites occur both on top of basal vitrophyre and in nonwelded base of unit.
Calico Hills Formation	Tac	35-290	High-silica rhyolite lava flows and related, petrographically similar, light-yellow, gray, and brown, block-and-ash-flow tuff, bedded airfall tuff, and tuff breccia, nonwelded to partially welded, thoroughly zeolitized at north end of exploration block; becomes vitric southward

Paintbrush Tuff

Table 3-1 (Continued)

Crater Flat Tuff	Prow Pass Member	Tcp	85-190	Crystal-rich rhyolite ash-flow tuff, nonwelded zones at top and base, moderately welded, devitrified interior with minor vapor-phase crystallization; nonwelded base is zeolitic; nonwelded top zeolitic in northern part of Yucca Mountain, but vitric to the south
	Bullfrog Member	Tcb	90-190	Crystal-poor, rhyolite ash-flow tuff, compound cooling unit, nonwelded top and base, nonwelded to densely welded interior with thickness and occurrence of welding zones highly variable, zeolitic in nonwelded zones
	Tram Member	Tct	155-385	Crystal-poor, rhyolite ash-flow tuff, compound cooling unit, zones of partial to dense welding vary from drill hole to drill hole; zeolitic in its nonwelded to partially welded parts, otherwise devitrified
	Dacite Flow Breccia (*)	Tfb	0-120	Flow breccia, lava, and tuffs, occurrence restricted to USW G-1; zeolites irregularly distributed throughout the unit.
	Lithic Ridge Tuffs	Trl	185-305	Crystal-poor, rhyodacitic ash-flow tuff, nonwelded to moderately welded; devitrified, contains few zeolite horizons.
	Unnamed Older Tuffs and Lavas(*)	Tot	365+	Ash-flow tuffs, lavas, reworked volcanic sediments; dacitic to rhyolitic compositions, contains few zeolite horizons; Includes units a, b, and c of USW G-1.

Note: (\*) – units described by Broxton et al. (1986) only.

The other is the sparse coverage of unwelded and altered parts of the Paintbrush Tuff (Tpc through Tpt), which, in turn, means sparse coverage of the vadose zone. This is true for the eastern part of Yucca Mountain in particular, where the coverage is limited to the Tuff of Calico Hills, at the base of the vadose zone.

### 3.1.2.1. Chemical Composition of the Glass and of the Altered Tuff

The chemistry of the glass typically corresponds to the liquid phase (melt) of erupted magma. The magma (and its product – volcanic tuffs) contains phenocrystals and lithic fragments, sometimes in abundance. The more fragments and phenocrystals that are present in the magma, the greater the difference between the glass and the whole-rock compositions. Therefore, the question arises: Is the chemistry of the glass determined by means of the EMPA technique a good proxy for the chemistry of the pristine tuff (i.e., tuff in its initial state before devitrification and subsequent alteration)?

Table 3-2

Stratigraphic setting of samples used in evaluations of the bedrock alteration  
at Yucca Mountain.

Unit	Boreholes										Sum
	USW G-2	USW G3 & GU-3	USW G-4	USW H-4	USW H-5	UE- 25a#1	UE- 25b#1	UE- 25p#1	J-13	Prow Pass	
	Glass (EMPA analyses)										
Tiva Canyon	-	3	-	-	4	2	-	-	-	-	9
Yucca Mountain	9	-	-	-	-	-	-	-	-	-	9
Bedded Tuff	5	-	-	-	-	16	-	-	-	-	21
Pah Canyon	3	-	-	-	-	-	-	-	-	-	3
Topopah Spring	-	19	-	-	1	1	-	-	8	11	40
Calico Hills	-	5	3	6	6	-	-	-	5	-	25
Prow Pass	-	1	-	-	3	1	-	-	-	-	5
Bullfrog	-	-	-	-	-	-	-	-	-	-	0
Tram	-	-	-	-	-	-	-	-	-	-	0
Dacite Flow Breccia	-	-	-	-	-	-	-	-	-	-	0
Lithic Ridge	-	-	-	-	-	-	-	-	-	-	0
Bedded Tuff	-	-	-	-	-	-	-	-	-	-	0
Older Tuffs	-	-	-	-	-	-	-	-	-	-	0
Sum	17	28	3	6	14	20	0	0	13	11	112

In the Yucca Mountain region, volcanic rock units contain from 0 to 15 % of phenocrystals as well as abundant pumice and lithic fragments of rhyolitic composition. Our calculations show that the addition of some 12 % of phenocrystals with compositions typical of Topopah Spring tuff to the glass of this unit does not affect the CaO content and results in a slight (within 0.5 to 1.5 wt. %) increase in Al<sub>2</sub>O<sub>3</sub>, K<sub>2</sub>O, and a decrease in SiO<sub>2</sub>. The results for the rest of the rock-forming oxides do not change. Based on that, we believe that the chemical composition of the glass provides a reliable representation of the initial composition of the tuffs. Substantial deviation of the whole-rock chemistry from the “baseline” glass chemistry may, therefore, be regarded as a manifestation of the epigenetic alteration processes. A comparison of the EMPA data obtained for glass with the whole-rock XRF data provides a powerful tool for assessing the degree of chemical alteration that the Yucca Mountain tuffs have undergone.

It must be noted that some of the tuffs are now hydrated, devitrified, and altered. Most of the older glass was destroyed during the Timber Mountain hydrothermal episode; consequently, the initial tuff composition is known only for upper part of the stratigraphic section, which includes the Prow Pass Member (T<sub>cp</sub>), the Tuff of Calico Hills (T<sub>ac</sub>), and the entire Paintbrush Tuff (T<sub>pc</sub> through T<sub>pt</sub>). For the underlying tuffs, there is no choice but to presume that their initial composition is comparable to that of the upper part. A high degree of homogeneity in the chemical composition of the glass samples, which represent as many as seven different stratigraphic units, suggests that this presumption is reasonable (see Figures 3-1-2 and 3-1-3). The fact that the chemical compositions of the altered tuffs from the lower units overlap with those from the upper units provides further assurances in this regard.

The chemical compositions of the glass and whole-rock samples of the altered tuffs are summarized in Figures 3-1-2 through 3-1-4. As can be seen from the figures, the glasses are high silica rhyolites containing sub-equal abundances of Na and K with only traces of alkaline-earth elements (Ca and Mg) and intermediate metals (Fe and Ti). Although hydrated, these glasses show no evidence of significant cation exchange with groundwater, which is, of course, the reason why they have survived. In spite of the diverse stratigraphic setting, a large percentage of the glass compositions is very tightly clustered, which implies a high degree of similarity for the initial composition of the entire sequence.

The Si/Al ratio is high, ranging between 5.2 and 5.6. However, seven samples out of 112 are depleted in SiO<sub>2</sub> and enriched in Al<sub>2</sub>O<sub>3</sub>, as indicated by the Si/Al ratio, which is lower, ranging between 4.44 and 5.12. The anomalous samples (7 out of 16 from the same stratigraphic unit) are from the eastern part of Yucca Mountain (drill hole UE-25a#1, Figure 3-1-1) and represent the Bedded Tuff unit (T<sub>b</sub>). This unit is situated between the Tiva Canyon and Topopah Spring Members (T<sub>pc</sub> and T<sub>pt</sub>, respectively), in the upper part of the vadose zone. The remaining nine samples from this unit, however, plot with the rest of the glass samples. Evidently, the samples, which are enriched in aluminum, represent a slightly altered and hydrated glass, rather

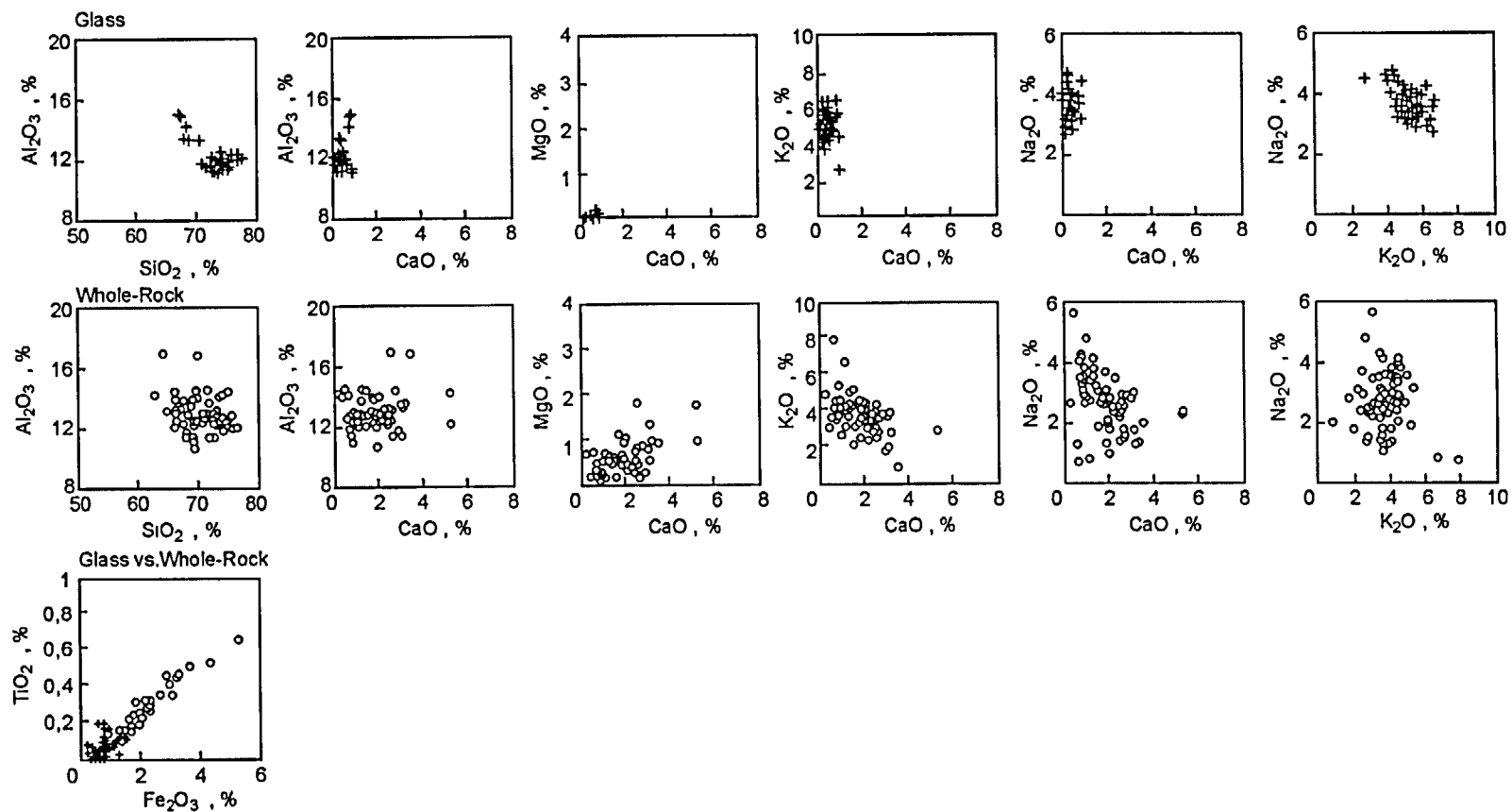


Figure 3-1-2. Comparison of contents of the rock-forming oxides in glass and devitrified tuffs. Glass data approximate the chemistry of the pristine (unaltered) tuff; whole-rock results integrate all chemical changes that the rock has experienced after emplacement. Glass compositions are by EMPA; whole-rock compositions are by XRF (by Broxton et al. 1986).

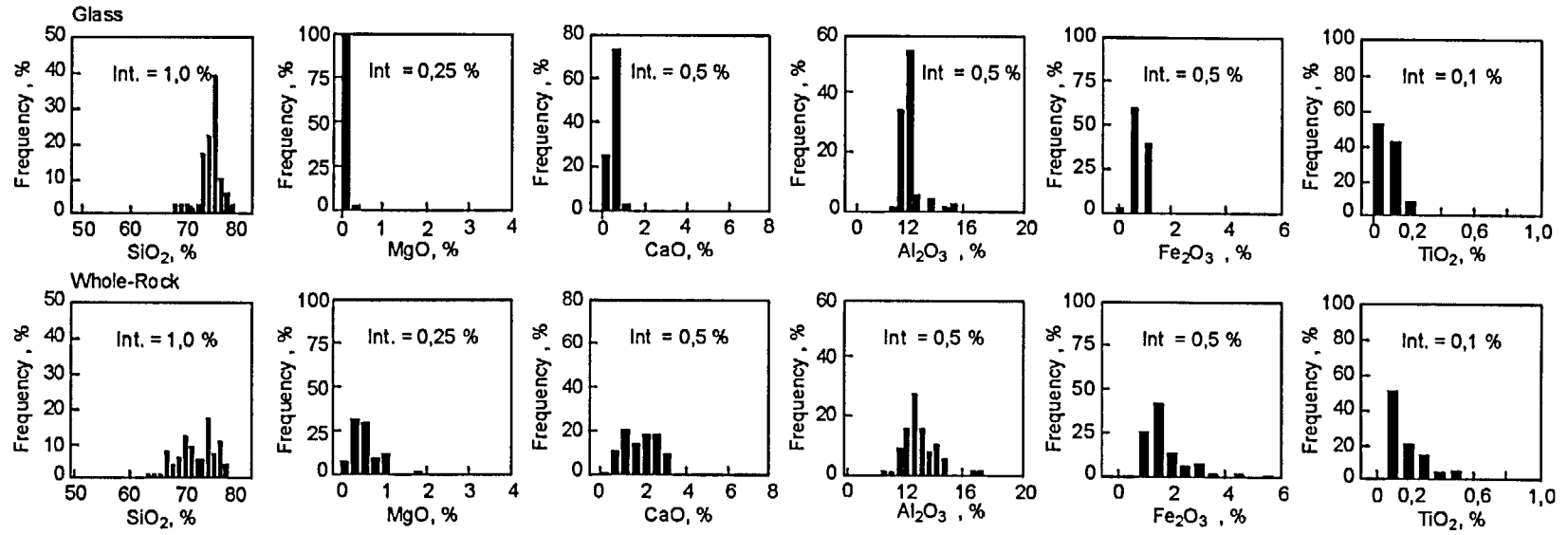


Figure 3-1-3. Comparison of contents of the rock-forming oxides in glass and devitrified Paintbrush, Calico Hills and Crater Flat tuffs. Glass data approximate the chemistry of the pristine (unaltered) tuff; whole-rock results integrate all chemical changes that the rock has experienced after emplacement. Glass compositions are by EMPA; whole-rock compositions are by XRF (by Broxton et al. 1986).

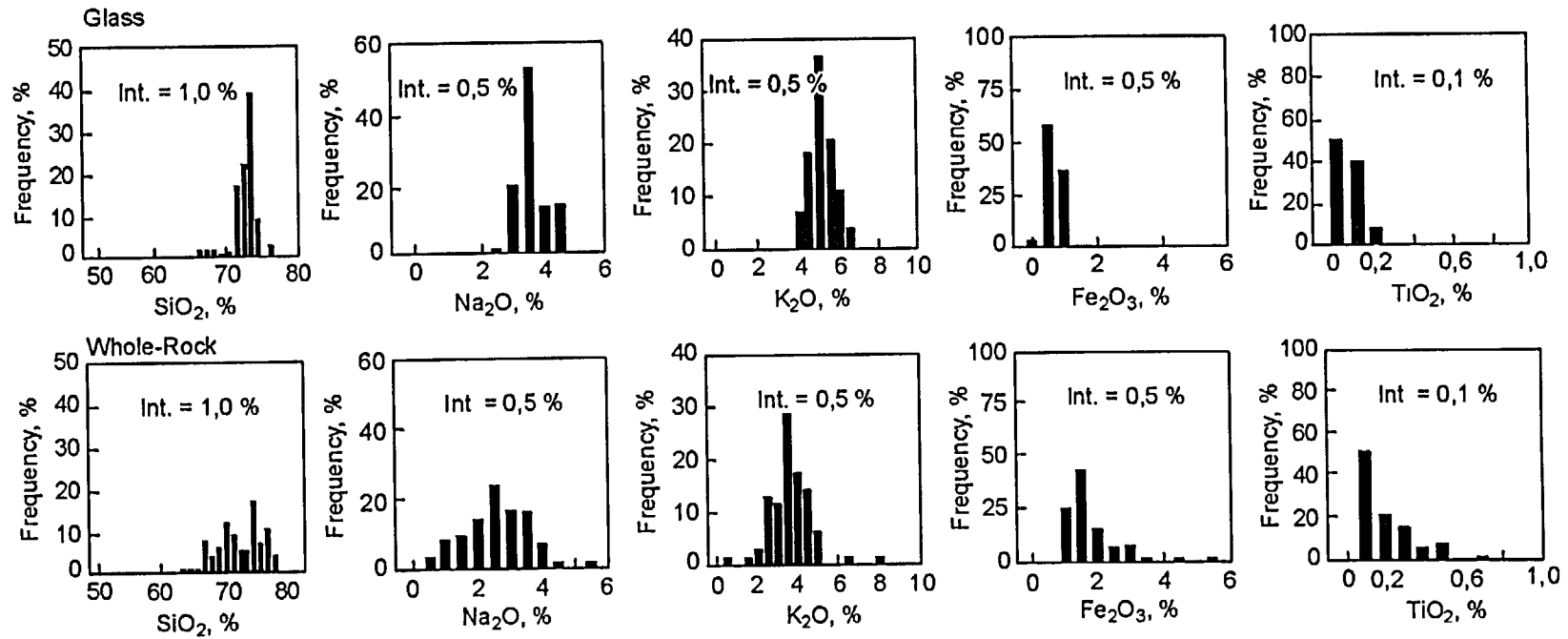


Figure 3-1-4. Comparison of contents of the rock-forming oxides in glass and devitrified Paintbrush, Calico Hills and Crater Flat tuffs. Glass data approximate the chemistry of the pristine (unaltered) tuff; whole-rock results integrate all chemical changes that the rock has experienced after emplacement. Glass compositions are by EMPA; whole-rock compositions are by XRF (by Broxton et al. 1986).

than a chemically different glass phase. The potential significance of this locally altered glass is addressed below.

Figures 3-1-2 through 3-1-4 show that the chemical composition of the altered tuffs displays significantly greater variability than the glass. The CaO, MgO, and Al<sub>2</sub>O<sub>3</sub> oxides are distinctly more abundant in the altered tuffs. The enrichment ranges between 0.5 and 5.0 wt. % for CaO, between 0.25 and 1.75 wt. % for MgO, and between 0.5 and as much as 5.0 wt. % for Al<sub>2</sub>O<sub>3</sub>. The gains have been accompanied by a depletion of the SiO<sub>2</sub> content, which is lower by between 4.0 and 10.0 wt. % as compared to the glass. Further, relative to the glass, a substantial portion of the altered tuffs is depleted in alkali metals, although a small number of samples is enriched by up to 2.5 wt. percent in oxides of these metals. The depletion is between 0.5 and 2.5 wt. % for Na<sub>2</sub>O, and between 0.5 and 3.0 wt. % for K<sub>2</sub>O. This deviation is substantially greater than can be accounted for by the addition of phenocrystals to the whole-rock analyses. Moreover, diagenesis does not normally cause any substantial change in the whole-rock composition. It must be concluded, therefore, that matter from an external source must have been introduced to explain the changes in the whole-rock geochemistry.

### 3.1.2.2. Suggested Mobility of Ti, Fe, and Al

Aqueous solutions, reacting with rocks, extract different elements in different proportions. The differences are explained by the variations in solubility of elements in water and their varying mobility under different conditions. Thermodynamic calculations reported by Palyanova et al. (2002) are summarized in Figure 3-1-5. They demonstrate that at temperatures from 25 to 100°C, Ca and Na are the most mobile components when meteoric water reacts with Yucca Mountain rhyolitic tuffs, whereas Fe and Al are less mobile. The mobility of Si, Mg, K and P is quite low. Among the last four elements, K and P are the most mobile of the group. The very low mobility of Al and Fe is typical of water-granite systems; in nature the low mobility is expressed through the formation of kaolinite and Fe-oxide minerals during chemical weathering or hydrothermal alteration (argillization) of granitic rocks (Barsukov and Borisov, 1989).

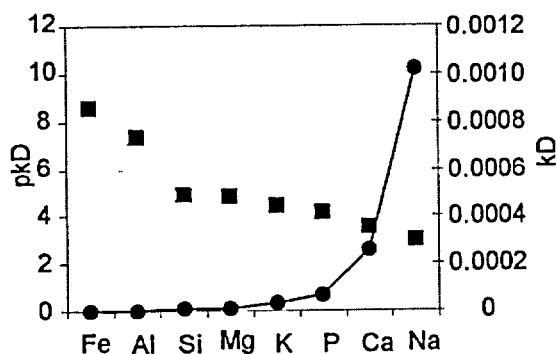


Figure 3-1-5. Partitioning of major rock-forming elements between aqueous solution and rock.  $kD$  – coefficient of partitioning (circles);  $pkD$  – inverse logarithm of the  $kD$  (squares). Calculations are based on the assumption that the fluid acquires its chemistry through interaction of rainwater with the Yucca Mountain rhyolite tuffs at  $T = 25$  to  $100$  °C. Calculated from the data reported by Palyanova et al. (2002).

It is noteworthy that all samples of the altered tuff are 0.1 to 0.5 wt. % richer in  $\text{TiO}_2$  and 0.5 to 4.5 wt. percent richer in  $\text{Fe}_2\text{O}_3$  than is the glass, as shown on Figures 3-1-2 and 3-1-4. Especially notable is the strong positive correlation between  $\text{TiO}_2$  and  $\text{Fe}_2\text{O}_3$ , which is shown in Figure 3-1-2 (glass vs. altered tuff cross-plot). Evidently, this correlation expresses the occurrence of these oxides in the form of titaniferous magnetite or some other Fe- and Ti-bearing minerals. The strong and concurrent enrichment in these metals, both of which are virtually immobile in a low- temperature and near-neutral pH environment, is highly problematic.

On one hand, the enrichment could be apparent, possibly expressing the presence of Ti- and Fe-bearing accessory minerals in the altered tuffs, which would be avoided during the microprobe analyses of the glass. On the other hand, it is possible that the enrichment is real, expressing an epigenetic alteration of the tuffs by acid or alkaline hydrothermal solutions. Some support for the latter possibility is provided by the fact that the strongly brecciated and mineralized tuffs, which are extensively exposed at the topographic surface, were found to be hosting seemingly authigenic, Ti- and Fe-bearing accessory minerals. In this regard, Chepizhko et al (1998) separated crystals of accessory titanite [ $\text{CaTi}(\text{SiO}_4)(\text{O},\text{OH},\text{F})$ ], magnetite [ $\text{FeFe}_2\text{O}_4$ ], and pyrite [ $\text{FeS}_2$ ] from large (1.5-5.5 kg) samples of the bedrock tuff. Similar crystals were separated from pipe-like bodies of breccia, which are cemented by authigenic opal and calcite, and from samples of veins in the bedrock, which are composed of micritic calcite+opaline, silica+minor sepiolite. Many of the separated crystals were observed to exhibit ontogenetic features indicative of an epigenetic hydrothermal origin for these crystals. This conclusion is consistent with the conclusions of Hanson et al. (1987), who regarded the host breccia in Trench #14 as a "*hydrothermal eruption breccia*".

Another noteworthy feature of the altered tuffs is that the  $\text{Al}_2\text{O}_3$  and CaO enrichments seem to be independent of each other, as shown on Figure 3-1-2 (CaO vs.  $\text{Al}_2\text{O}_3$  cross-plots for the whole-rock samples). The high degree (up to 5 wt. %) of the  $\text{Al}_2\text{O}_3$  enrichment implies that this enrichment is real rather than apparent. On the other hand, the conspicuous independence of the CaO and  $\text{Al}_2\text{O}_3$  abundances suggests that the enrichments were produced at different times and by chemically different alteration episodes.

The presence of  $\text{Al}_2\text{O}_3$  enrichment at Yucca Mountain is particularly noteworthy. This is because, at 25 °C and pH between 5.5 and 10, aluminum is practically insoluble in low ionic strength aqueous solutions, as given Wedepohl (1971). Very low aluminum abundance in J-12 and J-13 water, specifically 0.5 to 1.2 ppb, illustrates this point quite well. At higher temperatures, in epigenetic hydrothermal processes, the alumina enrichment is related to its low solubility at pH <8.5 (Pokrovsky, 1989) and is caused by removal of alkalis, alkali-earth elements and silica from the system. Thus, in most cases the

enrichment has a residual character. Deep alteration of alkaline (e.g., nepheline syenites) and acidic (e.g., rhyolites) rocks leads to the appearance of mineral assemblages containing Al-oxides and hydroxides, which confirms the very low mobility of alumina in the wide range of pH of natural hydrothermal solutions (Godovikov, 1987).

The Al<sub>2</sub>O<sub>3</sub> enrichment is evident at several locations scattered throughout Yucca Mountain. Further, this enrichment is not confined to the deeper tuffs, in the phreatic zone, but it is locally evident in the vadose zone. In this regard, the presence of Al<sub>2</sub>O<sub>3</sub> enriched glass in the Bedded Tuff (Tb), between the Tiva Canyon and Topopah Spring Members (Tpc and Tpt), in drill hole UE-25 a#1 has been mentioned above. Additionally, Al-rich, clinoptilolite and heulandite phases were identified by Broxton et al. (1986) at two locations, as noted in Livingston and Szymanski (1996). One of them is in the northern Yucca Mountain area, along a trace of the NW-SE trending shear zone (see Figure 3-1-1), in the Pah Canyon Member (Tpp) and the basal vitrophyre of the Topopah Spring Member (Tpt), in drill holes USW G-2 and G-1. The other is in the eastern part of the Mountain, along a trace of the Paintbrush fault zone (drill hole UE-25a#1), in the basal vitrophyre of the Topopah Spring Member (Tpt). Thus, the aluminum enrichment seems to have been concentrated along at least two fault zones. One of these fault zones is the horst-bounding Paintbrush fault, and the other is the NW-SE trending shear zone that represents, most probably, the Walker Lane deformation.

The Al-enrichment in the vadose zone indicates the open-system character of rhyolite alteration. The latter may be caused either by the removal of alkaline elements and silica, or by the input of Al. The first mechanism may be operational in any water-rock interaction system, including interaction of tuffs with meteoric waters as well as hydrothermal alteration. By contrast, input of Al is only possible by hot mineralized hydrothermal fluids. At Yucca Mountain, input of Al is suggested by the presence of the Al-rich zeolites discussed above. As for the Al-enriched glass, clear petrographic descriptions of samples are necessary in order to make a sound interpretation of the data (such descriptions have not been provided by Broxton et al. (1986) or other researchers who addressed the major element geochemistry of the Yucca Mountain tuffs).

Collectively, the preceding observations show that huge quantities of calcium and magnesium have been introduced into the interior of Yucca Mountain following the emplacement and iso-chemical devitrification of the tuffs. At the same time, huge quantities of silicon, sodium, and potassium were removed from it. The enrichment in allogenic alkaline earth elements (Ca and Mg) and the alteration of ash-fall tuffs both indicate that the initial composition was modified after the deuteric cooling as a result of the ionic exchange with aqueous solutions. In addition, there are indications that the chemistry of the altering solutions has changed over time, which suggests multiple alteration episodes. The addition of

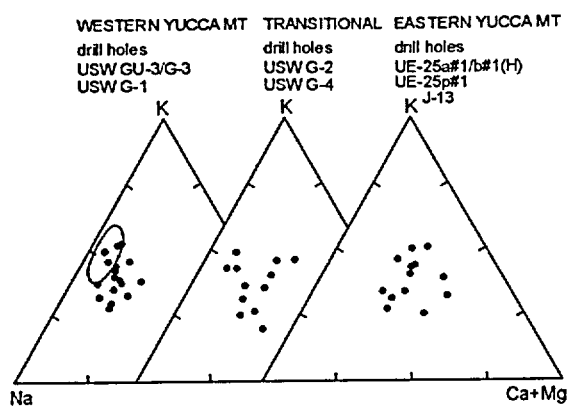


Figure 3-1-6. Relative concentrations of K, Na, and alkali-earth elements for whole-rock analyses of tuffs at Yucca Mountain. Shaded area shows field of unaltered rhyolite compositions. The data for Calico Hills and Crater Flat tuffs are from Broxton et al. (1986).

surface into unsaturated vitric tuffs.

### 3.1.2.3. Spatial Distribution of the Alteration

Further support for the hydrothermal affinity is derived from an analysis of the spatial distribution of the chemical alteration. This is because, in spite of the initially homogeneous composition, the present-

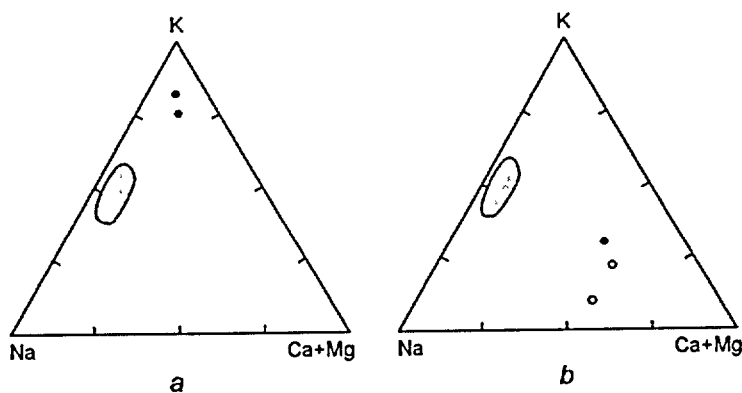


Figure 3-1-7. Relative concentrations of K, Na and alkali-earth elements for the whole-rock analyses of tuffs exposed on the surface of the Yucca Mountain. The shaded area shows field of unaltered rhyolite compositions (based on the glass analyses of Livingston 1993). Plotted by the whole-rock data by Broxton et al. (1986).

All five whole-rock samples, which are shown on this figure, have been collected from within the NW-SE trending shear zone, in the northern part of Yucca Mountain. They represent alteration-prone lithologies, such as nonwelded tuff and vitrophyre. *a* - Surface exposure of the nonwelded tuff of Calico Hills (Tac) at Prow Pass (see Figure 3-2). *b* - Nonwelded tuff from borehole cores. *Filled circles* - Pah Canyon Member (Tpp) in drill hole USW G-2, which at this location is exceptionally rich in smectite and zeolite (Broxton et al. 1986). *Open circles* - altered zone at the top of the basal vitrophyre of the Topopah Spring Member (Tpt) in drill hole USW G-1.

elements whose mobility is low in a low-temperature environment (e.g., magnesium) implies that this open-system alteration cannot be attributed to the exchanges with fresh (TDS of less than 1000 ppm) groundwater. The exchange with such groundwater would be feasible only in association with the diagenetic alteration of the tuffs near the ground surface. Instead, the addition of the allogenic cations seems to suggest that an epigenetic hydrothermal activity is responsible for them. This tentative conclusion contradicts a viewpoint that the alteration is the result of exchanges with "fresh" groundwater, which descended from the topographic

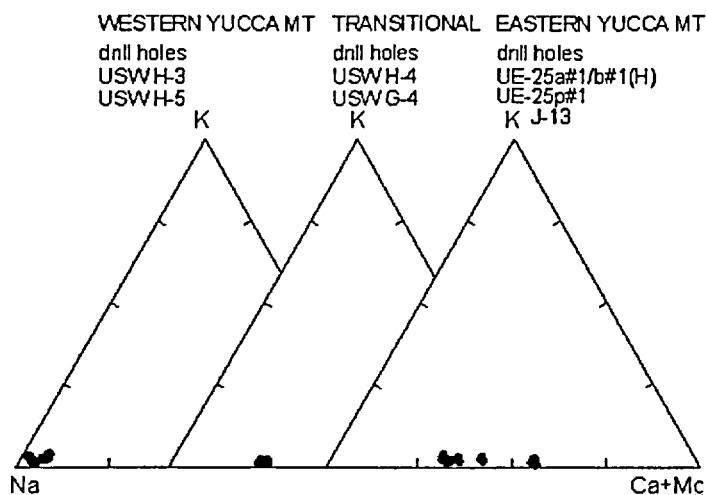


Figure 3-1-8. Major-cation chemistry of waters from Yucca Mountain drill holes.

day chemistry of the tuffs displays a surprisingly high degree of spatial heterogeneity, as shown on Figures 3-1-6 and 3-1-7.

Figure 3-1-6 was constructed based on the chemical analyses of samples, which represent the tuff units extending up to 100 m above the present-day water table and down to several hundreds of meters below it. By contrast, Figure 3-1-7 was constructed based on the analyses, which represent the central and upper parts (Tpp, Tpt,

and Tac units) of the present-day vadose zone.

Figure 3-1-6 shows that the chemical composition changes systematically, from east to west, across Yucca Mountain, over lateral distance of only about 5 km. The Ca and Mg enriched composition dominates in the eastern part where the present-day chemical state deviates most from the initial composition. In the western part, however, the stratigraphically equivalent tuffs have Na and K enriched compositions, which overlap the glass compositions to some extent. Typically, the western tuffs have higher Na/K and Na+K/Ca ratios. A transition zone, which is represented by samples from drill holes USW G-4 and G-2, separates the eastern and western alteration domains.

It is important to note that the changing chemical composition of the altered tuffs mirrors the systematically changing composition of the present-day aquifer water. Water, most enriched in alkaline-earth elements, resides in the eastern part of Yucca Mountain, along and around a trace of the Paintbrush fault. The major cation chemistry of this water (drill holes J-12, J-13, UE-25b#1, UE-25c#1 through #3, UE-25p#1, and UE-29a#2, see Figure 3-1-1) is given in Table 3-1-3 and illustrated in Figure 3-1-8.

The abundance of alkaline-earth elements in drill hole UE-25p#1, which penetrates the Paintbrush fault, increases down-dip of the fault. This increase parallels the down-dip increases in temperature and hydraulic head. For details of this phenomenon, see Craig and Johnson (1984) and Figure 1-30. Table 3-1-3 shows that, at a depth of 381-1197 m, the UE-25p#1 water contains 37 ppm of Ca and 10 ppm of Mg, whereas at a depth of 1297-1805 m the concentrations are 100 and 39 ppm, respectively. The *in situ* temperature (see Figure 1-28) and the abundance of alkaline-earth elements both decrease with the

westward increasing lateral distance from the fault, as shown on Figure 3-1-8. In the transition zone (drill holes USW G-4 and H-4, Figures 3-1-1 and 3-1-8), the Ca abundance is between 13 and 17 ppm and the Mg abundance between 0.2 and 0.29 ppm. However, to the west, in drill holes USW H-3 and H-5, the respective abundances range from 0.8 to 2.0 and from 0.01 to 0.02 ppm.

The gradual change in the chemical composition of the aquifer water indicates that hot fluids, enriched in alkaline earth elements, ascend along the Paintbrush fault from the underlying carbonate rocks of the basement. Upon reaching the overlying tuff units, the water appears to diffuse into these units and intermixes with the local alkali metal aquifer water, as shown on Figures 1-32 and 1-33. It is this lateral diffusion of the ascended water what seems to be expressed by the systematically changing chemistry of the altered tuffs, which is shown on

Figure 3-1-6. Thus, the Ca+Mg alteration and the  $Al_2O_3$  alteration both seem to be related to the Paintbrush fault as a structure, which exerts some influence on the spatial distribution of the chemistry of the altered tuffs.

It is important to note that the chemical heterogeneity of the altered tuffs is not confined to those stratigraphic units, which are situated near or below the present-day water table. Instead, this heterogeneity is also present in the vadose zone, where it seems to be expressed in as many as three stratigraphic units, as shown on Figure 3-1-7.

While considering the chemical alteration of those tuff units, which are situated above the present-day water table, it is important to recognize that a majority, but not all, of the preserved glass is concentrated in the vadose zone. This, of course, implies the absence of a spatially extensive saturation with high ionic strength solutions for extended periods of time. This statement does not necessarily mean that the relatively short-lived incursions of deep, hot and saline solutions were also absent. In the poorly conductive welded units, such incursions would have been narrowly confined to faults, and to the dilated and heavily fractured wallrock of these faults. In the more permeable ash-fall units, however, the invading solutions would spread laterally, forming bodies of perched water, which subsequently percolated downward.

Table 3-3

## Chemical composition of groundwater of eastern, central, and western parts of Yucca Mountain.

Well designation	pH (onsite)	pH (laboratory)	Water temperature (°C)	Dissolved constituents												Dissolved solids (calculated)	Solids (180°C)	
				Ca	Mg	Na	K	HCO <sub>3</sub> (onsite)	HCO <sub>3</sub> (laboratory)	Cl	SO <sub>4</sub>	SiO <sub>2</sub>	Li	Sr	F			
J-12	7.1	--	27.0	14	2.1	18	5	1	--	119	7.3	22	54	40	10	2.1	211	205
J-13	7.2	--	31.0	12	2.1	42	5	0	--	124	7.1	17	57	40	20	2.4	213	202
UE-25b#1	7.1	6.8	36.0	19	0.73	53	3	7	173	158	13	24	53	950	44	1.5	264	266
UE-25b#1	7.5	7.5	36.0	17	0.59	46	3	5	139	134	8.5	22	52	220	38	1.6	218	225
UE-25b#1	7.1	7.7	37.2	18	0.72	46	2	8	133	138	7.5	21	51	120	47	1.6	220	221
UE-25c#1	7.6	7.7	41.5	11	0.34	56	2	0	151	140	7.4	23	56	120	30	2.1	229	--
UE-25c#2	7.7	7.8	40.5	12	0.40	54	2	1	139	141	7.1	22	54	94	45	2.1	233	--
UE-c25#3	7.7	7.8	40.8	11	0.40	55	1	9	137	143	7.2	22	53	110	44	2.0	229	--
UE-25p#1	6.8	7.7	44.3	37	10	92	5	6	--	282	13	38	49	230	180	3.4	418	394
UE-25p#1	6.6	7.2	56	100	39	150	12	--	--	569	28	160	41	590	450	4.7	812	784
UE-29a#2	7.2	7.6	25.1	10	0.2	44	1	1	107	112	11	22	44	100	39	1.0	198	194
UE-29a#2	7.0	7.4	22.7	10	0.3	44	1	3	107	110	8.8	21	44	110	33	0.9	194	192
USW G-4	7.7	7.5	35.6	13	0.2	57	2	1	139	143	5.9	19	45	67	17	2.5	215	216
USWH-1	7.7	7.8	33.0	4.5	<0.1	51	2	4	--	115	5.7	18	47	40	5	1.2	--	176
USW H-1	7.5	8.0	34.7	6.2	<0.1	51	1	6	--	122	5.8	19	40	40	20	1.0	--	188
USW H-3	9.2	9.0	26.5	0.8	0.02	120	1	1	--	174	5.5	37	43	220	1	5.5	347	--
USW H-4	7.4	7.9	34.8	17	0.29	73	2	6	173	171	6.9	26	46	130	27	4.6	261	248

Table 3-1-3 (Continued)

Well designation	pH (onsite)	pH (laboratory)	Water temperature (° C)	Dissolved constituents												Dissolved solids (calculated)	solids (180°C)
				Ca	Mg	Na	K	HCO <sub>3</sub> (onsite)	HCO <sub>3</sub> (laboratory)	Cl	SO <sub>4</sub>	SiO <sub>2</sub>	Li	Sr	F		
USW H-5	7.9	8.0	35.3	2.0	<0.01	60	2.1	127	124	6.1	16	48	71	4	1.4	--	206
USW H-6	8.1	8.3	37.8	4.1	0.09	86	1.3	182	188	7.6	29	48	82	8	4.7	--	--
USW H-6	8.3	8.4	41.6	1.4	0.02	88	1.3	217	183	7.2	25	47	71	3	3.9	269	--
USW H-6	8.3	8.3	37.2	4.7	0.07	88	1.4	234	184	7.4	32	49	63	8	4.7	--	--
USW VH-1	7.9	8.0	35.2	11	1.6	79	1.9	167	158	11	44	50	90	70	2.7	280	287
USW VH-1	7.5	7.9	35.5	10	1.5	80	1.9	165	158	10	45	50	90	70	2.7	279	274
USW VH-1	7.5	8.0	35.5	9.9	1.5	78	1.8	162	158	10	44	49	90	60	2.7	275	277

Concentrations are reported in mg l<sup>-1</sup>, except for Li and Sr, which are reported in µg l<sup>-1</sup>. All the samples represent groundwater from the late Miocene tuffs, except for second UE-25p#1 sample that represents groundwater from carbonate rocks of the basement. First analysis UE-25#p1 is from depth 381-1197 m, second – from depth 1297-1805 m. From Benson and McKinley (1985).

Reacting with some of the vitric fragments, the spreading of initial solutions and eventual quasi-stagnant solutions would cause, first, the hydration and slight chemical alteration of these vitric fragments. If the exposure were long lasting or repetitive, these solutions would cause conversion of the vitric fragments into authigenic alteration minerals, such as zeolite and montmorillonite clays. It is the presence of these minerals that seems to be expressed by the deviations of chemical composition of the altered tuff from the initial composition, which is given by the stratigraphically equivalent glass. The fact that some fraction of the glass is still preserved does not mean that the host tuff remained unsaturated over the past 12.7 Ma. We believe that this fact means only that the incursions, if any, were of insufficient duration, chemistry, frequency, temperature, and spatial extent to achieve the complete conversion.

#### 3.1.2.4. K, Ca, and Mg Alteration in the Northern Sector

The enrichment in Al, Ti and Fe can also be related to the input or the residual enrichment (i.e., due to removal of other, more soluble components) of these elements by aqueous solutions. This enrichment clearly indicates a non iso-chemical process and chemically opened system but does not provide sufficient evidence for distinguishing between supergene and hypogene origins of solutions involved in the alteration process. In contrast to Al and Fe, Ca and Na would be selectively removed from the rock if the latter came in contact with fresh water in an open-system environment. K and Mg would be removed less readily than Na and Ca but much more readily than Al and Fe (Figure 3-1-5). Thermodynamic calculations by Palyanova et al. (2001) show that the resulting solution

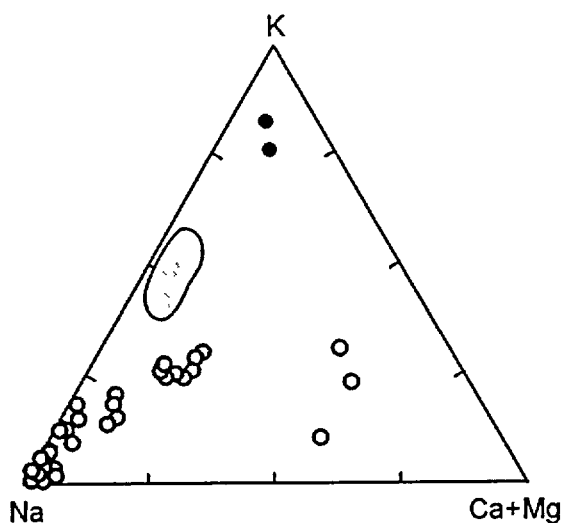


Figure 3-1-9. Comparison of chemistry of tuffs from the vadose zone at Yucca Mountain and fracture-based waters at Rainier Mesa, Nevada Test Site. *Black circles* – altered tuff Tac at Prow Pass; *open circles* – altered tuff Tpp and Tpt from USW G-1 and G-2; *gray circles* – vadose-zone water from Rainier Mesa tunnels in % of meq  $\Gamma^{-1}$ ; and *shaded area* – field of unaltered rhyolite compositions (based on chemistry of glass; Livingston, 1993).

from the reaction between meteoric water and Yucca Mountain rhyolite would not precipitate smectite or any substantial amounts of Ca–Na zeolites. Ca and K, in alteration assemblages, would be concentrated in carbonates, accessory zeolite, authigenic muscovite, and microcline (see Chapter 3-2).

Figure 3-1-9 shows that the altered Tuff of Calico Hills (Tac), which comprises the top of the vadose zone at Prow Pass, has an unusual major cation content, as compared to the rest of the altered

tuffs. Specifically, this alkali tuff is strongly enriched in potassium. It contains between 7.2 and 8.7 wt.%  $K_2O$  when normalized to the volatile-free composition, as given in Broxton et al. (1986). By contrast, in the northern and central parts of Yucca Mountain, the altered tuffs, including the Tuff of Calico Hills, contain only 3 or 4 wt.%  $K_2O$ , as given in Broxton et al. (1986).

According to Broxton et al. (1986) and Bish (1989), authigenic and K-bearing alteration minerals, such as adularia and hydromica (illite), occur at Yucca Mountain, but only below a depth of 834 m in the basal units (Tcb through Tot). On the other hand, although the initial abundance of potassium was substantial, (4-6 wt.% for the glass, Figure 3-1-2), the majority of it is tightly held by the primary alkali feldspars, such as orthoclase, sandinine, and microcline. These phases are all effective in resisting K-leaching by low-temperature and near-neutral pH water, which is at variance with the dissolution prone Na-feldspar that readily releases sodium. This differential resistance is the main factor, which is responsible for low K-abundance and high Na/K ratios in aquifers at Yucca Mountain, as shown in Table 3-1-3.

The average abundance of K is 3.7 ppm and the average value of Na/K ratio is 20.6, for aquifer water in the eastern part, whereas for the western part the average values are 1.8 ppm and 49.6, respectively. It is doubtful that such water could have been involved in producing a potassium alteration, which is observed at the Prow Pass outcrops. However, this alteration may have been produced by solutions, which have been involved in the formation of authigenic adularia and illite in the basal units (Tcb and Tot, see Table 3-1-1). Also, it appears that the past incursion of deep-seated water into the vadose zone is suggested. The NW-SE trending shear zone may have served as a pathway for the local ascent of K-enriched solutions.

Another northern location, within which major cation alteration of the vadose zone tuffs has been documented, is around drill holes USW G-1 and G-2, see Figure 3-1-1. In common with the Prow Pass exposures, this location is also within the trace of the NW-SE trending shear zone belonging to the Walker Lane wrench system. It can be seen from Figures 3-1-6 and 3-1-7 that the altered tuffs have an alkaline earth composition, which is very similar to that of the submerged tuffs in the eastern part. These tuffs contain more than 2.84 wt. % CaO and more than 0.94 wt. % MgO, when normalized to volatile-free compositions (Broxton et al. 1986). By comparison, the stratigraphically equivalent tuffs (Tpt and Tpp, see Table 3-1-1), which occur to the south, typically contain less than 0.65 wt. % CaO and 0.30 wt. % Mg. Thus, the altered tuffs, in the northern part, carry a three- to four-fold increase in the abundance of alkaline-earth elements. Further, according to Broxton et al. (1986), the rubidium and uranium contents are both depleted by a factor of more than two, as compared to the southern tuffs. The strontium

abundance is as high as 1600-1650 ppm, which is a factor of about 80 higher than that for the southern tuffs.

Because the alkaline earth enriched tuffs are situated up to 350 m above the present-day water table, the alteration in the northern part is potentially very important. Considering the strong chemical similarity with the submerged tuffs in the eastern Yucca Mountain, it is reasonable to suspect that past incursions of saline solutions may be responsible for this shallow alteration.

#### **3.1.2.5. Is the Presumption of a Supergene Epigenetic Alteration Feasible?**

The preceding analyses suggest that it is reasonable to attribute the observed alteration of the original composition of the tuffs to incursions of fluids from the deeper interior of Yucca Mountain. The involvement of allogenic elements and the spatial asymmetry of the alteration are particularly persuasive in this regard. Nevertheless, the appropriate question is: Is there a viable alternative? One may accept Hoover's concept, for example, and argue that the alkaline-earth alteration of the vadose zone tuffs is a product of fresh water that descended from the topographic surface. The transport of allogenic Ca and Mg in such a case would necessarily involve rainwater, which has dissolved air-borne dust deflated from local exposures of the basement.

To evaluate Hoover's alternative, it is necessary to consider the chemistry of rainwater, at the time of its residence in the vadose zone, for which it is known with confidence that the rainwater has descended from the topographic surface. The fact that water resides in the vadose zone alone is not sufficient in this regard. Although the chemistry of infiltrating rainwater is not known at Yucca Mountain, it may be assumed that this chemistry is similar to that which seeps into the Rainier Mesa tunnels. The latter chemistry is known based and shown on Figure 3-1-9.

The figure shows that the Rainier Mesa fracture-based water is sodium-potassium in its major cation chemistry, as would be expected for rainwater undergoing ionic exchange reactions with alkali tuffs.

Rainier Mesa is situated at an altitude of about 2200 m, in the northeastern Nevada Test Site, about 40 km to the northeast of Yucca Mountain. The thickness of the vadose zone and lithology of the tuffs are both comparable to those at Yucca Mountain. The higher value of the percolation flux and the resulting water, which seeps into the tunnels present the opportunity for obtaining samples of the fracture-based water. It is likely that this water consists largely of fresh atmospheric precipitation, descending from the topographic surface. The contamination by pore water, although evident in some of the samples, appears to be minimal.

Figure 3-1-9 shows that the infiltrating rainwater at Rainier Mesa is enriched in K and Na relative to Ca and Mg. The relative abundance of potassium is much less than that in the altered tuff at the Prow Pass exposures. In addition, the relative abundance of alkaline earth elements is much less than that in the altered tuffs, which were sampled (Tpp and Tpt units) in drill holes USW G-1 and G-2. The total dissolved cation abundance averages about 50 ppm. The average concentration of major cations is small: Ca - 8.41 ppm, Mg - 1.36 ppm, Na - 35.17 ppm, and K - 4.65 ppm.

A 1 m<sup>3</sup> of the Rainier Mesa fracture-based water is capable of introducing a maximum of 8.41 g of calcium and 1.36 g of magnesium. A 100 m tall and 1 m<sup>2</sup> column of altered tuff, which has been enriched by 2 wt. % CaO and 0.5 wt.% MgO, contains 4400 kg of allogenic CaO and 1100 kg of allogenic MgO. This enrichment involved the addition of 3140 kg of calcium and 663 kg of magnesium. A minimum of 373,200 m<sup>3</sup> and 487,500 m<sup>3</sup> of the water would be respectively required to introduce these quantities of calcium and magnesium. These volumes of fluid, in turn, require that the average value of the percolation flux, over the past 12.7 Ma, would be 29.4 and 38.4 mm·year<sup>-1</sup>, respectively.

A study involving the numerical simulations by Bodvarsson et al. (1997) revealed that, under the present-day climatic regime, a maximum value for the percolation flux is 4.9 mm·year<sup>-1</sup>. The study further suggested that this value could be as low as 1.0 mm·year<sup>-1</sup>, depending upon total flux of chloride at the topographic surface. Kwicklis (1996) estimated substantially lower values for the percolation flux based on the average residence times of bodies of perched water. These values are between 0.001 and 0.3 mm·year<sup>-1</sup>.

It thus becomes apparent that the minimum value of the percolation flux, which is required to introduce the implied quantities of the alkaline-earth elements, is at least a factor of six greater than the maximum estimate for the present-day percolation flux. The discrepancy is by far too large to be attributed to the past climatic changes. Rather, this discrepancy implies that there are reasonable grounds to remain skeptical about the diagenetic origin of the alkaline-earth alteration.

Even if the flux requirements have been met and if the tuffs are capable of completely depriving the rainwater of the dissolved alkaline-earth elements, the problem remains. How can the asymmetry from Figure 3-1-6 be explained, on one hand, and how can the alteration diversity from Figure 3-1-8 be explained, on the other? How is it, then, possible to accept the diagenetic tenet?

### 3.1.2.6. Concluding Remarks

In summary, the review of the chemical database for the tuff sequence at Yucca Mountain shows that vitric tuffs, which were precursors of the present-day tuffs, were generally high-silica alkali rhyolites with very similar chemistry. The present-day chemical composition of the majority of the tuffs deviates

from their original composition. The presence of complex chemical alteration of these tuffs, which involved ionic exchange reactions with aqueous solutions over the past 12.7 Ma, is therefore implied.

Some of the altered tuffs have managed to retain their initial alkali metal composition, but typically have higher Na/K and Na+K/Ca ratios as well as lower Al/Si ratio, as compared to the glass. The presence of authigenic and secondary Na- and K-feldspars both indicate that this alteration involved acid (or alkaline) solutions with elevated ionic strength. However, some of the altered tuffs have acquired the alkaline-earth composition, which implies that the alteration has a metasomatic character in the sense that the altering solutions acquired their chemistry from sources outside the tuffs. The most likely source corresponds to marine carbonates of the basement, which occur beneath the altered tuffs and outcrops around these tuffs.

The presence of two chemically distinct alteration suits indicates that the chemical compositions of the altering solutions have changed from Na+K composition to Ca+Mg composition, or vice versa. Altering solutions with both of the compositions seem to have intruded into the vadose and phreatic zones, which implies that both water levels and fluid chemistry have undergone substantial fluctuations in the past.

The spatial distribution of the secondary cation enrichment (K and Ca+Mg in particular) seems to be influenced by the location of the altered tuffs with respect to two prominent structural features of the local geology. One of these features is the Paintbrush fault zone, which forms the eastern horst-bounding fault zone. The other is the NW-SE trending shear zone, which seems to be expressing the presence of the Walker Lane deformation, in the northern part of Yucca Mountain.

### 3.1.3. Montmorillonite Alteration of the Tuffs

Smectite is a collective name for a group of clay minerals, which belong to the montmorillonite (dioctahedral) and saponite (trioctahedral) structural series. These series include expanding-lattice clay minerals with the general formula:  $R_{x+y}^+(Al_{2-x}Mg_x)^{-x}[(Si_{4-y}Al_y)^{-y}O_{10}](OH)_2nH_2O$ , where  $R$  denotes one or more of Ca, Na and K cations residing between batches built up of aluminosilica-oxygen tetrahedral layers (elements within brackets) and an octahedral layer of Al and Mg (elements within parentheses) between them. If each batch has the composition,  $Mg_2[Si_4O_{10}]$  or  $Al_2[Si_4O_{10}](OH)_2$ , no interlayer cations would have formed because the total charge of this batch would be zero. Typically, tetrahedral Si and octahedral Mg in smectite structures are replaced by Al, which leads to the appearance of a total negative charge. This charge is compensated partly by the corresponding replacement in the octahedral site and partly by incorporation of interlayer alkali cations, accompanied by interlayer water molecules. Dioctahedral smectites (montmorillonite series) are typically formed through epigenetic alteration of ferromagnesian minerals, feldspars, and volcanic glasses. Siliceous tuffs of the Yucca Mountain volcanic sequence have low Mg potential. Smectites with high Al content in the batch (montmorillonite–beidellite series) are expected to form. The batches of these smectites have a high negative charge and can be formed in alkaline solutions (pH > 5.5). The altered tuffs at Yucca Mountain are characterized by the ubiquitous presence of smectite, which has been found scattered throughout the entire 2-km thick explored section.

Vaniman et al. (1984), and Levy (1984) have used the microprobe to determine the chemical composition for a number of smectite specimens from drill holes USW G-2, G-3, and H-5, see Figure 3-1-1). Although microprobe analysis is not a typical (and clearly not the best) way for determining clay mineral composition\*, this database seems to indicate that the clays contain spatially varying abundances of Na, K, and Ca as exchangeable cations.

---

\* It is to be noted that the microprobe results obtained on clay minerals must be interpreted with caution. Smectites contain interstratal water and alkalis and alkali earth elements in the inter-layered position. Being weakly bonded, under the electron beam the water and alkalis evaporate and, therefore, are not detected in the analysis. This may lead to an apparent chemistry where alkali earth elements dominate among the interlayer components. The degree of the selective removal of alkalis from the analytic volume is affected by such parameters of the analysis as the size of beam, acceleration voltage, and signal collection time. The degree of ordering of the mineral may also play a role; the higher the ordering, the more alkalis are bonded by the aluminosilicate lattice and are lost during the analysis. The measured (apparent) K contents are expected to increase with increasing ordering of smectites, which will have nothing to do with the actual composition of smectites. Thus, in order to make the interpretation of the data less ambiguous, the information on the technical parameters of each microprobe run must be provided with the results. Unfortunately, the papers of Vaniman et al. (1984), and Levy (1984) do not provide this information.

Smectite specimens were typically found to display a tendency toward an increased Na abundance at a shallower depth, and an increased K abundance at a greater depth. Microprobe data for smectite specimens from USW G-3 drill hole shows a sub-equal Ca and Na abundance and a varying K abundance, with the latter having a tendency to increase below a depth of 1372 meters. Smectite specimens from the lower vitrophyre of the Topopah Spring Member, in drill hole USW H-5, were found to be Ca-rich with very low K and Na abundances. Similarly, at a depth less than 975 m, in drill hole USW G-2, the Ca abundance is greater than the combined Na+K abundance. Below this depth, however, the K abundance increases rapidly, so that at a depth greater than 1067 m potassium is the dominant cation.

It thus appears that in the western sector of Yucca Mountain the production of smectite involved ionic exchange reactions between the tuffs and two different chemical facies of the fluid. One of these facies had an alkali metal, K+Na, composition, whereas the other had an alkaline earth Ca+Mg composition, which is similar to the picture implied by the major cation data on Figure 3-1-6. The difference is that this figure shows the lateral variability, whereas the smectite database shows the same chemical variability but as a function of depth. The implication is that the tuffs at Yucca Mountain, as a whole, host two chemically and, most likely, temporally different alteration aureoles. The alkaline earth aureole is deep in the eastern sector, but thin and shallow in the western sector. The alkali metal aureole is expressed by the K-enrichment in the whole rock and in the smectite phases, as well as by the K-bearing alteration minerals, such as adularia and hydromica (see Bish 1989 and Broxton et al. 1986 for details). This aureole occurs throughout the entire Yucca Mountain and is best expressed in the basal units, such as Tcb through Tot. Because the K-enrichment becomes shallower and more intense to the north of Yucca Mountain, Broxton (1992) suggested that it probably reflects "*...widespread hydrothermal activity in areas marginal to the TM-OV [Timber Mountain-Oasis Valley] caldera complex.*"

The preceding discussion implies that both the K-rich smectite phases and the whole-rock K-enrichment are products of the Timber Mountain hydrothermal episode, which were formed about 10-11 Ma ago. It also implies that the alkali metal alteration aureole has been overprinted, later by the alkaline earth alteration aureole. The shape of the latter suggests that the Ca+Mg metasomatism expresses an upwelling of fluids from depth along the Paintbrush fault zone and a subsequent diffusion of these fluids into the vadose zone in the manner shown on Figures 1-30 and 2-1.

These ages suggest that the production of smectite commenced immediately after emplacement of the older tuffs. The presence of co-existing discrete illite and randomly interstratified smectite, however, has led Bish (1989) to conclude that the production of smectite continued long after the tuff emplacement. This conclusion was confirmed by WoldeGabriel (1993), who reported that two K/Ar ages from the illite/smectite fraction had less than 25 % of the collapsed illite layers. Samples G-2 3250, from the Prow

Pass Member (Tep), and G-1 5458.4, from the Unnamed Older Tuffs and Lavas (Tot), yielded ages of 12.7 +/-3.0 and 8.8 +/-1.0 Ma, respectively.

### 3.1.3.1. Geothermometry and Geochronology by smectite series: Background

There are two important properties of the montmorillonite smectite series, which make this series very useful from a geothermal reconstruction perspective. On one hand, the members of this series may be reliably dated using the K/Ar method, which makes it possible to employ these members as geochronometers. On the other, the associated alteration temperatures for the individual members may be inferred, under certain conditions, with some degree of confidence, which makes it possible to employ them as geothermometers.

The usefulness of the montmorillonite series for the purposes of geothermometry stems from the fact that smectite transforms via a series of two steps into illite, provided both the duration of thermal exposure and the supply of K and Al are sufficient. As it was previously shown, the dioctahedral smectite typical for siliceous tuff alteration should have aluminum dominating in octahedral batch sites while excess negative charge of the batch is controlled by  $Al^{3+} \rightarrow Si^{4+}$  substitution in tetrahedral batch sites. In an alkaline solution more Si substitutes for Al and more K, Na or Ca is acquired as exchangeable interlayer cations. If K and Al are the dominating cations, the structure of Al-smectite (beidellite type  $K_xAl_2[Si_{4-x}Al_xO_{10}](OH)_2nH_2O$ ) transforms into the illite-muscovite structure  $KAl_2[AlSi_3O_{10}](OH)_2$ . The reaction involves dehydration through loses of interlayer water and introduction of K as a batch bounding cation. This results in collapse of the interlayer distance from ~12-15 Å of the montmorillonite structure to ~10 Å of the muscovite structure. This reaction gives rise to clay minerals (alleverdite, kalkberg, and illite), for which both the expandability and the cation exchange capability decrease progressively with the reaction extent. Dehydration, which is necessary for interlayer distance collapse, requires an elevated temperature. The higher the temperature, the more water is lost, and the more smectite layers transform into illite-muscovite. This makes smectite  $\rightarrow$  illite transformations highly sensitive to the temperature.

The step-wise transformation of smectite has been observed in a wide range of alteration environments including burial diagenesis in sedimentary basins, epigenetic hydrothermal alteration of pelitic and volcanic rocks, and contact metamorphism. The transformation and its extent is a function of several factors including duration of the exposure, chemistry of the altering solutions, chemical composition of the precursor clay, and the alteration temperature (see Bish, 1989, and references therein for details).

Figure 3-1-10 is a summary diagram showing the relationship between the alteration temperature and the extent of the illitization reaction. It has been constructed based on field observations of clay

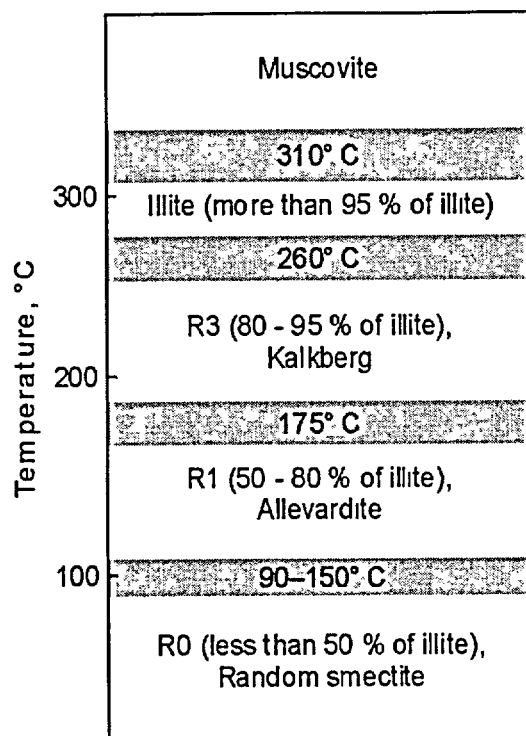


Figure 3-1-10. Relationship between alteration temperature and extent of illitization reaction. After Hoover and Altaner (1983).

mineralogy of pelitic rocks in sedimentary basins. Although the illitization reactions in solidified non-pelitic rocks have received considerably less attention, it is considered that the general trends with temperature hold for other rocks including siliceous tuffs.

The figure shows that in an alteration environment with the sufficient supply of potassium and aluminum, 100 % expandable smectite transforms by a series of intermediate steps into non-expandable illite, which becomes enriched in potassium and aluminum in the process. Smectite is randomly interstratified (R0-type of interstratification) and possesses less than 50 % of collapsed (illite) layers. Under the presence of potassium and aluminum, smectite is a stable mineral phase, but only at a relatively low-temperature. At temperatures about 90 to 150°C R0

smectite transforms into R1 illite/smectite or so called allevardite clay (50-80 % of collapsed illite layers; Hoover and Altaner (1983); Jennings and Thompson (1985).

Hoover and Altaner (1983) and Jennings and Thompson (1985) concluded that, at temperatures 90–150 °C, the smectite transformation is kinetically controlled. For time spans in excess of  $10^6$ - $10^7$  years, R0 smectite transforms into R1 at a temperature ranging from 90 to 100 °C. However, earlier, Hoover and White (1981) suggested that at this temperature, transformation of 100 % expandable smectite to a 20 % expandable illite/smectite would take more than  $10^4$ - $10^5$  years.

Over time spans, which are typically associated with magma chamber-supported hydrothermal systems (of the order of  $10^6$  years, see White (1957)), however, the R0 → R1 transformation requires temperatures that range from 130 to 150 °C. It is important to note that the presence of a 50-100 % expandable smectite does not necessarily mean that the host rock has not been subjected to temperatures more than 100°C after formation of this smectite. Instead, this presence merely indicates that either the supply of potassium and aluminum, or the duration of thermal exposure were insufficient.

At a temperature more than 150°C, the illitization reaction ceases to be kinetically controlled and the percentage of collapsed layers, or interstratification ordering, increases fairly independently of the

duration of thermal exposure. At a temperature of about 175 °C, and in a K- and Al-rich aqueous environment, R1 alleverdite clay becomes unstable and transforms into so-called kalkberg clay, as shown in Figure 3-1-10. The corresponding percentage of the collapsed layers ranges up to 95 percent (R3 type of interstratification). At a temperature of about 260°C, the illitization reaction is completed with the formation of non-expandable illite.

In addition to the alteration temperature and the duration of thermal exposure, the chemistry of the altering solution also plays an important role in controlling the extent of the illitization reaction. An increasing abundance of potassium and aluminum promotes this reaction. The presence of other cations (Ca, Mg, and Na), however, tends to inhibit it.

### 3.1.3.2. Spatial Distribution of the Montmorillonite Alteration Species

Figure 3-1-11 shows the extent of illitization reaction as a function of depth for the altered tuffs at Yucca Mountain. It is based on the X-ray powder diffraction data for clay minerals from drill holes USW G-1, G-2, G-3, and UE-25 p#1 (see Figure 3-1-1), as reported in Bish (1989).

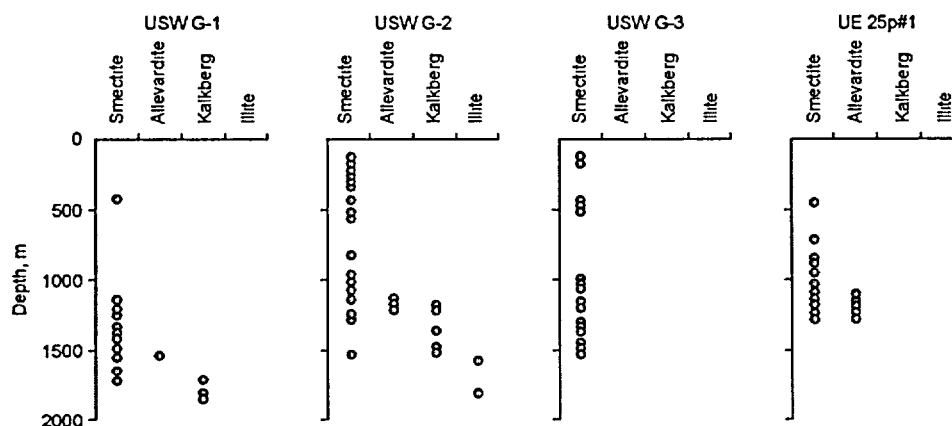


Figure 3-1-11. Extent of the illitization reaction as a function of depth in four boreholes, based on X-ray powder diffraction data from Chipera and Bish (1988) and Bish (1989).

The figure shows that the orderly-interstratified transformed clays were found in cores extracted from three drill holes, UE-25 p#1, USW G-1, and USW G-2. The southern most drill hole USW G-3 contains only the R0 smectite throughout the 1513 m explored depth.

All of the remaining drill holes, however, contain alleverdite clay (R1) at a depth ranging from 1072 m, in UE-25 p#1, through 1133 m, in USW G-2, to 1511 m, in USW G-1. Kalkberg clay has been

found in drill holes USW G-2 and G-1 at a depth of 1181 and 1718 m, respectively. Furthermore, discrete illite has been found in USW G-2 at a depth of 1576 m, as shown on Figure 3-1-11.

The depth distribution of clay minerals, in the interior of Yucca Mountain, exhibits two noteworthy features. **First**, the randomly interstratified smectite (R0) occurs below a depth at which the orderly-interstratified clays (allevardite, kalkberg, and illite) are present, as shown on Figure 3-1-11. In addition, one sample (G2-5369; Bish, 1989) has been found to contain both the discrete illite and the randomly interstratified smectite with about 80 % of expandable layers. This ubiquitous presence of the randomly interstratified smectite indicates that the tuffs have continued to be susceptible to smectite alteration long after high-temperature formation of the orderly-interstratified clays. Evidently, this alteration was occurring in an aqueous environment, which was inadequate to support the transformation into orderly-interstratified clays. Most likely, the duration of thermal exposure and/or the K- and Al-abundance were insufficient for this transformation to occur.

**Second**, the orderly-interstratified clays do not appear to be confined to a particular stratigraphic unit. For example, in USW G-2 allevardite clay occurs in the Tram Member of the Crater Flat Tuff (Tct; Table 3-1-1). In drill holes UE-25 p#1 and USW G-1, however, this clay has been found in the Lithic Ridge Tuff (Tlr) and in the Unnamed Older Tuffs and Lavas (Tot). Kalkberg clay has been found in the Tram Member (Tct) in USW G-2, but in USW G-1, this clay occurs in the Unnamed Older Tuffs and Lavas (Tot). The occurrence of illite is likewise independent of the stratigraphic framework. This clay has been found in USW G-1 in the Older Tuffs and Lavas (Tot), but in UE-25 a/b #1 it occurs in the Tram Member (Tct). The stratigraphy-independent occurrence of the orderly-interstratified clays is important. This is because such occurrence clearly indicates that the alteration is epigenetic, which means that it post-dates the emplacement and solidification (cooling) of, at least, the earlier tuffs.

### 3.1.3.3. Age and Significance of the Smectite Alteration Species

The timing of the formation of the orderly-interstratified clays is constrained by the K/Ar ages from kalkberg (samples G1-5637 and G2-3875) and illite (sample G2-5171) clays, as given in Bish (1989). The ages are  $10.9 \pm 0.6$ ,  $11.0 \pm 0.6$ , and  $11.0 \pm 0.6$  Ma, respectively. They are equivalent to the  $11.0 \pm 0.3$  Ma age of the Timber Mountain Tuff, as reported by Marvin et al. (1970). This tuff unit was erupted from the Timber Mountain Caldera, which is located to the north of Yucca Mountain (see Figure 1-2). In addition, Bish and Aronson (1993) reported one datum for smectite at  $9.4 \pm 0.6$  Ma. This sample, from drill hole USW G-2, is reported as sample Clay-07 in Feng et al. (1999).

The spatial and chronological correspondence indicates that the solidifying Timber Mountain granite massif provided heat, which fueled the circulation of K- and Al-enriched hydrothermal solutions.

The duration of thermal exposure (of the order of  $10^6$  years) and the solution chemistry (abundance of K and Al) were both sufficient to promote the illitization reactions, but only over a time span from 10 to 11 Ma ago. The absence of the younger orderly-interstratified clays indicates that such alteration environment, most probably, did not occur again over the past 10 Ma.

It thus becomes apparent that the alkali alteration aureole expresses hydrothermal processes supported by a "strong" heat source, in agreement with the inferred evolution of long-term behavior of the hydrologic system at Yucca Mountain (see Chapter 2-2). This aureole has been overprinted by the alkaline earth alteration aureole, which is in agreement with what the proposed conceptual model implies. Is this subsequent aureole the product of hydrothermal processes supported by "weak" heat sources? That is, indeed, a very appropriate question, and the development of the Yucca Mountain site as a repository hinges on the correct answer.

The 10-11 Ma age of the alkali alteration aureole constitutes grounds upon which reliable interpretations of the geologic record at Yucca Mountain can be founded. This age and the associated alteration environment (elevated K- and Al-abundance), both lead us to a number of important conclusions. For example, the Al-enrichment of the glass in drill hole UE-25a#1 which represents the Bedded Tuff (Tb) unit (see Table 3-1-2), high in the vadose zone, is clearly a product of the Timber Mountain hydrothermal metamorphism. The K- enrichment of the exposed whole-rock tuff (Tac, on Figure 3-1-9) at Prow Pass, in the northern sector, is likewise related to this metamorphism.

The preceding two examples indicate, on one hand, that the Timber Mountain hydrothermal metamorphism affected the tuffs of the present-day vadose zone. On the other hand, the preserved vitric state of the majority of these tuffs suggests that these tuffs have not been exposed to long-lasting hydrothermal circulations, such as those that were associated with the Timber Mountain hydrothermal metamorphism. These apparent contradictions may be reconciled by accepting the notion that only some faults served as pathways for ascent of the Timber Mountain hydrothermal solutions. Spatially, the Al- and K- enriched tuffs are associated with the Paintbrush fault zone (UE-25a#1) and the NW-SE trending shear zone (Prow Pass), which belongs to the Walker Lane wrench system, see Figure 3-1-1. Further, these locations also contain the tuffs, which host the orderly-interstratified smectites (i.e., UE-25p#1 and UE-25a/b#1 in the east and USW G-1 and G-2, in the north), as shown on Figures 3-1-1 and 3-1-11.

In addition, the alkali alteration aureole serves another very important purpose. It allows us to infer the thermal state of the vadose zone, including those tuffs that are exposed in the Exploratory Studies Facility, at a time of the cessation of the Timber Mountain hydrothermal episode. This thermal state, specifically the ESF *in situ* temperature, is crucial for rational interpretations of the fluid inclusion data and  $^{207}\text{Pb}/\text{U}$  ages, which were reported by Wilson and Cline (2001), Neymark et al. (2000, 2002), and

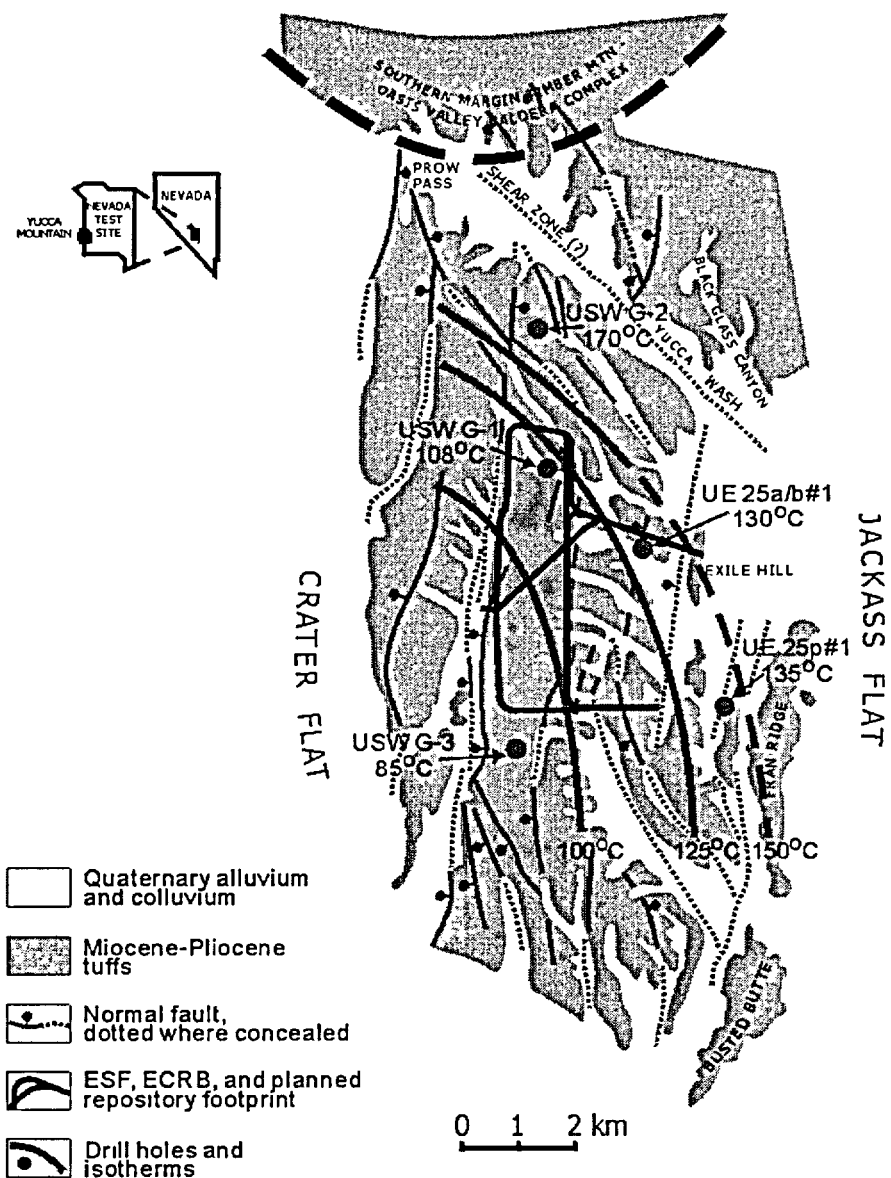


Figure 3-1-12. Alteration temperature at a depth (present-day) of 1 km at a time of smectite alteration of the tuffs at Yucca Mountain. K-Ar ages of kalkberg clay and illite indicate that this alteration is ~11 Ma old and is, most probably, a result of the Timber Mountain hydrothermal metamorphism.

Whelan et al. (2001). In this regard, two observations are critically important. These are: (1) the absence of orderly-interstratified clays in drill hole USW G-3 (see Figure 3-1-11), and (2) the presence of randomly interstratified smectite (G-1 5458.4 specimen) in drill hole USW G-1. WoldeGabriel (1993) reported the R0 smectite specimen at a depth of 1663.6 m (G-1 5458.4), which carries a K/Ar age of

8.8±1.0 Ma. The absence of orderly stratified clay in drill hole USW G-3 indicates that the average geothermal gradient, which was induced by the Timber Mountain hydrothermal metamorphism, was less than 72-85 °C km<sup>-1</sup>. Thus, the *in situ* temperature in the south ESF area (at a depth of about 200 m), during this metamorphism, was less than 34-37 °C. The G-1 specimen, on the other hand, indicates that the average geothermal gradient at the USW G-1 location, which was induced by the Timber Mountain hydrothermal episode, declined to 66-78 °C km<sup>-1</sup> by 8.8±1.0 Ma ago, which means that the *in situ* temperature at the ESF level must have been less than 33-36 °C, at a time when the G-1 5458.4 specimen was formed. Thus, the presence of ESF minerals, which carry apparent (see Chapter 3-7) <sup>207</sup>Pb/U ages of less than 8.8±1.0 Ma and at the same time contain two-phase fluid inclusions indicating elevated temperatures, indicates hydrothermal activity fueled by a heat source, other than the cooling of the Timber Mountain granitic batholith.

The spatial distribution of the maximum *in situ* alteration temperature, which was attained at a depth of 1.0 km during the Timber Mountain hydrothermal metamorphism, was reconstructed based on the data shown on Figure 3-1-11. The reconstructed temperatures are shown in Figure 3-1-12. They should be used to derive rational interpretations of the combined <sup>207</sup>Pb/U and fluid inclusion database. We will interpret this database at a time when it is released and available for scientific scrutiny.

Two notable features of the thermal field are shown by the figure. First, the temperature diminishes to the southwest away from the Timber Mountain Caldera from about 170°C, in the northern segment, to 100°C, in the western and central segments of Yucca Mountain. Second, the isotherms display a tendency to be aligned parallel to traces of the NW-SE trending shear zone and the Paintbrush fault zone. Both of these structures have been noted earlier as influencing the spatial distribution of chemical alteration of the tuffs at Yucca Mountain.

### **Concluding Remarks**

In summary, the presence of orderly-interstratified smectite clays in the interior of Yucca Mountain provides evidence for the involvement of hydrothermal solutions in causing alteration of the tuffs. This conclusion therefore constitutes a partial validation of the inferred long-term behavior of the hydrologic system. It is clear that the solidifying granite batholith, underneath the Timber Mountain Caldera, has acted as a "strong" heat source, which fueled the hydrothermal flow. The alkali tuffs have served as a source of the dissolved cations, K and Al in particular.

The duration of thermal exposure, the *in situ* temperature, and the aqueous chemistry were all sufficient to support the illitization reactions, but only over a time span from ~11 to 10 Ma ago. The hydrothermal flow affected to some extent the tuffs, which underlie the central and northern sectors of

Yucca Mountain and locally include those that comprise the present-day vadose zone. It is likely that both the Paintbrush fault zone and the NW-SE trending shear zone served as pathways for the ascent of K- and Al-bearing hydrothermal solutions. Chemically and spatio-temporally, the Timber Mountain hydrothermal metamorphism differs from the alkaline earth metasomatism, which appears to be a product of later ionic exchange reactions between the altered tuffs and some allogenic solutions.

Thermodynamic calculations by Palyanova et al. (2002) demonstrated that the equilibration of meteoric waters with Yucca Mountain tuffs would not result in formation of abundant smectite. Quite the opposite, in the equilibrium assemblage, K and Al would be distributed between authigenic kaolinite, muscovite, and microcline. Potassium appears to be a moderately mobile cation (see Figure 3-1-7<<SS: 3-1-5?>>) and would be readily removed from the system if the system is chemically open and the degree of reaction is low. Thus, elevated temperatures and the additional input of potassium are necessary to produce the smectite/illite alteration. Because no K source is known at the surface of Yucca Mountain, the suggestion of a dominant role for surficial water in the alteration of tuffs appears to be untenable.

### 3.1.4. Zeolite Alteration of the Tuffs

Zeolites are hydrous aluminosilicate mineral phases whose chemical composition and structure are derived from feldspars. The structure of zeolites is a 3D framework with sodium, calcium, and potassium (rarely barium and strontium) as the major exchangeable cations, positioned in big voids of the structure along with water molecules. Typically, these phases are characterized by a ratio,  $Al+Si / (non\text{-}hydrous\ oxygen)$ , of about 0.5, by an easily reversible loss of water, and by fusion and swelling upon heating. They occur as authigenic minerals in a number of geologic environments. In marine and saline-alkaline lake environments they form "during and after burial, generally by reaction of pore water with solid aluminosilicate materials (e.g. volcanic glass, feldspar, biogenic silica, and clay minerals)" (Hay, 1978). They are also quantitatively significant in hot spring environments and in hydrothermally altered silicic and basic volcanic rocks (e.g., Lebedev, 1979).

Formation of zeolite phases involves nearly neutral to alkaline aqueous solutions operating in a wide range of temperatures. Aqueous silica activity, absolute and relative cation abundances, temperature, and pH are all-important parameters, governing which zeolite species will form, or whether they will form at all.

#### 3.1.4.1. Background

Iijima (1975 and 1980) compiled the typical vertical zonation of zeolite mineralogy from a number of thick silicic tuff sequences, which have been metamorphosed by burial in a marine environment. This zonation is shown on Figure 3-1-13.

Figure 3-1-13 shows that the typical sequence of altered tuffs consists of four zones, each of which is associated with the characteristic mineralogical assemblage. The uppermost, Zone I, includes a zeolite-free rock and contains unaltered volcanic glass and its low-temperature derivatives, such as opal, smectite, and cristobalite. As the temperature increases up to 60 °C, this zone grades into the alteration Zone II, which includes clinoptilolite and mordenite (alkali series) or clinoptilolite and

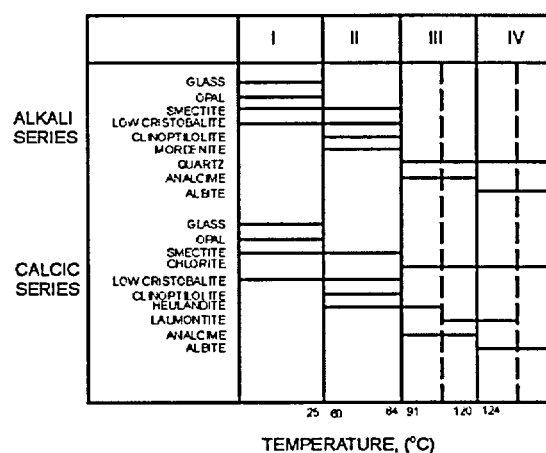


Figure 3-1-13. Four mineralogic zones (I through IV; by Iijima, 1975 and 1980) of the zeolitic alteration and the dependence of zonation on the alteration temperature. Reproduced from Smith and Caporuscio (1981).

heulandite (calcic series). At an 84 to 91 °C temperature, the Zone II assemblage begins to convert into analcime (alkali series) or to analcime plus laumontite/heulandite (calcic series), the presence of which characterizes the alteration Zone III. These alteration minerals replace the precursor zeolite species, which then co-exist as relicts. The alteration Zone IV is characterized by the presence of albite (alkali series) or of albite plus laumontite (calcic series), which denotes alteration temperatures of more than 120-124 °C.

The ranges of alteration temperature, which are shown on Figure 3-1-13, have been inferred based on the mineralogical zonation, as is typically observed in a marine alteration environment. Here, the abundance of dissolved cations is high (Na – 10,560 ppm; Mg – 1,270 ppm; Ca - 400 ppm; and K - 380 ppm; Wedepohl, 1971). Smyth and Caporuscio (1981), however, have extrapolated the marine temperature ranges to include other Na-rich alteration environments, such as saline alkali lake ( $\text{Na}+\text{K} \cong 10^5$  ppm plus negligible Ca) and weakly alkaline geothermal ( $\text{Na} \cong 10^3$  ppm) environments. The results of these extrapolations are shown on Figure 3-1-14.

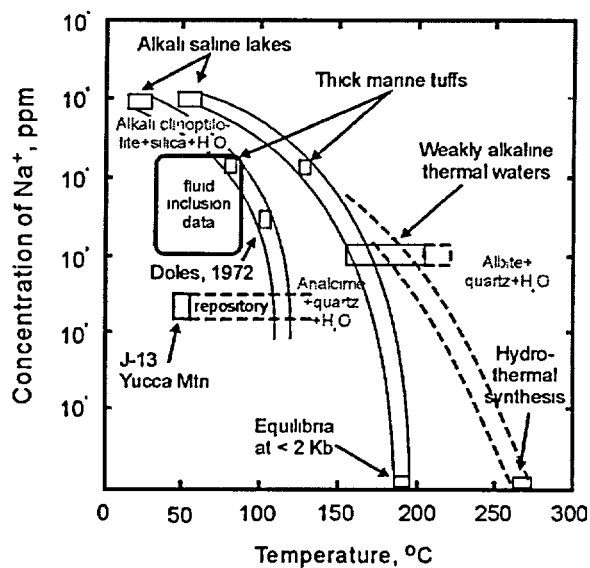


Figure 3-1-14. Zonation of the zeolitic alteration as a function of the alteration temperature for various abundances of sodium. From Smith and Caporuscio (1981). Parameters of fluids that circulated through the vadose zone of Yucca Mountain in the past (box "fluid inclusion data") are shown for comparison (constructed based on the data of Dublyansky et al., 2001).

Figure 3-1-14 shows that the Zone II/Zone III transition takes place at a temperature ranging from about 25°C, for saline-alkali lakes, through about 87-90°C, for marine deposits, to about 110°C, for weakly alkaline hydrothermal deposits. For the Zone III/Zone IV transition the corresponding temperatures are ~55, 130, and 175°C, for a salinity equivalent of about  $10^5$  ppm Na.

The alteration temperatures, which correspond to the Zone II/Zone III and Zone III/Zone IV transitions in a weakly alkaline environment (110 and 175°C, respectively), may be appropriate for the reactions that are expressed at Yucca Mountain. This is because, as Dublyansky et al. (2000) have demonstrated, the salinity of aqueous solutions entrapped in inclusions hosted by the ESF calcite are between 0.00 and 2.07 wt.% NaCl equiv., with an average of 0.57 wt.% NaCl equiv. (or  $\sim 2.2 \cdot 10^3$  ppm Na).

The investigation of Chipera and Bish (1997) demonstrated the influence of relative activities of Ca, Na and K along with temperature and aqueous silica activity on the zeolite assemblages. They studied

the stability of the various species by means of thermodynamic modeling using estimated thermodynamic properties (heat capacity, Gibbs free energy and enthalpy of formation at 298 °K, and entropy) for these species. The primary reason for using the estimated properties, even though these parameters have been measured for many zeolite species, is the highly variable chemistry. In spite of this shortcoming, the results are useful to some extent in reconstructing the geochemical regimes under which a particular zeolite assemblage has been formed. The usefulness is somewhat limited, however, because the species variability is expressed in the form of its dependence on the aqueous silica activity and on relative values of the cation abundances. The results of thermodynamic modeling from Chipera and Bish (1997) are reproduced as Figure 3-1-15.

Figure 3-1-15 shows the stability of zeolite species as a step-function of the temperature. The assemblages shown are typical of hydrothermally altered silicic volcanic rocks. The figure shows that the presence of chabazite, erionite, and phillipsite are indicative of an alteration environment with an elevated abundance of potassium. By contrast, an elevated abundance of calcium is required for the formation of heulandite, stilbite (stellerite), wairakite, and laumontite. The presence of more siliceous zeolite species (clinoptilolite and mordenite) is indicative of an environment with intermediate values of the K/Ca ratio for the dissolved cations. The elevated abundance of Na, at the expense of Ca, enhances the analcime stability field.

Figure 3-1-15 further shows that the temperature is an important parameter, which exerts a strong influence on the stability fields for almost all zeolite species. The increasing temperature has the principal effect of enhancing the stability field for analcime and suppressing the fields for the remaining species. In addition, the elevated temperature enhances the stability fields for calcic zeolites, at the expense of the stability fields for clinoptilolite and mordenite and, to a lesser degree, for the potassic species.

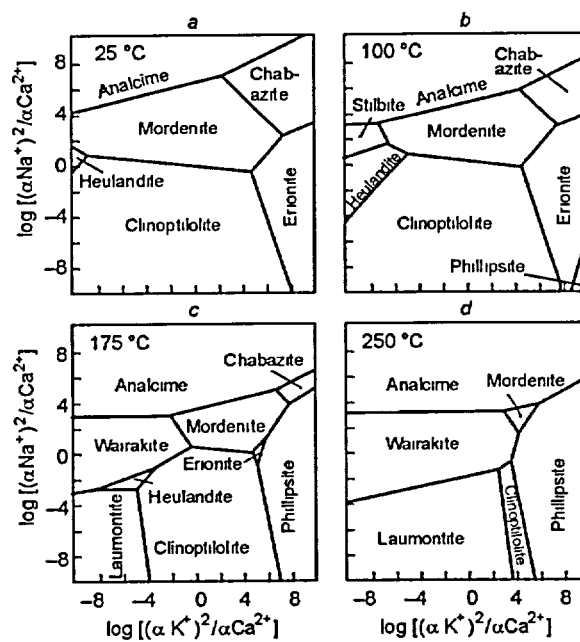


Figure 3-1-15. Stability diagrams for zeolite minerals in hydrothermally altered silicic-volcanic rocks, based on thermodynamic modeling at different temperatures and at aqueous silica activity in equilibrium with cristobalite. From Chipera and Bish (1997).

Some of the zeolite species are stable only at elevated temperatures, and their presence in an assemblage may be employed for temperature estimation. In this regard, the presence of wairakite, laumontite, and phillipsite are indicative of environments with temperatures  $\geq 100$  °C. Similarly, the presence of stilbite (stellerite) may be regarded as evidence for the alteration temperature being somewhere within the 100-175 °C range.

Zeolite species, which have been identified at Yucca Mountain, occur in the form of whole-rock secondary constituents (clinoptilolite/heulandite, mordenite, analcime, and laumontite) or of authigenic fracture coatings (analcime, chabasite, erionite, phillipsite, mordenite, and heulandite). The results of thermodynamic modeling of the stability fields for these species are shown on Figure 3-1-16.

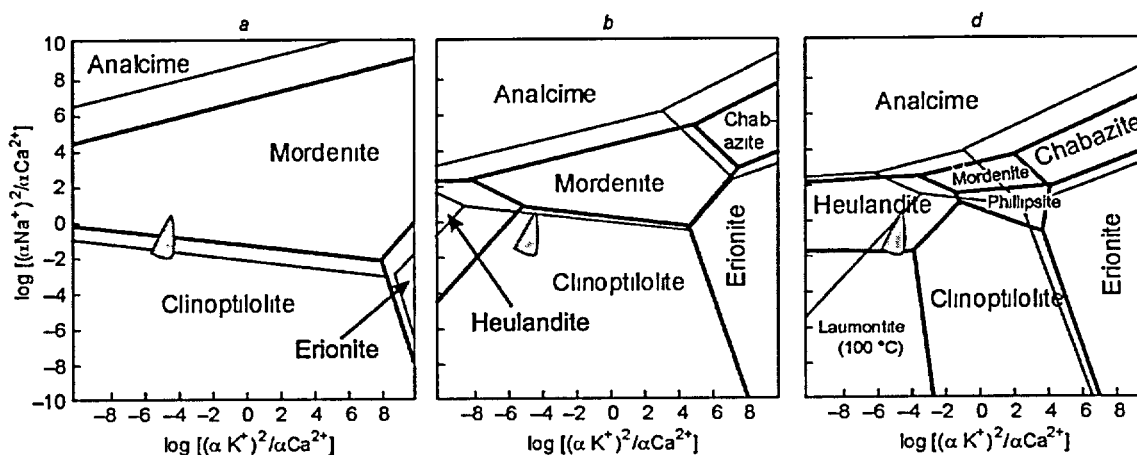


Figure 3-1-16. Stability diagrams for zeolite minerals found at Yucca mountain, based on the results of thermodynamic modeling at 35°C (*thin lines*) and 100°C (*heavy lines*). Aqueous silica activity in equilibrium with: *a* – amorphous silica, *b* – cristobalite, and *c* – quartz. *Shaded area* – present-day groundwater chemistry at Yucca Mountain. From Chipera and Bish (1997)

The relative chemistry of the present-day water is shown in Figure 3-1-16 for reference. The calculations were made for the alteration temperatures of 35 and 100 °C and for the silica saturation levels in equilibrium with amorphous silica, with cristobalite, and with quartz.

By comparing the respective stability diagrams in Figures 3-1-15 and 3-1-16, it can be seen that the stability fields for the Yucca Mountain zeolite species are identical to those, which were obtained for geothermal environments. This observation alone is a sufficient basis for the rejection of view that the origin of zeolite phases at the Nevada Test Site was caused by the interaction of tuffs with downward percolating ambient-temperature meteoric waters.

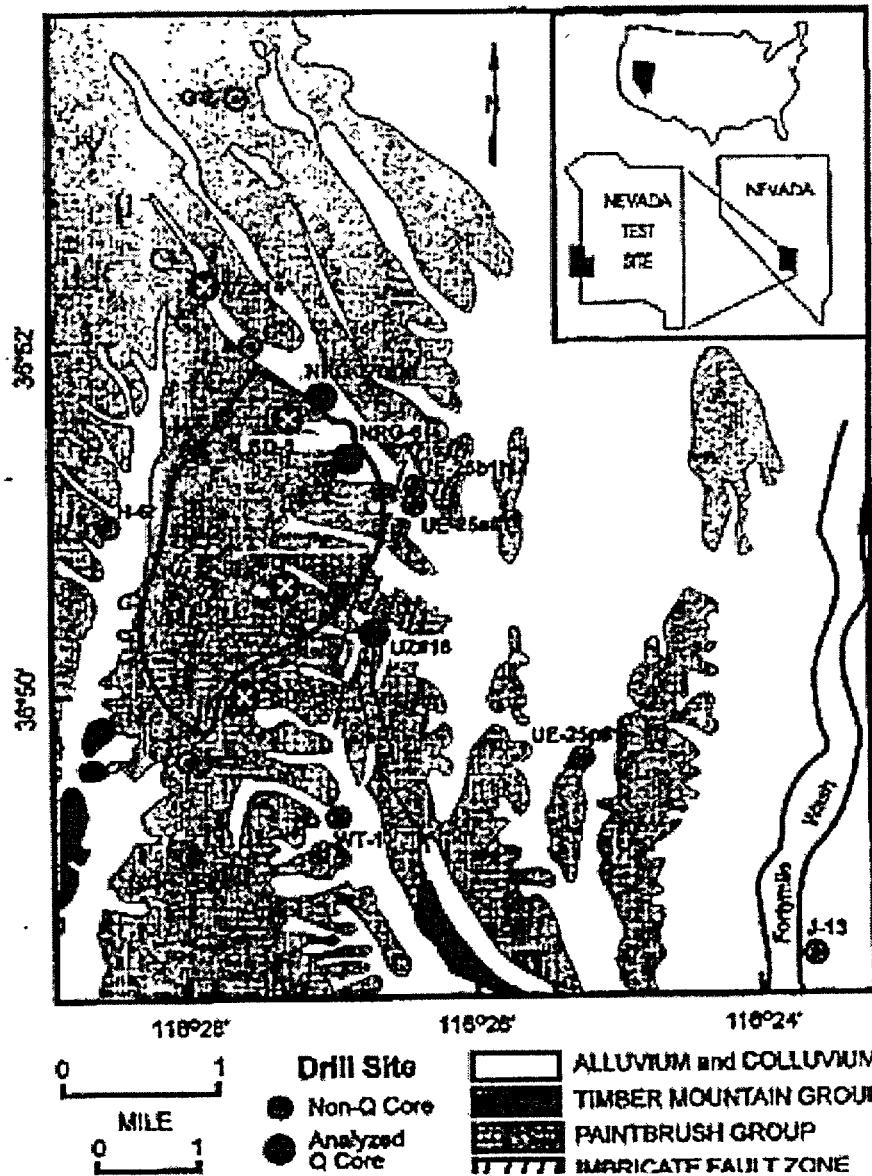


Figure 3-1-17. Map showing location of drill holes from which the inventory of zeolites was derived. Modified from Chipera et al. (1997).

Figure 3-1-16 illustrates two additional points. First, for each of the zeolite species the level of aqueous silica activity exerts a significant influence on the corresponding stability fields. The fields for clinoptilolite and mordenite dominate at the silica activity in equilibrium with amorphous silica, but they are greatly reduced at the quartz saturation levels. The calcic (heulandite and laumontite) and potassic (chabasite and phillipsite) species are stable only at the quartz saturation level.

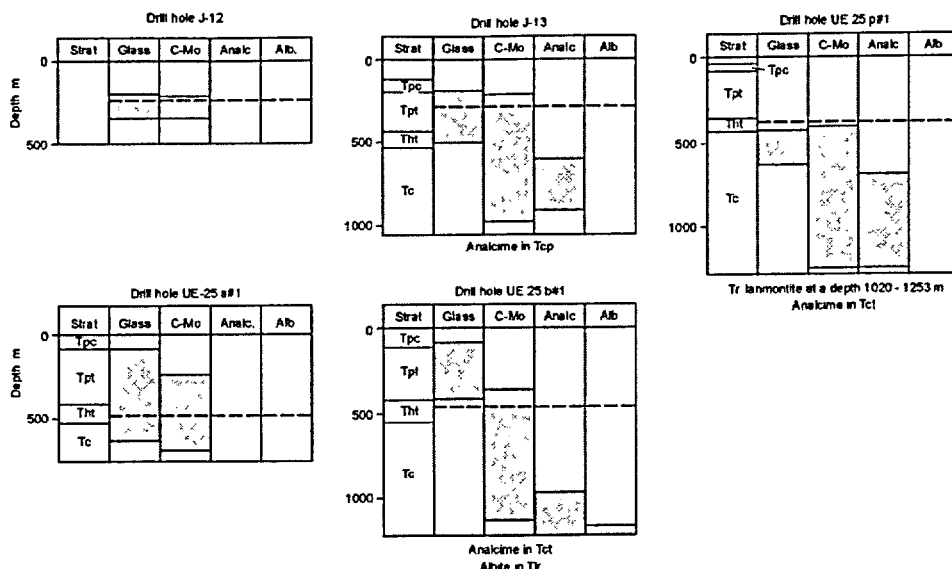


Figure 3-1-18. Mineralogy of zeolite alteration of the bulk tuffs in the eastern Yucca Mountain (including hanging wall and footwall of the Paintbrush fault zone) as a function of depth. Depth intervals in which occasional glass, clinoptilolite and mordenite (C-Mo), analcime (Analc.), and albite (Alb.) were encountered. Dashed line – static water table. Based on data from Bish and Chipera (1989).

Second, temperature seems to be acting in harmony with aqueous silica activity levels. The stability fields for the siliceous species (clinoptilolite and mordenite) are reduced at the elevated temperature, whereas the fields for heulandite and erionite are enhanced. With the aqueous silica activity in equilibrium with quartz, the increasing temperature has the effect of producing the stability fields for laumontite and phillipsite and, at the same time, of enhancing the stability fields for heulandite and erionite.

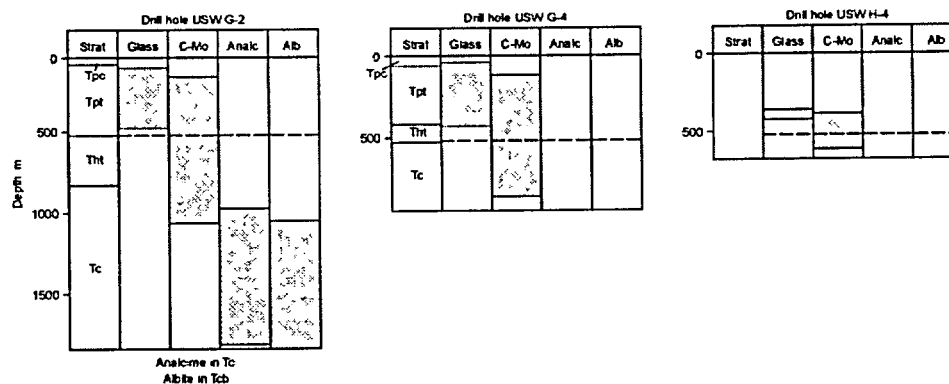


Figure 3-1-19. Mineralogy of zeolite alteration of the bulk tuffs in the central Yucca Mountain as a function of depth. Depth intervals in which occasional glass, clinoptilolite and mordenite (C-Mo), analcime (Analc.), and albite (Alb.) were encountered. Dashed line – static water table. Based on data from Bish and Chipera (1989).

### 3.1.4.2. Database

The inventory of zeolite species hosted by the altered tuffs at Yucca Mountain, is shown on Figures 3-1-18 through 3-1-24. This inventory is in the form of a distribution of the zeolite and glass phases as a function of depth at which they were found in 21 drill holes. Locations of these drill holes are shown in Figure 3-1-17.

The inventory represents a compilation of the XRD results and the SEM and optical identifications, as given in Bish and Vaniman (1985), Carlos et al. (1995-a)., The generalized distributions for glass, for clinoptilolite and mordenite (Zone II, Figure 3-1-13), for analcime (Zone III), and for albite (Zone IV) are shown on Figures 3-1-18 through 3-1-20. The distributions on Figures 3-1-21 and 3-1-22 are a more detailed presentation of the species, which reside in the present-day vadose zone. The generalized and detailed distributions were determined based on the analyses of whole-rock samples of the tuffs. By contrast, the distributions that are shown on Figures 3-1-23 and 3-1-24 pertain to the fracture-based species, which commonly are intergrown or interlayered with major calcite and/or silica polymorphs.

Clinoptilolite and heulandite are isostructural mineral phases and, because of that, they are not readily distinguishable, one from the other. The original investigators made no distinction between the

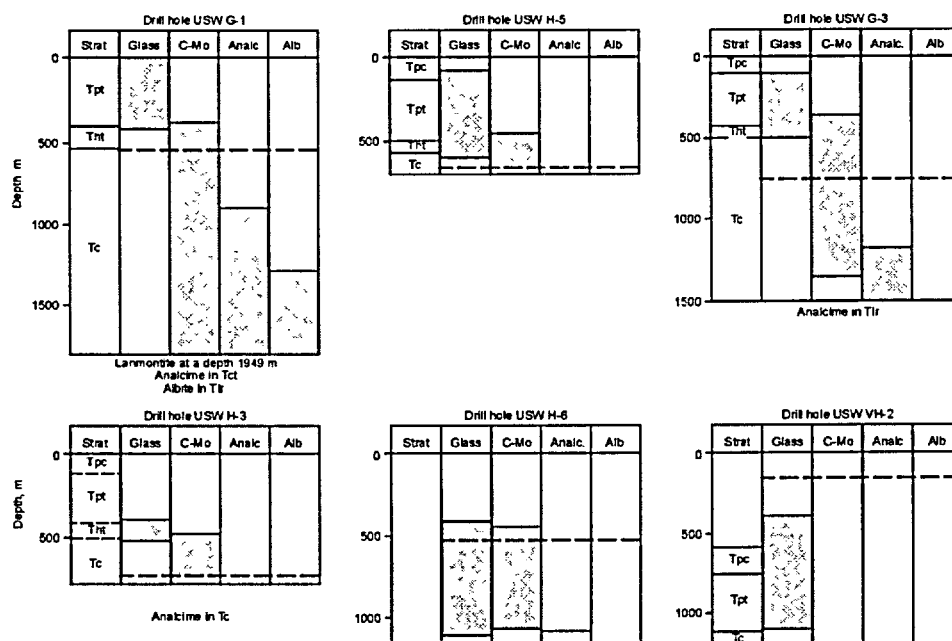


Figure 3-1-20. Mineralogy of zeolite alteration of the bulk tuffs in the western Yucca Mountain as a function of depth. Depth intervals in which occasional glass, clinoptilolite and mordenite (C-Mo), analcime (Analc.), and albite (Alb.) were encountered. Dashed line – static water table. Based on data from Bish and Chipera (1989).

two species. Thus, it is likely that the distributions, which are shown on Figures 3-1-18 through 3-1-24, misrepresent some heulandite as clinoptilolite. Chemical analyses of "clinoptilolite" from the Paintbrush Tuff, for example, show that the dominant cation is Ca and the Si/Al ratio is between 3.4 and 3.8. These characteristics indicate that the "clinoptilolite" is in fact heulandite (Boles, 1972).

In addition, Carlos et al. (1995) reported that the questionable samples from fractures in drill hole USW G-4 were heated to 450 °C, for 15 hours, to determine if their structure would collapse as expected for heulandite. The observed response (partial collapse) confirmed that these fracture coatings were indeed group-II heulandite. This response is similar to that, which was observed for clinoptilolite found above the upper vitrophyre of the Topopah Spring Tuff in a 3 m-thick zeolitized zone in drill hole UE-25 UZ #16. However, chemical analyses of clinoptilolite-group zeolites occurring below the Paintbrush Tuff, in the western Yucca Mountain where the alkaline earth alteration aureole is shallow and thin, indicate that these zeolites are clinoptilolite but not heulandite. The heulandite vs. clinoptilolite distinction is important. This is because the former would be expected to be associated with the overprinting alkaline earth alteration aureole, whereas the latter would tend to be associated with the overprinted alkali metal alteration aureole (see Figure 3-1-15).

The zeolite inventory and the environmental circumstances surrounding the formation of the inventoried zeolite species have far reaching implications for interpreting the zeolite alteration of the tuffs at Yucca Mountain. In the following evaluation we will attempt to answer the question whether the

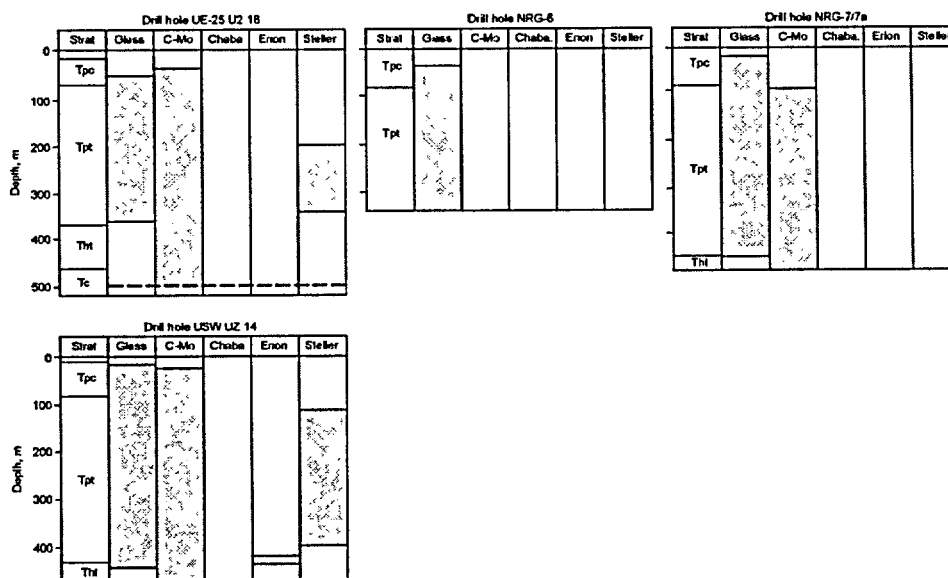


Figure 3-1-21. Mineralogy of zeolite alteration of the bulk tuffs in the vadose zone at Yucca Mountain as a function of depth. Depth intervals in which occasional glass, clinoptilolite and mordenite (C-Mo), chabasite (Chaba.), erionite (Erion.), and stellerite (Steller.) were encountered. Dashed line – static water table. Based on data from Chipera and Bish (1995) and Chipera and Bish (1997).

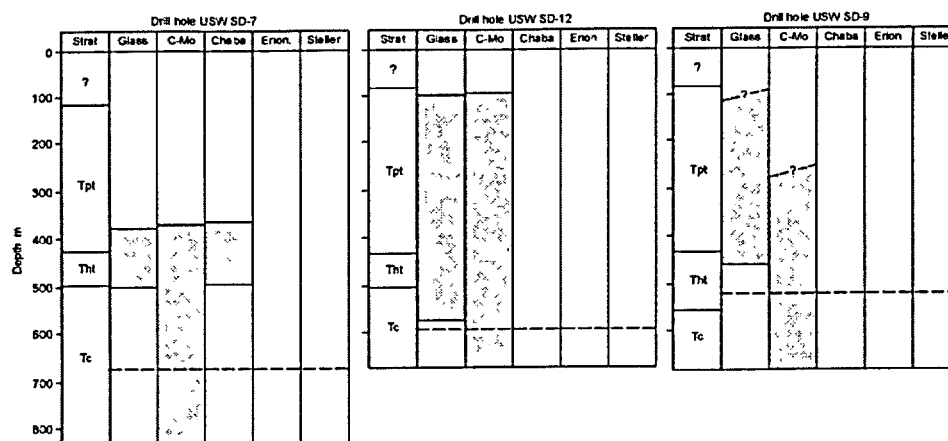


Figure 3-1-22. Mineralogy of zeolite alteration of the bulk tuffs in the vadose zone at Yucca Mountain as a function of depth. Depth intervals in which occasional glass, clinoptilolite and mordenite (C-Mo), chabasite (Chaba.), erionite (Erion.), and stellerite (Steller.) were encountered. Dashed line – static water table. Based on data from Chipera and Bish (1995) and Chipera and Bish (1997).

zeolitic alteration is the result of a long-term evolution of the hydrological system, which included hydrothermal processes supported first by "strong" and then by "weak" heat sources. The spatial distribution of the zeolite species in the interior of Yucca Mountain provides the basis for a number of important inferences, which constitute the grounds upon which the origin of these species can be founded.

### 3.1.4.3. Spatial Distribution of the Glass in Relation to the Present-day Water Table

Figures 3-1-18 through 3-1-24 as a group indicate that the top of the glass-free section lacks a consistent relationship to the present-day water table. These figures show that, throughout most of the horst of Yucca Mountain (see Figure 3-1-17), the glass-bearing tuffs are generally confined to the lower parts of the present-day vadose zone. However, they also show that the situation is quite different in the adjacent tectonic depressions, Jackass Flats to the east and Crater Flat to the west. In western Jackass Flats, the preserved glass has been found deep below the present-day water table, at a depth of about 230 m in drill holes J-12 and J-13, as shown in Figure 3-1-18. In central Crater Flat, the glass has been found in drill hole USW VH-2 at a depth of 920 m below the present-day water table, as shown in Figure 3-1-20.

The preserved glass has also been found in the phreatic zone directly underneath of Yucca Mountain. Such glass occurs at a depth of 213 m in UE-25a#1, at a depth of 275 m in UE-25 p#1, and at a depth of 580 m below the water table in USW H-6, as shown on Figures 3-1-18 and 3-1-20. In some instances (J-12, J-13, and USW VH-2), the preserved glass comprises the dense vitrophyre of the Topopah Spring Member. In the other instances (J-13, UE-25 p#1, UE-25 a#1, and USW H-6), however,

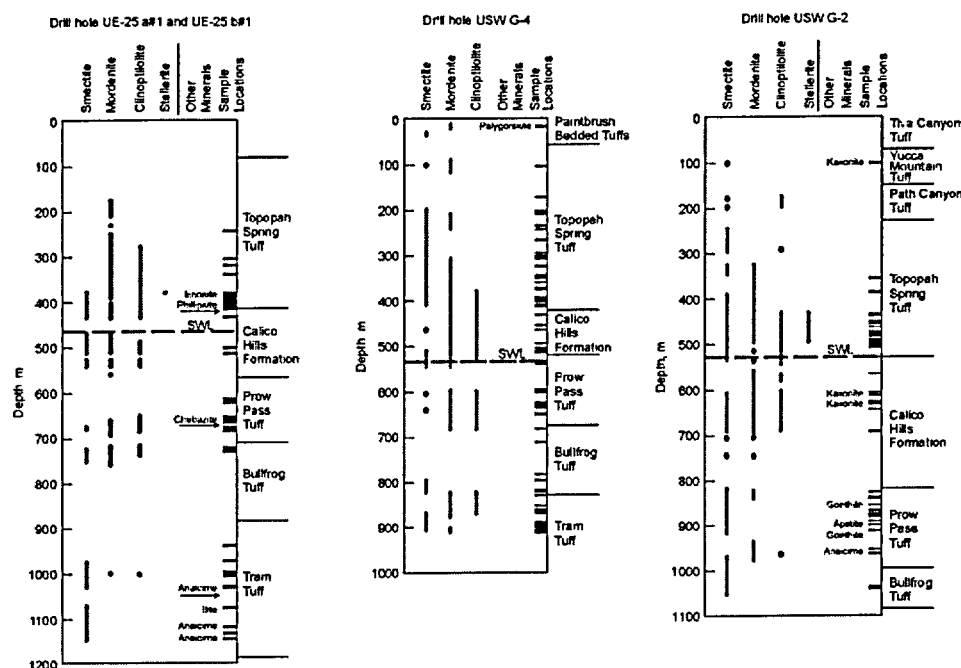


Figure 3-1-23. Mineralogy of fracture-lining zeolites in the altered tuffs in the eastern and central Yucca Mountain as a function of depth. SWL – static water table. Based on data from Carlos et al. (1995-a).

the preserved glass occurs within the non-welded or partially welded Tuff of Calico Hills and the underlying Crater Flat Tuff.

The preservation of some glass deep below the present-day water table is important. This is because it demonstrates that, under the present-day geochemical regime, the conversion of glass into zeolite phases proceeds at exceedingly low rates or not at all. The present-day regime is characterized by low abundance of the dissolved cations (Mg - 2 ppm, Ca - 13 ppm, K - 5 ppm, and Na - 50 ppm; Ogard and Kerrisk, 1984). In addition, this regime is associated with low temperatures (less than 40 °C, Sass et al., 1987) and with a near neutral pH (6.8-9.0, Benson and McKinley, 1987). To speed up the conversion process a more severe geochemical environment seems to be required. An ascent of hot and chemically complex solutions from the deep interior of Yucca Mountain would have the effect of producing such an environment.

#### 3.1.4.4. Vertical Zonation

The degree or grade of zeolite alteration of the tuffs at Yucca Mountain increases with depth in a manner similar to that, which has been observed in a different environment by Sheppard (1971) and Hay (1978). It may be recalled that Iijima made his observations in association with the burial metamorphism of volcanic ash-beds in thick sedimentary sequences. On the other hand Sheppard (1971) and Hay (1978) proposed that similar zonation could be produced by slow percolation of meteoric water through a tuff.

Nonetheless, Gottardi and Galli (1985) stated that the zonation produced by the meteoric water alteration would be virtually indistinguishable from the one produced by burial metamorphism.

The pro-grade alteration is expressed, at Yucca Mountain, by the fact that the top of the albite-bearing tuffs occurs a few hundred meters below the top of the analcime-bearing tuffs, as shown on Figures 3-1-18 through 3-1-20. The figures further show that both of these alteration horizons occur well below the base of the glass-bearing tuffs.

The depthward-increasing grade of the alteration, undoubtedly, expresses the depth-ward increasing temperature at a time when the zeolitization reactions took place. The highest level of albitization occurs at a depth of only 1082 m in drill hole USW G-2, which is much shallower than the depth that is typically

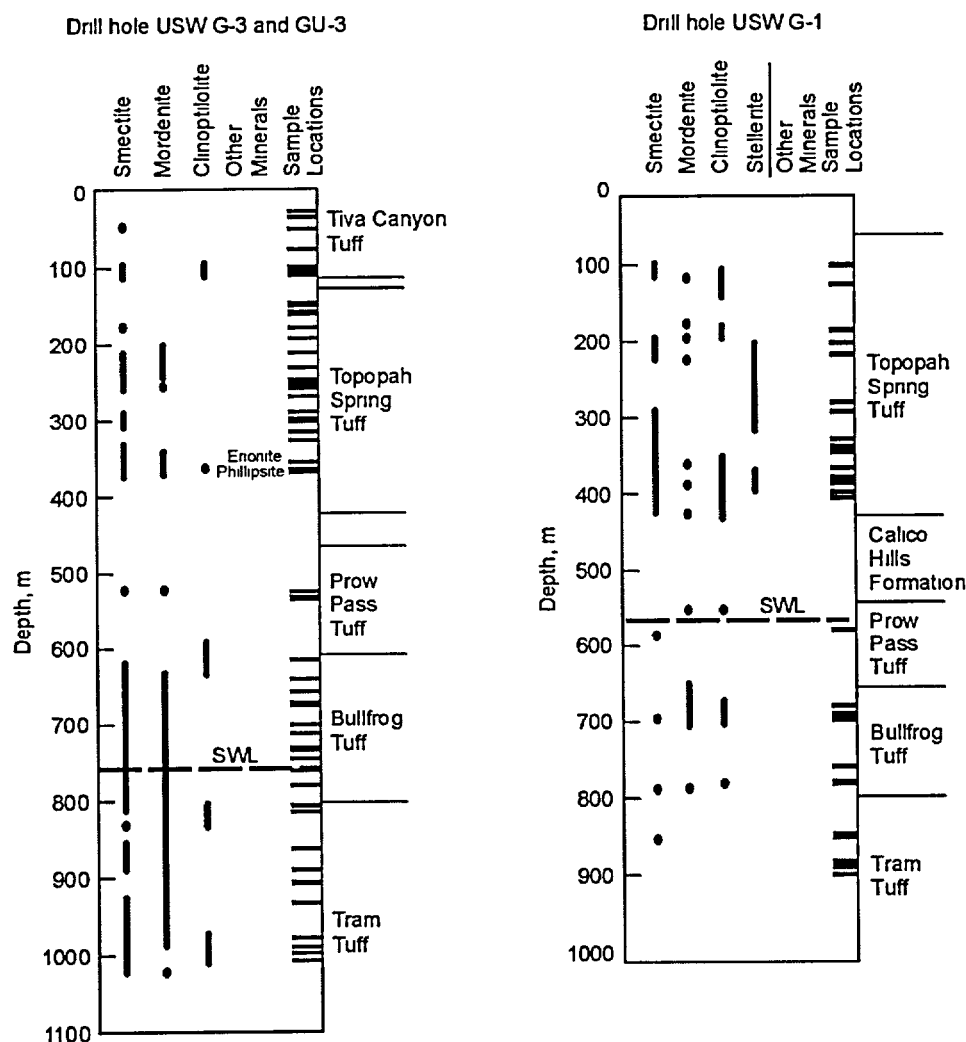


Figure 3-1-24. Mineralogy of fracture-lining zeolites in the altered tuffs in the western Yucca Mountain as a function of depth. SWL – static water table. Based on data from Carlos et al. (1995-a).

observed in association with burial metamorphism. It is regarded as indicating that, in the past, the geothermal gradient was much steeper than the one, which exists now in the interior of Yucca Mountain.

The geothermal gradient, at a time of the zeolite alteration, may be reconstructed based on Figure 3-1-14 and on the assumption that the altering solutions were similar to those that were responsible for the deposition of the ESF calcite. According to Dublyansky et al. (2001), this calcite precipitated from aqueous solutions having salinities between  $10^3$  and  $10^4$  ppm NaCl-equiv. Thus, the alteration temperatures, which are required for the formation of analcime and albite inferred from Figure 3-1-14, must exceed 110 and 175 °C, respectively. These alteration temperatures lead to a conclusion that the geothermal gradient has had a spatially varying value from a minimum of  $78 \text{ }^\circ\text{C}\cdot\text{km}^{-1}$  (USW G-3) to a maximum of  $150 \text{ }^\circ\text{C}\cdot\text{km}^{-1}$  (J-13 and USW G-2).

The average value of the thermal conductivity for the tuffs at Yucca Mountain is given in Sass et al. (1987) as about  $1.73 \text{ W}\cdot\text{m}^{-1}\cdot\text{K}^{-1}$ . Thus, the reconstructed values of the geothermal gradient lead to a conclusion that, at a time when the analcime and albite formed, the heat flow was between 135 and as much as  $260 \text{ mW}\cdot\text{m}^{-2}$  (or 3.2 and 6.1 HFU respectively) These intensities are possible but only in association with the waning stages of cooling and solidification of volcanic rocks or in association with active hydrothermal systems, as Figure 1-20-*b* illustrates. It is clearly erroneous to associate them with a supergene epigenetic alteration environment.

#### **3.1.4.5. Age Relationship between the Zeolite Alteration and the Deuteric Alteration**

In the preceding section, we demonstrated that the isogradal surfaces (i.e. surfaces that separate one alteration grade from the other) of the montmorillonite (alkali) alteration aureole do not correspond to the stratigraphic boundaries. This means that, in different drill holes, the top of a particular alteration zone occurs in different stratigraphic units. The stratigraphy-independent positions of the isogradal surfaces distinguish the epigenetic hydrothermal alteration from the deuteric alteration of the tuffs.

It is important to note that the zeolite isogradal surfaces do not conform to the stratigraphic boundaries of the tuff sequence. As shown on Figures 3-1-18 through 3-1-20, the top of the analcime-bearing zone occurs in drill holes UE 25-p#1, UE 25-a/b#1, and USW G-1 within the Tram Member (Tct) of the Crater Flat Tuff. However, in drill holes J-13, USW G-2, and USW G-3, the equivalent surface occurs within the Prow Pass Member (Tcp), or within the Lithic Ridge Tuff (Tlr). Furthermore, the top of the albite zone occurs in drill holes UE 25-a/b#1 and USW G-1 within the Lithic Ridge Tuff (Tlr). In drill hole USW G-2, however, the equivalent surface is within the Bullfrog Member (Tb).

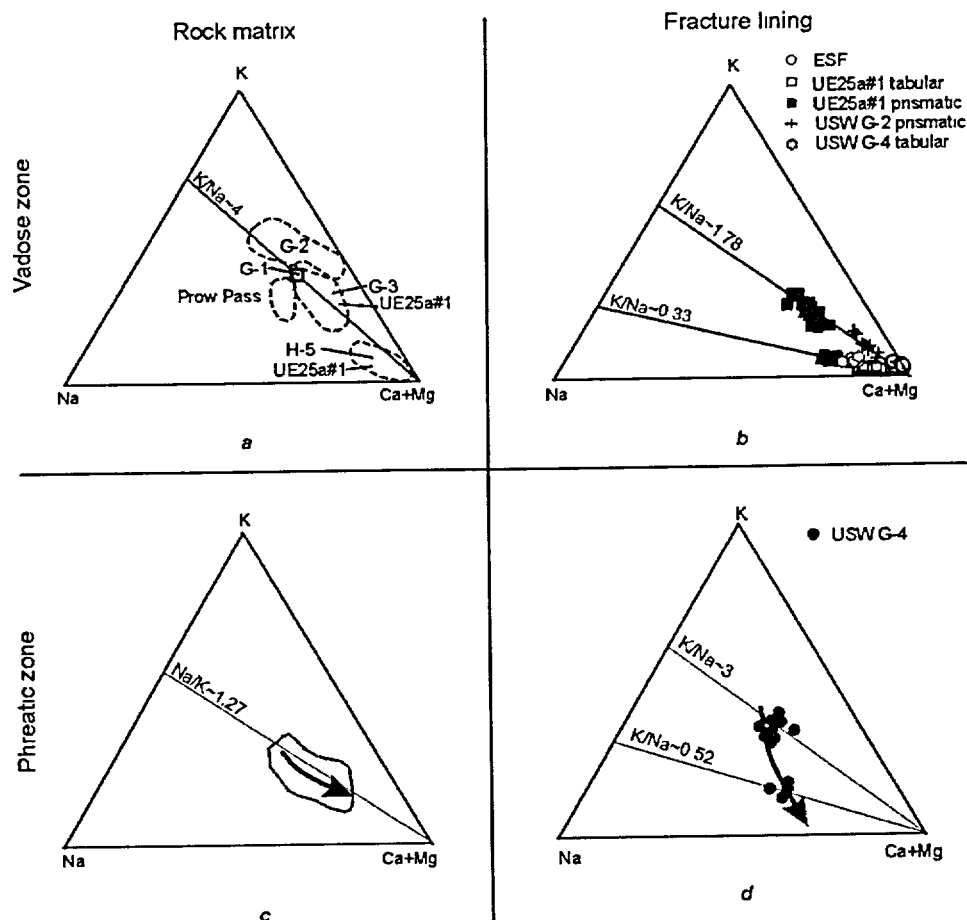


Figure 3-1-25. Chemical compositions of the rock matrix (*a* and *c*) and the fracture lining (*b* and *d*) clinoptilolite/heulandite zeolites from volcanic tuffs of the Yucca Mountain area. *a* and *b* - zeolites from vadose zone; *c* and *d* - zeolites from phreatic zone (drill hole USW G-4). Arrows indicate the direction of chemical change with increasing depth (from ~630 m to ~820 m). Rock-matrix zeolite compositions are shown as areas. Note that fracture-based zeolites show two distinct trends with different K/Na ratios.

Based on data from Carlos (1987), Livingston (1993), Carlos et al. (1995-a), Dublyansky and Reutsky (1995), Smirnov and Dublyansky (2001).

The discordant relationship between the stratigraphic boundaries and the isogradal surfaces indicates that the zeolite alteration is clearly not of a deuteric origin. The evidence unequivocally indicates that this alteration is secondary in the sense that it post-dates the cooling and solidification of the tuffs. Thus, as is the case with the smectite alteration, some of the zeolitic alteration has been produced, at least in part, by epigenetic hydrothermal metamorphism. Does the alteration express only the Timber Mountain metamorphism, or is it polygenetic, which includes the effects of hydrothermal processes supported by "weak" heat sources?

#### 3.1.4.6. Fracture-Based Zeolite Species

The presence of zeolite species at Yucca Mountain is not restricted to the rock matrix. These species also occur in the form of fracture-lining mineral phases (Carlos et al., 1995-a). The whole-rock zeolite alteration is restricted mainly to those units, which are composed of ash-fall and non-welded tuffs, and occur between the ash-flow units with densely welded and devitrified interiors. After emplacement, these tuffs remained vitric and in that state were highly susceptible to alteration because of the instability of the glass in the presence of corrosive groundwater.

By contrast, the fracture-lining zeolites occur indiscriminately throughout the stratigraphic section, including the devitrified interiors of the ash-flow tuffs, as shown on Figures 3-1-23 and 3-1-24. These figures show that the mineralogy of the fracture-lining zeolites is similar to the mineralogy of zeolites from the rock matrix, which includes clinoptilolite/heulandite, mordenite, stellerite, chabazite, erionite, phillipsite, and analcime. Figure 3-1-25 compares the major cation chemistry of the rock-matrix and the fracture-lining clinoptilolite/heulandite zeolites from a similar depth.

The fracture-lining clinoptilolites/heulandites in both the vadose (Figure 3-1-25-b) and phreatic (Figure 3-1-25-d) zones split into two trends dominated by either sodium or potassium. The separation of zeolites from altered tuffs is less apparent. Rock matrix clinoptilolites/heulandites produce a potassium-enriched compositional trend (Figure 3-1-25-a and -c). Even though the chemistry of the fracture-lining zeolites from the vadose zone is fairly similar to the chemistry of the rock-matrix zeolites from the same depth, the fracture zeolites show characteristically higher contents of sodium and alkali earth elements.

The chemistry of zeolites collected from the ESF is particularly noteworthy. The ESF heulandites reside in fractures that intersect the least zeolitized rocks. There is no data available on the chemistry of zeolites in this particular depth range; a comparison with the rock-matrix zeolites from the closest depths demonstrates that the ESF zeolites are maximally enriched in alkali earth elements and depleted in alkalis. This chemistry is similar to that of the latest tabular heulandites from the USW G-4 and UE25a#1 located in the vicinity of the ESF.

Zeolites from fractures in the phreatic zone are similar in their chemistry to the respective rock matrix zeolites (see Figure 3-1-25-c and -d). They exhibit higher contents of alkalis compared to their vadose zone counterparts.

The observations presented above allow us to draw the following conclusions.

The similarity of the chemical compositions of fracture- and rock-matrix zeolites suggests that the chemistry of the fracture zeolites is, at least partially, controlled by the chemistry of the bedrock tuffs.

The existence of the two trends of fracture-zeolite compositions indicates different compositions of fluids during different stages of zeolite deposition (this is consistent with early conclusions by Carlos et al. 1995-a). The chemistry change within each trend involved an increase in the contents of alkali earth elements from early to late mineral forming stages while maintaining the same alkali element ratios (see Figure 3-1-25).

The variable compositions of the rock matrix zeolites reflect, most probably, a variable chemistry of the fluids that circulated through the tuffs. Variations in the chemistry of clinoptilolites might be caused either by ionic exchange of the earlier formed zeolites with the late fluids, or by the deposition of late generations of alkali earth zeolite species.

The occurrence of zeolites with different chemistries at similar depths suggests that the chemical compositions of the fluids were not controlled by the length of the infiltration path, as would be expected for zeolites of the supergene origin. The results of the thermodynamic modeling (see Figures 3-1-15 and 3-1-16, as well as Chapter 3-2) make a strong case for the deposition of fracture heulandites at shallow depths caused by the intrusion of heated fluids enriched in alkali earth elements into the rocks in the vadose zone well after the major episode of zeolitization of the Yucca Mountain tuffs.

The presence of fracture-lining zeolite species is important. This is because their presence indicates that their formation involved a process, which included, first, the dissolution of the glass and second, their precipitation from ionic solutions. Some of the rock matrix species could have been formed directly from the glass, through the hydration of it, rather than by the precipitation from ionic solutions. Such, however, cannot possibly be the case for the fracture lining zeolite species.

For precipitation of the fracture lining zeolites, the ionic solutions must have been carrying all of the zeolite-forming cations, including aluminum, which is practically insoluble in low temperature (25-35 °C) solutions with pH between 4.5 and 10, as given in Wedehpohl (1971). Thus, the presence of fracture-lining zeolite species indicates that they have been precipitated from solutions with elevated temperatures and ionic strengths, which is consistent with an epigenetic hydrothermal origin.

#### **3.1.4.7. Multiple Episodes of the Zeolite Alteration and Mineralization**

Both the fracture-lining species and the rock matrix species appear to be the result of multiple and discrete episodes of zeolite alteration and mineralization. Two lines of evidence are important in this regard. First, the altered tuffs, as a whole, host two chemically distinct zeolite facies. One of them includes the calcic zeolite species (stellerite, heulandite, and laumontite), which must have been formed by ionic exchange reactions between the alkali glass, and solutions having a very small abundance of K, as Figures 3-1-15 and 3-1-16 imply. By contrast, the other zeolite facies is composed of alkali zeolites

with clinoptilolite dominating. The alkali facies is split into two series: the sodic series ( $K/Na \sim 0.3$ ) and the potassic series ( $K/Na \sim 1.7 - 4.0$ ). Apparently, mordentite from the fracture-lining also belongs to the sodic series. The formation of potassic zeolites is, most likely, related to the chemistry of the fracture-hosting tuffs, with which the mineral forming solutions interacted.

Second, in two drill holes, laumontite has been found in the form of a mineral phase, which spatially co-exists with the orderly-interstratified clays, allevardite in UE-25 p#1 and kalkberg in USW G-1. Laumontite requires the presence of abundant calcium concurrently with a negligible abundance of potassium (Figures 3-1-15 and 3-1-16), whereas the orderly-interstratified clays require a K-rich but Ca-poor environment. It is thus clear that these chemically incompatible species could not have been formed at the same time and under the same chemical regime. In addition, Carlos et al. (1995-a) have presented evidence to the effect that some of the calcic species, heulandite in particular, are products of at least two temporally discrete mineralization episodes. In this regard, the investigators have established that the fracture-lining heulandite is developed in the form of two morphologically distinct habits, an earlier tabular heulandite and a later prismatic heulandite. As shown in Figure 3-1-26, the younger prismatic heulandite is enriched in Mg but depleted in Sr, as compared to the older tabular heulandites. This chemical bi-modality documents two separate episodes of the heulandite deposition from chemically different solutions, which have bathed the older crystals in Mg-enriched and Sr-depleted solutions.

#### 3.1.4.8. Geologic Ages of the Potassic and Calcic Zeolite Species

The combined database pertinent to the alteration and mineralization of the tuffs allows for inferences to be drawn in regard to the probable absolute age of the alkali zeolite species and to the relative age of the calcic species. To this end, it is helpful to consider first the geothermal implications of the zonation, then the affinity between the zeolite and montmorillonite alterations, and finally, the crosscutting relationship between the calcic species and other fracture-lining minerals.

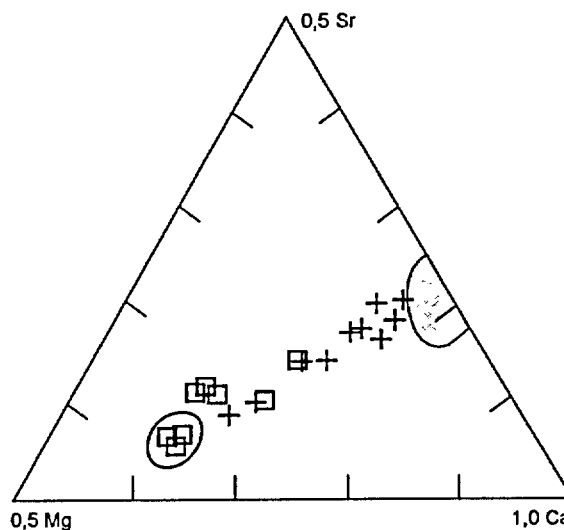


Figure 3-1-26. Ternary diagram showing compositions for fracture-lining heulandite crystals. *Shaded area* - cores of earlier tabular crystals; *crosses* - intermediate zones of tabular crystals; *open boxes* - rims of tabular crystals; and *unfilled area* - later prismatic crystals, which overgrew tabular ones. Based on Carlos et al., (1995-a).

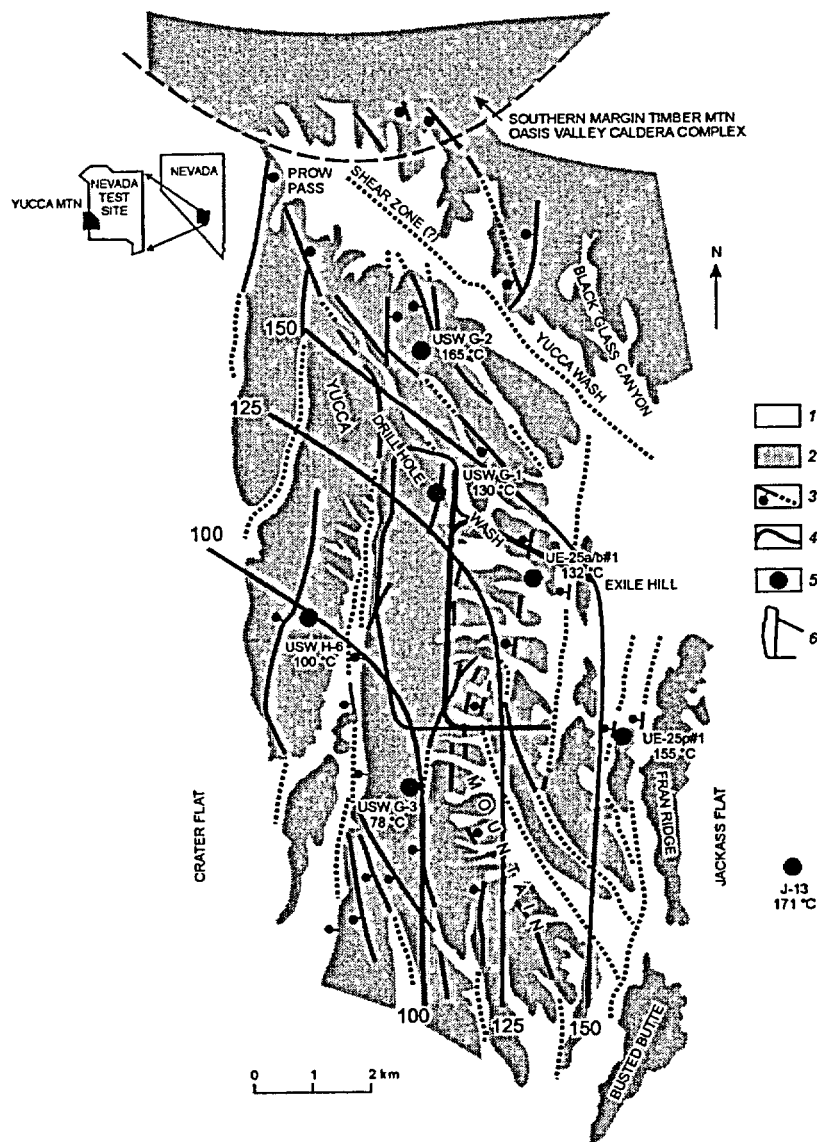


Figure 3-1-27. Alteration temperature at a depth (present-day) of 1 km at a time of zeolitic alteration of the tuffs at Yucca Mountain. 1 - Quaternary alluvium and colluvium; 2 - Miocene-Pliocene tuffs; 3 - normal faults, bar and ball on the downthrown side, dotted line shows concealed part; 4 - isotherm, °C; 5 - boreholes; and 6 - Exploratory Studies Facility with proposed repository outline.

The age of the formation of analcime and albite is implied in Figure 3-1-27. This figure shows the reconstructed alteration temperature at a depth of 1 km at a time when alteration Zone III (analcime) and Zone IV (albite) were formed.

Figure 3-1-27 is directly comparable to Figure 3-1-12. Both of them show that the temperature distribution, which has been reconstructed based on the zeolite zoning, is similar to a reconstruction based

on the distribution of the orderly-interstratified clays. Thus, the similarity of the respective thermal regimes suggests that these alterations are contemporaneous products of the Timber Mountain hydrothermal metamorphism, which took place some 10-11 Ma ago.

Both the illitization reactions and the formation of the potassium-enriched zeolite species (e.g. clinoptilolite) require an abundant supply of K, concurrently with a restricted supply of calcium. Thus, the whole-rock K-alteration at Prow Pass, the orderly-interstratified clays, and the zeolite species, which belong to the potassic species, are probably contemporaneous and, most likely all of them are products of the Timber Mountain hydrothermal metamorphism. This conclusion is in agreement with the timing of the K-metasomatism of the Calico Hills Tuff (T<sub>ac</sub>). The author drew these inferences based on the elemental enrichment and depletion patterns, which he observed in an area to the south of the Timber Mountain-Oasis Valley Caldera complex.

Mineralogical studies of the fracture-lining mineral coatings by Carlos et al. (1995-a) are particularly useful for inferring the relative age of the calcic zeolite species, stellerite and heulandite in particular. These studies revealed that these calcic zeolite species are common accessory minerals in those fracture-based mineral coatings, which occur in the present-day vadose zone at Yucca Mountain, see Figures 3-1-23 and 3-1-24.

Importantly, Carlos et al. (1995-a) observed crystalline calcite overlying the older tabular heulandite crystals in some coatings, and this calcite was observed to be overgrown by small prismatic heulandite crystals. Stellerite was noted in some of the coatings to occur over tridymite or directly on the rock surface, which suggests that this species began forming in the early stages of the calcic zeolitization. However, stellerite was also observed to occur in the form of single crystals or sprays of crystals sometimes in association with both prismatic and tabular (older) heulandite crystals. Furthermore, stellerite crystals in association with prismatic heulandite crystals were also observed to overlie calcite, which implies that these calcic species were deposited after the calcite and after the tabular heulandite. In some other coatings, additional late calcite was noted to occur over both stellerite and heulandite.

Studies of the fracture- and lithophysal cavity-lining minerals from the Exploratory Studies Facility by Smirnov and Dublyansky (2000 and 2001) are also noteworthy in the context of interpreting the relative age of the calcic zeolite species. These studies demonstrated that the ESF coatings contain silica polymorphs, uraniferous opal and chalcedony, in addition to containing abundant calcite and accessory minerals, including the calcic zeolite species, heulandite in particular. These studies are consistent with the earlier observations by Carlos et al. (1995-a) that the calcic zeolite species are broadly contemporaneous with the fracture-lining calcite.

Recently, Wilson and Cline (2001) and Neymark et al. (2000, 2002) have shown that the ESF uraniferous chalcedony and opal, at various depths, from within the coatings carry apparent  $^{207}\text{Pb}/\text{U}$  ages, which are no greater than about 10 Ma. Smirnov and Dublyansky (2001) showed that prismatic heulandite overgrows bladed calcite, which was dated between 6 and 2 Ma ago (Wilson and Cline, 2000; Neymark et al., 2000; Whelan et al., 2001). Our analysis, however, shows (see Chapter 3-7) that these ages are most likely erroneous and do not reflect the true age of deposition for the ESF fracture- and lithophysal cavity-lining coatings. The actual ages might be much younger. This conclusion is supported by the fact that Paces et al. (1996) have shown that the uraniferous chalcedony and opal from the bottom and interior of the coatings carry  $^{230}\text{Th}/\text{U}$  ages of about 250-330 Ka, as shown on Figure 2-35. Although these ages are also doubtful, we may be certain that the dated silica polymorphs are very young indeed, because the  $^{234}\text{U}/^{238}\text{U}$  and  $^{230}\text{Th}/^{234}\text{U}$  ratios significantly deviate from the secular equilibrium values.

The  $^{207}\text{Pb}/\text{U}$  ages may therefore be taken to indicate that the precipitation of the calcite-bearing coatings, and the precipitation of stellerite and heulandite, contained therein, post-dates the Timber Mountain hydrothermal metamorphism. Thus, it is possible that the calcite-, heulandite-, and stellerite-bearing mineral coatings do express late hydrothermal processes, which would have been fueled by "weak" heat sources. This possibility is in harmony with the earlier drawn inferences concerning the crosscutting relationship between the alkali metal and alkaline earths alteration aureoles. What remains to be done, to complete the validation of the proposed conceptual model, is to demonstrate the hydrothermal origin for the calcic zeolite species, on one hand, and for the associated calcite, on the other.

#### 3.1.4.9. Origin of the Calcic Zeolite Species

The geologic ages for the calcic zeolite species have been inferred. It is appropriate now to address circumstances, which have led to their formation. In this regard, the spatial variability of the chemical compositions of clinoptilolite (some of it may actually be heulandite) is particularly revealing. This variability has been documented by Broxton et al. (1986) based on microprobe analyses of mono-mineral specimens, which were separated from whole-rock samples of the various tuffs. The results of these analyses are summarized in Figures 3-1-28 through 3-1-35. The variability in the upper tuffs, specifically in the Paintbrush Tuff (Tp) and in the Tuff of Calico Hills (outcrops at Prow Pass), is shown on Figure 3-1-28.

Figure 3-1-28 shows that the major cation composition changes from K-rich, at Prow Pass, to Ca+Mg-rich to the south in the proposed repository area. Concurrently, the abundance of calcium increases up the stratigraphic section, with most of the K-enriched clinoptilolite occurring at the base of the Tuff of Calico Hills (Tac).

The two-fold K-enrichment pattern, which Figure 3-1-28 implies, expresses an overprinting of the two chemically distinct alteration facies. The chemical variability of clinoptilolite, therefore, expresses, in part, an alteration of the glass by Ca+Mg solutions, but also, in part, expresses cation exchanges between the K-rich zeolites and the late Ca+Mg solutions.

Clinoptilolite, which occurs to the south of Prow Pass, is enriched in Ca, as shown on Figure 3-1-28. According to Broxton et al. (1986), this species is associated with Si/Al ratios between 4.0 and 5.0 and with an elevated abundance of magnesium, between 0.6 and 1.5 wt.% MgO. Thus, the Mg enrichment of zeolites may reveal a genetic link between zeolites and the calcite mineralization in the vadose zone.

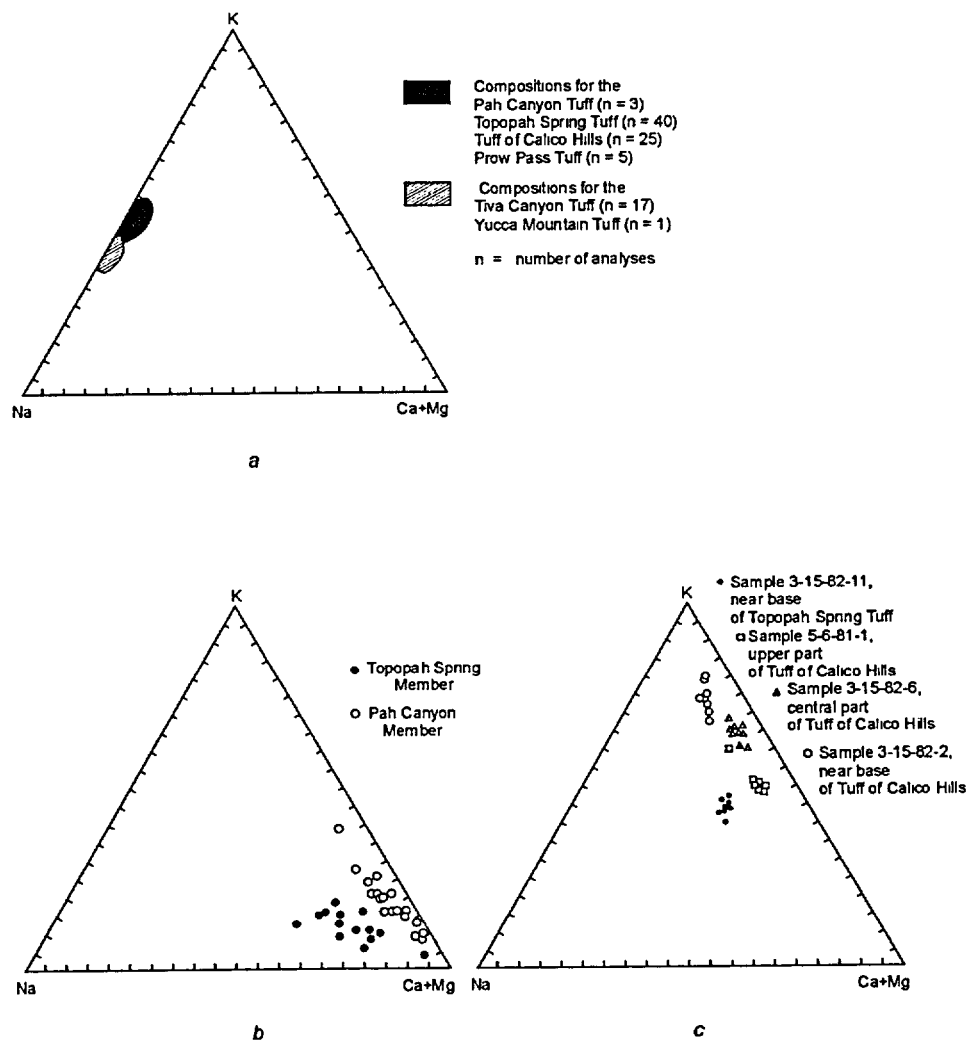


Figure 3-1-28. Relative concentrations of alkali and alkali-earth elements for glass and clinoptilolite from vadose zone in the repository block and at Prow Pass. *a* - glass; *b* - clinoptilolite from the vadose zone in the repository block; and *c* - clinoptilolite from surface exposure of the Tuff of Calico Hills at Prow Pass. From Broxton et al. (1986).

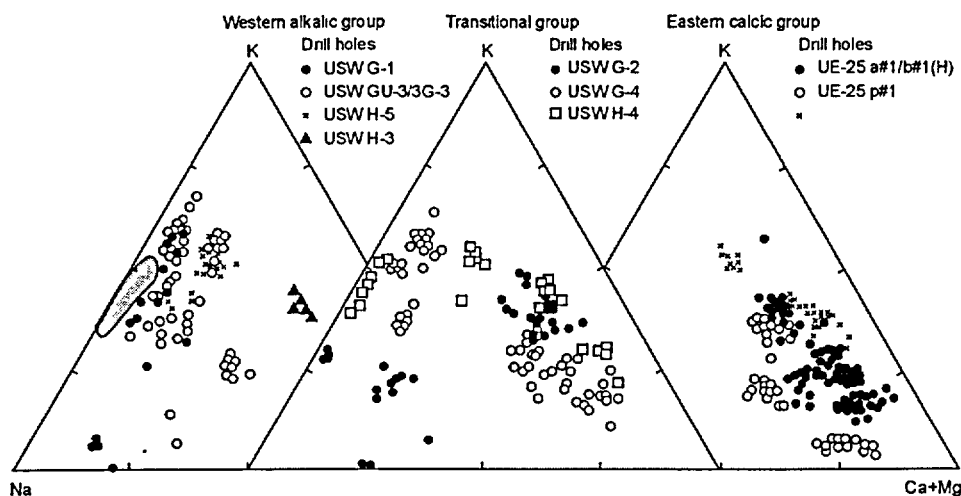


Figure 3-1-29. Relative concentrations of alkali and alkaline-earth elements in clinoptilolites from the tuff underlying Paintbrush Tuff formation. Shaded area represents field of compositions for rhyolitic glasses of Yucca Mountain. From Broxton et al. (1986).

Calcite from the ESF was found to show complex patterns of Mg enrichment at early, intermediate and late stages of growth (Smirnov and Dublyansky, 2001; Wilson and Cline, 2001). Heulandites associated with the secondary open-space minerals in the ESF show a wide range of Mg contents from 0.21 to 1.07 formulae units (Smirnov and Dublyansky, 2001).

Levy (1984) has shown that some specimens of the southern "clinoptilolite" are associated with thermal stability, which is typical for heulandite. However, the remaining "clinoptilolite" specimens displayed a thermal stability intermediate between that of heulandite and that of clinoptilolite, which leads to the conclusion that these specimens belong, in fact, to group 2 of Boles (1972). Gottardi and Galli (1985) showed a relationship between the thermal stability of minerals of the heulandite-clinoptilolite series and their compositions. On the basis of their data, zeolites of group 2 typically have  $Si/Al \geq 4$  and  $Ca+Mg > Na+K$ . Thus, these "clinoptilolite" specimens represent the calcic alteration series, and are believed to be a heulandite. In common with the Mg-enriched calcite of Wilson and Cline (2001) and the Mg-enriched prismatic heulandite of Carlos et al. (1995-a) they post-date the Timber Mountain hydrothermal metamorphism.

We now examine the lateral variability of the major cation composition of those "clinoptilolite" species, which occur below the Paintbrush Tuff, in the remaining units (Tac through Tlr) of the stratigraphic section. These units comprise the lower parts of the vadose zone and upper parts of the phreatic zone. The lateral variability, from east to west across Yucca Mountain, is shown on Figure 3-1-29.

Figure 3-1-29 shows that, as lateral distance increases to the west away from the Paintbrush fault, the cation compositions vary systematically. This important trend is identical to the one, which is shown on Figure 3-1-6 for the major cation composition of whole-rock samples of the altered tuffs. For both of these phases, Ca+Mg compositions dominate in the eastern Yucca Mountain near the trace of the Paintbrush fault zone, whereas the western part is characterized by the presence of Na+K compositions. The area encompassing drill hole sites USW G-2, G-4, and H-4 is a transition zone containing "clinoptilolite" species having intermediate compositions.

Like Broxton et al. (1986), we attributed the changing composition, which is shown in Figures 3-1-6 and Figure 3-1-29, to the diffusion of Ca+Mg-enriched aquifer fluids from the Paintbrush fault zone into the wallrock. However, in contrast to Broxton et al. (1986) who concluded that the changing composition applied only to the tuffs in the phreatic zone, we have concluded that the fluid diffusion is expressed high in the vadose zone, as Figure 3-1-28 implies. The presence of the calcic species both above and below the present-day water table has led us to the conclusion that the overprinting alteration aureole is thin and shallow to the west, but thick and deep in the eastern sector. The shape of this alkaline earth aureole is exactly what the proposed conceptual model implies (see Figure 2-1).

We now examine the shape of the alkaline earth alteration aureole more closely, in particular as this shape relates to the Paintbrush fault zone and to the NW-SE trending shear zone from the Walker Lane wrench system. Figures 3-1-30 through 3-1-35 have been constructed with this specific purpose in mind.

Figures 3-1-30 and 3-1-35 depict a variability of the major element chemistry of the "clinoptilolite" species as a function of stratigraphic depth across Yucca Mountain. The data depicted are based on official DOE literature. These figures are in the form of ternary diagrams, and show that the Ca+Mg-rich "clinoptilolite" species are distributed throughout the interior of Yucca Mountain in a strongly asymmetrical manner.

The overall pattern is one where the relative abundance of Ca+Mg and the depth extent of the Ca+Mg-rich "clinoptilolite" species both diminish to the south and to the west, away from a high along the subject fault zones. The Ca+Mg-rich species are much more abundant throughout this high. Furthermore, they are the dominant zeolite species down to a depth, which ranges from 820 m (drill hole USW G-2) to at least 1200 m (drill holes UE-25 a/b#1 and UE-25 p#1), as shown on Figures 3-1-30 through 3-1-32. Thus, it is evident that these calcic zeolite species occur both above and below the present-day water table.

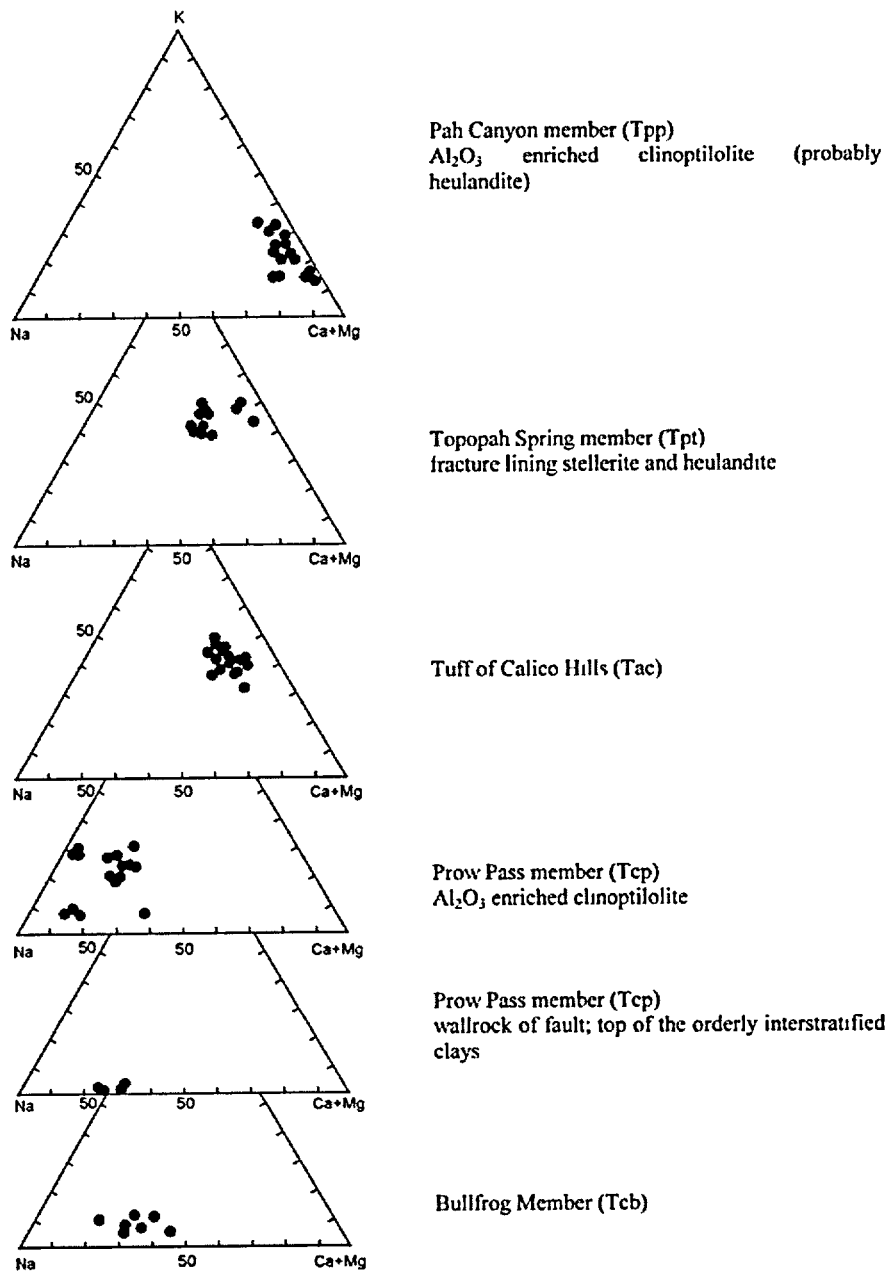
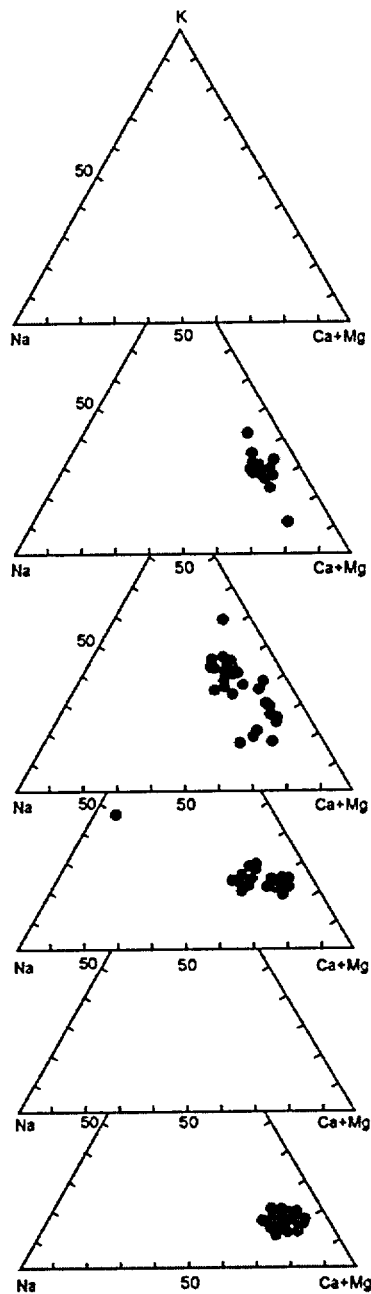


Figure 3-1-30. Diagram of exchangeable cation compositions for clinoptilolites in drill hole USW G-2 as a function of stratigraphic depth. Modified from Caporuscio et al. (1982), Bish and Chipera (1989), and Carlos et al. (1995).



Pah Canyon Member (Tpp)

Topopah Spring Member (Tpp);  
fracture-lining stellerite and  
 $Al_2O_3$ -enriched clinoptilolite  
(most probably heulandite),  
erionite and phillipsite (fracture  
lining).

Tuff of Calico Hills (Tac)

Prow Pass Member (Tcp);  
fracture-lining chabasite

Prow Pass Member (Tcp)

Bullfrog Hills Member (Tcb);  
analcime and illite in the  
underlying Tram Member,  $Al_2O_3$ -  
enriched clinoptilolite

Figure 3-1-31. Diagram of exchangeable cation compositions for clinoptilolites in drill hole UE-25 a/b#1 as a function of stratigraphic depth. Based on data from Broxton et al. (1986), Bish and Chipera (1989), and Carlos et al. (1995).

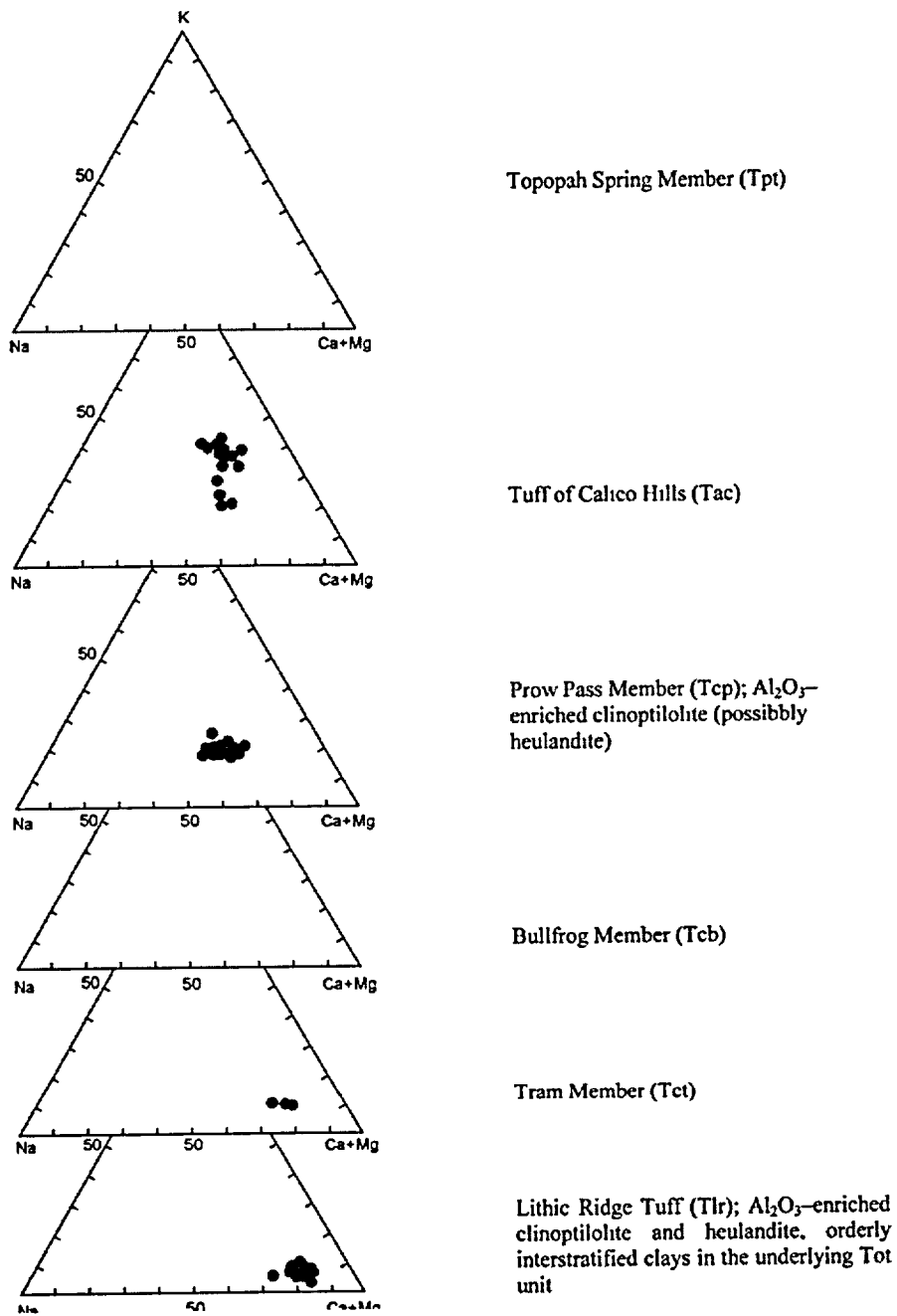


Figure 3-1-32. Diagram of exchangeable cation compositions for clinoptilolites in drill hole UE-25 p#1 as a function of stratigraphic depth. Based on data from Broxton et al. (1986), Bish and Chipera (1989), and Carlos et al. (1995).

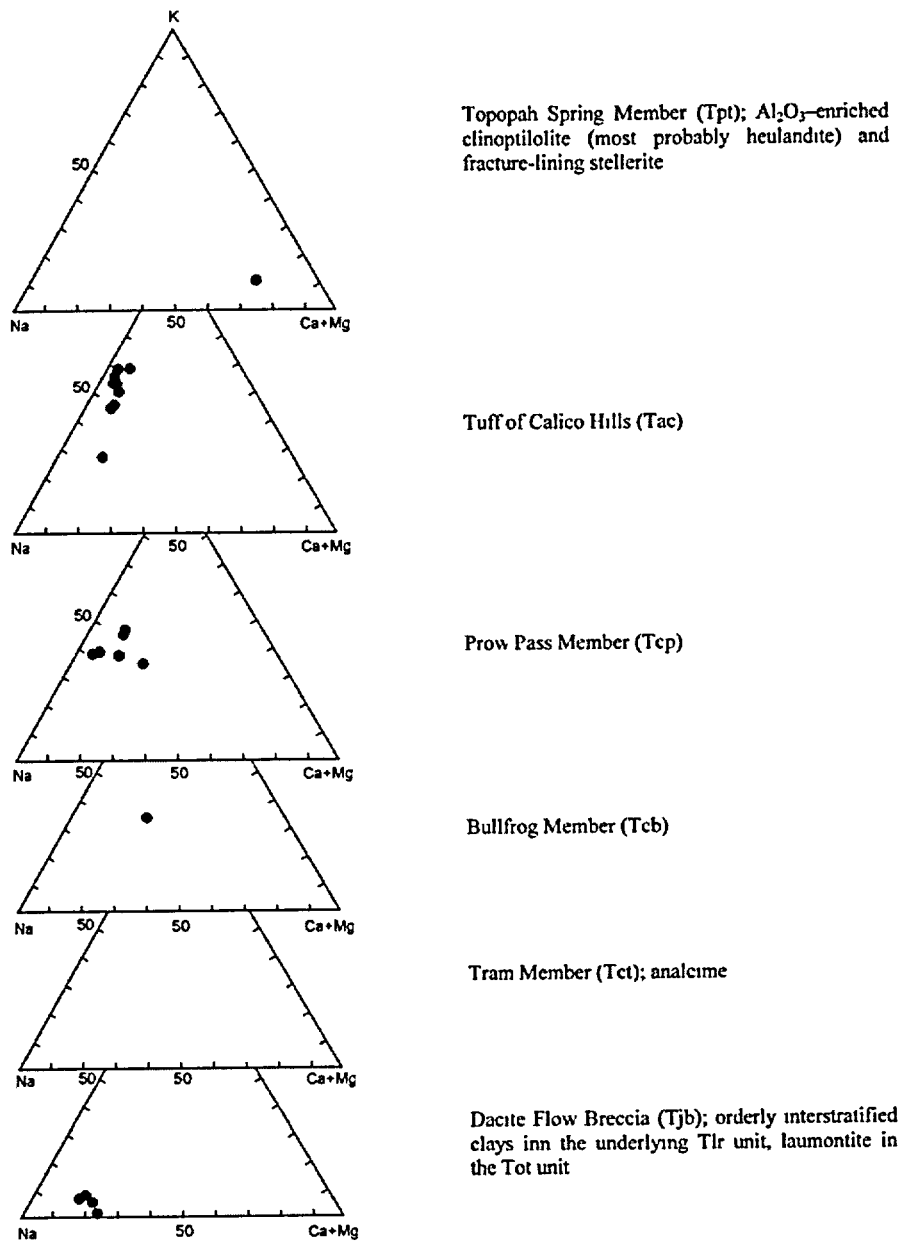


Figure 3-1-33. Diagram of exchangeable cation compositions for clinoptilolites in drill hole USW G-1 as a function of stratigraphic depth. Based on data from Broxton et al. (1986), Bish and Chipera (1989), and Carlos et al. (1995).

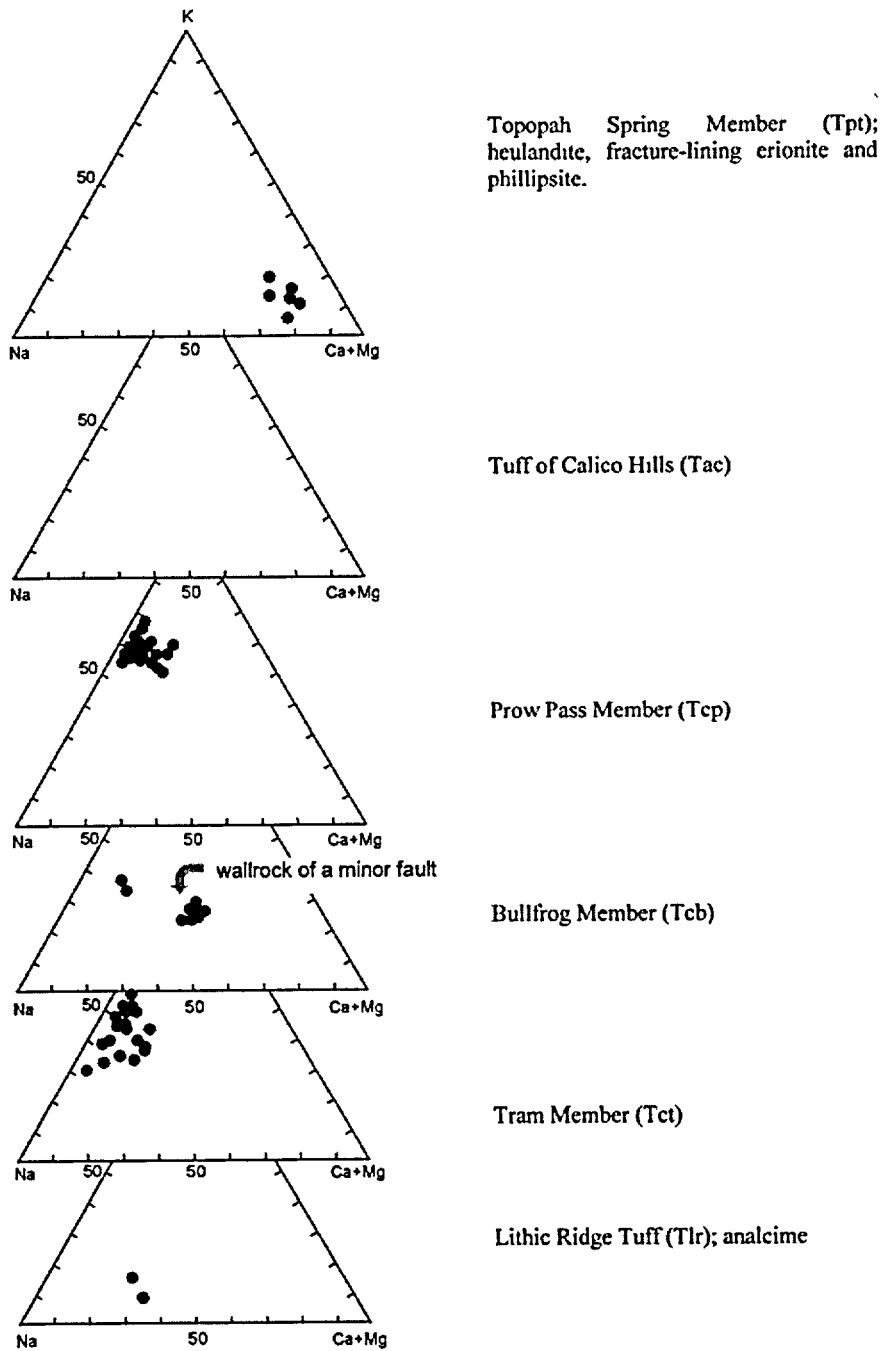


Figure 3-1-34. Diagram of exchangeable cation compositions for clinoptilolites in drill hole USW G-3 as a function of stratigraphic depth. Based on data from Broxton et al. (1986), Bish and Chipera (1989), and Carlos et al. (1995).

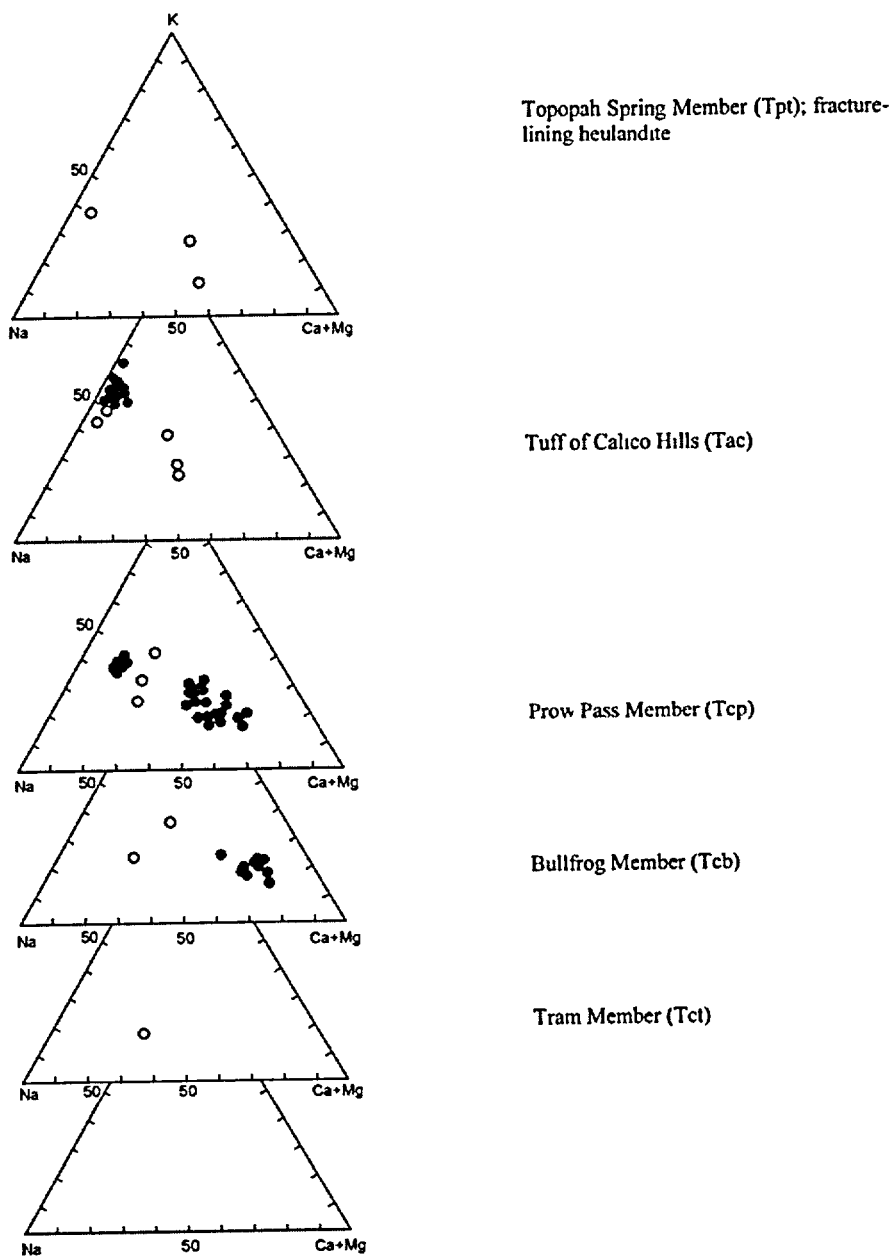


Figure 3-1-35. Diagram of exchangeable cation compositions for clinoptilolites and the whole rock in drill hole USW G-4 as a function of stratigraphic depth. *Filled symbols* - clinoptilolite; *open symbols* - whole-rock sample. Based on data from Broxton et al. (1986) and Carlos et al. (1995-a).

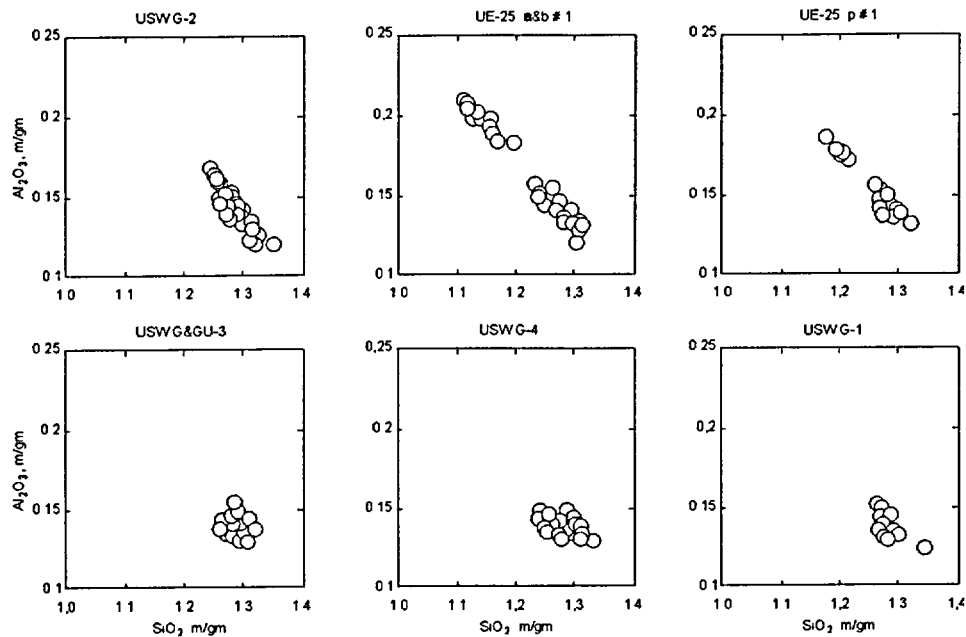


Figure 3-1-36. Silica and  $\text{Al}_2\text{O}_3$  contents of clinoptilolites from six drill holes at Yucca Mountain normalized to total abundance of  $\text{SiO}_2$ ,  $\text{Al}_2\text{O}_3$ ,  $\text{CaO}$ ,  $\text{MgO}$ ,  $\text{K}_2\text{O}$ , and  $\text{Na}_2\text{O}$ . Note bi-modal clinoptilolite compositions from drill-holes located at the northeast and eastern part of Yucca Mountain (upper row) and unimodal compositions of clinoptilolites from the rest of the drill holes (lower row). From Livingston and Szymanski (1996). Based on chemical data from Broxton et al. (1986).

To the south and to the west, however, the abundance of Ca+Mg-rich "clinoptilolite" species diminishes, and the presence of them is restricted to the Paintbrush Tuff above a depth of about 400 m, as shown on Figures 3-1-33 and 3-1-34. This chemical trend parallels the trend defined by the reconstructed alteration temperatures, which are shown on Figures 3-1-12 and 3-1-27. It also parallels a trend defined by the Al-rich "clinoptilolite", which is shown in Figures 3-1-36.

Figure 3-1-36 shows that drill holes with a high abundance of calcium-rich "clinoptilolite" species (USWG-2, UE-25 a/b#1, and UE-25 p#1) are the same holes where the  $\text{Al}_2\text{O}_3$  content for these species has a bi-modal distribution. It is noteworthy that all of these drill holes lie to the northeast and to the east of the 150-°C isotherm (see Figure 3-1-27).

The Paintbrush fault zone and the NW-SE trending shear zone are both situated immediately to the northeast and to the east of the 150-°C isotherm. We believe that these fault zones have served as pathways for the ascent of hydrothermal fluids, which were responsible for the production of the alkali metal alteration aureole at the time of the Timber Mountain hydrothermal metamorphism. The presence

nearby of the orderly-interstratified clays of the Al-rich "clinoptilolite" species and of the higher-grade zeolite species (analcime and locally albite) support this conclusion.

The presence nearby of the Ca+Mg-rich "clinoptilolite" species, deep in the section and below the present-day water table, strongly suggests that these two faults also served as pathways for the later ascent of alkaline earth solutions. The ascending hydrothermal character of these solutions is clearly indicated by the presence nearby of laumontite (boreholes UE-25p#1 and USW G-1; Figures 3-1-32 and 3-1-33) and stellerite, otherwise known as stilbite. The later mineralization occurs in association with tabular (older) and prismatic (younger and Mg- and Sr-enriched, see Figure 3-1-26) heulandite. It overgrows and is overgrown by calcite (Carlos et al., 1995-a). It has been found in boreholes UE-25 a#1, USW G-1 and USW G-2 mainly above the present-day water table (see Figures 3-1-23 and 3-1-24).

Laumontite requires for its formation a solution, which is strongly depleted in the dissolved alkali metals (Na and K), and a temperature exceeding 100°C (see Figures 3-1-15 and 3-1-16). Likewise, stellerite (stilbite), generally known to be associated with hydrothermally altered silicic tuffs, requires for its formation a solution, which is strongly depleted in K, and a temperature of about 100°C (see Figure 3-1-15). The chemistry of solutions required for formation of these two zeolites precludes the involvement of the Timber Mountain hydrothermal solutions, and the required temperature precludes the involvement of ordinary aquifer fluids or infiltrating rainwater. The widespread occurrence of the alkaline-earth zeolite species in the present-day vadose zone implies the possible episodic repetition of higher water levels, higher heat flow and temperature, higher pH, and higher abundance of the dissolved cations, over the past 8-9 Ma. The zeolite metasomatism, its spatial extent and mineralogical association, in particular, provide strong evidence for past, but short-lived, amplification or amplifications of the present-day, quasi-stable Paintbrush geothermal anomaly see Figures 1-31 through 1-33.

#### **3.1.4.10. Concluding Remarks**

The analysis of the distribution of zeolite species in the interior of Yucca Mountain leads to a conclusion that the Mountain hosts two chemically distinctive alteration aureoles, which is in harmony with the proposed conceptual model. The alkali (Na and K) alteration aureole was, most likely, contemporaneous to the orderly interstratified clays produced by the Timber Mountain hydrothermal metamorphism, about 10-11 Ma ago. It is present mainly below the Paintbrush Tuff, and consists of three broadly pervasive alteration zones, which are at variance with the stratigraphic boundaries that dip gently to the south and to the west. The alkali zeolite species occur sporadically in the Paintbrush Tuff, or in the vadose zone, where these species (chabazite, erionite, and phillipsite) seem to be narrowly confined to faults and fractures.

The alkaline earth (Ca and Mg) alteration aureole is younger, and this aureole overprints the pervasive Timber Mountain hydrothermal metamorphism. It has the shape of double inter-grown mushroom stems, which are rooted in the Paintbrush fault zone and in the NW-SE trending shear zone in conformity with the proposed conceptual model. The juxtaposed west and southwest pileuses of this double mushroom are located in the area of the proposed facility. The corresponding tuffs host the calcic zeolite species (stellerite, heulandite, and laumontite) in the form of both the fracture-lining minerals and the matrix alteration minerals. In addition, these tuffs also host products of the (earlier) Timber Mountain hydrothermal metamorphism such as some of the siliceous species (clinoptilolite and mordenite), orderly interstratified clays, analcime, and albite. Crosscutting relationships among the fracture-lining calcic species provide evidence for multiple episodes of the deposition of stellerite and heulandite. In addition, these relationships indicate that these zeolite species are contemporaneous with the fracture-lining calcite-opal-quartz-fluorite assemblages.

Although the R0 smectite is ubiquitously distributed in the interior of Yucca Mountain, late orderly-interstratified clays seem to be absent. Some of this smectite post-dates the Timber Mountain hydrothermal metamorphism, which is indicated by its coexistence with the orderly-interstratified clays and by the K/Ar ages that are associated with it. The absence of evidence for the smectite transformation implies that the duration of thermal exposure was insufficient or the solution chemistry was inadequate to support the illitization reactions, which is what the conceptual model demands. Smectite specimens from the lower vitrophyre of the Topopah Spring Member, in drill hole USW H-5, were found to be Ca-rich with very low K and Na abundance. This together with the presence of zeolite species, requiring for their formation a virtual absence of potassium indicates that the altering solutions must have been practically free of this dissolved cation.

It thus appears that the task of validating the proposed conceptual model has been successfully completed. The critically important conclusion in this regard is the one concerning the hydrothermal origin of the alkaline earth zeolite alteration and mineralization. It is appropriate, therefore, to consider whether there is a rational alternative to the conceptual model. The only alternative approach, which has been proposed, discounts the presence of laumontite and stellerite (stilbite) and the established asymmetry of the alkaline earth alteration aureole. This approach has the effect of preserving the Peterman et al. (1993) insistence that the alteration is telling us only that the process "*occurred under whole open-system conditions*". Giving the alternative approach some benefit of the doubt, we defer a final, categorical validation of the proposed conceptual model to the fluid inclusion data, which establishes the salinity and temperature of fluids responsible for the precipitation of the calcite that is coeval with the calcic zeolite

species. We do so as further confirmation of the conceptual model without detracting from what we consider is a complete validation of it provided thus far.

### 3.1.5. *K/Ar Ages of the Alkali and Alkaline-Earth Zeolite Species*

Zeolite species are open-framework aluminosilicate minerals, which are best known for their absorptive, molecular sieve, ion exchange, and catalytic properties. These properties express the presence of large cavities and channels in the zeolite framework. The openings allow cations, water molecules, and certain gases to move in and out of the crystal structures. From the standpoint of the K/Ar dating, this implies poor retention of the radiogenic argon and potassium within.

To be useful for the purposes of K/Ar dating, however, it is essential that a mineral phase have a capacity for retaining  $^{40}\text{K}$  and  $^{40}\text{Ar}$  produced by  $^{40}\text{K}$  decay, and of resisting post-depositional alteration. Because of their properties, zeolite species are not regarded as ideal material for the application of the K/Ar dating method, and the dates are often viewed with suspicion, although there has been limited research done in this area. Nevertheless, the K/Ar method has been used to date clinoptilolite elsewhere, and the results have been regarded as geologically reasonable.

It has been suspected, for the past decade (see Szymanski, 1992), that the clinoptilolite specimens from the vadose zone at Yucca Mountain could be, in fact, representing the alkaline earth alteration aureole. These "clinoptilolite specimens" carry K/Ar ages between 2.0 and about 9.0 Ma (WoldeGabriel et al., 1993). However, clinoptilolite specimens from the phreatic zone, which clearly do represent the older alkali alteration aureole, carry K/Ar ages that correctly reflect the fact that this aureole is a product of the Timber Mountain hydrothermal metamorphism (Szymanski, 1992). The Yucca Mountain Project scientists regard the late K/Ar ages from the vadose zone as apparent (erroneous), reflecting either a gain of  $^{40}\text{K}$  or a loss of  $^{40}\text{Ar}$ . Nevertheless, these scientists consider the older ages as accurately reflecting the age of formation of the host clinoptilolite specimens, because these ages are confirmed by K/Ar ages from the orderly-interstratified clays (WoldeGabriel et al., 1993).

We reject the Project Scientists' notion of  $^{40}\text{K}$  gain by pointing out that, in contrast to the Timber Mountain hydrothermal solutions, the later solutions were alkaline earth in their chemical character. These solutions cannot therefore be held responsible for introducing allogenic  $^{40}\text{K}$ . We also reject the notion of certain (for sure)  $^{40}\text{Ar}$  loss; the lower  $^{40}\text{Ar}$  contents could be taken to mean either that the loss of  $^{40}\text{Ar}$  occurred or the younger ages are correct. In order to accept one of these two possibilities, one would need adequate justification. We pose the question: If it were presumed that the  $^{40}\text{Ar}$  loss did occur, how have the old (>9 Ma) saturated-zone clinoptilolite specimens managed to retain completely, the radiogenically produced  $^{40}\text{Ar}$ ?

Keeping in mind the preceding reservations, we regard all of the K/Ar ages as potentially correct in indicating that the alkaline earth alteration aureole post-dates the Timber Mountain hydrothermal metamorphism. These ages do not need to be accurate, which most likely they are not, to make this point. The fact that the tuffs at Yucca Mountain contain two chemically and chronologically distinct alteration aureoles is sufficient, in our opinion, to validate the proposed conceptual model.

### 3.1.5.1. Sample Preparation and Analytical Methods

Researchers at the Los Alamos National Laboratory have attempted to constrain the timing of the zeolite alteration at Yucca Mountain and to expand upon the earlier K/Ar studies of the smectite alteration (Bish and Aronson, 1993). They have employed for this purpose the ubiquitously present clinoptilolite specimens, some of which may in fact be the isostructural heulandite (see discussion in the previous section).

The resulting ages were reported and analyzed in WoldeGabriel (1993), and Faiia et al. (2000). These ages represent five outcrop samples from the northern sector of Yucca Mountain and 22 core samples from five drill holes (USW G-1, G-2, G-3, G-4, and UE-25p#1). The dated samples contained more than 30 % clinoptilolite fraction in the whole-rock samples. They represent the altered tuffs below and above the present-day water table and provide adequate spatial coverage of the area.

The samples were crushed and pulverized and a mixture of the alteration products (clays, zeolite species, feldspars, and silica polymorphs) was extracted by sedimentation in deionized water. Ten out of twenty two core samples were subjected to further purification using a mixture of *s*-tetrabromoethane and acetone. This mixture had a density between 2.1 and 2.45 g·cm<sup>-3</sup>, and was used to separate clinoptilolite from the denser primary and authigenic minerals by centrifugation. Although clinoptilolite is less dense than other common minerals found in the tuff matrix, the heavy-liquid separation was not entirely effective.

The mineral separates were analyzed by X-ray diffraction using random and oriented mounts. Standard XRD patterns were then used to identify zeolite species and the associated alteration minerals. The purified separates contained more than 75 % of the clinoptilolite fraction, except for some samples from the Tram Tuff, which contained finely crystalline quartz and minor amounts of feldspar. Opal-CT, cristobalite, quartz, and K-bearing mineral phases (mordenite, feldspar, and illite/smectite) were common impurities in the clinoptilolite separates. Heating experiments were carried out on the clinoptilolite separates and the results indicated the absence of heulandite. The clinoptilolite-rich separates were selected for K/Ar dating using an MS10 mass spectrometer.

### 3.1.5.2. Reliability of K/Ar Ages

In order to examine the effects of heavy-liquid purification, WoldeGabriel et al. (1992) performed K/Ar dating of treated and untreated separates from the same samples. The results indicate that the dated samples responded variably to the treatment. The K/Ar apparent age increased for two out of ten of the purified separates, which indicates that these two particular separates contained relatively young authigenic and K-bearing impurities, such as mordenite and/or adularia for example. For most of the purified separates, however, the apparent age decreased, which indicates that these separates contained relatively old K-bearing mineral phases, either primary or secondary. The remaining three separates, however, maintained their age within the range of experimental errors. The variability of the purification effects indicates that the deposition of K-bearing minerals, including zeolite species and feldspars, is a polygenetic or multi-episode process. This variability suggests a continuation of the zeolite alteration after cessation of the Timber Mountain hydrothermal metamorphism, and it indicates that some of the K/Ar ages are average (mixed) ages for two or more end-members of the mixture.

The effects of the post-deposition cation exchanges was examined by K/Ar dating of the pristine separates and separates from the same sample exchanged with NaCl and BaCl<sub>2</sub>, as described in WoldeGabriel et al. (1992). A series of ion-exchange experiments was also conducted by WoldeGabriel (1995) using Ca-, Cs-, K-, and Na-chloride solutions and a clinoptilolite-rich sample from the late Miocene Sucker Creek Formation from eastern Oregon. The exchange experiments collectively revealed that alkaline and saline solutions could strip the potassium from the clinoptilolite specimens without significantly affecting the <sup>40</sup>Ar abundance.

Fluids with elevated salinity (up to 10<sup>3</sup> and 10<sup>4</sup> ppm NaCl equiv.) have been found by Dublyansky et al. (2001) to be entrapped inside fluid inclusions in the ESF calcite, which clearly post-dates the Timber Mountain hydrothermal episode. In addition, this late calcite has been observed by Carlos et al. (1995-a) to be intergrown with Mg- and Sr-enriched heulandite and stellerite. It is likely, therefore, that the older zeolite species from the vadose zone were undergoing cation exchange reactions with fluids, which were both saline and alkaline in composition. Thus, the cation exchange between K-bearing clinoptilolite with the saline and alkaline solutions would have the effect of stripping the potassium without significantly affecting the <sup>40</sup>Ar abundance. The stripping would have the effect, in turn, of increasing the apparent K/Ar ages, but not decreasing them.

As noted earlier, K/Ar ages greater than about 9 Ma are in conformity with the K/Ar ages from the orderly-interstratified clays, which are unquestionably retentive of both K and <sup>40</sup>Ar. These ages therefore must be accepted as generally reliable, so that only the reliability of the younger ages is open to question.

Consequently, the removal of potassium via ionic exchange reactions is an effect, which is irrelevant to the considerations undertaken herein.

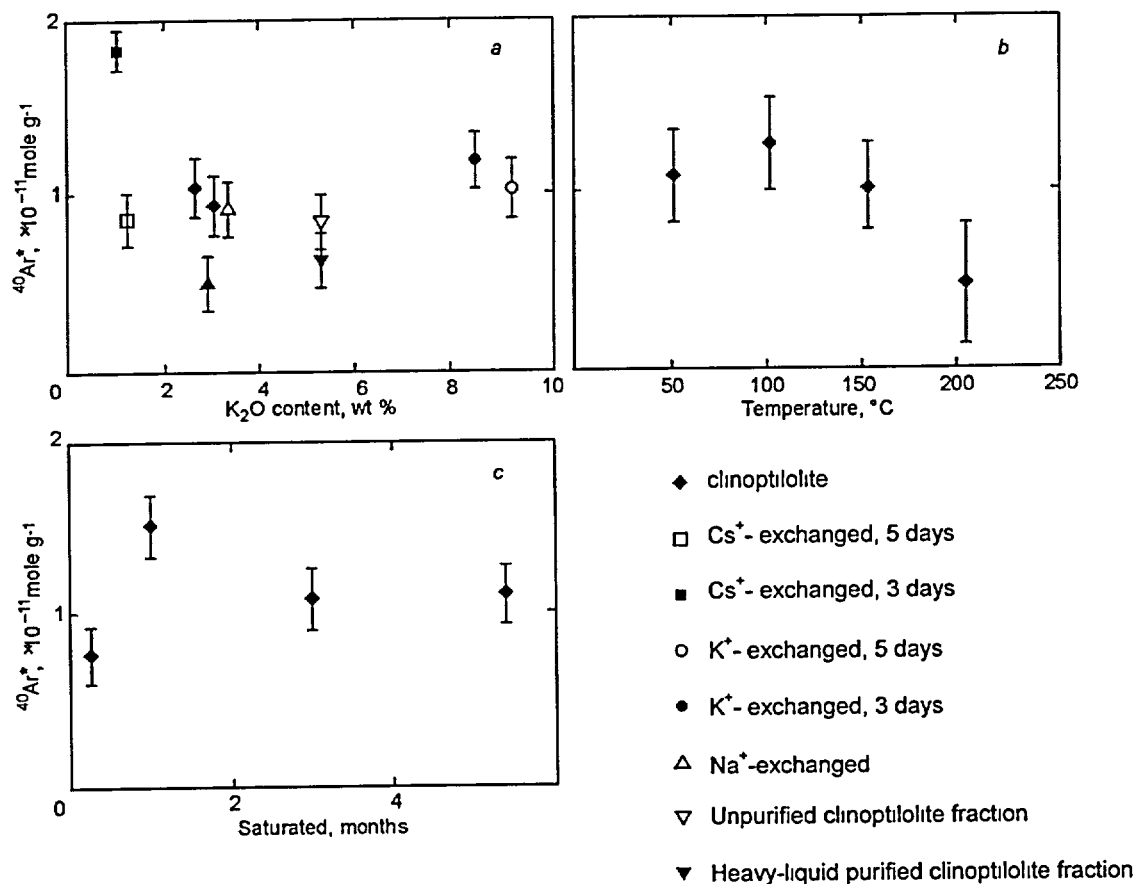


Figure 3-1-37. Radiogenic Ar content of ion-exchanged (a), dehydrated at different temperatures in a vadose environment (b), and heated at 100°C in a H<sub>2</sub>O-saturated environment (c) clinoptilolite. From WoldeGabriel (1995).

WoldeGabriel (1995) has also evaluated the Ar and K retention capability of clinoptilolite, based on dehydration experimental studies of clinoptilolite specimens from the late Miocene Sucker Creek Formation of eastern Oregon. In contrast to the cation exchange experiments, the results of these studies are potentially important for interpreting the younger K/Ar clinoptilolite ages from the Yucca Mountain tuffs. This is because they show that water plays a vital role in stabilizing the clinoptilolite framework, which controls the retention of  $^{40}\text{Ar}$ . Particularly important is the fact that the argon depletion has been observed in clinoptilolite that was dehydrated by heating it at different temperatures for 16 hours, as shown on Figure 3-1-37.

Figure 3-1-37-*b* shows that specimens of the Sucker Formation clinoptilolite, which have been dehydrated at progressively higher temperatures, seem to have begun losing  $^{40}\text{Ar}$  at a temperature of about  $100^\circ\text{C}$ . WoldeGabriel (1995) reported that similar results were obtained from clinoptilolite specimens, which have been exchanged with a Na-bearing solution for five days. However, Figure 3-1-37-*c* shows that the comparable  $^{40}\text{Ar}$ -depletion was not observed for the water-saturated experiments, during which the Sucker Formation clinoptilolite separate was heated at a temperature of  $100^\circ\text{C}$  for a period as long as six months. Argon depletion was observed in the water-saturation experiments, but at the higher temperature, between 100 and  $150^\circ\text{C}$ . Thus, we do not know whether the differing responses are attributable to the differing aqueous environments (saturate vs. unsaturated), or conversely, whether these responses are attributable to the differing  $^{40}\text{Ar}$ -depletion activation temperatures.

The experimental results as a whole allow for making three points. **First**, the heavy-liquid purification experiments indicate that the zeolite alteration at Yucca Mountain is not a discrete, in time, event. Instead, the results are telling us that the K/Ar ages pertain to a mixture of older and younger alteration products, which implies a continuation of the zeolite alteration after cessation of the Timber Mountain hydrothermal metamorphism. **Second**, the cation exchange experiments suggest that there is a potential for post-depositional loss of  $^{40}\text{K}$ , which would have the effect of increasing the measured age. **Third**, the dehydration experiments indicate that there is a potential for  $^{40}\text{Ar}$  loss, because of the dehydration at an elevated (above  $100^\circ\text{C}$ ) temperature.

We do not know whether the  $^{40}\text{Ar}$ -loss activation temperature is comparable to the one, under which the vadose zone tuffs were altered after the cessation the Timber Mountain hydrothermal metamorphism. The alteration temperature information depicted in Figures 3-1-12 and 3-1-27 indicate that the residual temperature at the proposed repository level could not have been higher than about  $40\text{-}50^\circ\text{C}$ . The zeolite dehydration would have the effect of decreasing the  $\text{H}_2\text{O}$  content, on one hand, and of decreasing the corresponding K/Ar age, on the other. Thus, the central questions are whether tuff dehydration is possible in a vadose environment (nearly 100 % relative humidity) and whether there is any evidence for it.

Table 3-4

Mineralogical composition of clinoptilolite separates from the altered tuffs at Yucca Mountain. From WoldeGabriel et al. (1993).

Sample ID	Stratigraphic Units	Depth (m)	Size Fraction ( $\mu\text{m}$ )	Authigenic Minerals*
3-15-82-8	Calico Hills	outcrop	1-3	CPT, MOR, opal-CT
3-15-82-8	Calico Hills	outcrop	3-20	CPT, MOR, opal-CT
82FB-4	Calico Hills	outcrop	3-20	CPT, MOR, opal-CT
USWG-11561	Calico Hills	475.8	1-3	CPT, MOR, opal-CT
USWG-11819	Prow Pass	554.4	1-3	CPT, MOR, opal-CT, quartz
USW G-1 2190 8-2190 0	Prow Pass	667.5	1-3	CPT, MOR, FEL, opal-CT, quartz
USWG-1 3288 5-3288 6	Tram	1002.2	1-3	CPT, MOR, quartz, FEL, ANL, US
USW G-1 5458 4-5458.5	Tuff (Unit B)	1663.6	1-3	CPT, quartz, FEL, I/S
USW G-1 5560	Tuff (Unit C)	1694.7	1-3	CPT, MOR, quartz, I/S, FEL
USW G-2 762	Topopah Spring	232.2	1-3	CPT, opal-CT
USW G-2 2430	Calico Hills	740.7	1-3	CPT, MOR, opal-CT, I/S, FEL
USW G-2 1691-1691 5	Topopah Spring	515.5	1-3	CPT, MOR, opal-CT
USW G-2 3191.5-3192.0	Prow Pass	972.9	1-3	CPT, quartz, FEL, I/S
USW G-2 3250-3250 7	Prow Pass	990.6	1-3	CPT, ANL, MOR, quartz, FEL, I/S
USW GU-3 1874	Prow Pass	571.2	1-3	CPT, opal-CT
USW G-3 2013 1-2013 4	Bullfrog	613.6	1-3	CPT, opal-CT
USW G-3 3589	Tram	1094.1	1-3	CPT, quartz, FEL, I/S
USW G-3 3854 7-3854.9	Tram	1174.9	1-3	CPT, FEL, MOR, quartz, I/S
USW G-4 1381	Topopah Spring	420.9	1-3	CPT, opal-CT
USW G-4 1685.2-1685 4	Calico Hills	513.6	1-3	CPT, opal-CT
USW G-4 1734 3-1734 6	Calico Hills	528.5	1-3	CPT, MOR, opal-CT
USW G-4 1763 2-1763 5	Prow Pass	537.4	1-3	CPT, opal-CT, MOR, FEL, quartz

Table 3-4 (Continued)

Sample ID	Stratigraphic Units	Depth (m)	Size Fraction ( $\mu\text{m}$ )	Authigenic Minerals*
USW G-4 1779 6-1779 9	Prow Pass	542.2	1-3	CPT, opal-CT, MOR, FEL, quartz
USW G-4 1788 4-1788 7	Prow Pass	545	1-3	CPT, opal-CT, FEL, quartz
UE-25P#1 1740-1750	Prow Pass	530 4	1-3	CPT, opal-CT, MOR, FEL
UE-25P#1 1790-1800	Prow Pass	545 6-548 6	1-3	CPT, MOR, opal-CT

CPT-clinoptilolite  
MOR-mordenite  
FEL-feldspar  
ANL-analcime  
I/S-illite/smectite

Notes: \* Most of the feldspar and quartz are primary. Clinoptilolite is the dominant mineral, except for quartz in some of the deeper units, and comprises more than 75 wt.% of the separates.

### 3.1.5.3. K/Ar Database

An inventory of the K/Ar dated samples of clinoptilolite from Yucca Mountain is presented in Table 3-1-4. This table lists the samples, specifies the stratigraphic position, and identifies the associated authigenic minerals.

The results of the laboratory analyses ( $\text{K}_2\text{O}$  abundance,  $^{40}\text{Ar}$  abundance, and calculated K/Ar age) are shown in Tables 3-1-5-a through -c.

Figures 3-1-38 through 3-1-42 are ternary diagrams showing the major cation composition of whole-rock samples of the tuff and of zeolite species, plotted individually for the respective drill holes as a function of the stratigraphic depth. Additionally, these figures identify the corresponding K/Ar age, the major cation composition of the dated sample (if known), and the associated alteration minerals. They were prepared with the intention of establishing a means for associating the K/Ar dated specimens with the respective alteration aureole.

While considering the K/Ar ages of the clinoptilolite specimens, it is important to keep in mind the central issue to be resolved by these ages. This issue is not whether the ages are accurate *per se*; we know that they are not. Rather, the issue is to establish whether, indeed, the zeolite species occur at Yucca Mountain in the form of two chronologically and chemically distinct facies, and further whether the alkaline earth facies are younger.

Table 3-5 a

K/Ar analyses of clinoptilolite (1-3  $\mu\text{m}$  and 3-20  $\mu\text{m}$  fractions) separates from the altered tuffs at Yucca Mountain.  
From WoldeGabriel et al. (1993).

Sample ID	Depth (m)	Stratigraphic Unit	Depth to Water Table* (m)	Size Fraction ( $\mu\text{m}$ )	Weight (g)	K <sub>2</sub> O wt %	<sup>40</sup> Ar§ (10 <sup>-11</sup> mol/g)	<sup>40</sup> Ar§ (%)	Age† (m.v., $\sigma$ )
3-15-82-8	Outcrop	Calico Hills	**	1-3	0.1599	5.49	2.0271	8	2.6±0.8
3-15-82-8	"	"	"	1-3	0.1677	6.13	3.1094	15	3.5±0.5
3-15-82-8	"	"	"	3-20	0.1685	5.83	1.6997	10	2.0±0.4
3-15-82-8	"	"	"	3-20	0.1765	5.47	1.1439	8	1.5±0.4
USW G-I 5458.4-5458.5	1663.6	Older Tuffs	571.7	1-3	0.1837	3.58	6.1866	22	12.0±0.9
USW G-I 5560	1694.7	"	"	1-3	0.1653	3.25	5.7686	23	12.3±0.9
USW G-2 1691-1691.5	515.4	Topopah Spring	524.9	1-3	0.1548	4.13	2.3731	10	4.0±0.7
USW G-2 2430	740.7	Calico Hills	"	1-3	0.1672	3.47	2.2875	17	4.6±0.5
USW G-2 3250-3325.7	990.6	Prow Pass	"	1-3	0.1925	1.64	3.1446	17	13.3±1.0
USW GU-3 1874	571.2	"	750.3	1-3	0.1697	3.99	1.4002	8	2.4±0.6
USW GU-3 2013.15-2013.4	613.6	Bullfrog	"	1-3	0.1573	4.64	2.5681	19	3.8±0.3
USW G-3 3854.7-3854.9	1174.9	Tram	"	1-3	0.1664	4.02	6.0061	45	10.4±0.3
USW G-4 1381	420.9	Topopah Spring	539.5	1-3	0.1895	4.79	2.8756	9	4.2±0.9
USW G-4 1685.2-1685.4	513.6	Calico Hills	"	1-3	0.1560	5.42	3.5271	22	4.5±0.3
USW G-4 1788.4-1788.7	545.2	Prow Pass	"	1-3	0.1629	6.85	7.1259	34	7.2±0.3
UE-25P#1 1740-1750	530.4-545.6	"	383.9	1-3	0.1527	4.72	5.6841	18	8.4±0.8
UE-25P#1 1790-1800	545.6-548.6	"	"	1-3	0.1803	3.24	3.9166	19	8.4±0.8

§ Radiogenic

† Determined from decay constants and isotopic abundance of <sup>40</sup>K according to Steiger and Jager, 1977

\* Data on water table depth from surface are from Robison, 1984.

\*\* Depth, to water table not known

$\sigma$  Total percentage error

Table 3-5 b

K/Ar analyses of clinoptilolite (1-4  $\mu\text{m}$  and 3-20  $\mu\text{m}$  fractions) separates from the altered tuffs at Yucca Mountain, before and after heavy-liquid treatment. From WoldeGabriel et al.(1993).

Sample ID	Depth (m)	Stratigraphic	Unit	Depth to Water Table <sup>#</sup> (m)	Size Fraction ( $\mu\text{m}$ )	Weight (g)	K <sub>2</sub> O wt %	<sup>40</sup> Ar§ (10 <sup>-11</sup> mol/g)	<sup>40</sup> Ar§ (%)	Age† (m.y., $\sigma$ )
USWG-1 1561a	475.8	Calico Hills		571.7	1-3	0.1254	4.96	1.5677	8	2.2±0.6
USW G-1 1561b	475.8	"		"	1-3	0.1340	4.96	1.4006	10	2.0±0.4
USW G-1 1561 <sup>+</sup>	475.8	"		"	1-3	0.1349	4.99	2.2210	15	3.1±0.4
USW G-1 1561 <sup>+</sup>	475.8	"		"	1-3	0.1628	4.87	1.3491	7	1.9±0.6
USW G-1 2190.8-2190.9	667.5	Prow Pass Member		"	1-3	0.1760	4.86	4.7995	26	6.9±0.4
USW G-1 2190.8-2190.9 <sup>+</sup>	667.5	"		"	1-3	0.1372	4.38	2.7158	7	4.3±1.0
USW G-1 3288.5-3288.6	1002.2	Tram Member		"	1-3	0.1535	4.85	7.3396	35	10.5±0.4
USW G-1 3288.5-3288.6 <sup>+</sup>	1002.2	"		"	1-3	0.1301	4.64	6.7043	35	10.0±0.4
USW G-2 3191.5-3192.0	972.9	Prow Pass Member		524.9	1-3	0.1500	3.73	5.6058	27	10.4±0.6
USW G-2 3191.5-3192.0 <sup>+</sup>	972.9	"		"	1-3	0.0524	2.30	2.3145	20	7.0±0.7
USW G-3 3589	1094.1	Tram Member		750.3	1-3	0.1569	6.12	8.2727	33	9.9±0.5
USW G-3 3589	1094.1	"		"	1-3	0.1800	5.66	8.0722	44	10.0±0.3
USW G-3 3589 <sup>+</sup>	1094.1	"		"	1-3	0.0714	5.10	6.6200	29	9.0±0.5
USW G-4 1734.3-1734.6	528.5	Calico Hills		539.5	1-3	0.1548	3.28	1.8338	5	3.8±1.0
USW G-4 1734.3-1734.6 <sup>+</sup>	528.5	"		"	1-3	0.1467	3.29	2.2847	4	4.8±2.0
USW G-4 1763.2-1763.5	537.4	Prow Pass Member		"	1-3	0.1572	3.09	1.9400	10	4.4±0.8
USW G-4 1779.6-1779.9	542.2	"		"	1-3	0.1623	7.13	7.6142	43	7.4±0.2
USW G-4 1779.6-1779.9 <sup>+</sup>	542.2	"		"	3-20	0.1744	4.34	2.7582	24	4.4±0.3
USW G-4 1779.6-1779.9 <sup>+</sup>	542.2	"		ii	1-3	0.1721	4.30	2.5421	18	4.1±0.4
UE-25P#1 1740-1750 <sup>+</sup>	530.4-545.6	"		383.9	3-20	0.2141	2.60	2.2415	11	6.0±1.0

§ Radiogenic

† Determined from decay constants and isotopic abundance of <sup>40</sup>K according to Steiger and Jager (1977)

+ Heavy liquid treated

# Data on water table depth are from Robison (1984)

$\sigma$  Total percentage error

Table 3-5 c

K/Ar analyses of clinoptilolite (1-3  $\mu\text{m}$  and 3-20  $\mu\text{m}$  fractions) separates from the altered tuffs at Yucca Mountain, before and after cation exchange experiments. From WoldeGabriel et al. (1993).

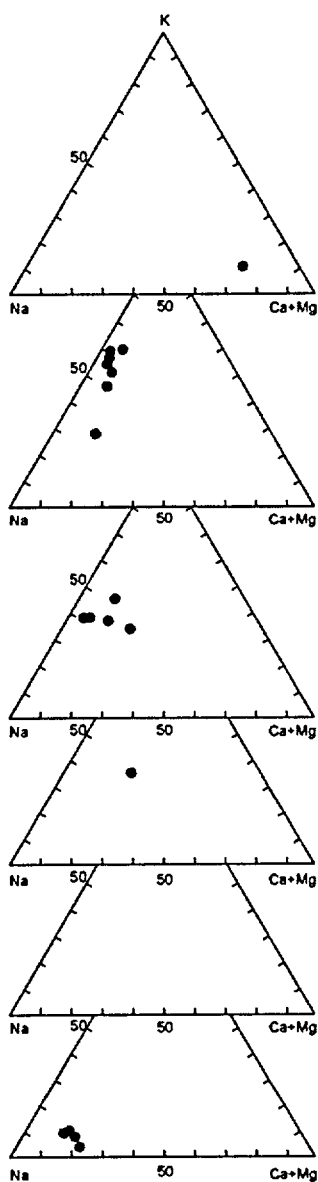
Sample ID	Depth (m)	Stratigraphic Unit	Depth to Water Table <sup>#</sup> (m)	Size Fraction ( $\eta\text{m}$ )	Weight (g)	K <sub>2</sub> O wt. %	<sup>40</sup> Ar§ (10 <sup>-11</sup> mol/g)	<sup>40</sup> Ar§ (%)	Age† (m v., $\sigma$ )
USWG-11819	664.4	Prow Pass	571.7	1-3	0.1961	4.91	3.7616	18	5.310.5
USW G-11 1819-NaCl, 48 hr.	554.4	"	"	1-3	0.1532	3.55	3.5081	19	6.9 $\pm$ 0.6
USW G-11 1819-BaCl <sub>2</sub> , 48 hr.	554.4	"	"	1-3	0.1540	3.20	3.4008	16	7.4 $\pm$ 0.8
USW G-11 1819-BaCl <sub>2</sub> , 72 hr.	554.4	"	"	1-3	0.1708	3.97	4.7366	20	8.3 $\pm$ 0.7
USWG-11819-CsCl, 72 hr.	554.4	"	"	1-3	0.2439	3.63	4.5633	14	8.7 $\pm$ 1.0

§ Radiogenic

† Determined from decay constants and isotopic abundance of <sup>40</sup>K according to Steiger and Jager (1977)

# Data on water table depth are from Robison (1984)

$\sigma$  Total percentage error



Tpt: Samples 1156 through 1356 contain trace of major fracture-lining heulandite and lesser stellerite

Tac: Sample 1561a  $2.2 \pm 0.1 \rightarrow 3.1 \pm 0.5$  Ma,

a) vadose zone b) chemistry of the separate:

Ca+Mg=3.3 wt. %, K=55.3 wt. %, and 39.2 wt. %

Tac: Sample 1561b  $2.0 \pm 0.1 \rightarrow 1.9 \pm 0.8$  Ma,

The chemistry same as above

Tcp: Sample 1819  $5.4 \pm 0.1$  Ma,

a) vadose zone b) chemistry of the separate:

Ca+Mg=12wt.%, k=40.9wt.%, and 47.5wt. %

Tcp: Sample 2190  $6.9 \pm 0.1 \rightarrow 4.3 \pm 1.2$  Ma,

a) phreatic zone b) chemistry of the separate unknown

Tcb: Sample 3286  $10.6 \pm 0.2 \rightarrow 10.0 \pm 0.4$  Ma,

a) phreatic zone b) chemistry of the separate unknown

Tct

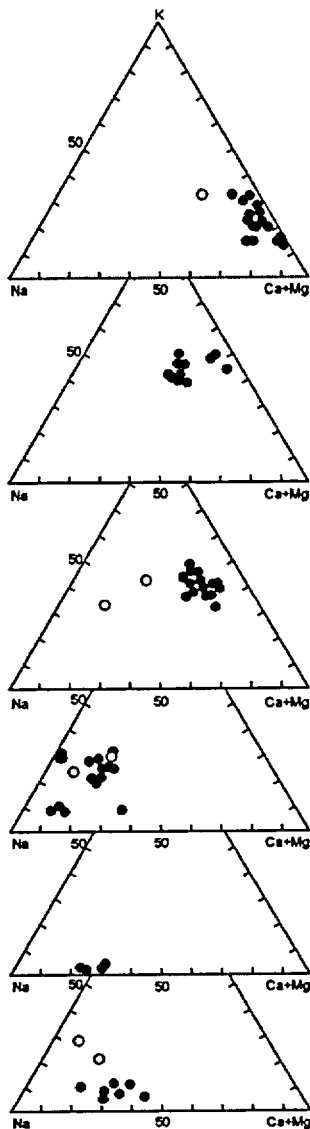
Tfb - Tot: Sample 5458  $12 \pm 0.9$  Ma,

a) phreatic zone b) chemistry of the separate unknown

Tfb - Tot: Sample 5560  $12.3 \pm 0.9$  Ma,

Same as above

Figure 3-1-38. Chemistry of the K/Ar dated separates and of chemistry and mineralogy of their surrounding, drill hole USW G-1. Based on data from Broxton et al. (1986), Bish and Chipera (1989), Carlos et al. (1990), WoldeGabriel et al. (1992), and WoldeGabriel (1993).



Tpp

Tpt: Sample 762 0 9 Ma,  
 a) vadose zone b) chemistry of the separate.  
 Ca+Mg=55.2 wt. %, K=39.1 wt. %, and Na= 5.7 wt. %  
 Samples 1447 through 1687 contain trace – major  
 fracture-lining heulandite and stellerite, Carlos et al.  
 (1990)

Tpt: Sample 1691 4 1±0.1 Ma,  
 a) vadose zone b) chemistry of the separate av (2):  
 Ca+Mg=33.95 wt. %, K=48.15 wt. %, and Na=17.9 wt.  
 %

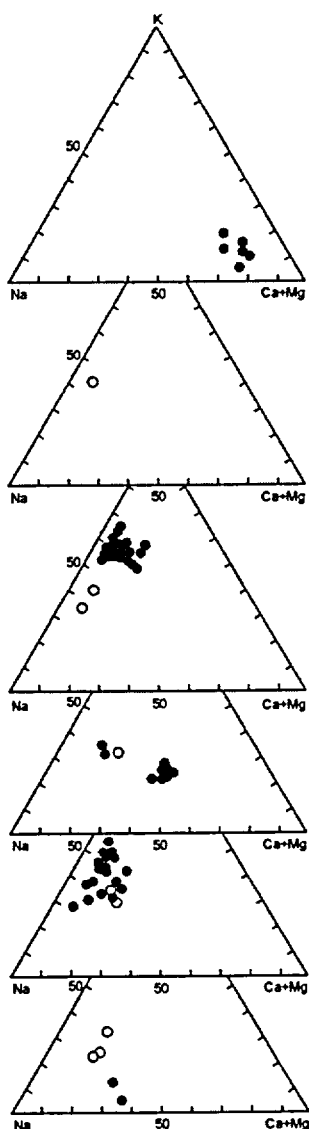
Tac: Sample 2430 4 6±0.2 Ma,  
 a) phreatic zone b) chemistry of the separate av (2):  
 Ca+Mg=42.9 wt. %, K=41.55 wt. %, and 15.55 wt. %  
 Chemistry of tuff. Ca+Mg=24.8 wt. %, K=45.7 wt. %, and Na=29.5 wt. %

Tct: Sample 3191 10.6±0.2 Ma,  
 a) phreatic zone b) chemistry of the separate av (3):  
 Ca+Mg=20.2 wt. %, K=21.48 wt. %, and 57.81 wt. %  
 Chemistry of tuff. Ca+Mg=12.2 wt. %, K=43.3 wt. %, and Na=44.5 wt. %

Tcp

Tcb

Figure 3-1-39. Chemistry of the K/Ar dated separates and or chemistry and mineralogy of their surrounding, drill hole USW G-2. Based on data from Broxton et al. (1986), Bish and Chipera (1989), Carlos et al. (1990), WoldeGabriel et al. (1992), and WoldeGabriel (1993).



Tpt

Tac

Tcb, Sample 1874 2.5±0.2 Ma,

a) vadose zone b) chemistry of the separate av (4) Ca+Mg=16.28 wt. %, K=55.5 wt. %, and Na=28.64 wt. %, c) Sample 1189 contains major fracture-lining heulandite, Carlos et al. (1990)

Tcb, sample 2013 3.9±0.1 Ma

a) phreatic zone, b) chemistry of dated separate: unknown

Tct: Sample 3589a 9.5±0.2 Ma.

a) phreatic zone b) chemistry of the separate av (2) Ca+Mg=8.4 wt. %, K=54.65 wt. %, and 36.95 wt. %  
Chemistry of tuff Ca+Mg=22.1 wt. %, K=33.5 wt. %, and Na=44.4 wt. %

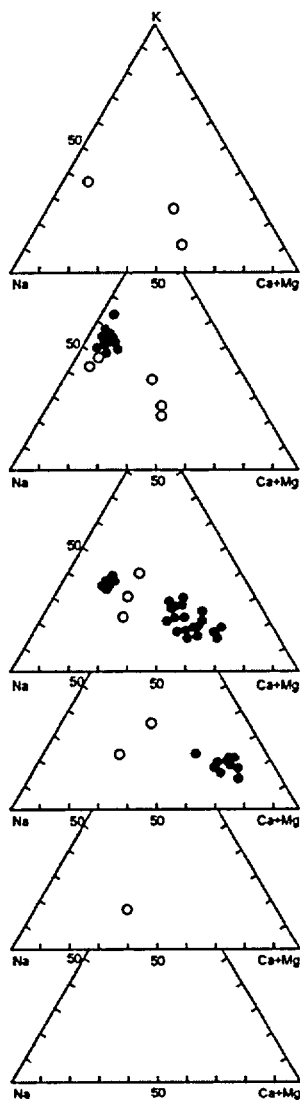
Tct: Sample 3589a 3589b 10.0±0.2 Ma

the same as above

Tir: Sample 3854 10.4±0.3 Ma.

a) phreatic zone b) chemistry of the separate: unknown  
Chemistry of tuff Ca+Mg=17.8 wt. %, K=30.5 wt. %, and Na=51.7 wt. %

Figure 3-1-40. Chemistry of the K/Ar dated separates and or chemistry and mineralogy of their surrounding, drill hole USW G-3/GU-3. Based on data from Broxton et al. (1986), Bish and Chipera (1989), Carlos et al. (1990), WoldeGabriel et al. (1992), and WoldeGabriel (1993).



Tpt: Sample 1381  $4.2 \pm 0.1$  Ma.

a) vadose zone, b) chemistry of dated separate: unknown, c) samples 1354 through 1381 contain major fracture-lining heulandite, Carlos et al. (1990), and d) the dated separate is overlain and underlain by whole-rock samples enriched in alkaline-earth.

Tac: Sample 1685  $4.6 \pm 0.1$  Ma.

a) vadose zone, b) chemistry of the dated separate-unknown, c) the dated separate is overlain and underlain by whole-rock samples enriched in alkaline-earth

Tac: Sample 1734  $3.9 \pm 0.2 \rightarrow 4.8 \pm 2.4$  Ma.

the same as above

Tcp: Sample 1763  $4.4 \pm 0.2$  Ma.

a) vadose zone b) chemistry of the separate av (7). Ca+Mg=15 wt. %, K=38 wt. %, and Na=47 wt. %.

Tcp: sample 1779  $7.5 \pm 0.1 \rightarrow 4.1 \pm 0.3$  Ma

a) phreatic zone, b) chemistry of dated separate: unknown, c) the dated separate is overlain and underlain by whole-rock samples enriched in alkaline-earth.

Tcp sample 1788  $7.3 \pm 0.1 \rightarrow 4.1 \pm 0.3$  Ma

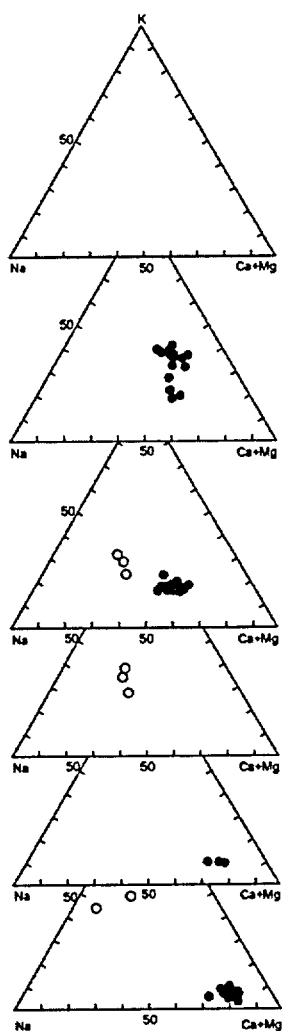
the same as above

Tcb Sample 2716  $12.3 \pm 0.8$  Ma.

a) phreatic zone b) the dated separate consists of mordenite, c) the chemistry of dated separate: unknown, d) chemistry of the whole-rock tuff Ca+Mg=26.4 wt. %, K=26.5 wt. %, and 47 wt. %

Tct

Figure 3-1-41. Chemistry of the K/Ar dated separates and or chemistry and mineralogy of their surrounding, drill hole USW G-4. *Open circles* – whole rock sample (XRF analyses), *solid circles* – separated zeolites (EMPA). Based on data from Broxton et al. (1986), Bish and Chipera (1989), Carlos et al. (1990), WoldeGabriel et al. (1992), and WoldeGabriel (1993).



Tpt

Tac

Tcp: Sample 1740-1750  $8.5 \pm 0.2 \rightarrow 6.0 \pm 0.2$  Ma.

a) phreatic zone b) chemistry of the separate: unknown. c) chemistry of the whole-rock tuff Ca+Mg=24.4 wt %, K=33.6 wt %, and Na=42.1 wt %

Tcp: Sample 1790-1800  $8.4 \pm 0.8$  Ma.

a) phreatic zone b) chemistry of the separate: Ca+Mg=50 wt %, K=19.4 wt %, and Na=30.5 wt %, c) chemistry of the whole-rock tuff Ca+Mg=29.1 wt %, K=28.4 wt %, and Na=42.6 wt %.

Tcb

Tct

Tlr

Figure 3-1-42. Chemistry of the K/Ar dated separates and or chemistry and mineralogy of their surrounding, drill hole UE-25 p#1. *Open symbols* – whole-rock sample, *solid symbols* – clinoptilolite. Based on data from Broxton et al. (1986), Bish and Chipera (1989), Carlos et al. (1990), WoldeGabriel et al. (1992), and WoldeGabriel (1993).

How much younger is a question, which is not germane to the considerations undertaken herein. What is germane, however, is to establish whether the younger zeolite facies expresses the same process as the calcite-silica deposits in the Exploratory Studies Facility and at the ground surface. We do know with confidence that the later deposits have been forming intermittently over the past 12 Ma, including the late Quaternary (see Figure 2-15 for example).

#### 3.1.5.4. The K/Ar Clinoptilolite Ages as a Function of Depth

Some degree of confidence in the general reliability of the K/Ar clinoptilolite ages is provided, in our opinion, by the distribution of these ages as a function of depth. Figure 3-1-43 shows this distribution for both the vadose and phreatic zones in relation to the K/Ar ages from the  $^{40}\text{K}$  and  $^{40}\text{Ar}$  retentive, orderly-interstratified clays.

Figure 3-1-43 contains two important features. **First**, the clinoptilolite ages at a shallow depth, including the vadose zone, are consistently younger than the deeper ones. **Second**, the deeper ages, from the phreatic zone, overlap with the K/Ar ages from the orderly-interstratified clays, kalkberg and illite in particular. This overlap demonstrates that some of the clinoptilolite specimens, those in the phreatic zone in particular, have the capacity to retain both the initial  $^{40}\text{K}$  and the  $^{40}\text{Ar}$  produced therefrom. There are no grounds therefore for a wholesale dismissal of the K/Ar ages as completely erroneous.

Are the consistently younger ages from the shallower specimens a result of contamination of these specimens by some young K-bearing mineral phase or phases? Figure 3-1-43 presents a comparison of the K/Ar ages from those clinoptilolite specimens that have been separated by sedimentation in deionized water with the ages of those specimens, which have been subsequently purified in heavy liquid (shown as open symbols). The figure shows that both the purified and the unpurified clinoptilolite specimens express

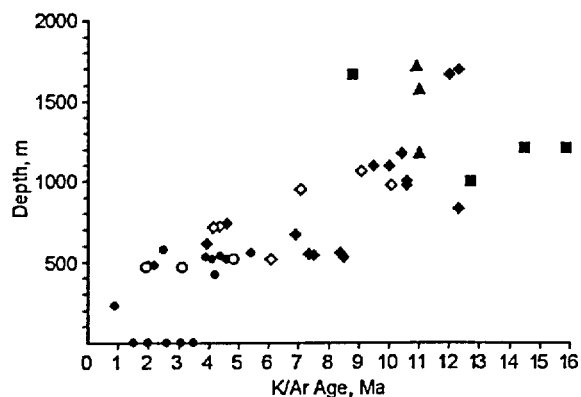
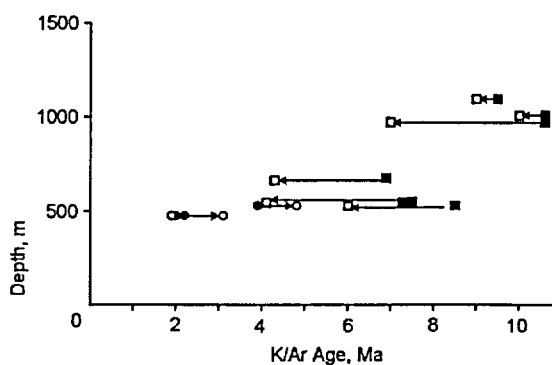


Figure 3-1-43. K/Ar ages of the untreated and heavy-liquid purified clay and clinoptilolite separates as a function of depth. *Squares* and *triangles* – montmorillonite clay by WoldeGabriel (1993) and Bish (1989); *circles* – vadose zone clinoptilolite; *diamonds* – phreatic zone clinoptilolite; *open symbols* – heavy-liquid purified separates; and *filled symbols* – untreated separates. Based on data from WoldeGabriel et al. (1992) and WoldeGabriel (1993).

Note that the two oldest reported ages (14.49 and 15.88 Ma; samples G1 3940-a and -b from WoldeGabriel, 1993) are clearly artifacts, since they are greater than the age of the host Lithic Ridge tuff (13.9 Ma)

the depthward increase of the K/Ar ages. Evidently, the contamination by a young and K-bearing mineral phase is not a factor, which is responsible for this increase.

We now examine more closely the K-contamination issue. Figure 3-1-44 shows the effects of the clinoptilolite purification in heavy liquid, which amounts to removal of heavier K-bearing minerals, such as K-feldspar (adularia), for example. It shows that the shallow specimens respond differently to purification than the deeper ones from the phreatic zone. The shallow specimens either remain unchanged (one specimen) or become older, whereas the deeper ones invariably become younger.



species have the capacity for resisting the alteration, so that they satisfactorily conserve  $^{40}\text{K}$  and  $^{40}\text{Ar}$ . Thus, these phases, the ones from the phreatic zone in particular, can be dated and they form a basis for unraveling the alteration history at Yucca Mountain.

The younger population of the dated clinoptilolite specimens from the phreatic zone occurs between a depth of about 800-m and the present-day water table (see Figure 3-1-43). These specimens carry the apparent K/Ar ages between  $3.9\pm 0.1$  to  $8.5\pm 0.2$  Ma (see Table 3-1-5 and Figure 3-1-43). If it were assumed that they have lost some of the  $^{40}\text{Ar}$  due to heating at a temperature of about  $100\text{ }^{\circ}\text{C}$  (see Figure 3-1-37), the question how it is possible to achieve such a result without heating up the underlying aquifer would arise. There is no choice but to recognize that the subject specimens were formed at a time after the Timber Mountain hydrothermal metamorphism, or more likely, they represent older K-bearing mineral phases, which are variably overgrown by or intermixed with younger ones.

#### 3.1.5.5. The Problem with Clinoptilolite Dehydration

Why the apparent K/Ar clinoptilolite ages from the vadose zone decrease systematically with decreasing depth is a question of major importance. The answer to this question is approached first by recognizing that the  $^{40}\text{Ar}$ -abundance, as shown on Figure 3-1-45, is the major difference, which distinguishes younger and older clinoptilolites.

Figure 3-1-45 shows that, for the entire population of clinoptilolites, the  $\text{K}_2\text{O}$ -abundance is comparable except for two or three older specimens for which this abundance is slightly above 5.5 wt.% (Figure 3-1-45-a). It also shows that the  $^{40}\text{Ar}$ -abundance increases in proportion to the increasing K/Ar apparent age, as it should (Figure 3-1-45-b).

The  $^{40}\text{Ar}$ -abundance vs. depth gradient has led WoldeGabriel (1995) to attribute this gradient to dehydration of the clinoptilolite specimens *in situ* in the vadose zone. This dehydration would have caused the, diminishing with depth,  $^{40}\text{Ar}$  loss, which would be expressed in the form of the observed gradient. This hypothesis seems to be consistent with the results of dehydration experiments on the Sucker Formation clinoptilolite, which are shown on Figure 3-1-37-b. It is important because this hypothesis allows the Department of Energy to maintain a belief that most zeolite alteration occurred at the same time as the tuff emplacement (U.S. DOE, 1998). Nevertheless, there are at least three observations, which do not allow us to accept the dehydration hypothesis.

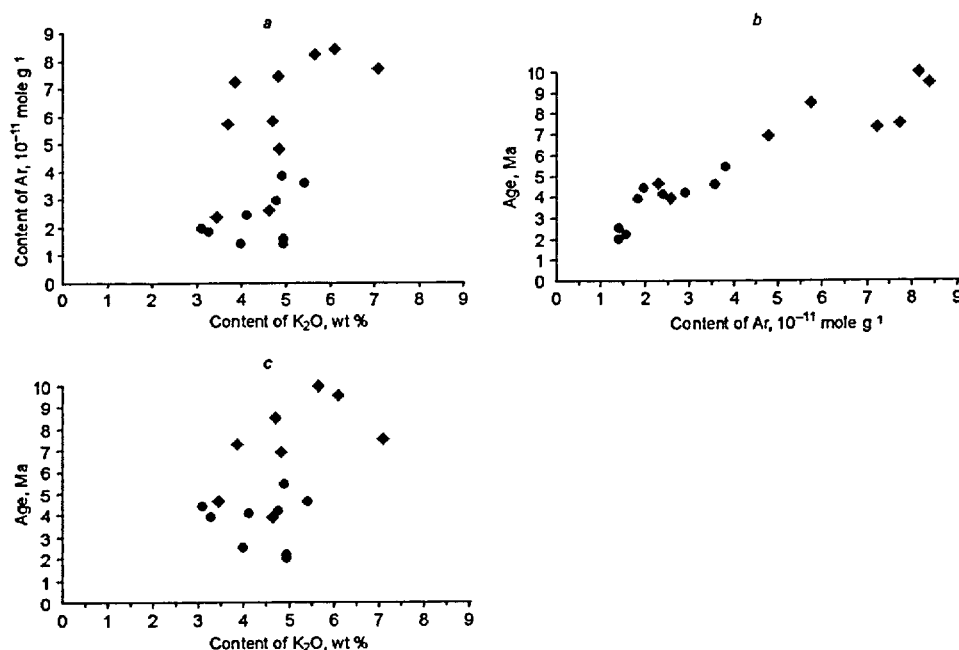


Figure 3-1-45. Cross-plots for the clinoptilolite separates: *a* -  $K_2O$  vs Ar; *b* - Ar vs. K/Ar age; and *c* -  $K_2O$  vs K/Ar age. *Circles* – clinoptilolite from the vadose zone; *diamonds* – clinoptilolite from the phreatic zone. Based on data from WoldeGabriel (1991), WoldeGabriel et al. (1992) and WoldeGabriel (1993).

First, based on the results of laboratory experiments alone, we do not know what the minimum value for the long-term Ar-loss activation temperature is. It is apparent from the Figure 3-1-37-*b* that, in experiments, dehydration begins at temperatures between 150 and 200 °C. Paleogeothermal data indicate, however, that the rocks in the vadose zone of Yucca Mountain have not had temperatures this high since the emplacement and initial cooling of the tuffs. As we have stated before, the average geothermal gradient, which was induced by the Timber Mountain hydrothermal metamorphism, did not exceed 72-85 °C·km<sup>-1</sup>, which translates into a 34-38 °C range of temperatures at the potential repository horizon. Some of the presumably dehydrated clinoptilolite specimens were collected directly at the topographic surface of Yucca Mountain (see Table 3-1-5-*a*). Thus, a necessary condition for DOE's dehydration hypothesis would require the long-term activation temperature to be close to the present-day ambient temperature, which is about 15 °C. Finally, the vadose zone is characterized by a high relative humidity ( $R_h = 90$ -100%), which poses a thermodynamic obstacle to zeolite dehydration.

Second, the dehydration hypothesis presumes that all of the K/Ar dated clinoptilolite specimens, including those residing in the upper aquifer, have been formed either immediately following emplacement of the tuffs or during the Timber Mountain hydrothermal metamorphism. Thus, this hypothesis not only does not account for the young specimens present below the present-day water table (see Figure 3-1-43), but it is inconsistent with these specimens. Although the position of the water table

may have been substantially higher in the past, it is totally without merit to suggest that past levels were some 200-300 m lower than they are now.

Third, the dehydration hypothesis does not seem to be supported by differing responses of the dated clinoptilolite specimens to the heavy-liquid purification procedure, which are shown on Figure 3-1-44. The figure shows that the dated specimens that represent the present-day vadose zone responded to the purification procedure by increasing their apparent age. By contrast, those of the dated specimens that represent the phreatic zone responded to this procedure by decreasing their apparent ages. The differing responses imply that relatively old K-bearing minerals, most probably adularia and/or mordenite contaminate the upper (younger) clinoptilolite specimens. These responses, therefore, further imply that the actual ages of the upper specimens are even younger than the apparent ages. In the same vein, the responses imply that the dated specimens from the phreatic zone, which are older, are overgrown by the younger K-bearing mineral phases, most likely mordenite. It is reasonable to assume that the upper specimens have been formed in the tuff, which already has been altered by K-rich solutions, so that they have become contaminated by the older K-bearing mineral phases, such as authigenic adularia. Likewise, it is reasonable to assume that the late growth was accompanied by a concurrent deposition of clinoptilolite and mordenite elsewhere, so that the older mineral phases in the phreatic zone have become overgrown by them.

#### 3.1.5.6. What Does the Apparent K/Ar Age vs. Depth Gradient Express?

The apparent K/Ar age vs depth gradient requires a contradiction-free explanation. Such an explanation may be constructed by first recognizing that the development of the laterally extensive zeolite horizons, such as those in the interior of Yucca Mountain, requires the presence of a vitric precursor material. This precursor material is then converted *in situ* into various zeolite species via hydration and ionic exchange reactions by fluids having the appropriate abundances of cations, aqueous silica, temperature, etc.

Nevertheless, zeolite species could also crystallize directly from ionic solutions, provided these solutions are sufficiently enriched in silica, aluminum, and alkali or alkaline earth cations. The precipitated zeolite species would be relatively scarce, occurring in the form of fracture- and cavity-lining coatings. Although such zeolite species do occur in the vadose zone (e.g., Carlos et al. 1995), we are not concerned here with such species, because the dated specimens are mostly from the altered rock matrix.

The rate of *in situ* conversion of volcanic glass is a process, which must vary in space and in time, reflecting both the changing alteration environment (temperature, fluid chemistry, salinity etc.) and the alteration-induced decreases of permeability. Further, the average long-term conversion rates increase

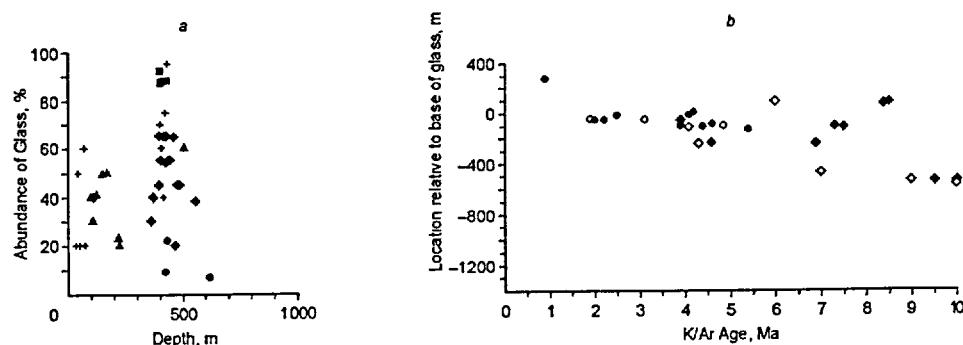


Figure 3-1-46. Abundance of the glass phase in rhyolite tuffs as a function of depth (a) and distribution of K/Ar ages relative to the present-day base of vitric zone (b).

a - Drill holes: circles - UE-25p#1; squares - USW G-1; triangles - USW G-2; diamonds - USW G-3; and crosses - USW G-4. Deepest known occurrence of the glass phase in drill hole UE-25 p#1 at depth of 613 m. In this drill hole, however, only traces of glass (less than 20 wt. %) were encountered. b - Clinoptilolite samples: circles - from the vadose zone; diamonds - from the phreatic zone; filled symbols - unpurified; and open symbols - purified.

Based on data from Bish and Chipera (1989), WoldeGabriel et al. (1992), and WoldeGabriel (1993).

with depth, which reflect the increasing temperature and availability of appropriately saline solutions. As the conversion progresses, the vitric material becomes gradually depleted and the rates of production of zeolite species diminish steadily. Eventually, the complete depletion of the vitric reservoir must take place, at which time further progress of the alteration is no longer possible, although temperature- or ionic exchange reaction-induced transformations may continue. Because the long-term alteration rates increase with depth, the complete reservoir depletion is most readily accomplished in deeper stratigraphic units, and gradually progresses toward the topographic surface.

The progressive depletion of the vitric reservoir in this manner results in the zeolite species being inevitably associated with three features. First, they exhibit multi-generation mineral agglomerates, or compounds. Second, at and near the ground surface the late generations are more abundant than the older ones. Third, the abundance of the older generations increases with depth, at the expense of the younger ones, so that the apparent K/Ar ages must increase with depth. All these three features are clearly expressed in the tuffs at Yucca Mountain.

Figure 3-1-46 confirms the preceding remarks. It shows the spatial extent of the present-day vitric zone and the generalized relationship between this zone and the apparent K/Ar clinoptilolite ages.

Figure 3-1-46-a shows that the vitric zone extends to a depth ranging from 424 m (drill hole USW G-1) to 618 m (drill hole UE-25p#1) and further that the glass abundance varies substantially between 9 and 95 wt.%. This zone hosted the K/Ar dated clinoptilolite specimens, which have yielded the apparent

ages between  $1.5 \pm 0.4$  and  $8.5 \pm 0.2$  Ma, as shown in Figure 3-1-46-*b* and Table 3-1-5. The older age is "mixed", which is indicated by the decreased age ( $6.0 \pm 1.0$  Ma, sample UE-25p#1 1740-1750, Table 3-1-5-*b*) of the heavy-liquid purified specimen.

Figure 3-1-46-*b* shows further that those specimens that have been produced by the Timber Mountain hydrothermal metamorphism, occur at a depth of about 400 m below the vitric zone, which roughly corresponds to the top of the analcime zone. These clinoptilolites seem to be those least affected by the purification procedure, which implies that the overgrowth by younger K-bearing mineral phases is at a minimum. The 400 m-thick section between the base of the vitric zone and the top of the analcime zone, which hosted those clinoptilolite specimens, yielded apparent ages between  $1.9 \pm 0.8$  and  $7.5 \pm 0.1$  Ma (Figure 3-1-46-*b*). Here, the response to the purification procedure is mixed, which means that some of the purified specimens yielded ages that are older than their unpurified counterparts, and vice versa. This response implies that some older K-bearing mineral phases (Timber Mountain) contaminate the youngest clinoptilolite specimens and, at the same time, some of the older clinoptilolite species are overgrown by the more recently produced minerals.

In light of the preceding observations, the apparent K/Ar age vs. depth gradient suggests an interpretation, which follows. The Timber Mountain hydrothermal episode has produced a high (more than  $100$  °C) temperature, which has persisted at a depth in excess of 800-m, for a period spanning between 1.0 and 1.5 Ma. The result of such prolonged thermal exposure of the tuffs was fairly intense and caused a pervasive alteration (both zeolite and montmorillonite) of these tuffs. The vitric reservoir was largely depleted at that time and, consequently, further zeolite alteration was effectively inhibited or arrested.

However, higher in the section, the Timber Mountain hydrothermal metamorphism was increasingly less intense and pervasive. In the densely welded units, such as the Topopah Spring and Tiva Canyon Members, this metamorphism appears to have been narrowly confined to faults and fractures. Here, the rate of vitric reservoir depletion was substantially lower and much of the glass phase escaped the conversion into the various zeolite species. Subsequent alteration events could have used the remaining glass to produce younger clinoptilolite species and other alteration minerals, including feldspar, smectite, silica polymorphs, heulandite, stellerite, laumontite, calcite, etc., as well. Some of the newly produced mineral phases were growing over the older ones, including the older clinoptilolite species. The resulting radiometric age overprinting, being a depth-dependent process is expressed in the form of the observed apparent K/Ar age vs. depth gradient. In reality, this gradient expresses a diminishing with depth probability of encountering the youngest alteration products.

### 3.1.5.7. Major Cation Composition as a Function of the Apparent K/Ar Ages

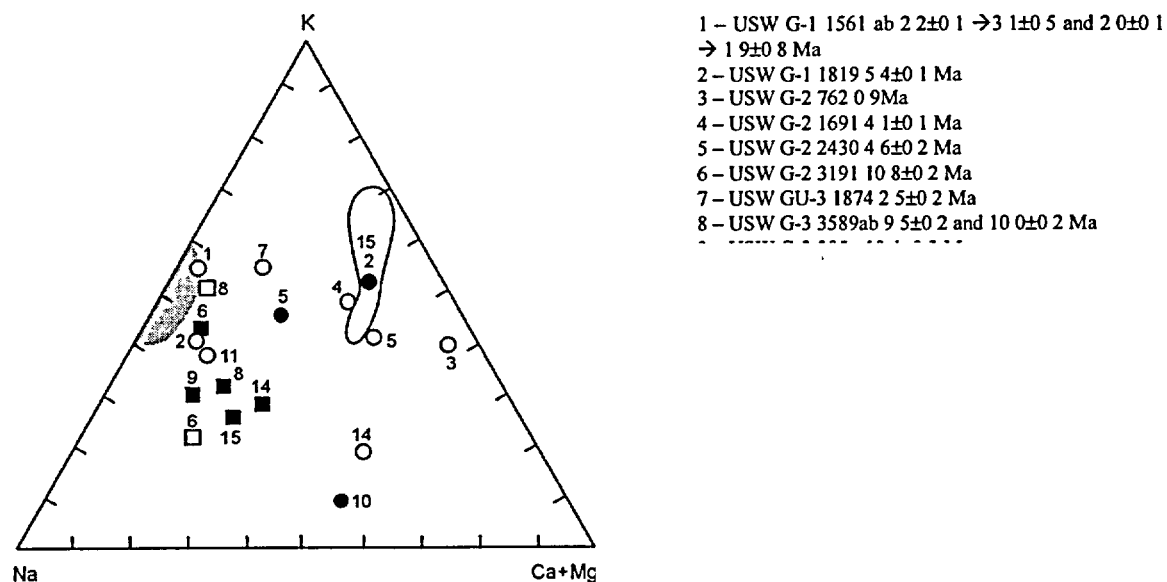


Figure 3-1-47. Compositions of the whole-rock tuffs and K/Ar dated clinoptilolite separated from these tuffs. *Open symbols* – dated clinoptilolite separates; *filled symbols* – corresponding whole-rock compositions; *circles* – K/Ar ages less than  $8.4 \pm 0.8$  Ma; and *squares* – K/Ar ages  $9.5 \pm 0.2$  to  $10.6 \pm 0.2$  Ma. *Shaded area* – unaltered glass compositions; *open area* – compositions of tuffs from surface outcrops at Prow Pass. Based on data from Broxton et al. (1986), WoldeGabriel et al. (1992), and WoldeGabriel (1993). Samples listed in the table under #12 and #13 are not shown on the diagram, since their chemistry was not reported.

It is important to note that the apparent K/Ar ages from the separated clinoptilolite specimens, support the earlier inferred overprinting of the Timber Mountain alteration by the alkaline-earth alteration aureole. This support is illustrated on Figure 3-1-47.

The figure shows the major cation compositions of the clinoptilolite separates and the associated whole-rock tuffs in relation to the apparent K/Ar ages. It also shows that the younger (less than 8.5 Ma) ages are associated with those alteration products, which are more enriched in Ca+Mg+K alkaline earth elements, as compared to the older alteration products. This enrichment may reasonably be attributed to the selectivity of clinoptilolite with respect to K, on one hand, and the increased abundance of the dissolved alkaline earth elements in fluids, which were involved in producing the overprinting, on the other.

Figure 3-1-47 further shows that some of the alteration products plot near the composition field for the parental glass, whereas the others deviate from this field by varying degrees. This pattern indicates that the glass conversion involved, first, hydration of the glass and, then, the continued ionic exchange reactions with alkaline earth bearing fluids. Because of these exchange reactions, the older alteration products acquired Na-rich compositions but the subsequent products acquired Ca+Mg-rich compositions.

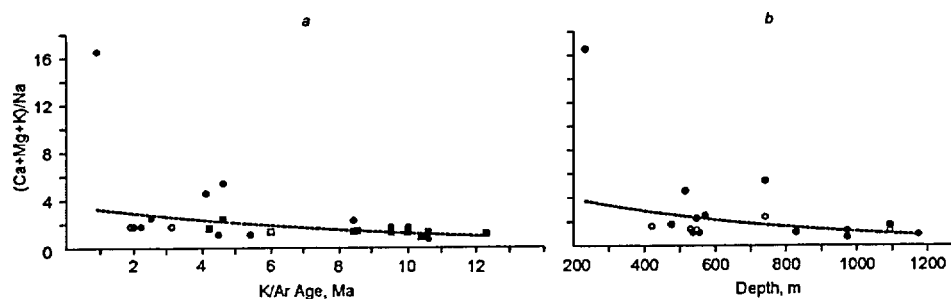


Figure 3-1-48.  $(Ca+Mg+K)/Na$  ratios from the dated clinoptilolite separates and the whole-rock tuffs from which these separates were extracted as a function of K/Ar apparent age (a) and depth (b).

a – Filled symbol – untreated specimen; open symbol – heavy-liquid purified specimen; circle – clinoptilolite separate; and square – tuff (whole rock analysis) from which the separate was extracted. b – Filled symbol – clinoptilolite separate; open symbol – tuff (whole rock analysis) from which the separate was extracted. Based on data from Broxton et al. (1986), WoldeGabriel et al. (1992) and WoldeGabriel (1993).

It is reasonable to conclude, therefore, that the apparent K/Ar ages reinforce the inferences drawn earlier concerning the relative ages of the two alteration aureoles.

Figure 3-1-48 depicts the  $(Ca+Mg+K)/Na$  ratios for the clinoptilolite separates and for the spatially associated whole-rock tuffs, which are plotted as a function of the apparent K/Ar ages and as a function of depth. It can be seen that average value of this ratio declines gradually as the depth and the apparent age increases. The gradual decline of this ratio expresses the gradually increasing with depth contribution of the Na-rich end-member, and thus, the increasing "signal" of the Timber Mountain hydrothermal metamorphism.

Figures 3-1-38 through 3-1-42 summarize all available data concerning the spatial distribution of the apparent K/Ar ages in the interior of Yucca Mountain. These figures also summarize all available data concerning the distribution of the chemical composition of the alteration products in relation to the present-day hydrologic setting. Collectively, these figures emphasize the following two important points:

First, the presence of relatively young alkaline earth enriched clinoptilolite specimens is not confined to the vadose zone, but instead, such specimens are also present in the phreatic zone. The same altering solutions were evidently acting upon the glass and produced alteration phases irrespective of the present-day hydrologic setting, which indicates that this setting is not a permanent feature of the hydrologic system at Yucca Mountain. Both depth and configuration of the potentiometric surface (water table) changed over time in response to hydrodynamic instabilities, which were induced by coupled episodic alterations of the *in situ* stress and temperature fields.

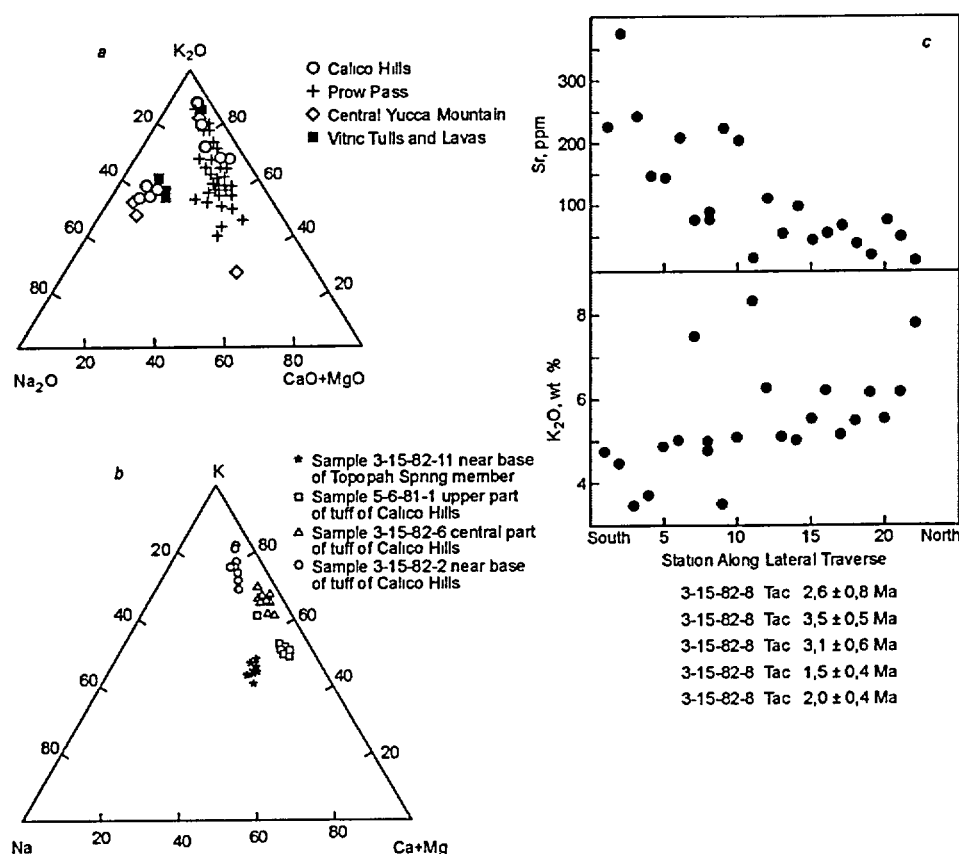


Figure 3-1-49. Chemistry of the K/Ar dated separates and/or chemistry and mineralogy of their surrounding surface outcrops of the Tuff of Calico Hills at Prow Pass in the northern Yucca Mountain area. From Broxton (1992) (a and b), Broxton et al. (1986) (c), and age dates from WoldeGabriel (1993); sample 3-15-82-8 is from the outcrop of the Calico Hills tuff; see Table 3-1-5-a). Tuff units sampled in the south-north profile (graph c) are not specified in the original paper.

Second, the spatial distribution of the alkaline earth alteration aureole is highly asymmetric, relative to both the topographic surface and the stratigraphic boundaries. This alteration aureole is thick in the north and east sectors of Yucca Mountain, where it extends to the phreatic zone. At Prow Pass, it occurs directly at the topographic surface and extends below the Tuff of Calico Hills (Tac) to some unknown depth. The alteration overprinting is clearly expressed by the major cation composition of both the whole-rock tuff and the corresponding clinoptilolite specimens, in addition to being expressed by the inversely correlated Sr- and K- enrichments. The major cation compositions and the inversely correlated enrichments are shown on Figure 3-1-49.

Figure 3-1-49 indicates that the K-enriched whole rock and clinoptilolite species (Timber Mountain K-metasomatism) were interacting with Ca+Mg+Sr-bearing solutions. This figure also shows that the

doubly altered clinoptilolite specimens (4) carry apparent K/Ar ages between  $1.5 \pm 0.4$  and  $3.5 \pm 0.5$  Ma. The overprinting Sr-enrichment varies laterally, which demonstrates that this enrichment was not caused by infiltrating rainwater, on one hand, and that it is most probably fault-based, on the other.

Returning to the shape of the alkaline earth alteration aureole, Figure 3-1-30 indicates that in USW G-2 the bottom of this aureole is between the Tuff of Calico Hills (Tac) and the Prow Pass Member (Tcp). However, in USW G-4 this bottom is deeper, between the Bullfrog Member (Tcb) and the Tram Member (Tct), as shown on Figure 3-1-35. In drill hole UE-25p#1 the bottom of the alkaline earth alteration aureole is below the Lithic Ridge Tuff (Tlr) (see Figure 3-1-32), extending all the way down to the Paleozoic carbonates of the basement.

By contrast, in the west and south sectors of Yucca Mountain, the alkaline earth alteration aureole is both thinner and shallower. In drill holes USW G-1 and USW GU-3, the bottom of this aureole is confined to the Paintbrush Tuff (Tpt), as shown on Figures 3-1-33 and 3-1-34.

The asymmetry of the overprinting aureole creates the illusion that in the south and west sectors of Yucca Mountain the alteration and the corresponding calcite-silica vein mineralization are restricted to the vadose zone (whereas in reality, this alteration extends well into the phreatic zone in the northern and eastern sectors). Many scientists (see Paces et al., 1996 and Denniston et al., 1997), who are associated with the Yucca Mountain Project, do not appear to be aware of this illusion. They simply use the, changing with depth, properties ( $^{87}\text{Sr}/^{86}\text{Sr}$ ,  $\delta^{13}\text{C}$ , REE patterns, etc.) of the calcite-silica deposits from the south and west sectors to "demonstrate" the association of these deposits with the topographic surface.

#### 3.1.5.8 Concluding Remarks

In summary, there are no rational grounds to support the viewpoint that the K/Ar ages, particularly those from specimens that, spatially, are associated with the alkaline earth alteration aureole, are erroneous because of the post-depositional losses of  $^{40}\text{Ar}$ . Nevertheless, these ages are apparent in a sense that they are composite or mixed ages from variable agglomerates of K-bearing minerals, some of which were overgrown by younger species and some of which are contaminated by the older species. It is clear, however, that these apparent ages do provide important insights into the alteration history of the tuffs at Yucca Mountain.

Particularly important is the fact that the apparent clinoptilolite K/Ar ages do not contradict the conclusion that the zeolite and whole-rock chemical alteration has continued long after cessation of the Timber Mountain hydrothermal metamorphism. On the contrary, these ages validate the earlier inference that the alkaline earth alteration aureole overprints (post-dates) the alkali alteration aureole, which has been produced by the Timber Mountain hydrothermal metamorphism. These ages therefore can be

regarded as recording the intermittent ascension of alkaline earth solutions, from the basement into the overlying tuffs over the past 8-9 Ma, which in principle further validates the conceptual model proposed in Part II of this book.

## Chapter 3-2. Thermodynamic modeling of rhyolite – meteoric water interaction at Yucca Mountain

*By G.P. Palyanova, S.Z. Smirnov, and Y.V. Dublyansky*

### Table of contents

<b>Chapter 3-2. Thermodynamic modeling of rhyolite – meteoric water interaction at Yucca Mountain</b>	<b>110</b>
3.2.1. Model formulation	111
3.2.2. Input parameters	111
3.2.3. Calculation method	113
3.2.4. Results	115
3.2.4.1. Submodel 1 - Interaction of rainwater equilibrated with atmospheric CO <sub>2</sub> (pCO <sub>2</sub> = 0.003 bar) with rhyolite at T = 25-100°C	115
3.2.4.2. Submodel 2 - Interaction of rainwater equilibrated with soil CO <sub>2</sub> (pCO <sub>2</sub> =0.01 bar) with rhyolite at T = 25°C	119
3.2.4.3. Submodel 3 - Interaction of rainwater equilibrated with CaCO <sub>3</sub> with rhyolite at T = 25-100°C	119
3.2.4.4. Saturation of Yucca Mountain ground waters in respect to the secondary minerals	120
3.2.5. Evaluation of secondary assemblages observed at Yucca Mountain in light of the results of the thermodynamic modeling	121
3.2.5.1. Estimation of the reaction advancement rate (or rock-to-water ratio, R/W)	122
3.2.5.2. Mineral assemblages	123
3.2.6. Concluding remarks	125

## Chapter 3-2. Thermodynamic modeling of rhyolite – meteoric water interaction at Yucca Mountain

*By G.P. Palyanova, S Z Smirnov, and Y.V. Dublyansky*

As stated in Chapter 3-1, the only conceptual alternative to the proposed hydrothermal upwelling model is a model attributing the deposition of secondary minerals in the vadose zone to rainwater, percolating through the mountain and reacting with soils and the bedrock tuffs. This concept was presented in numerous publications (e.g., Roedder et al. 1994, Paces et al., 1998, Whelan and Moscati, 1998, and others) and is presently endorsed by U.S. DOE as the "official" model (U.S. DOE 1998 and 2001).

After the discovery in the secondary minerals in Yucca Mountain of the two-phase fluid inclusions, indicating temperatures of the mineral forming waters of up to 85°C (Dublyansky and Reutsky, 1995; Dublyansky et al. 1998, 1999, and 2001), the "rainwater concept" had to be modified to accommodate these new data. It now envisages a process involving the percolation of rainwater through a hot rock mass in the vadose zone. At least two models were advanced in order to explain how the rocks in the vadose zone become hot. Marshall and Whelan (2000) suggested that the rock mass was conductively heated by a putative magma chamber, residing underneath the Timber Mountain caldera, some 8-10 km north of Yucca Mountain. In turn, Whelan et al. (2001) suggested that the rocks in the vadose zone could have been heated by conductive heat transfer from thermal waters that circulated under the mountain (at a depth of  $\cong$  1000 m) during the Timber Mountain Caldera hydrothermal event 10-11 Ma ago. (The thermal history of Yucca Mountain will be discussed in Chapter 3-8).

In this section we evaluate the thermodynamic constraints on the composition of minerals that may be expected to form within the "rainwater concept". Specifically, we attempt to evaluate whether the formation of such mineral phases as calcite, quartz, amorphous silica, fluorite, and other minerals reported from the Yucca Mountain unsaturated zone is thermodynamically possible in the postulated setting. More data on the subject matter can be found in Palyanova et al. (2002).

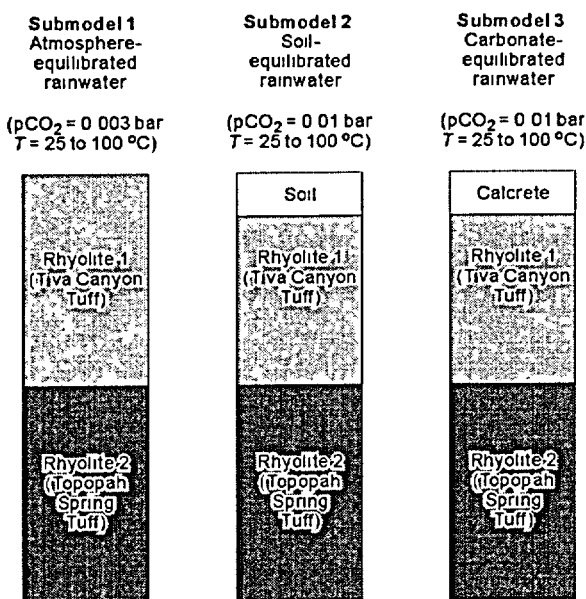


Figure 3-2-1. Composition of rock columns in three submodels examined by thermodynamic modeling.

### 3.2.1. Model formulation

In our analysis, the mineral forming solution acquires its mineral composition as it percolates through a column of rocks. We examined the following three hypothetical situations (Figure 3-2-1). *Submodel 1*: the rock column is composed of rhyolitic tuffs, and percolating water is equilibrated with atmosphere ( $p\text{CO}_2 = 0.003$  bar); *Submodel 2*: the same, except percolating water is equilibrated with soil atmosphere ( $p\text{CO}_2 = 0.01$  bar); and *Submodel 3*: Before entering the tuffs, water equilibrates with carbonate deposits. We believe that the natural system at Yucca Mountain is more adequately approximated by the open

system and have carried all the calculation at  $p\text{O}_2 = 0.2$  bar, corresponding to the atmospheric values.

### 3.2.2. Input parameters

**Tuff.** We assume that percolating water interacts with tuffs that have already passed the stage of diagenesis and vapor-phase alteration/zeolitization. This permits the usage of actual chemical compositions of the Yucca Mountain tuffs as input parameters. For this study we obtained X-ray fluorescence analyses of the Tiva Canyon and Topopah Spring tuffs collected in the ESF. Special precautions were taken to obtain chemical data from unaltered tuff samples. The results of the analysis are given in Table 3-2-1.

Table 3-2-1

## Chemistry of volcanic rocks used for thermodynamic modeling (wt. %)

Specimen #	569209	569201	569208	569205
ESF Station	North portal	76+17.8	14+25	35+89
Tuff (stratigraphic Unit)	Tiva Canyon	Topopah Spring upper vitrophyre	Topopah Spring crystal-rich	Topopah Spring middle non-lithophysal
TiO <sub>2</sub>	0.16	0.34	0.50	0.11
SiO <sub>2</sub>	76.03	69.32	67.86	76.03
Al <sub>2</sub> O <sub>3</sub>	12.95	14.81	16.39	12.71
Fe <sub>2</sub> O <sub>3</sub>	1.14	1.97	2.47	1.36
MgO	0.10	0.25	0.31	0.08
MnO	0.14	0.14	0.15	0.14
CaO	0.25	1.08	1.36	0.57
Na <sub>2</sub> O	3.83	3.91	4.56	3.48
K <sub>2</sub> O	4.76	5.26	5.96	4.95
P <sub>2</sub> O <sub>5</sub>	0.01	0.06	0.10	0.03
F*	0.01	0.032	0.032	0.017
LOI	0.62	2.72	0.33	0.52
Total	99.99	99.86	99.99	99.98

XRF analyses were performed in the Institute of Mineralogy and Petrography, Russian Academy of Science, Siberian Branch, Novosibirsk, Russia. Analyst L.D. Kholodova. \* - Fluorine was determined by photospectrometric method in the Analytical Center of United Institute of Geology, Geophysics and Mineralogy, Russian Academy of Science, Siberian Branch, Novosibirsk, Russia. Analyst I.M. Fominykh.

Table 3-2-2

## Compositions of rainwater and groundwater from wells drilled within proposed repository area

Well #	Depth, m	Ca	Mg	Na	K	Cl	SO <sub>4</sub>	Si	F	HCO <sub>3</sub>	TDS	Saturation at		pH
												25°C	100°C	
Rain water	0	0.02	0.02	0.03	-	0.07	0.04	0.01	-	0.38	30	-	-	-
USW G-4	mean	0.3	0.0	2.5	0.1	0.2	0.2	0.8	0.1	2.3	320	Qtz, Chl	Cat	7.7
UE 25b#1	863-875	0.5	0.1	2.0	0.1	0.2	0.2	0.9	0.1	2.5	340	Qtz	Cat	7.6
UE 25p#1 (shallow)	381-1197	0.9	0.4	4.0	0.1	0.4	0.4	0.4	0.2	4.6	520	Qtz, Chl	Cat	6.8
UE 25p#1 (deep)	1297+	2.5	1.6	6.5	0.3	0.8	1.7	0.7	0.3	9.4	1,140	Cat, Qtz, Chl, FI	Cat, FI	6.6

Notes: Contents are in mmole·l<sup>-1</sup>; TDS is in ppm. Cat – calcite; Qtz – quartz; Chl – chalcedony; and FI – fluorite. All groundwater data are from volcanic aquifer except UE25 p#1 (deep) representing carbonate aquifer in Paleozoic rocks underlying the Miocene volcanic sequence at Yucca Mountain. Data on rainwater are from Yang et al (1996), on groundwater – from Ebinger (1992).

For the modeling we used two model compositions: (1) Rhyolite 1 corresponding to the Tiva Canyon tuff (Table 3-2-1, sample 569209) and (2) Rhyolite 2 corresponding to the average composition of the Topopah Spring tuff from Table 3-2-1.

**Water.** We used the composition of rainwater from the Yucca Mountain area, as reported by Yang et al. (1996) and presented in Table 3-2-2. For the Submodel 3 calculations ("carbonate rainwater"), this water was "saturated" with calcium carbonate before interaction with rhyolites.

Taking into account the data presented above, as well as compositions of the groundwaters tapped by boreholes in the Yucca Mountain area (Table 3-2-2), for modeling the rhyolite-water system we used a 14-component system: Si-Al-Na-K-Ca-Mg-Fe-F-Cl-P-S-C-H-O. In order to simplify calculations we excluded Ti, which does not form separate mineral phases in rhyolite. Also, we counted MnO along with FeO. The method of this approach was developed by Ryzhenko et al. (1996).

Since the modeling was carried out at constant  $P$  and  $T$ , according to the Gibbs rule, the non-variant composition of the modeled 14-component system must consist of the 11 solid phases and an aqueous fluid. Calculations revealed that the number of solid phases at high rock-to-water (R/W) ratios reaches 10. The water fluid, therefore, may be unsaturated with respect to some phases. These might be chlorides of N, K, Mg, pyrite, or gypsum. Their precipitation is possible only from the highly mineralized solutions ( $R/W \geq 2 \cdot 10^2$ ). Such high rock-to-water ratios, however, seem to be unrealistic for Yucca Mountain setting.

### 3.2.3. Calculation method

For thermodynamic calculations we used a set of computer codes, *Hch* by Shvarov (1999), which employs a minimization of free energy approach. The starting thermodynamic parameters for the dissolved species and mineral phases, pertinent to the rhyolite-water system, were compiled from a database by Robie and Hemingway (1995), and databases *UNITHERM* (Shvarov, 1999), *SUPCRT98* (Shock and Helgeson 1988; Sverjensky et al. 1991, 1997; Shock et al. 1997). Most calculations were performed for  $T = 25$  °C and  $P_{tot} = 1$  bar; some calculations were carried out for  $T = 50, 75,$  and  $100$  °C and  $P_{tot} = 100$  bar. For calculations of the activity coefficients of the dissolved species in the *Hch* code we used the Debye-Huckel equations (third approximation). The list of minerals, taken into account for modeling the water-rhyolite interaction, consisted of the 54 phases. The water phase of the studied system is described by a set of 114 dissolved species (Table 3-2-3).

Thermodynamic calculations were done by the method of the reaction rate, which is expressed through the rock-to-water (R/W) ratio. This parameter is widely used in geochemical modeling as an indicator of (a) intensity of water exchange, or (b) volume ratios between the solid and aqueous phase, or

(c) depth of water infiltration. The modeled R/W ratios (which is, the amount of rock, in kg, reacted with 1 kg of water) varied from  $10^{-5}$  to  $10^2$ . These values generally bracket the total range reported for hydrogeologic systems in crystalline rocks.

Table 3-2-3

## Minerals and aqueous species considered in the thermodynamic model

Element	Minerals	Aqueous species
Si	SiO <sub>2</sub> (quartz, silica glass, chalcedony), CaSiO <sub>3</sub> (wollastonite), CaMgSi <sub>2</sub> O <sub>6</sub> (diopside), CaAl <sub>2</sub> Si <sub>3</sub> O <sub>8</sub> (anorthite), CaAl <sub>2</sub> Si <sub>2</sub> O <sub>6</sub> (OH) <sub>4</sub> (lawsonite), CaAl <sub>2</sub> Si <sub>4</sub> O <sub>12</sub> *4H <sub>2</sub> O (laumontite), CaAl <sub>2</sub> Si <sub>7</sub> O <sub>18</sub> *6H <sub>2</sub> O (heulandite), Mg <sub>2</sub> SiO <sub>4</sub> (forsterite), MgSiO <sub>3</sub> (enstatite), KAISi <sub>3</sub> O <sub>8</sub> (microcline, sanidine), KMg <sub>3</sub> AlSi <sub>3</sub> O <sub>10</sub> (OH) <sub>2</sub> (phlogopite), KFe <sub>3</sub> AlSi <sub>3</sub> O <sub>10</sub> (OH) <sub>2</sub> (annite), KAl <sub>3</sub> Si <sub>3</sub> O <sub>10</sub> (OH) <sub>2</sub> (muscovite), Fe <sub>2</sub> SiO <sub>4</sub> (fayalite), Fe <sub>3</sub> Al <sub>2</sub> (SiO <sub>4</sub> ) <sub>3</sub> (almandine), Fe <sub>4</sub> Al <sub>4</sub> Si <sub>2</sub> O <sub>10</sub> (OH) <sub>8</sub> (daphnite), K <sub>0.6</sub> Mg <sub>0.25</sub> Al <sub>2.3</sub> Si <sub>3.5</sub> O <sub>10</sub> (OH) <sub>2</sub> (illite), NaAlSi <sub>3</sub> O <sub>8</sub> (albite), Na(AlSi <sub>2</sub> O <sub>6</sub> )*H <sub>2</sub> O analcite, NaCa <sub>2</sub> Mg <sub>4</sub> Al <sub>3</sub> Si <sub>6</sub> O <sub>24</sub> H <sub>2</sub> (pargasite), NaAl <sub>3</sub> Si <sub>3</sub> O <sub>10</sub> (OH) <sub>2</sub> (paragonite)	H <sub>3</sub> SiO <sub>4</sub> , H <sub>3</sub> SiO <sub>4</sub> <sup>-</sup> , SiF <sub>4</sub> , SiF <sub>5</sub> <sup>-</sup> , SiF <sub>6</sub> <sup>2-</sup> , Si(OH) <sub>2</sub> F <sub>2</sub> , HSiO <sub>3</sub> <sup>-</sup> , NaHSiO <sub>3</sub>
Al	Al <sub>2</sub> O <sub>3</sub> (corundum), KAISi <sub>3</sub> O <sub>8</sub> (microcline, sanidine), KMg <sub>3</sub> AlSi <sub>3</sub> O <sub>10</sub> (OH) <sub>2</sub> (phlogopite), KFe <sub>3</sub> AlSi <sub>3</sub> O <sub>10</sub> (OH) <sub>2</sub> (annite), KAl <sub>3</sub> Si <sub>3</sub> O <sub>10</sub> (OH) <sub>2</sub> (muscovite), K <sub>0.6</sub> Mg <sub>0.25</sub> Al <sub>2.3</sub> Si <sub>3.5</sub> O <sub>10</sub> (OH) <sub>2</sub> (illite), KAl <sub>3</sub> [SO <sub>4</sub> ] <sub>2</sub> (OH) <sub>6</sub> (alunite)	Al <sup>3+</sup> , Al(OH) <sup>2+</sup> , Al(OH) <sub>2</sub> <sup>+</sup> , Al(OH) <sub>3</sub> , Al(OH) <sub>4</sub> <sup>-</sup> , AlF <sup>2+</sup> , AlF <sub>2</sub> <sup>+</sup> , AlF <sub>3</sub> , AlF <sub>4</sub> <sup>-</sup> , AlOH <sup>+</sup> , AlOH <sub>2</sub> <sup>+</sup> , Al(OH) <sub>2</sub> F
K	KAISi <sub>3</sub> O <sub>8</sub> (microcline, sanidine), KMg <sub>3</sub> AlSi <sub>3</sub> O <sub>10</sub> (OH) <sub>2</sub> (phlogopite), KFe <sub>3</sub> AlSi <sub>3</sub> O <sub>10</sub> (OH) <sub>2</sub> (annite), KAl <sub>3</sub> Si <sub>3</sub> O <sub>10</sub> (OH) <sub>2</sub> (muscovite), K <sub>0.6</sub> Mg <sub>0.25</sub> Al <sub>2.3</sub> Si <sub>3.5</sub> O <sub>10</sub> (OH) <sub>2</sub> (illite), KAl <sub>3</sub> [SO <sub>4</sub> ] <sub>2</sub> (OH) <sub>6</sub> (alunite), K-montmorillonite	K <sup>+</sup> , KOH, KCl, KSO <sub>4</sub> <sup>-</sup> , KHSO <sub>4</sub>
Na	NaAlSi <sub>3</sub> O <sub>8</sub> (albite), Na(AlSi <sub>2</sub> O <sub>6</sub> )*H <sub>2</sub> O analcite, NaCa <sub>2</sub> Mg <sub>4</sub> Al <sub>3</sub> Si <sub>6</sub> O <sub>24</sub> H <sub>2</sub> (pargasite), NaAl <sub>3</sub> Si <sub>3</sub> O <sub>10</sub> (OH) <sub>2</sub> (paragonite), Na-montmorillonite	Na <sup>+</sup> , NaOH, NaSO <sub>4</sub> <sup>-</sup> , NaCl, NaF, NaCO <sub>3</sub> <sup>-</sup> , NaHCO <sub>3</sub> , NaHS, NaHSiO <sub>3</sub>
Ca	CaAl <sub>2</sub> Si <sub>3</sub> O <sub>8</sub> (anorthite), CaAl <sub>2</sub> Si <sub>2</sub> O <sub>6</sub> (OH) <sub>4</sub> (lawsonite), CaAl <sub>2</sub> Si <sub>4</sub> O <sub>12</sub> *4H <sub>2</sub> O (laumontite), CaAl <sub>2</sub> Si <sub>7</sub> O <sub>18</sub> *6H <sub>2</sub> O (heulandite), Ca-montmorillonite, CaF <sub>2</sub> (fluorite), Ca(OH) <sub>2</sub> <sup>-</sup> (portlandite), CaCO <sub>3</sub> (calcite, aragonite), CaSO <sub>4</sub> *2H <sub>2</sub> O (gypsum), Ca <sub>5</sub> (PO <sub>4</sub> ) <sub>3</sub> (OH) (apatite-OH), Ca <sub>5</sub> (PO <sub>4</sub> ) <sub>3</sub> F (apatite-F), CaSO <sub>4</sub> (anhydrite)	Ca <sup>2+</sup> , CaOH <sup>+</sup> , CaCO <sub>3</sub> , CaHCO <sub>3</sub> <sup>+</sup> , CaSO <sub>4</sub> , CaF <sup>+</sup> , CaCl <sup>+</sup> , CaCl <sub>2</sub> , CaHSiO <sub>3</sub> <sup>+</sup>
Fe	Fe <sub>2</sub> O <sub>3</sub> (hematite), Fe <sub>3</sub> O <sub>4</sub> (magnetite), FeOOH (goethite), FeS <sub>2</sub> (pyrite, marcasite), Fe <sub>2</sub> SiO <sub>4</sub> (fayalite), Fe <sub>3</sub> Al <sub>2</sub> (SiO <sub>4</sub> ) <sub>3</sub> (almandine), Fe <sub>4</sub> Al <sub>4</sub> Si <sub>2</sub> O <sub>10</sub> (OH) <sub>8</sub> (daphnite), KFe <sub>3</sub> AlSi <sub>3</sub> O <sub>10</sub> (OH) <sub>2</sub> (annite), FeCO <sub>3</sub> (siderite)	Fe <sup>2+</sup> , Fe(OH) <sup>+</sup> , Fe(OH) <sub>2</sub> , Fe(OH) <sub>3</sub> <sup>-</sup> , FeSO <sub>4</sub> , FeCl <sup>+</sup> , FeCl <sub>2</sub> , Fe <sup>3+</sup> , Fe(OH) <sup>2+</sup> , Fe(OH) <sub>2</sub> <sup>+</sup> , Fe(OH) <sub>3</sub> , Fe(OH) <sub>4</sub> <sup>-</sup> , FeF <sup>2+</sup> , FeCl <sup>2+</sup>
Mg	Mg(OH) <sub>2</sub> (brucite), Mg <sub>2</sub> SiO <sub>4</sub> (forsterite), CaMgSi <sub>2</sub> O <sub>6</sub> (diopside), MgSiO <sub>3</sub> (enstatite), Mg-montmorillonite, NaCa <sub>2</sub> Mg <sub>4</sub> Al <sub>3</sub> Si <sub>6</sub> O <sub>24</sub> H <sub>2</sub> (pargasite), CaMg(CO <sub>3</sub> ) <sub>2</sub> (dolomite), MgCO <sub>3</sub>	Mg <sup>2+</sup> , MgOH <sup>+</sup> , MgCO <sub>3</sub> , MgHCO <sub>3</sub> <sup>+</sup> , MgSO <sub>4</sub> , MgF <sup>+</sup> , MgCl <sup>+</sup> , MgCl <sub>2</sub> , MgOHCl, MgHSiO <sub>3</sub>

Table 3-2-3 (continued)

Minerals and aqueous species considered in the thermodynamic model

Element	Minerals	Aqueous species
P	Ca <sub>5</sub> (PO <sub>4</sub> ) <sub>3</sub> (OH) (apatite-OH), Ca <sub>5</sub> (PO <sub>4</sub> ) <sub>3</sub> F (apatite-F)	PO <sub>4</sub> <sup>3-</sup> , HPO <sub>4</sub> <sup>2-</sup> , H <sub>2</sub> PO <sub>4</sub> <sup>-</sup> , H <sub>3</sub> PO <sub>4</sub> , P <sub>2</sub> O <sub>7</sub> <sup>4-</sup> , HP <sub>2</sub> O <sub>7</sub> <sup>3-</sup> , H <sub>2</sub> P <sub>2</sub> O <sub>7</sub> <sup>2-</sup> , H <sub>3</sub> P <sub>2</sub> O <sub>7</sub> <sup>-</sup> , H <sub>4</sub> P <sub>2</sub> O <sub>7</sub> , HPO <sub>3</sub> <sup>2-</sup> , H <sub>2</sub> PO <sub>3</sub> <sup>-</sup> , H <sub>3</sub> PO <sub>3</sub>
C	C (graphite), CaCO <sub>3</sub> (calcite, aragonite), CaMg(CO <sub>3</sub> ) (dolomite), MgCO <sub>3</sub> (magnesite), FeCO <sub>3</sub> (siderite)	CO <sub>2</sub> , HCO <sub>3</sub> <sup>-</sup> , CO <sub>3</sub> <sup>2-</sup> , CH <sub>4</sub> , C <sub>2</sub> H <sub>6</sub> , HCOO <sup>-</sup> , HCOOH, CH <sub>3</sub> COO <sup>-</sup> , CH <sub>3</sub> COOH
S	S (sulfur), CaSO <sub>4</sub> *2H <sub>2</sub> O (gypsum), FeS <sub>2</sub> (pyrite, marcasite), KAl <sub>3</sub> [SO <sub>4</sub> ] <sub>2</sub> (OH) <sub>6</sub> alunite, CaSO <sub>4</sub> (anhydrite)	H <sub>2</sub> S, HS <sup>-</sup> , S <sub>2</sub> <sup>2-</sup> , S <sub>2</sub> O <sub>3</sub> <sup>2-</sup> , SO <sub>2</sub> , SO <sub>3</sub> <sup>2-</sup> , HSO <sub>3</sub> <sup>-</sup> , HSO <sub>4</sub> <sup>-</sup> , SO <sub>4</sub> <sup>2-</sup>
F	CaF <sub>2</sub> (fluorite), Ca <sub>5</sub> (PO <sub>4</sub> ) <sub>3</sub> F (apatite-F)	F <sup>-</sup> , HF, HF <sub>2</sub> <sup>-</sup>
Cl	NaCl (halite)	Cl <sup>-</sup> , HCl, NaCl, ClO <sup>-</sup> , HClO, ClO <sub>2</sub> <sup>-</sup> , HClO <sub>2</sub> , ClO <sub>4</sub> <sup>-</sup>
H		H <sub>2</sub> , H <sup>+</sup> , OH <sup>-</sup> , H <sub>2</sub> O
O		O <sub>2</sub>

### 3.2.4. Results

#### 3.2.4.1. Submodel 1 - Interaction of rainwater equilibrated with atmospheric CO<sub>2</sub> (pCO<sub>2</sub> = 0.003 bar) with rhyolite at T = 25-100°C

The evolution of mineral assemblages at different temperatures is shown in Figure 3-2-2. At  $T = 25$  °C and  $P_{tot} = 1$  bar and increasing R/W ratios, equilibrium mineral assemblages evolve in the manner described in the following paragraphs (see Figure 3-2-2-*a* and -*b*).

The first phase precipitation from rainwater that reacted with rhyolite occurred at  $R/W = 10^{-5}$ . At this point the secondary assemblage consisted of major quartz, kaolinite and accessory hematite. (It is to be noted that in this thermodynamic model hematite can be regarded as an analogue of Fe- and Mn-oxides). At  $R/W = 10^{-4}$  to  $10^{-3}$  kaolinite gives way to major microcline and muscovite in association with quartz. At these R/W ratios, accessory calcite and dolomite began to form along with F-apatite. Albite appeared in the major-mineral assemblage at  $R/W=10^{-2}$ . Fluorite appeared in tiny amounts among accessory minerals only at  $R/W = 10^0$ . Negligible amounts of gypsum (not shown in Figure 3-2-2) appeared at an extremely large R/W ( $\sim 10^1$ ). Waters reacting with rhyolite evolved with an increasing R/W ratio from silica-chloride-sulfate (at  $R/W = 10^{-5}$ ) through silica-potassium-sodium-bicarbonate (at  $R/W = 10^{-4}$ ) to

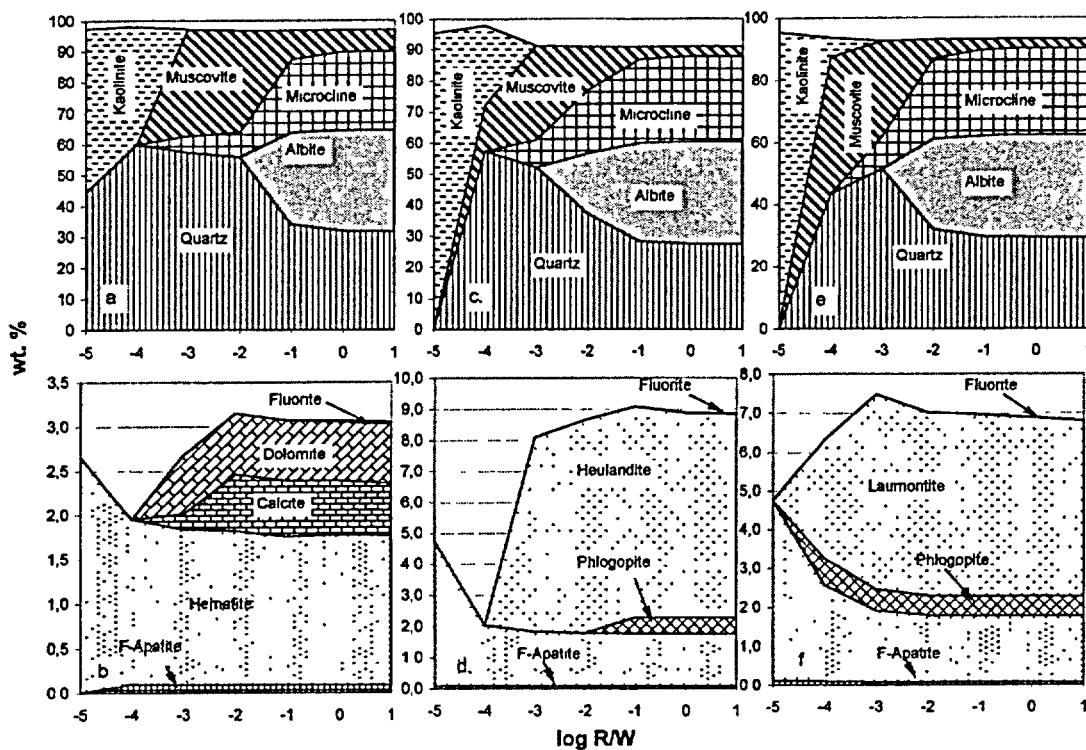


Figure 3-2-2. Thermodynamically stable mineral assemblages for Submodel 1 (atmosphere-equilibrated rainwater reacting with rhyolite tuff). Upper row – major minerals; lower row – accessory minerals. *a* and *b* –  $T = 25^\circ\text{C}$ ,  $P_{tot} = 1$  bar; *c* and *d* –  $T = 50^\circ\text{C}$  and  $P_{tot} = 100$  bar; *e* and *f* –  $T = 100^\circ\text{C}$  and  $P_{tot} = 100$  bar.

sodium-bicarbonate (at  $R/W \geq 10^{-3}$ ) (Table 3-2-4). The initial acidic pH of the rainwater (3.82) increased with increasing  $R/W$  toward near-neutral and later alkaline values (up to 9.4).

Molal concentrations of the components in the aqueous phase at elevated temperatures (50 and 100 °C) are shown in Table 3-2-5, and the proportions of the mineral phases in Figure 3-2-2-*c* through *f*. The figure shows that major mineral assemblages at  $T = 50$  and  $100^\circ\text{C}$  ( $P_{tot} = 100$  bars) are similar to those forming at  $T = 25^\circ\text{C}$ . The formation of the major minerals (except kaolinite), however, begins at higher  $R/W$  ratios. The most important changes are established for accessory minerals. At  $T > 50^\circ\text{C}$  carbonates do not form, while zeolites (heulandite and laumontite) and phlogopite dominate along with hematite. Small amounts of fluorite may form, at any temperatures, only at a very high  $R/W$  ratio ( $\geq 10^0$ ).

The concentration of dissolved elements changes with increasing temperature, but nevertheless, the dominant components at  $25^\circ\text{C}$  and at higher temperatures are the same (compare Tables 3-2-4 and 3-2-5). No significant changes in pH are detected in the Submodel 1 at elevated temperatures.

Table 3-2-4

Model compositions of water solution forming through reaction of rainwater  
with Yucca Mountain rhyolites at  $T = 25^{\circ}\text{C}$  and  $P_{tot} = 1$  bar.

Element	Reaction advancement degree (rock-to-water ratio, RW)						
	$10^{-5}$	$10^{-4}$	$10^{-3}$	$10^{-2}$	$10^{-1}$	$10^0$	$10^1$
Solution, log m <sub>i</sub>							
Si	-4.00	-4.00	-3.96	-3.82	-3.82	-3.82	-3.82
Al	-5.70	-8.47	-7.80	-7.00	-7.00	-7.02	-8.00
	-8.08	-8.03					
K	-4.66	-3.66	-3.92	-4.64	-4.64	-4.60	-4.59
		-3.92					
Na	-4.60	-3.60	-2.60	-1.60	-1.59	-1.55	-1.54
Ca	-5.66	-4.70	-4.02	-4.92	-4.92	-4.89	-4.89
	-3.25	-3.36					
Fe	-8.96	-9.44	-9.44	-9.44	-9.44	-9.44	-9.43
Mg	-6.14	-5.14	-5.48	-6.57	-6.55	-6.48	-6.47
Cl	-4.17	-4.17	-4.17	-4.17	-4.17	-4.17	-4.17
F	-6.75	-5.82	-4.82	-3.82	-2.82	-2.28	-2.26
	-6.82						
P	-6.96	-9.28	-11.41	-12.68	-10.10	-10.36	-10.34
	-6.70	-11.92					
C	-5.00	-3.42	-2.59	-2.96	-1.70	-1.72	-1.72
	-3.00	-2.96					
S	-4.37	-4.37	-4.37	-4.37	-4.37	-4.37	-4.37
TDS, ppm	18	55	250	670	1870	1930	1950
	101	112					
pH	4.03	7.88	8.71	9.48	9.47	9.44	9.44
	8.29	8.34					
Eh, mV	0.98	0.75	0.7	0.66	0.66	0.66	0.66

**Note:** If compositions are shown on two lines, the upper line corresponds to the "atmospheric CO<sub>2</sub>-equilibrated" model water and the lower line corresponds to the "soil CO<sub>2</sub>-equilibrated" model water. If only one value appears in a cell, the model results are similar for both types of model waters.

Table 3-2-5

Model compositions of water solutions resulted from reaction of rainwater with Yucca Mountain rhyolites at  $T = 50$  and  $100^\circ\text{C}$ ,  $P_{tot} = 100$  bars

Element	T°C	Reaction advancement degree (rock-to-water ratio, RW)						
		$10^{-5}$	$10^{-4}$	$10^{-3}$	$10^{-2}$	$10^{-1}$	$10^0$	$10^1$
		Content in solution, log m <sub>i</sub>						
Si	50	-3.72	-3.57	-3.49	-3.34	-3.34	-3.39	-3.44
	100	-3.72	-3.04	-2.82	-2.80	-2.82	-2.96	-4.00
Al	50	-6.57	-7.38	-6.68	-6.17	-6.17	-6.28	-6.35
	100	-6.89	-5.92	-5.09	-5.01	-5.10	-5.46	-5.48
K	50	-5.66	-3.82	-4.17	-4.64	-4.64	-4.52	-4.59
	100	-4.66	-4.19	-4.52	-4.59	-4.49	-4.11	-4.14
Na	50	-4.66	-3.60	-2.60	-1.96	-1.96	-1.85	-1.92
	100	-5.66	-4.70	-7.14	-7.10	-6.77	-5.82	-2.05
Ca	50	-5.66	-4.70	-4.64	-5.13	-5.13	-5.04	-5.10
	100	-5.66	-4.96	-6.30	-6.38	-6.26	-5.60	-5.64
Fe	50	-8.82	-9.13	-9.13	-9.12	-9.12	-9.13	-9.19
	100	-8.35	-8.51	-8.48	-8.48	-8.49	-8.49	-8.52
Mg	50	-6.14	-5.14	-6.17	-6.85	-6.85	-6.60	-6.66
	100	-6.14	-5.14	-8.24	-8.33	-8.09	-7.08	-7.10
Cl	50-100	-4.17	-4.17	-4.17	-4.17	-4.17	-4.17	-4.17
F	50	-6.74	-5.82	-4.82	-3.82	-2.82	-2.21	-2.19
	100	-6.74	-5.82	-4.82	-3.82	-2.82	-2.08	-2.10
P	50	-6.96	-8.72	-9.74	-8.82	-9.21	-9.62	-9.68
	100	-6.96	-8.96	-7.62	-7.80	-8.31	-9.35	-9.38
C	50	-5.29	-5.14	-2.64	-2.07	-2.09	-6.96	-2.25
	100	-5.54	-4.03	-2.92	-2.85	-2.96	-3.31	-3.34
S	50-100	-4.37	-4.37	-4.37	-4.37	-4.37	-4.37	-4.37
pH	50	4.01	7.96	8.81	9.30	9.28	9.19	9.18
	100	4.02	7.83	8.89	8.96	8.87	8.50	8.50
Eh	50	0.94	0.69	0.63	0.60	0.60	0.60	0.61
	100	0.86	0.57	0.50	0.49	0.50	0.52	0.52

### 3.2.4.2. Submodel 2 - Interaction of rainwater equilibrated with soil CO<sub>2</sub> (pCO<sub>2</sub>=0.01 bar) with rhyolite at T = 25°C

Equilibrium mineral assemblages obtained within the Submodel 2 are the same as in the calculations for the rhyolite/water interaction within Submodel 1. At R/W = 10<sup>-5</sup> the assemblages consist of quartz, kaolinite, and hematite. At R/W = 10<sup>-4</sup> F-apatite appeared. Microcline, muscovite, calcite, and dolomite joined the assemblage at R/W = 10<sup>-3</sup> to 10<sup>-2</sup>, while kaolinite disappeared at R/W = 10<sup>-2</sup>. Fluorite appeared in the system somewhat earlier (at R/W = 10<sup>-1</sup>) than in the system equilibrated with atmospheric CO<sub>2</sub>. Gypsum appeared at R/W = 10<sup>2</sup>. Thus, the major effect of the excess CO<sub>2</sub> added to the system is that the solubility of fluorite decreased and it appeared as a mineral phase at lower reaction advancement rates (or rock-to-water ratios). Differences in the proportions of precipitating quartz, microcline, albite and muscovite were insignificant.

The increase of pCO<sub>2</sub> (up to 0.01 bar) led to a corresponding increase of the HCO<sub>3(aq)</sub> abundance, and an increase in the acidity of the model solutions. The solutions, forming as the result of interaction with rhyolite at pCO<sub>2</sub> = 0.01 bar and R/W ≥ 10<sup>-3</sup>, had a sodium-bicarbonate composition with a higher total mineralization (for example at R/W = 10<sup>1</sup> for pCO<sub>2</sub> = 0.01 bar the [Na] = 0.16 m and [HCO<sub>3</sub>] = 0.14 m, whereas for pCO<sub>2</sub> = 0.003 bar, [Na] = 0.029 m and [HCO<sub>3</sub>] = 0.019 m). For all R/W ratios, the pH of solutions with pCO<sub>2</sub> = 0.01 bar was lower than the pH for solutions with pCO<sub>2</sub> = 0.003 by ≅ 0.7 units. Generally, water containing an excess of CO<sub>2</sub> has a somewhat higher ability to react with rhyolites.

### 3.2.4.3. Submodel 3 - Interaction of rainwater equilibrated with CaCO<sub>3</sub> with rhyolite at T = 25-100°C

In order to model a hypothetical situation in which the percolating rainwater passes through a layer of calcretes or carbonatized soil before reacting with the tuffs, we calculated the composition of the solutions, which equilibrated with calcite. The pH of such solutions was as high as 8.29 and the [Ca] = 5·10<sup>-4</sup> m. In reality, solutions with a pH intermediate between “normal” rainwater values of 3.82 to the “carbonate-equilibrated water” values of 8.29 may exist. For further calculations we conservatively used waters with the highest degree of saturation with respect to calcite.

Figure 3-2-3 shows the compositions of secondary assemblages that originated from carbonate-equilibrated rainwater reacting with tuffs at different R/W ratios and temperatures. It is obvious that the major differences between the models involving carbonate-free and carbonate-bearing waters appeared only at small R/W ratios (< 10<sup>-3</sup>). At T = 25°C and R/W = 10<sup>-5</sup>, the content of calcite in the mineral assemblage may reach ≅ 12 wt. %. With an increasing R/W ratio, the share of calcite decreased and its precipitation became impossible at R/W = 10<sup>-2</sup>. The calcite fraction was greater in assemblages forming at elevated temperatures, but its precipitation ceased at smaller R/W ratios (10<sup>-5</sup> to 10<sup>-3</sup>). The most important

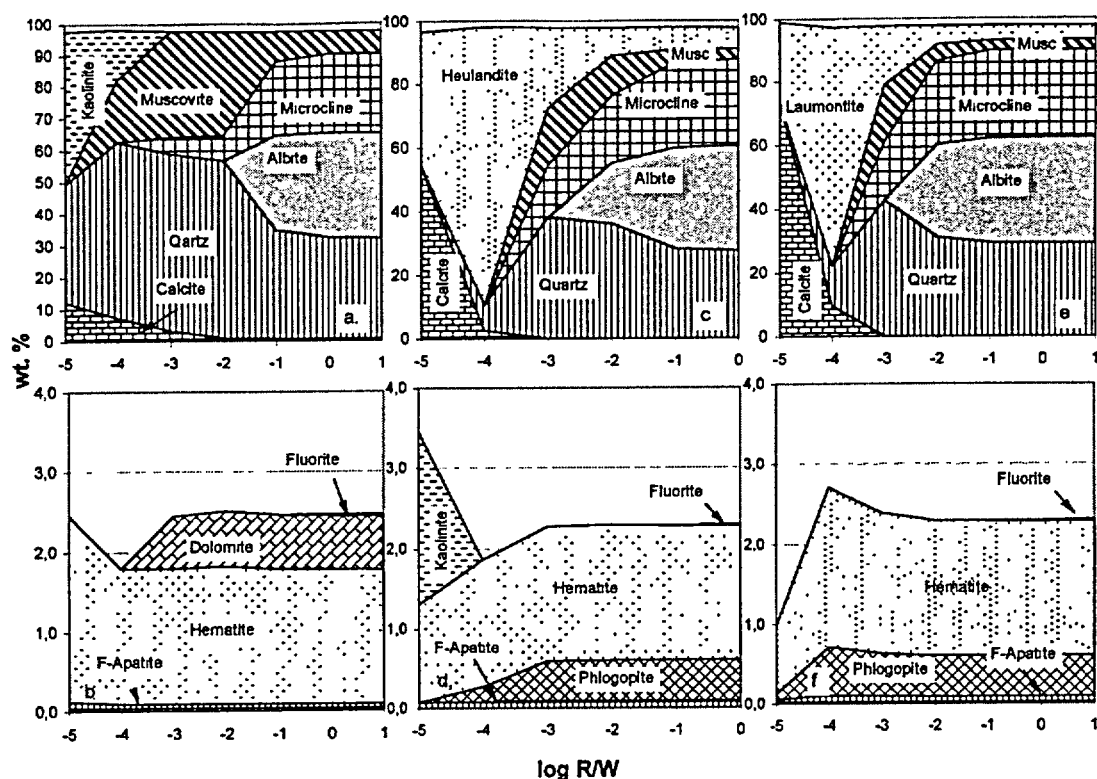


Figure 3-2-3. Thermodynamically stable mineral assemblages for Submodel 3 (carbonate-equilibrated rainwater reacting with rhyolite tuff). Upper row – major minerals; lower row – accessory minerals. *a* and *b* –  $T = 25\text{ }^{\circ}\text{C}$ ,  $P_{tot} = 1\text{ bar}$ ; *c* and *d* –  $T = 50\text{ }^{\circ}\text{C}$  and  $P_{tot} = 1\text{ bar}$ ; *e* and *f* –  $T = 100\text{ }^{\circ}\text{C}$  and  $P_{tot} = 1\text{ bar}$ .

feature of the assemblages, formed at higher temperatures (50 to  $100^{\circ}\text{C}$ ) was the domination of zeolites at smaller  $R/W$  ratios. At  $R/W > 10^{-3}$  the overall character of the assemblages became similar to that of the "carbonate-free rainwater" model. As the reaction advancement rate increased, carbonate-equilibrated rainwater became more alkaline, and at  $R/W \geq 10^{-3}$  it acquired a pH similar to that of carbonate-free water.

As is apparent from Figure 3-2-3, the accessory minerals are dominated by hematite. Fluorite appeared only at  $R/W > 10^{-1}$  and in extremely small amounts.

#### 3.2.4.4. Saturation of Yucca Mountain ground waters in respect to the secondary minerals

According to our thermodynamic calculations the major species of silicon at a pH, ranging from 3.8 to 9.5, is  $\text{H}_4\text{SiO}_4$ . At a given pH, potassium, sodium, calcium and magnesium existed in the cationic form ( $\text{K}^+$ ,  $\text{Na}^+$ ,  $\text{Ca}^{2+}$  and  $\text{Mg}^{2+}$ ). The iron was transported as  $\text{Fe}(\text{OH})_3$ . Chlorine and fluorine formed anions  $\text{Cl}^-$  and  $\text{F}^-$ . Sulfur occurred in the solution as the sulfate-ion  $\text{SO}_4^{2-}$ . As the pH changes from weakly acidic to alkaline, the dominant forms of aluminum and carbon changed from  $\text{Al}(\text{OH})_3$  to  $\text{Al}(\text{OH})_4^-$  and from  $\text{H}_2\text{CO}_3$  to  $\text{HCO}_3^-$ .

Table 3-2-6

Calculated saturation of the present day ground water from the Yucca Mountain area  
in respect to some important secondary minerals

T, °C	Well	Cat	Flu	Chl	Qtz	SiO <sub>2</sub> (a)
25	UE 25b#1	-	-	-	-	-
	USW G-4	-	-	+	-	-
	UE 25p#1 (deep)	+	+	+	+	-
50	UE 25b#1	+	-	-	-	-
	USW G-4	-	-	-	-	-
	UE 25p#1 (deep)	+	-	-	-	-
100	UE 25b#1	+	-	-	-	-
	USW G-4	+	-	-	-	-
	UE 25p#1 (deep)	+	-	-	-	-

**Notes:** Cat - calcite, Qtz - quartz, Chl - chalcedony, Flu - fluorite, and SiO<sub>2</sub>(a) – amorphous silica + - water is saturated, - - water is unsaturated. Wells UE 25b#1 and USW G-4 represent volcanic aquifer; well UE 25p#1 (deep) represents carbonate aquifer in Paleozoic rocks beneath Yucca Mountain. Based on the data from the Table 3-2-2.

In order to assess the degree of saturation of different waters at Yucca Mountain relative to the potentially possible saturation levels in the studied system, we used the data from Table 3-2-2 and the *Hch* computer code. The results are shown in Table 3-2-6. It is apparent from the table that waters from the volcanic aquifer tapped by different boreholes are saturated with respect to silica minerals but are unsaturated with respect to calcite at temperatures less than 50-75 °C. By contrast, the waters of the carbonate aquifer tapped by the deep part of the UE 25p#1 borehole are saturated with respect to both calcite and fluorite over the whole temperature range (from 25 to 100 °C) and with respect to silica minerals at temperatures up to 50 °C.

### *3.2.5. Evaluation of secondary assemblages observed at Yucca Mountain in light of the results of the thermodynamic modeling*

In order to evaluate the Yucca Mountain Project's "rainwater" concept of mineral deposition at Yucca Mountain, we addressed the following questions:

- What are the realistic reaction advancement rates (or R/W ratios) that could have been achieved during the interaction between percolating rainwater and tuffs?

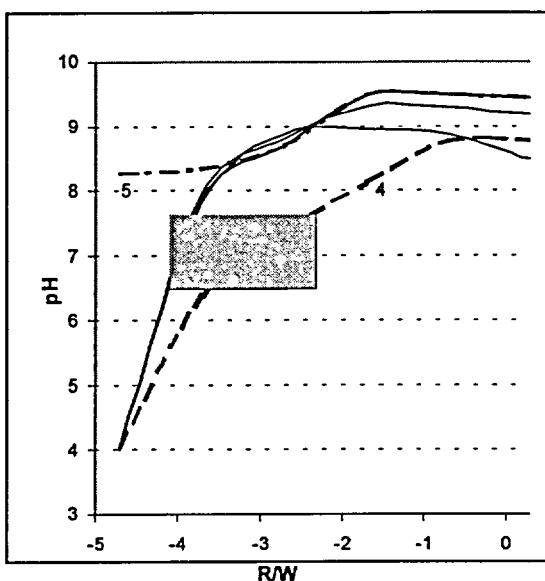


Figure 3-2-4. pH vs. R/W diagram for model solutions forming through rainwater-rhyolite interaction at  $T = 25$  to  $100^{\circ}\text{C}$ . 1 -  $T = 25^{\circ}\text{C}$  and  $p\text{CO}_2 = 0.003$  bar, 2 -  $T = 50^{\circ}\text{C}$  and  $p\text{CO}_2 = 0.003$  bar, 3 -  $T = 100^{\circ}\text{C}$  and  $p\text{CO}_2 = 0.003$  bar, 4 -  $T = 25^{\circ}\text{C}$  and  $p\text{CO}_2 = 0.01$  bar, 5 - carbonate equilibrated water at  $T = 25^{\circ}\text{C}$ . Shaded area - pH range for present day ground waters of volcanic aquifer and corresponding R/W interval.

reaction models. The modern-day groundwater from the rhyolite aquifer at Yucca Mountain has a pH ranging from 6.6 to 7.7. Within the carbonate-free rainwater reaction model, percolating water reaches these pH values at  $R/W \leq 10^{-4}$  ( $T = 25^{\circ}\text{C}$ ). Rainwater equilibrated with soil  $\text{CO}_2$  would reach the modern-day pH at a higher R/W ratio of  $\cong 10^{-3}$ . Rainwater equilibrated with carbonate would acquire a pH of 1 to 2 units greater than that of the present-day waters even at an extremely small R/W ratio.

Another way of assessing the R/W ratio is provided by the total mineralization of the ground waters (TDS). The TDS values of modern waters from the volcanic aquifer at Yucca Mountain fall between 300 and 1,100 ppm (see Table 3-2-2), which corresponds to model R/W ratios of  $10^{-3}$  to  $10^{-2}$ . Besides being similar in terms of their pH and total mineralization, the model waters with  $R/W = 10^{-4}$  to  $10^{-3}$  have similar, although not identical, chemical compositions (Figure 3-2-5). We estimate, therefore, that the most realistic R/W ratios that were achieved in the meteoric water/tuff interaction did not exceed  $10^{-3}$ . Assuming that temperature does not affect the pH significantly at the small R/W ratios, we believe the reaction advancement rates were similar within a 25 to  $100^{\circ}\text{C}$  interval.

- How similar are the chemical compositions of the actual Yucca Mountain ground waters and the model solutions?
- How similar are the compositions of the observed and the model mineral assemblages?

### 3.2.5.1. Estimation of the reaction advancement rate (or rock-to-water ratio, R/W)

Groundwater of the rhyolite aquifer has resided in the volcanic rocks for thousands of years; hence, it may be considered to be the result of a quite evolved interaction between meteoric precipitation and rhyolites. The pH of such waters may, therefore, be used to establish an upper bound on the pH values expected for waters reacting with the tuffs. Figure 3-2-4 shows the pH vs R/W ratio dependence for both carbonate-free and carbonate-equilibrated rainwater

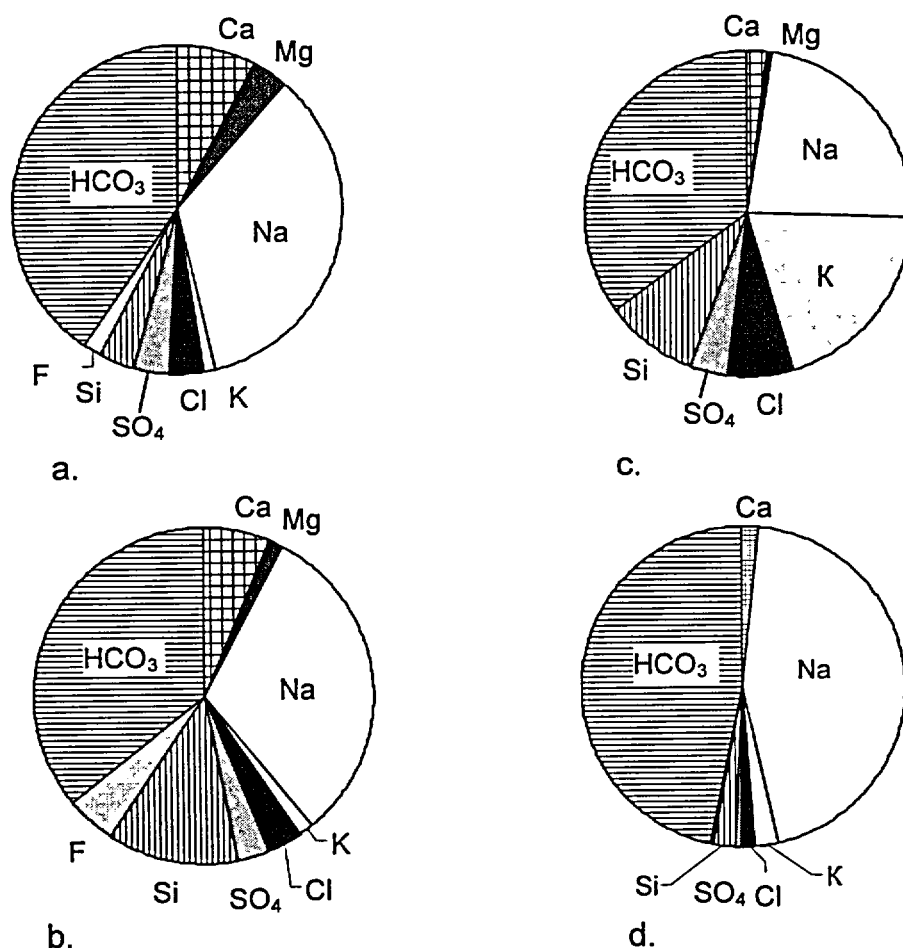


Figure 3-2-5. Compositions of present day ground waters (*a – b*) compared with model compositions at  $R/W = 10^{-4}$  to  $10^{-3}$  (*c – d*).

*a* – UE-25p#1 381-1197 m; *b* – USW G4; *c* – model composition at  $R/W=10^{-4}$ ; *d* – model composition at  $R/W=10^{-3}$

### 3.2.5.2. Mineral assemblages

The peculiarities of the Yucca Mountain secondary mineral assemblages, as they are observed in the whole-rock alteration and fractures, were partly covered in Chapter 3-1 and will be further discussed in detail in Chapter 3-4. In short, the dominating whole-rock alteration minerals are silicates (clay and hydromica minerals, zeolites), while fracture-lining parageneses are dominated by calcite and silica polymorphs. The zoned distribution of secondary minerals was detected on both the repository block scale and the individual mineral crust scale.

If the assessment of the  $R/W$  ratios made above is correct, the major minerals in the secondary assemblages should be quartz, kaolinite, microcline, and muscovite. In the early stages of the rock-water

interaction (low R/W), kaolinite and quartz dominate in the calculated mineral assemblage. In the more advanced stages, kaolinite does not form, but muscovite and microcline form instead. Similar assemblages would have formed through the interaction between hydrothermal chloride-carbonate acidic hydrothermal solutions with liparitic rocks at 150°C, as was demonstrated by Barsukov and Borisov (1989).

The whole-rock alteration assemblages at Yucca Mountain differ substantially with the calculated thermodynamically stable assemblages. The observed assemblages of clinoptilolite, heulandite and smectite clays do not match the assemblages forming in both carbonate-free and carbonate-equilibrated rainwater models. The Figure 3-2-3 clearly shows that heulandite- or laumontite-dominated associations may form at estimated realistic R/W ratios, but only at elevated temperatures and from carbonate-saturated fluids. Calculated equilibrium assemblages, however, do not contain any clay minerals because Al is consumed by zeolite. At somewhat higher R/W ratios, smaller amounts of secondary microcline and muscovite would be in equilibrium, and Al would redistribute between these minerals.

According to the Ostwald step rule, smectites and hydromica, which have common structures and compositions, can be regarded as metastable analogues of muscovite. It thus becomes apparent that the secondary mineral assemblages described in Chapter 3-1 could be metastable assemblages, indicating relatively short residence times of fluids and their specific chemistry (excess of K). These features make untenable the hypothesis that the Yucca Mountain secondary minerals are the result of the downward percolation of meteoric waters.

Major minerals of fracture lining assemblages are calcite and silica polymorphs (quartz, chalcedony, and opal; see Section 3.4.3.1. for details). Thermodynamic modeling unequivocally demonstrates that calcite cannot be formed as a major component of the paragenesis through the interaction of rainwater with Yucca Mountain rhyolites. Even after being equilibrated with carbonate prior to interaction with rhyolite, meteoric waters percolating from the surface would form silicate-dominated assemblages at the estimated range of pH.

The set of accessory minerals in the modeled assemblages is dominated by hematite. By contrast, the actually observed assemblages contain only minor amounts of hematite, which, most likely, is syngenetic with tuffs (vapor-phase alteration stage). In the thermodynamic calculations, hematite may be regarded as an analogue of manganese oxides. At Yucca Mountain, the Mn-oxides are subordinate (at least in the ESF mineral assemblages). They are confined primarily to thin fractures, the formation of which is thought to be prior to the "main stage" calcite (Carlos et al., 1995-*b*).

The appearance of accessory heulandite in silica- and calcite-dominated fracture linings at Yucca Mountain (Smirnov and Dublyansky, 2001-*a* and *b*) is possible only at elevated temperatures ( $\geq 50^\circ\text{C}$ ).

The most important conclusion from the thermodynamic modeling, however, is that fluorite would not form in secondary mineral assemblages at the estimated R/W ratios. The formation of fluorite through the interaction of surficial water with rhyolites required extremely high R/W ratios, which seems to be totally unrealistic for mineral deposits formed in the vadose zone at a depth of only 50 to 300 m from the surface (i.e., flow path for hypothetical mineral forming rainwater would be very short). In addition, fluorite always occurred as an accessory mineral in the model assemblages, whereas at Yucca Mountain fluorite was also found in mono-mineral occurrences (Smirnov and Dublyansky, 2001-*a*; see Section 3.4.3.2.2. for details).

The aggregate-scale mineral zoning was reported for the Yucca Mountain mineral assemblages (Smirnov and Dublyansky 2000-*a*), but this zoning does not correspond to the thermodynamically defined sequence described above. The large-scale vertical zoning of secondary minerals, expected for the "rainwater" concept is not observed in the repository block. The Yucca Mountain Project researchers interpret zoning with an elevated abundance of silica minerals near the North portal of the ESF (see Section 3.4.4.2.) as an expression of vertical zoning (because the ESF North Ramp inclination intersects the stratigraphically higher Tiva Canyon tuff near the North Portal and it penetrates deeper in the Topopah Spring tuffs) (Whelan, 2000, pers. comm.). If this was, indeed, the case, the character of the zoning (quartz and chalcedony located closer to the surface and calcite dominating the deeper parts of the mountain) would be exactly opposite to the thermodynamically controlled sequence in which calcite must be more abundant at lower R/W ratios (i.e., closer to the surface) and getting more scarce as the R/W ratios increase deeper along the percolation path.

### *3.2.6. Concluding remarks*

The results of our thermodynamic modeling indicate that mineral assemblages, similar to those observed in the Yucca Mountain vadose zone, cannot form as the result of an interaction of downward percolating rainwater with calcretes and rhyolitic tuffs. There are fundamental discrepancies between the observed and the thermodynamically stable compositions for both major and accessory minerals. A number of minerals that, based on thermodynamics, should have been formed (e.g., major kaolinite, muscovite, microcline, albite and accessory hematite) are not observed in the Yucca Mountain mineral assemblages at all. On the other hand, the most abundant accessory minerals from actual Yucca Mountain assemblages, fluorite and heulandite, should not form from percolating waters at realistic R/W ratios.

In order to address the recent modification of the "rainwater concept", which now envisages percolation of rainwaters through the hot rock mass, we examined the thermodynamics of the system in the 25-100 °C temperature interval. Calculations show that increased temperatures do not change

significantly the composition of the depositing mineral phases. Increased temperatures, therefore, do not make the observed and the calculated compositions of mineral assemblages compatible.

An additional corroboration of this conclusion comes from our calculations, which demonstrate that modern waters from volcanic aquifers (which reflect a rather evolved degree of water-rock interaction) cannot serve as the parent solutions for the secondary mineral assemblages observed in the Yucca Mountain vadose zone.

The only natural waters known at Yucca Mountain that are compatible with the chemistry of secondary mineralization are the waters of the deep carbonate aquifer tapped under Yucca Mountain by the UE25 b#1 borehole. Even at 25 °C, these waters are saturated with respect to all major secondary minerals of the Yucca Mountain assemblage, as well as to the most abundant accessory mineral – fluorite.

## Chapter 3-3. Calcite-Silica Deposits at the Topographic Surface

*By J.S. Szymanski and Y.V. Dublyansky*

### Table of contents

<b>Chapter 3-3. Calcite-Silica Deposits at the Topographic Surface</b>	<b>128</b>
3.3.1. Field Appearances and the Questions They Provoke	130
3.3.2. Lithofacies	136
3.3.2.1. AMC breccias	136
3.3.2.2. Bedrock veins and slope-parallel calcretes	140
3.3.2.3. Carbonate coatings of clasts	145
3.3.3. Stable isotopes	147
3.3.3.1. Carbon isotopes	147
3.3.3.1.1. Pedogenic setting	147
3.3.3.1.2. Spring setting	151
3.3.3.2. Oxygen	152
3.3.3.2.1. Pedogenic setting	152
3.3.3.2.2. Spring setting	153
3.3.3.3. Isotopic trends and correlations in pedogenic calcite and aquifer water	154
3.3.3.3.1. Pedogenic carbonates	154
3.3.3.3.2. Aquifer water	155
3.3.3.4. Isotopic trends and correlations in travertine calcite	155
3.3.3.5. Discussion: The use of stable carbon and oxygen isotopes as environmental indicators	155
3.3.3.5.1. Comparative approach	155
3.3.3.5.2. Trend analysis	156
3.3.3.5.3. Correlation analysis	156
3.3.4. Isotopes of the $^{238}\text{U}$ Decay Series	157
3.3.5. Pb-Isotope Ratios	160
3.3.6. Redox Potential	164
3.3.7. Gases trapped in fluid inclusions	167
3.3.8. Trace-element geochemistry of surface deposits	170
3.3.9. Rare Earth Elements	172
3.3.10. Concluding Remarks	176

## Chapter 3-3. Calcite-Silica Deposits at the Topographic Surface

*By J.S. Szymanski and Y.V. Dublyansky*

The topographic surface and alluvial, colluvial and soil deposits of the environs of Yucca Mountain are extensively coated and cemented with calcium-bearing deposits. In some places, horizons of eolian sand and coarse colluvium, which may be two to three meters thick, are cemented with micritic calcite and to a lesser degree by opaline silica. Field relationships indicate that these deposits are very young. Cracks and fractures in the tuffs also, in places, host veins of the micritic calcite and silica. The bedrock consists of alkali tuffs that contain very little Ca, so that the obvious question is what is the source of calcium in the carbonate-silica deposits. Even a brief inquiry in that regard leads to a conclusion that this source must be an ancient (early Paleozoic) sequence of marine carbonates of the basement. Extensive outcroppings of these carbonates occur to the west, to the east, and to the south of Yucca Mountain; they also occur underneath it, as was demonstrated in the course of exploratory drilling (e.g., borehole UE25 p#1).

How the minerals were transported to the topographical surface is the difficult question. The Yucca Mountain Project scientists believe that the minerals were transported laterally in the form of windblown, calcium bearing dust. Formation of the calcite-opal deposits is envisioned as a variant of the pedogenic (or soil-forming) process, whereby extraneous carbonate material accumulates in soils, alluvium, colluvium, and on the bedrock surfaces, through multiple cycles of dissolution and deposition caused by interactions between atmospheric precipitation and soil gases (the "rainwater concept"). By contrast, our opinion is that many of these carbonate-silica minerals were formed as a result of the discharge, at the topographic surface of Yucca Mountain, of waters that ascended along fault zones from great depth (the "hydrothermal upwelling concept").

In support of the officially adopted "rainwater" concept, the Yucca Mountain Project scientists present a set of facts, which they regard as indisputable. They suggest that the facts indicate that the deposits in question were formed from meteoric water, that this water was cool at the time of deposition, that it was not present-day aquifer water, etc. The summary of the arguments is provided in the recent U.S. DOE Yucca Mountain Science and Engineering Report (U.S. DOE, 2001):

Several types of isotopic data can be used to demonstrate that local groundwater was not involved in the formation of the Trench 14 veins. ... Oxygen isotopes in the calcite found in veins at Trench 14

indicate that their origin would have been at unreasonably low temperatures if they had been precipitated from either of the aquifers beneath Yucca Mountain. Carbon isotopes preclude involvement of the deepest groundwater aquifer at Yucca Mountain. Strontium in the vein deposit has a greater proportion of the isotope strontium-87 than strontium found in either aquifer beneath Yucca Mountain, which precludes the involvement of either aquifer in the formation of the veins. In contrast, the isotopic composition of strontium in the Trench 14 deposits is within the range of measured for soil deposits, which is permissive evidence for formation of the deposits by soil-forming process. The uranium-234/uranium-238 activity ratio in groundwater beneath Yucca Mountain is anomalously large relative to most groundwaters (greater than 5 in the volcanic aquifer). In comparison, the uranium-234/uranium-238 activity ratio values for both soils and the calcite from Trench 14 are less than 1.5. This isotopic system again shows that the local groundwater could not have formed the deposits, but that they may be closely related to soil-forming process. Finally, lead isotope data also support a pedogenic origin for the calcite and identify a detrital origin as the probable source of the silicate lead. (pp. 4-400 - 4-401).

It is our opinion that, even though these purported facts may be compatible with the "rainwater" origin, none of them definitely proves that the deposits were formed from "*infiltrating rainwater in a desert environment.*" For example, the fact that a slope-parallel calcrete deposit and a bedrock vein share the same stable and radiogenic isotope signatures means no more than that both of them share the same origin, it offers no proof about what the origin is. The fact that the radiogenic isotope signatures of the present-day aquifer fluids (which occur hundreds of meters below the surface) are different from those of the parental fluids for the subject deposits does not mean that minerals and waters fell from the sky to produce these minerals. The fact that the subject deposits carry uraniumogenic Pb indicates only that the lead originated in marine carbonates, but it suggests nothing about how it was transported to the surface. The fact that the deposits carry similar stable isotope signatures as those in pedogenic carbonates indicates that they may be related, but it tells nothing about which one is the parent and which one is the daughter.

On the other hand, some properties and features of the near-surface calcite-silica deposits do not seem to have a rational explanation within the pedogenic ("rainwater") model of formation.

In this chapter consideration shall be given to the field occurrences, the lithofacies and their textures, the stable and radiogenic isotope signatures, the presence of trace elements and the contents of other important elements. This chapter is based on data from the published literature or officially released government (U.S. DOE and State of Nevada) documents and on the database that has been obtained by the authors to fill in the gaps.

The authors' intention herein was to develop a stand-alone chapter, which would be sufficient to validate the conceptual model proposed in Part II of this monograph. This approach was deemed

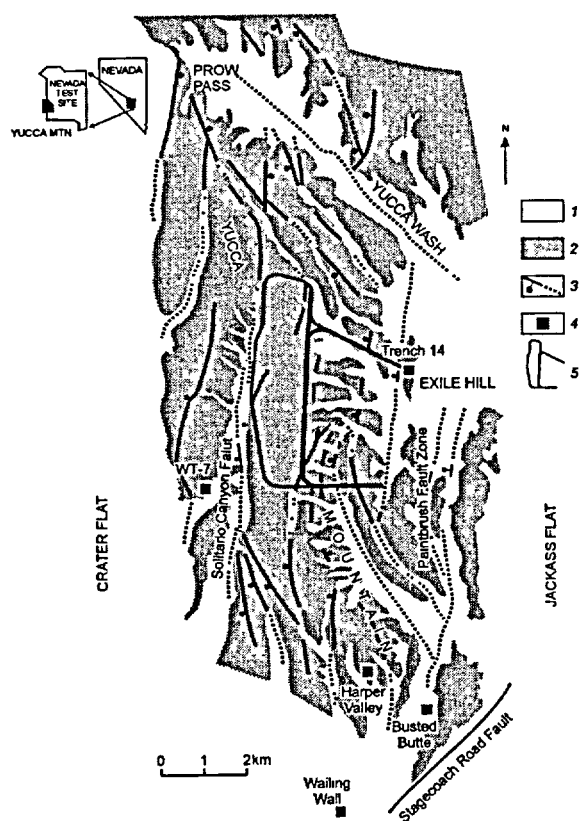


Figure 3-3-1. Occurrences of surface carbonate-silica deposits discussed in the text. 1 – alluvium and colluvium; 2 – Miocene volcanic rocks; 3 – faults; 4 – locations of surface deposits; and 5 – footprint of the ESF tunnel and the planned repository outline.

faults: Trench #14 (hereinafter, Trench 14) and Busted Butte exposures along the Paintbrush fault zone (including the Bow Ridge fault); the WT-7 exposure along the Solitario Canyon fault zone; and the so-called Wailing Wall exposure along a splay from the Stagecoach Road fault system. Locations of these exposures are given in Figure 3-3-1.

Attention must be directed to these particular exposures for two reasons. First, Trench 14, Busted Butte, and the WT-7 exposures are situated within the horst-bounding fault zones, so that they are underlain by locally prominent geothermal anomalies, as shown on Figure 1-31. Second, the Wailing Wall exposure is situated within or near the location of Site#106, a sample from which has been shown by Szabo et al. (1981) to carry  $^{230}\text{Th}/\text{U}$  age of  $78 \pm 5$  Ka. The authors described the sample as: "*Seep-deposited tufa or calcrete intercalated in Q2 alluvium. Shows some evidence of spring-water deposition.*"

The Wailing Wall outcrop is located about 10 km to the south of the proposed repository, as shown on Figure 3-3-1. The wallrock consists of severely brecciated and silicified welded tuff of the

particularly appropriate because it is known with certainty that the deposits in question are of a late Quaternary age based on their directly observable stratigraphic relationships. Therefore, the importance of the origin of the deposits on the licensing of the Yucca Mountain site as the host site for the first national high-level nuclear waste disposal facility is critically important.

### 3.3.1. Field Appearances and the Questions They Provoke

The controversial calcite-silica deposits occur along youthful faults, which are readily recognizable in the field by displaced tuff units, slickensided surfaces of scarps, and brecciated and mineralized zones. In places, where faults are exposed by trenching, the deposits occur in the form of subvertical seams or veins (along or near the fault planes), which grade into subhorizontal aprons, or layers of calcrete at the ground surface. Several of the deposits are located along major

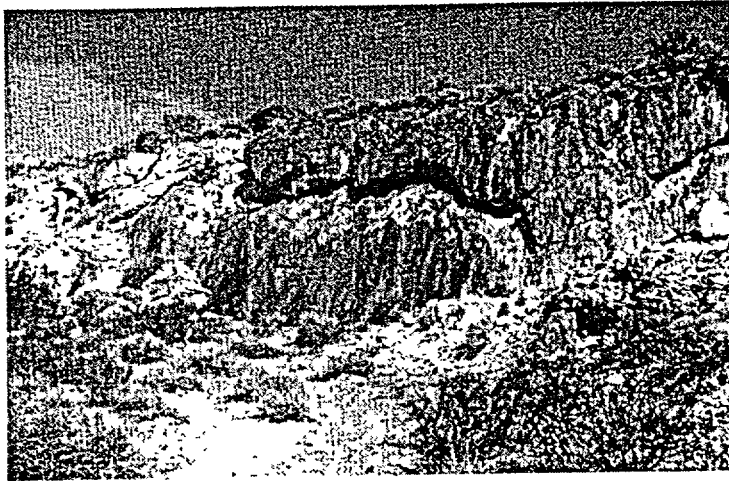


Figure 3-3-2. Calcite/opal (white material) directly along fault, Wailing Wall. Away from the fault the mineralization dies out. The fault is part of the Stagecoach Road fault system and is recognizable by slickensides and offset beds. Photo: C.A. Hill, from Hill et al. (1995).

Topopah Spring Member. Here, a two to three meter-tall fault-scarp, the face of which consists of a grooved and slickensided plane with an oblique slip vector, is partially covered by eolian sand. A sub-vertical seam of carbonate and opaline silica, up to 1.0 m-thick, occupies the fault-contact between the bedrock and the scarp infilling sand (Figure 3-3-2).

The down-thrown block of infilling sand is cemented near the fault plane, but is loosely distributed

away from it. Thus, it is evident that the carbonate-opalite seam was emplaced at a time when the scarp was covered by loose sand. The emplacement of the seam presents the question: How is it possible for opalite (pure  $\text{SiO}_2$ ) to fill the opening between the tuff and the loose sand producing seams up to three cm thick, absent the involvement of a silica-saturated and upwardly flowing fluid?

The **Busted Butte** outcropping is located several kilometers to the southeast of the proposed facility, on the east and west sides of Busted Butte (see Figure 3-3-1). Here, valley erosion has dissected sand ramps, thus exposing the Topopah Spring bedrock with some brecciated traces of the Paintbrush fault zone, including recent slip-planes and associated scarps. At a time when the fault rupture occurred, these scarps were buried beneath sand ramps tens of meters thick. One of these scarps is shown in Figure 3-3-3-b.

A curving slip plane emerges directly from the scarp, which propagates to the ground surface and displaces the overlying sand ramp by 3-4 meters. Near its base, the sand contains a layer of the Bishop Ash tuff (age 760 Ka). Thus, it is certain that a late Quaternary fault rupture is exposed at this location. The curving slip plane contains a vein composed of carbonate and silica, including sand grains cemented by them. The vein narrows toward the underlying scarp but it thickens and splits into multiple branches within a few meters of the ground surface. The calcite-silica deposits then continue down slope from the vein in the form of a cemented "apron", or a slope calcrete, as shown on Figures 3-3-3-b and 3-3-3-c.

The exposure indicates that a pile of loose sand tens of meters thick separated, and the resulting curving fracture was in-filled with and cemented by allogenic carbonate and opalite. It is difficult if not

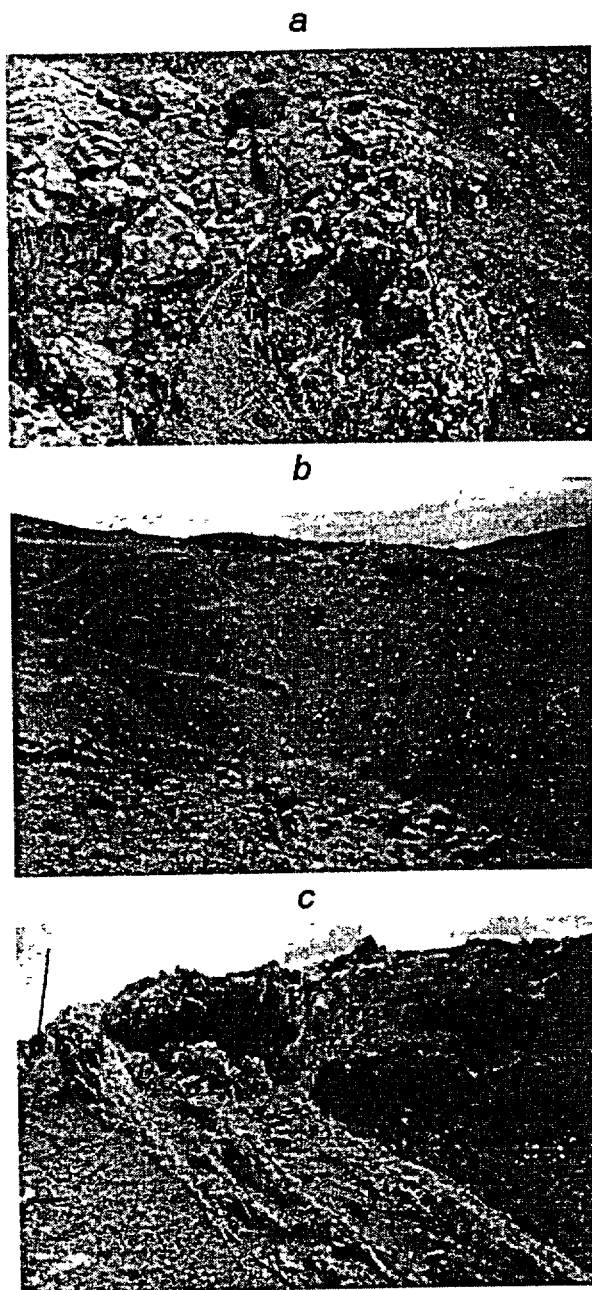


Figure 3-3-3. West slope of Busted Butte, Nevada Test Site. *a* – fault scarp with silica-cemented mosaic breccia (note lens cap for scale); *b* – bent calcite vein in sand ramp steaming from the fault scarp (figure in red marks the location of the fault breccia outcrop) and turning into the slope-parallel “apron” at the ramp surface; and *c* – close-up of the merging vein and “apron” (note abundant rootcasts). Photo Y. Dublyansky.

impossible to perceive, within a context of the rainwater hypothesis, how it is possible to keep this fracture open, and to coat and cement it with carbonate and silica. Discussing this deposit, Hill and Dublyansky (1999, p. 77) argued: *"Since it takes thousands to hundreds of thousands of years to build up a thick pedogenic deposit (300000 years to develop a platy K horizon according to Taylor 1986, Taylor and Huckins 1995), how can a large accumulation of pedogenic calcite/opal take place in such an environment? Unconsolidated sand cannot support an open fracture for a year, let alone for thousands of years. We bring up this point because it is a major stumbling block to a pedogenic model for the COD [calcite-opal deposits] vein and slope deposits at Busted Butte."* To the best of our knowledge, nowhere in the Yucca Mountain publications, the mechanism

of formation of the Busted Butte veins has been discussed.

The exposure called **Trench 14** was excavated across the Bow Ridge fault, a north-south trending subsidiary fault within the western part of the Paintbrush fault zone. As with the Busted Butte exposure, this exposure is also underlain by the Paintbrush geothermal anomaly (see Figure 1-31). It is located just to the east of Exile Hill, directly above the north portal of the Exploratory Studies Facility (see Figure 3-3-1). The bedrock is composed of densely welded tuff, which belongs to the Tiva Canyon Member, in

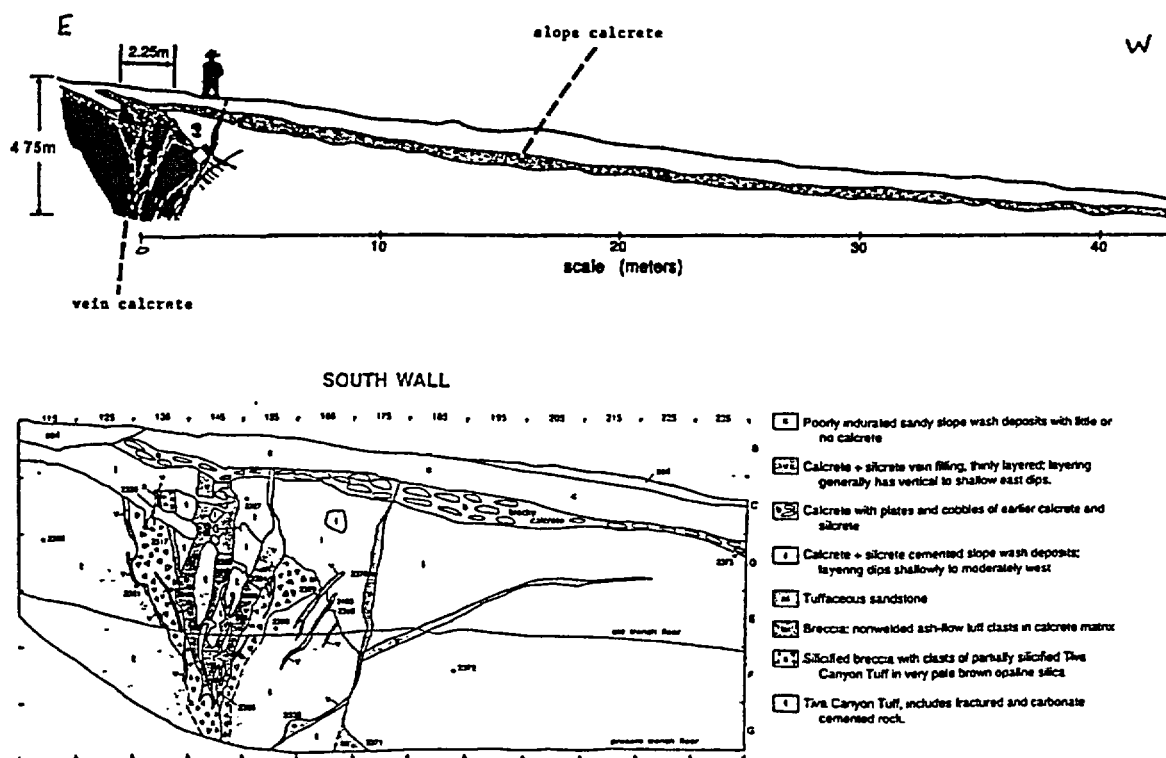


Figure 3-3-4. Geologic map of part of the south wall of Trench 14: general view (from U.S. DOE, 1993) and detailed map of the vein zone (by Taylor and Husking, 1995, as reported in NBMG/UNR, 1999).

fault contact with the vitroclastic tuff of the Rainier Mesa Formation. The fault scarp is locally up to 3-4 m high, and the down-thrown block is filled with variably cemented colluvium, which has been derived mainly through denudation of the scarp and of the up-slope bedrock. There is a spectacular calcite-opaline silica vein emplaced directly within the fault plane, which upon reaching the ground surface continues in the form of a slope-parallel calcrite "apron" (see, Figure 3-3-4).

The veins in the north and south walls of Trench 14, which is only a few meters wide, differ in appearance. In the south wall, the vein narrows toward the floor but thickens and splits out into a few branches near the ground surface (Figure 3-3-5-a). By contrast, the north wall contains a one to two meter thick vein grading at the top into the slope-parallel apron, or calcrite. Here, the vein is almost free of detritus and extends vertically into the ground surface (Figure 3-3-5-b).

Both of the opposing trench walls contain many puzzling features. One such feature is the presence of seams of opalite (pure opaline silica), which in places are up to a few cm thick. In the up-slope part of the south wall, between the brecciated bedrock and the boulder derived there from, there is a 30-40 cm thick carbonate coating of the apparent bedrock surface (see Figure 3-3-5-a). This coating contains

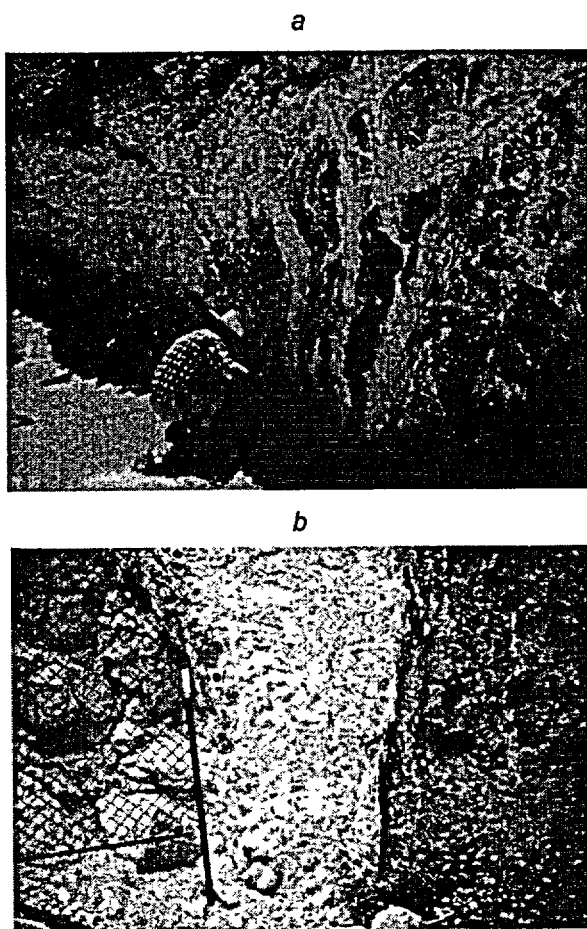


Figure 3-3-5. Calcite-opal surface deposits exposed in Trench 14, Exile Hill, eastern slope of Yucca Mountain. *a* - south wall; note sub-horizontal calcite-silica deposits between the bedrock and the boulder, as well as inclined  $\sim 20^\circ$  to the west seam of opalite. *b* - north wall; 0.8 to 1.0 m-thick vein composed of micritic calcite and opal. The vein is emplaced between Miocene tuff (right) and colluvial boulder deposits (left).

several of the opalite seams, which are inclined ( $10\text{-}15^\circ$ ) to the west in the down-slope direction. The seams are also present in the north wall, particularly in the down-slope part of the vein near the contact with the Rainier Mesa Tuff (see Figure 3-3-5-*b*). In this wall, however, the seams are steeply ( $60\text{-}70^\circ$ ) inclined to the east, which is in the up-slope direction. There again, it is difficult if not impossible to explain, within a context of the rainwater hypothesis, the formation of a few cm thick opaline seams, which are oppositely inclined yet seemingly contemporaneous.

The WT-7 exposure has been excavated on the eastern slope of the Boomerang Point near the mouth of Solitario Canyon. The occurrence belongs to the hanging wall of the Solitario Canyon fault, and is located a kilometer or two to the west of the footprint of the proposed Yucca Mountain facility (see Figure 3-3-1). It occurs above the northern flank of the Solitario Canyon geothermal anomaly (see Figure 1-31). The bedrock is composed of densely welded tuff, which belongs to the Tiva Canyon Member. The exposure contains a pipe-like body of breccia, consisting of an extensive maze of carbonate and opalite veins emplaced between angular fragments of the *in situ* dilated tuff (Figure 3-3-6).

To the south of the WT-7 exposure, the breccia body is overlain by a layer of colluvium topped by a soil horizon, which appears to be composed mainly of cemented but undilated (grain-supported textures) eolian sand and windblown dust. Draping over the dilated bedrock and the overlying detritus, there is an inclined "apron" composed of carbonate, containing nodules of opal (Figure 3-3-7). Carbonate-opal deposits commonly contain variable amounts of detrital material, ranging in size from sand to gravel and small boulders. Parts of the deposits are virtually detritus-free.

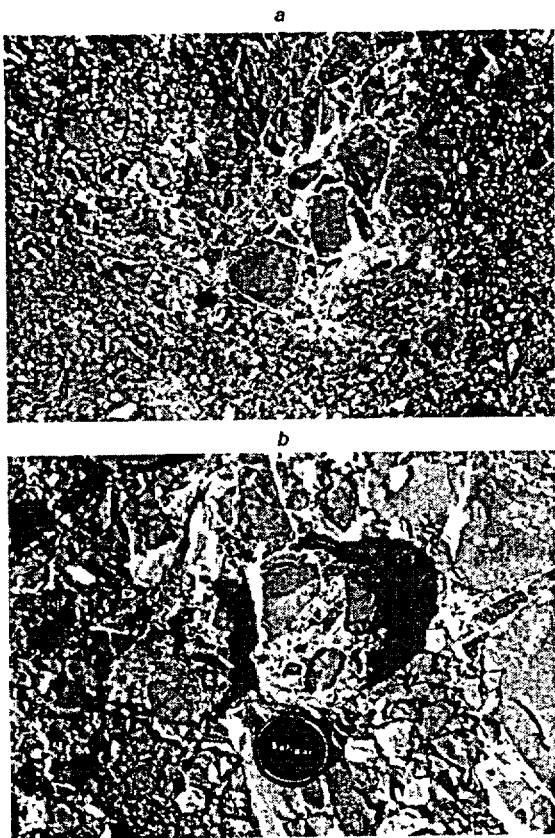


Figure 3-3-6. Mosaic breccia at WT-7 drill pad.  
Photo: Y. Dublyansky.

The WT-7 exposure indicates that the *in situ* dilatatory brecciation of the bedrock is contemporaneous with the deposition of the carbonate and opalite veins, all of which appear to be free of, or contain very little detritus. This exposure also indicates that the brecciation is very young, geologically speaking, and no older than say mid-Quaternary. The brecciation appears to be similar to that, which Nelson and Giles (1985) observed elsewhere in association with bodies of hydrothermal eruption breccia. The *in situ* fragmentation of the bedrock, the isotropic character of the dilatatory separation of the breccia clasts, and the precipitation of authigenic cement around the separated clasts is a dominant feature of the WT-7 exposure. It is our opinion that all of these observations cannot be explained without calling for the involvement of a detonation-like (isotropic) increase of gas pressure followed by a silica- and carbonate-saturated upward-flowing fluid.

### 3.3.2. Lithofacies

The calcite-silica deposits, which occur at the topographic surface of Yucca Mountain, are developed as a whole in the form of four morphologically distinct members, or lithofacies. These are the so-called AMC (authigenic-mineral-cemented) breccias, veins in the bedrock, slope-parallel calcretes within and on top of the overburden, and carbonate coatings of alluvial and colluvial clasts. The term "lithofacies" is used herein to emphasize the broad genetic affinity of the members to each other, on one hand, and the differing modes and environments of deposition, on the other.

We use, as a working model, the following sequence of lithofacies: mosaic breccias → bedrock veins → calcretes → clast encrustations. In the sequence, each lithofacie is a more distal (in terms of time and space) derivative of the previous one. In addition, since emplacement of all lithofacies occurred at or near the topographic surface, all of the lithofacies are likely to be affected, in some degree, by supergene (pedogenic) processes. The involvement of the supergene processes increases from proximal to distal facies, being the least in the AMC breccias and the greatest (perhaps dominant) in the clast encrustations.

#### 3.3.2.1. AMC breccias

The AMC breccias occur along several of the fault scarps, where they form dike-like and pipe-like bodies. We regard these bodies as being among the most thought-provoking geologic objects, which an observer encounters in traversing Yucca Mountain from east to west. Surprisingly, they are present near the ground surface only, so even the shallowest parts of the several miles long Exploratory Studies

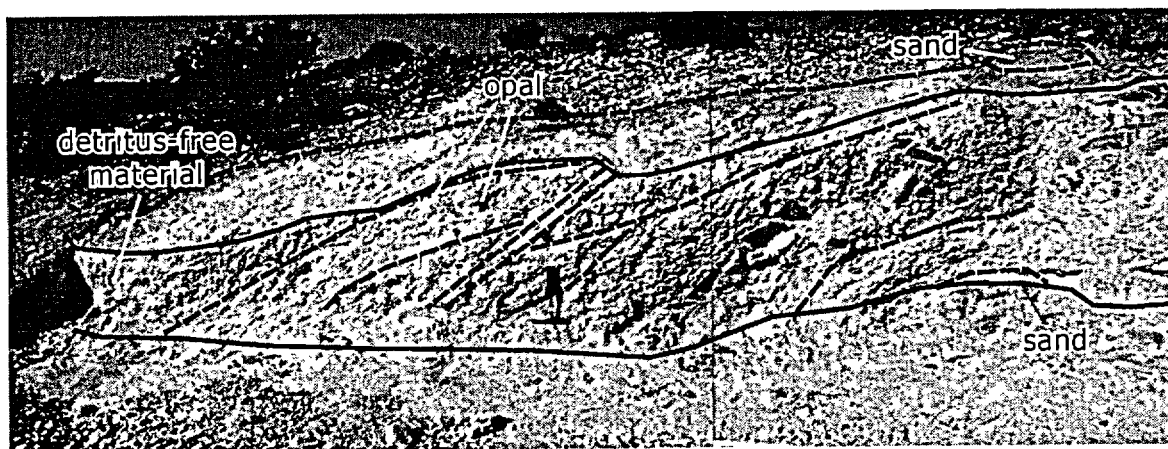


Figure 3-3-7. Slope deposits at the WT-7 exposure. The deposits overly the *in situ* dilated welded tuffs. Pockets of eolian sand are present beneath the slope carbonate-silica deposits (cemented) as well as above it (non-cemented). Carbonate-silica deposits in places contain detrital material, including boulders (central part of the photograph). In other places they are detritus-free (calcite+opal). Photo: Y. Dublyansky.

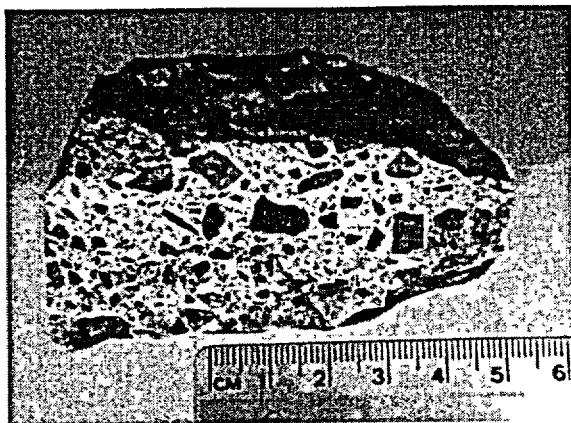


Figure 3-3-8. Hand specimen of the fault-associated mosaic breccia at Busted Butte (see Figure 3-3-3-a). Photo Y. Dublynsky.

Facility are completely devoid of them. Examples of the AMC breccia exposures are shown on Figures 3-3-3-a and 3-3-6.

A typical hand specimen of the breccia consists of angular or, less commonly, sub-rounded fragments of welded tuff, which are embedded in a matrix composed of opaline silica and, to a lesser extent, carbonate. There are three truly remarkable features associated with the breccia bodies. First, many hand specimens from several locations display a "matrix" support texture, which means that the compositional clasts

are not in direct contact with each other, but instead "float" in the authigenic cement. Second, in those hand-specimens for which there are strong indications that the compositional clasts have been derived from the same block of tuff, the amount of volumetric strain (distention) is very large, between several to tens of percent. Third, the volumetric strain is remarkably isotropic, which means that the amount is comparable in all three mutually perpendicular directions (see, Figure 3-3-8).

Szymanski (1989) concluded that the AMC breccias are polygenetic materials, which means that they were formed by at least two processes. Some, he concluded, are so-called "explosive" breccias, whereas the others are so-called "fragmentation" breccias. The adjective "explosive" was used to denote a breccia for which the formation of both the compositional clasts and the authigenic cement have a common cause and require a large build-up and very fast release of gas or fluid pressure. Such pressure build-up implies past occurrences of hydrothermal explosions, or of gas (vapor)-assisted seismic pumping phenomena, or perhaps of the implosions of fault wallrocks charged with gas in association with their sudden separation. By contrast, the adjective "fragmentation" was used to denote a breccia for which formation (fragmentation) of the compositional clasts and precipitation of the authigenic cement was caused by two different processes operating at the same time and space. An example of such processes is the mass wasting and filling of a bedrock opening, either structural (fault-plane separation) or erosional, within which silica and carbonate precipitate from the super-saturated solutions. The "floating" texture could be regarded, as Szymanski (1989) has claimed, as evidence for the rates of cement formation being as high as the rate of clast supply. Alternatively, these textures could be regarded as expressing the introduction of clasts into mineral gels having specific gravity similar to that of the clasts.

Experts are sharply divided in their opinions about the processes, which were actually involved in formation of the AMC breccia bodies at Yucca Mountain and in particular, the pipe-like bodies along the horst-bounding faults. A five-member panel, which was convened by the DOE to peer-review the Site Characterization Plan, concluded that the Trench 14 AMC breccia body might reasonably be regarded as a "*hydrothermal eruption breccia*" (Hanson et al., 1987).

Petrographic examinations of thin sections of samples of the AMC breccias, from the Trench 14 and Busted Butte exposures, by Levy and Naeser (1991) revealed two significant observations. "*Plant remains have been observed in all samples examined for this study*". "*Some of the carbonate-rich fracture cements contain so many root casts that non-root mineral deposits from any source could only compose a small portion of the total cement*". These two observations led Levy and Naeser (1991) to conclude that the "*AMC breccias probably formed by varying combination of surface erosion and deposition ... and recent near-surface fault movement Most of the authigenic mineral cementation of AMC breccia is related to surficial pedogenic processes, as shown by the abundance of plant remains*".

Similar conclusions were expressed by the National Academy of Sciences/National Research Council seventeen-member panel, which was convened by the DOE to review the upwelling water controversy and provide the appropriate recommendations. The panel concluded that: "*... the fault breccia cement at Trench #14 and Busted Butte is of pedogenic or surficial origin, based on the presence of older detrital zircons, grain size and structural characteristics, and is not of hydrothermal origin*" (NAS/NRC, 1992).

Other investigators, however, draw quite different conclusions. In this regard, Somerville et al. (1992) examined an assay database from seven samples of the Trench 14 AMC breccia, as developed by Castor et al. (1989) and Weiss (1990) and concluded that, relative to the stratigraphically equivalent background (Tiva Canyon Tuff), the breccia cement is "*... enriched in the base metals, noble metals, and pathfinder elements*". Specifically, it has been shown that the cement was enriched in Ag (factor of 16), As (factor of 3.6-36), Cu (factor of 4), Au (factor of 5), Mo (factor of 18-650), Pb (factor of 65), and Sb (factor 25-100).<sup>\*</sup> Somerville et al. (1992) concluded "*... fragmentation involved in the formation of mosaic breccia almost certainly occurred under conditions of high pressures and rapid release of strain energy*." Further, researchers of the Nevada Bureau of Mines and Geology (NBMG/UNR, 1999) reported "clearly anomalous" contents of Au (15-16 ppb) in fault gouge and breccia samples from two trenches intersecting the northern extension of the Solitario Canyon fault. Discussing breccias from Trench 14 and

---

<sup>\*</sup> It is to be noted that, according to the numeric data reported in the NBMG/UNR (1999), the bulk breccia samples (i.e., tuff clasts and the carbonate-silica cement) are commonly depleted in these elements relative to the bedrock tuff specimens. This discrepancy in the numeric data cannot be reconciled without further verification program.

Busted Butte, Neymark et al. (1995) stated: "*When normalized to average concentration data of the unaltered HSR [high-silica rhyolite] from the Tiva Canyon Tuff ... and Topopah Spring Tuff ... unleached breccia samples ... show significant enrichment (up to a factor of 20) in Ca, Sr, and Ba...The data may be explained by the presence of calcite (CaCO<sub>3</sub>) which contains large concentrations of Sr and Ba...*" (p.9).

The viewpoint of Somerville with co-authors has been confirmed by petrographic studies of the Trench 14 and Busted Butte AMC breccia by scientists from the Siberian Branch of the Russian Academy of Sciences. In this regard, Dublyansky and Lapin (1996) reported that the samples exhibit granoblastic and crustification textures and show evidence for multiple episodes of authigenic cement precipitation and recrystallization. The authors further reported that the cement partly consisted of zeolite-chlorite-silica assemblages, with chlorite filling in central parts of the interstitial space and zeolite-silica forming alternating bands within the outer parts. In addition, they observed that alternating bands of such typical hydrothermal mineral phases as chlorite, jasperoid, and prehnite, were present around edges of the clasts in the Trench 14 breccia body. Dublyansky and Lapin (1996) stated: "... *we did not find any root casts in breccia cement, which is surprising, taking into account the...quotations above [i.e. from Levy and Naeser (1991)]*". They also concluded "... *AMC breccias show all the petrographic features typical of low-temperature hydrothermal processes from elsewhere; thus, they are interpreted as being formed in association with epithermal activity.*"

Microscopic studies of the AMC breccias were also made by Harmon (1993), who examined two samples, one (#5h) from the WT-7 exposure and the other (#19e) from the Wailing Wall exposure. The following two quotations sum up the results for the respective samples:

This sample [#5h from WT-7] consists predominantly of carbonate in which there are numerous sub-parallel veinlets of quartz. Under high magnification, the veinlets quartz is observed to be zoned, the central portions consisting of clear euhedral quartz crystals and the outer zone being comprised of fine-grained cryptocrystalline quartz (opal). Some of the veinlets contain unfamiliar tubular structures of undetermined composition. Neither their origin nor their significance is known, they could be organic, or could represent a low-temperature epithermal fluid flow structures. The latter explanation is preferred as there are mammillated surfaces on some of the voids, which appear to consist of similar material. The clear euhedral quartz crystals are totally lacking in fluid inclusions, except for a few very small (<1 μm) monophasic (?) inclusions.

This [#19c from the Wailing Wall] is a mixed carbonate/silica sample (#19e) containing numerous small void spaces, which have been filled with secondary silica. The silica deposited within the "vuggy" areas is zoned from an early fine-grained microcrystalline silica (opal) to a later clear crystalline quartz, which forms subhedral to euhedral crystals with doubly-terminated bipyramidal forms. These appear to be isolated within the carbonate component of the sample, so their relationship

to the vug-filling quartz in the sample is unclear. ...In places, the quartz crystals contain abundant, but minute ( $<1 \mu\text{m}$ ) fluid inclusions not suitable for thermometric analysis. Many are not easily resolved, but appear as solid "specks" within the host quartz. Two kinds of the inclusions appear to be present in the sample, a monophasic gaseous type and a 2-phase liquid-vapor variety. The latter have a high degree of fill (i.e. ratio of liquid to total volume of about 0.9).

Harmon (1993) makes three important points. First, the WT-7 sample (#5h) contains veinlets partially composed of euhedral crystals of quartz, which contain tubular structures possibly representing fluid-flow structures. A judgment by Levy and Naeser (1991) that they appear to be root casts is questionable. Second, euhedral quartz was observed to be present in both of the samples, which implies an epithermal deposition environment but not an ordinary soil-forming process. Third, quartz in the Wailing Wall sample (#19e) was found to contain very small two-phase fluid inclusions with consistent vapor/liquid ratios. Even though the homogenization temperatures for these inclusions have not been determined (inclusions were deemed to be not amenable to the fluid inclusion thermometric studies due to the small sizes, by authors of the report), the very presence of such two-phase inclusions implies that the deposition temperature for the host quartz was greater than approximately  $40\text{-}50^\circ\text{C}$ , which is at least  $15^\circ\text{C}$  greater than the surface temperature. A possibility exists that depositional temperatures have been even greater, similar to the homogenization temperature of  $145^\circ\text{C}$  reported by Vaniman et al. (1984) from the euhedral drusy quartz collected in Trench 14, which intersects the trace of the Bow Ridge fault at Exile Hill on the eastern slope of Yucca Mountain.

It thus appears that the observations of Harmon (1993) on the #19e sample from Wailing Wall are important, because these observations indicate the presence of deep-seated (hypogene) fluids at the present-day topographic surface at some time in the past. Furthermore, the #19e sample represents bedrock that underlies Site #106 of Szabo et al. (1981). This site contains a few meter-thick calcite-silica deposits, interpreted by Szabo et al. (1981) as "*seep deposited tufa*" showing "*some evidence of spring-water deposition*". A sample of these deposits yielded a U/Th age of about 78 Ka, as given in Szabo et al. (1981). This allows us to consider a possibility that the observations of Harmon (1993) pertain to geologic processes which either took place in Late Quaternary or their activity have continued into that time.

### **3.3.2.2. Bedrock veins and slope-parallel calcretes**

The bedrock veins are invariably emplaced within the horst-bounding fault zones, although lesser faults contain them as well. Typically, these veins are wedge-shaped, so that the thickness diminishes from 1.0-1.5 m at the ground surface to tens of cm, at a depth of a few meters. Hill et al. (1995) have documented that, at the scale of hand-specimens, they display a variety of textures, which range from banded, through laminated and vesicular, to powdery, as shown on Figure 3-3-9.

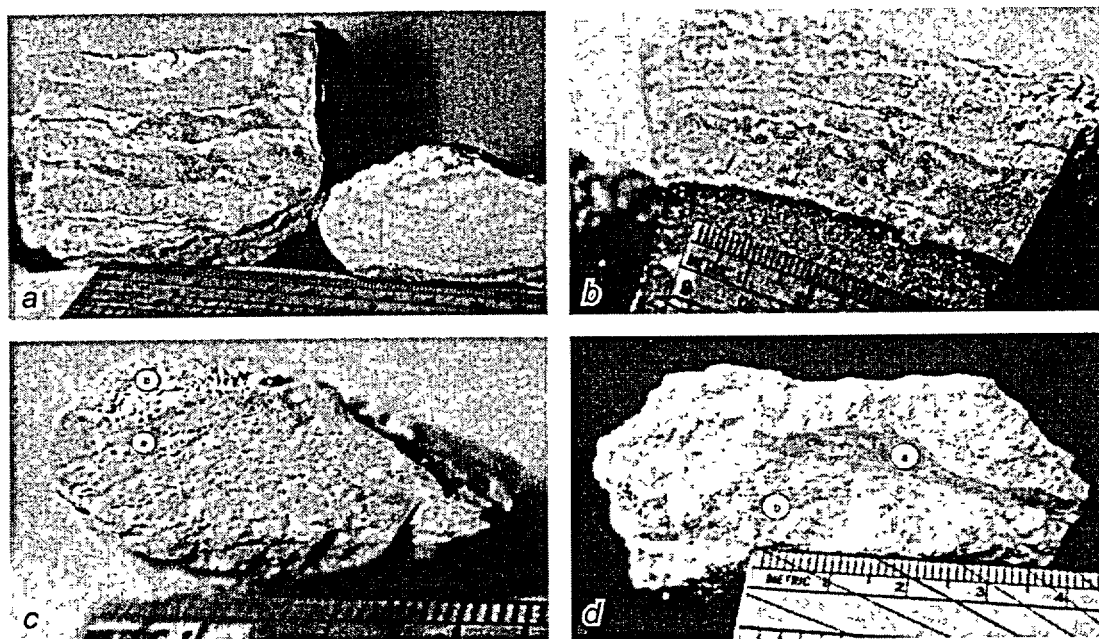


Figure 3-3-9. Textures of the vein/slope deposits. *a* – Two banded samples from Wailing Wall, showing bands (a few centimeters thick) of alternating mixed, massive, or powdery texture; *b* - Laminated/banded texture where the individual layers are a few millimeters thick (sample from WT-7 site); *c* – Vesicular texture of both buff-colored calcite/opal (*a*) and in powdery-textured matrix (*b*). Sample from Trench 14; *d* - Invasive texture where dense, buff-colored, calcite/opal (*a*) has invaded a powdery-textured mass composed primarily of calcite (*b*). Sample from Wailing Wall. Photos: C.M. Schluter; from Hill et al. (1985).

X-ray diffraction data from Vaniman et al. (1988) show that the bedrock veins consist of abundant calcite, opal-CT, lesser amounts of opal-A, sepiolite, and either chain silicate clays or smectite. The presence of sepiolite is particularly noteworthy. As stated in Hill et al. (1995), "... *sepiolite may be pedogenic but in the Basin and Range Province it is often related to hydrothermal water upwelling along fault zones where the source of Mg and Si for the mineral is dolomite and volcanic rocks in the subsurface...*"

The slope-parallel calcretes occurring at and around Yucca Mountain are part of the overburden, which covers the bedrock and fills the adjacent tectonic depressions. These calcretes occur both within and on top of the overburden, and are developed in the form of detrital clasts of various sizes cemented by carbonate and, to a lesser extent, by silica. They form discrete horizons or layers within three types of the overburden deposits, which are sand ramps, colluvium and alluvium derived from the tuffs, and colluvium and alluvium derived from marine carbonates of the basement (e.g., at the foothills of Bare Mountain). The fact that the calcretes are scattered throughout the interior of the overburden indicates that the introduction of authigenic cement occurred at the ground surface and that the introduction was an

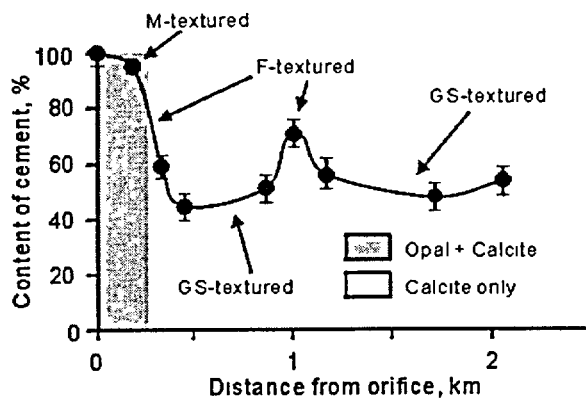


Figure 3-3-10. Changes in the contents of the authigenic cement and textures of slope calcretes in the 2 km-long profile in the vicinity of the Solitario Canyon Fault (WT-7). A decrease in content of cement is accompanied by a textural transition from matrix (M) through floating (F) to grain-supported (GS) textures. An increase in the content of cement and appearance of F textures at approximately 1 km reflects the passage of the profile within approximately 100 m from another inferred orifice. Note that opal was found in samples only from near the inferred "orifice".

intermittent, re-occurring process. The analyses of rock cores extracted from drill hole USW VH-2 (see Chapter 2-4 and Figure 2-20) indicate that this process has been intermittent over the past 13 Ma.

The natural exposures of sand ramps, which have been dissected by erosion, indicate that the introduction of authigenic cement has continued intermittently over the late Quaternary. These calcrete-bearing sand ramps are especially well preserved along the Paintbrush fault zone, at Busted Butte and along western flank of Fran Ridge. They are up to tens of meters thick and record the deposition of eolian sand, over the past say 0.5 Ma (based on the presence at the base of sand deposits of a discrete layer of basaltic Bishop Ash deposited 570 Ka). The sand ramps

contain, at the top and in the interior, three discrete layers of calcite- and opaline silica-cemented sand, up to 1.5 m thick. Fault slip-planes, which propagate upward from the bedrock scarp and displace the overburden by up to 3-4 meters, contain calcite-silica cement in the form of a curving high-angle vein (see Figure 3-3-3). The vein is an aggregate of many veinlets. At the ground surface, this vein grades into or intersects an inclined layer of slope-parallel calcrete (see Figure 3-3-3-c), which contains abundant plant remains in the form of root-casts.

X-ray diffraction data from Vaniman et al. (1988) show that the mineral compositions of the calcretes and of the veins in the overburden are identical to each other and similar to the mineral compositions of the bedrock veins and of the AMC breccia cements. In all of these lithofacies, the authigenic cements consist of micritic calcite, opal-CT, lesser opal-A, poorly crystallized smectite, and chain silicate clays. The clast population of the slope-parallel calcretes is variable and includes sand- and silt-sized fragments of minerals (quartz, plagioclase, feldspar, pyroxene, and amphibole), fragments of tuff and glass, and fragments of re-worked calcite-silica cement.

In the Solitario Canyon fault zone, the slope-parallel calcretes developed down-slope from the WT-7 drill pad exhibit a number of noteworthy features. The abundance of opaline silica, relative to micritic calcite, and the purity of the authigenic cement diminish with increasing lateral distance away and down-

slope from the suspected orifice (indicated by the presence of the AMC breccias and bedrock veins), intersected by the drill pad (Figure 3-3-10).

Figure 3-3-10 shows that the authigenic cement is pure (largely devoid of detrital fines), at and near the "orifice", and opal constitutes a significant fraction of it, up to 30 % or more. As the lateral distance increases, however, the contribution of opal decreases rapidly, relative to the carbonate, and the authigenic cement becomes increasingly more contaminated by detrital fines.

The downslope-diminishing abundance of the opal, concurrently with the increasing abundance of carbonate and detrital fines, raises the question of how this trend can be explained. The answer is readily apparent if it is presumed that the authigenic cement was precipitated from solutions, which were discharged along the fault zone, and then flowed down-slope into the subsiding Crater Flat depression. The rapidly diminishing temperature of the fluid would have the effect of diminishing the  $\text{SiO}_2$ -solubility, but without comparably diminishing the  $\text{CaCO}_3$ -solubility, so that the relative amount of the precipitated  $\text{CaCO}_3$  would increase down-slope.

The decreasing intensity of mineral precipitation along the flow path would cause the authigenic minerals to be more vulnerable to contamination by detrital fines. Such relationships are commonly observed at travertine-depositing springs.

By contrast, the competing hypothesis, which is the atmospheric (wind blown dust) derivation of the authigenic cement, does not appear to be capable of providing a comparably rational interpretation. Here, we again draw attention to the exceptional purity of authigenic mineralization emplaced on the mountain slope (inclination 10 to 20°) within and on top of the colluvial and eolian material. For example, a bowl-shaped, approximately 70 cm-thick deposit exposed on the left side of the excavation (see Figure 3-3-7) is composed of massive and exceptionally pure authigenic mineralization (72.3 % calcite and 27.7 % opal-C; detrital material is absent based on microscopic and XRD data).

Guthrie et al. (1995) studied the mineral composition of modern dusts in the vicinity of Yucca Mountain. The dusts contain 45-47 wt. % feldspar, 18-22 % quartz, 6-8 % smectite, 3-4 % zeolite (clinoptilolite), 1-3 % mica, as well as minor amounts of tridymite, cristobalite, chlorite, amphibole, and hematite. Calcite was found in trace amounts or, in some samples, was not determined at all. Hill and Livingston (1993) reported similar results (<0.2 % carbonate) for eolian deposits sampled at Busted Butte and Lathrop Wells. We can see no plausible mechanisms capable of transforming the eolian dust source-term into the pure calcite-opal deposits, similar to that found at WT-7. This stumbling block disappears if one considers the spring-orifice model of formation for these deposits. Even in the spring environment, the deposits must be deposited quickly in order to avoid contamination by detrital material. The rate of



Figure 3-3-11. M-textured (matrix) carbonate slope deposit at Boomerang point, eastern Crater Flat, in the vicinity of the mouth of the Solitario Canyon. Clasts comprise less than 10 % of the total rock volume. Photo Y. Dublyansky.

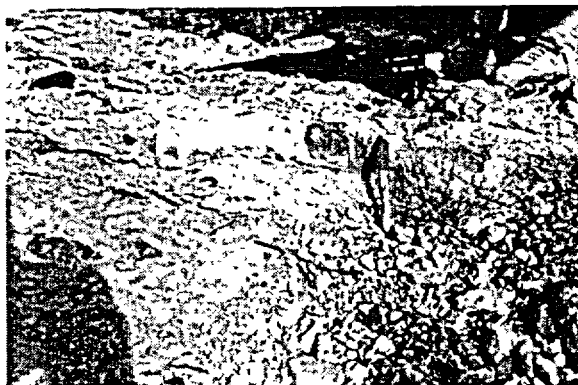


Figure 3-3-12. F-textured carbonate slope deposit at Bare Mountain, western Crater Flat. Clasts comprise more than 10 % of the total rock volume. They are "suspended" in the cement and do not touch. Photo: Y. Dublyansky.

carbonate deposition, thus, must have been many orders of magnitude greater than the eolian carbonate accumulation rates of  $0.3$  to  $5.0 \text{ g}\cdot\text{m}^{-2}\cdot\text{yr}^{-1}$  estimated for the southwestern United States (Machette, 1985; Rheis et al. 1992). The fast rates of deposition may be responsible for the micritic, or cryptocrystalline, character of the carbonate mineralization.

The macroscopic (hand-specimen) textures of the slope-parallel calcretes also change systematically with increasing lateral distance from the suspected orifice. At and near the orifice, the calcretes are typically M-textured (matrix-texture), which means that they contain less than 10% of detrital clasts and consist almost entirely of authigenic cement (Figure 3-3-11).

As the lateral distance increases, however, the volumetric ratio between the compositional clasts and the authigenic cement increases gradually, so that the calcretes become at first F-textured (floating texture). This texture means that the authigenic cement comprises between 90 and about 30 % of the total volume, so that the compositional clasts "float" in the authigenic cement (i.e., the clasts do not touch each other), as shown on Figure 3-3-12.

As the lateral distance increases further, the slope-parallel calcretes eventually become GS-textured (grain-supported texture). This texture means that the detrital clasts are in direct contact with each other and that the authigenic cement occupies the "undiluted" pore space (Figure 3-3-13).

The down-slope grading textures (from matrix (M), through floating (F), to grain-supported (GS)) require an explanation. Here again, the answer is readily apparent if it were presumed that the authigenic cement has precipitated from solutions, which were discharged along the Solitario Canyon fault zone, and flowed down-slope into the Crater Flat depression. The down-slope diminishing temperature and rates of CO<sub>2</sub>-degassing for the fluid would have had the effect of diminishing the precipitation rates for the authigenic cement, in the down-slope direction, along the increasingly longer flow path. Concurrently, the increasing length of the flow path would have had the effect of changing the mode of the fluid flow, initially from a surface run-off to, eventually, a flow path through the accumulations of colluvial or alluvial detritus. Thus, in the context of this scenario, the GS texture expresses the subterranean flow, whereas the M and F textures express the surface flow, or flow in an open space, such as an open fault. The switch from the M-texture into the F-texture, however, expresses the diminishing rate of precipitation of the authigenic cement. By contrast, the competing "rainwater" hypothesis does not appear to be capable of providing a suitable explanation for these features.

### 3.3.2.3. Carbonate coatings of clasts

The carbonate coatings of clasts occur in much of the area irrespective of the carbonate content of the bedrock, and in particular in places where the run-off of rainwater flows over unconsolidated colluvium and soil horizons or ponds along bedrock scarps. In addition, these coatings are also found on slopes of volcanic cones and in the subsurface, in loose colluvium at the top and in-between layers of cemented calcrete. This ubiquitous presence implies that, by contrast to the slope-parallel calcretes, the



Figure 3-3-13. GS-textured (grain-supported) carbonate slope deposit in Solitario Canyon, eastern Crater Flat. Clasts are in contact with each other and carbonate cement fills in the space between them. Photo: Y. Dublyansky.

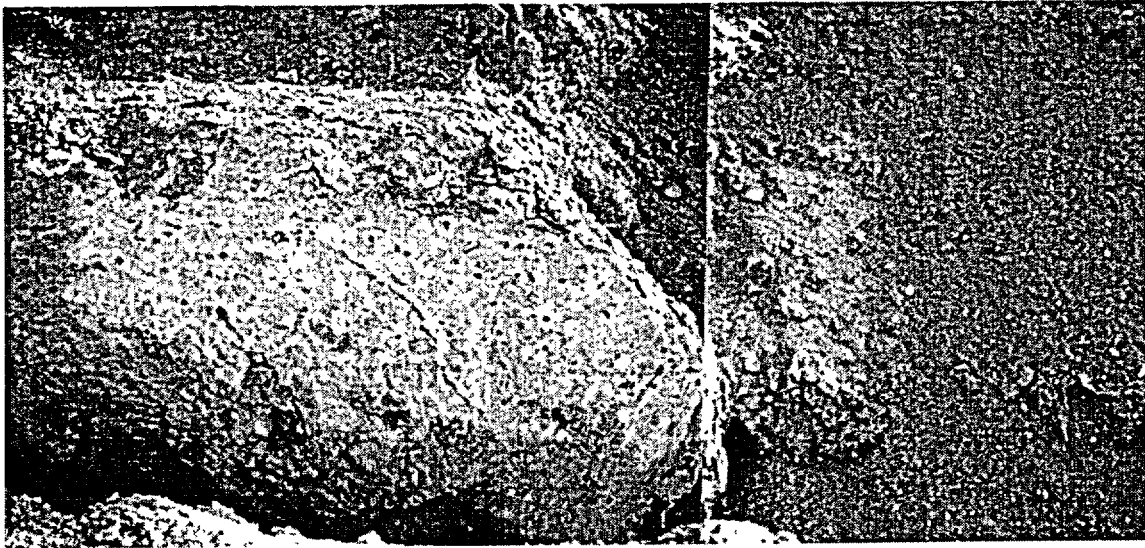


Figure 3-3-14. Calcite-silica deposits exposed in trench excavation at the Stagecoach Road Fault zone. Massive calcite-silica deposits are present in the footwall, but are absent in the hanging wall (right side of the photograph), where loose non-cemented alluvium and eolian sand are present. Surface of calcite-silica deposits and the fault scarp are covered with thin white layer of material, re-mobilized by run-off. Some clasts in the gray alluvium carry white carbonate encrustations. Photo: Y. Dublyansky.

carbonate coatings are formed continuously through evaporation of run-off and, most certainly, without the involvement of deep and chemically evolved fluids.

The presence of carbonate coatings of clasts on the steep slopes of volcanic (basalt scoria) cones indicates that, in part, the run-off acquires the dissolved calcium through leaching of the bedrock and, in part, through dissolution of the windblown dust. This dust is and always has been deflated from all outcroppings of the pre-existing rocks, including the tuffs, the Paleozoic carbonates, and the older calcretes as well. The presence of secondary accumulations of thin and discrete layers of pure carbonate on top of the controversial "calcrete" deposits, however, indicates that the dissolved calcium is also acquired through leaching of these deposits. This parent → daughter relationship between the calcite-opal vein- and calcrete deposits (parent) and the secondary accumulations (daughter) is illustrated on Figure 3-3-14.

### 3.3.3. *Stable isotopes*

Surface deposits in the Yucca Mountain area have been studied by means of the stable isotope method. The results obtained were interpreted as demonstrating a pedogenic origin for these carbonates (e.g., Quade and Cerling, 1990, NAS/NRC, 1992, Vaniman and Whelan, 1994, Whelan and Moscati, 1998, and many others). Below we address the carbon and oxygen isotope geochemistry of the carbonates, and evaluate the validity of the conclusions regarding the origin of the Yucca Mountain surface deposits reached by the Yucca Mountain Project researchers.

It should be borne in mind that both  $\delta^{13}\text{C}$  and  $\delta^{18}\text{O}$  values of the freshwater carbonate deposits may be altered after deposition (Choquette, 1968), which makes environmental interpretation of these values somewhat uncertain. (This does not hold, however, for crystalline carbonates formed in the subsurface, for which alteration of the isotope properties does not happen; Ohmoto, 1972). Nevertheless, it is an opinion accepted by the scientific community that stable isotopic values of carbonates do have certain value as environmental indicators (Faure, 1987).

Below we evaluate the supply of carbon and oxygen that participate in the formation of calcite deposits in two model settings: the pedogenic setting (i.e., inside or just below the soil layer) and the spring or travertine setting. The pedogenic setting is envisaged as one, where calcium carbonate is deposited in the soil or other substratum far from possible spring orifices. We believe this to be a close approximation for cobble coatings and incrustations. The spring or travertine setting is that of the hot or warm spring, discharging on the Earth's surface and precipitating carbonate (travertine). These two settings may be viewed as the two end-member environments. Water discharging at the thermal spring, as it flows away from the orifice, evolves toward the compositions of the soil fluids. Thus, "travertine" calcite, may gradually acquire properties, characteristic of the "pedogenic" calcite, but not vice versa.

#### 3.3.3.1. Carbon isotopes

##### 3.3.3.1.1. Pedogenic setting

There exist, generally, four "reservoirs" or "pools" of carbon that contribute to soil  $\text{CO}_2$  and the deposition of pedogenic calcite.

**Carbonate rock-derived  $\text{CO}_2$**  supplies isotopically heavy carbon for pedogenic carbonates. The latter are believed to form, at least in part, by re-deposition of wind-blown carbonaceous dust deflated from the outcrops of carbonate rocks. Marine limestones have  $\delta^{13}\text{C} = 0 \pm 4 \text{‰}$  (Craig, 1953) so that soil

waters may receive some contribution of relatively heavy carbon from dissolution of these carbonates, although the contribution is believed to be minor (McConnaughey et al., 1994).

**Atmospheric CO<sub>2</sub>** is the second heaviest source of CO<sub>2</sub> of the four source terms. It has a stable and homogenized  $\delta^{13}\text{C} = -6\text{‰}$  (pre-industrial value). Concentration of CO<sub>2</sub> in atmospheric air is low ( $p\text{CO}_2 \cong 10^{-3.5}$  or about 0.003), which means that, in order to make a significant contribution, water equilibrated with an atmospheric reservoir must be volumetrically dominant in the calcite-forming solution. This may be realized at the very top of the soil profile (surface or first few centimeters of depth), as well as deeper in porous, well-ventilated substrates devoid of vegetation (e.g., fresh eolian sands, regolith, etc.).

**Plant-derived CO<sub>2</sub>** produces isotopically light carbon. At least 50 % of the CO<sub>2</sub> in the soil is derived from the decomposition of soil organic matter, which includes root exudates (Parker et al., 1983) with the rest being respired by root systems. The content of carbon dioxide in the soil atmosphere may be several orders of magnitude higher than in the atmosphere. For example, Atkinson (1977) has demonstrated that the soils in the temperate climates contain between 0.03 and 11.5 % CO<sub>2</sub> (mean 0.9 %).

Isotopic values of CO<sub>2</sub> respired by plants and released due to the root decomposition may vary significantly, depending on the type of vegetation. According to Salomons and Mook (1986), plants with a C<sub>3</sub> metabolic pathway (Calvin cycle) generate CO<sub>2</sub> with isotopic compositions of -22 to -34 ‰ (with a maximum at  $-27 \pm 2\text{‰}$ ); plants with a C<sub>4</sub> pathway (Hatch-Slack cycle) range from -9 to -19 ‰ (maximum at  $-12 \pm 2\text{‰}$ ); and plants with a CAM pathway (Crassulacean acid metabolism) show intermediate values (generally around -17 ‰, but in arid areas acquire values close to those of C<sub>4</sub> plants (Wells, 1976).

**Deep-seated CO<sub>2</sub>** is the least known and commonly neglected component of the mix. It comprises CO<sub>2</sub> evolving from the underground aquifer and mixed with the CO<sub>2</sub> of the vadose zone. The mantle-derived CO<sub>2</sub> is thought to have  $\delta^{13}\text{C}$  values in the range -8 to -5 ‰. In the volcanic and geothermal areas, values of the igneous  $\delta^{13}\text{C}$  range typically from 0 to -9 ‰ (Deines, 1980). Substantially lighter  $\delta^{13}\text{C}$  values may appear if there is an ongoing bacterial or inorganic oxidation of methane, which is strongly enriched in <sup>12</sup>C relative to the oxidized carbon species. The occurrence of "light" (<sup>12</sup>C-enriched) carbon in the near-surface setting, either in the form of gases or as secondary calcite, is used as an aid in prospecting for petroleum and natural gas deposits (Donovan et al., 1974; Stahl, 1977; Fuex, 1977). By contrast, CO<sub>2</sub> liberated by decarbonation of carbonate rocks during contact metamorphism is about 6 ‰ richer in <sup>13</sup>C than the original carbonate (Shieh and Tailor, 1969; Turi, 1986), which is believed to result in deposition of isotopically "heavy" travertines (e.g., in Italy; Turi, 1986).

In the vicinity of Yucca Mountain, soils commonly contain CO<sub>2</sub> with abnormal  $\delta^{13}\text{C}$  values that may be as low as -23 to -27 ‰ (Thorstensen et al., 1989; White and Chuma, 1987; see Figure 2-24). Such

low values cannot be accounted for by the local plant community input, so that the most likely source of this CO<sub>2</sub> is oxidation of CH<sub>4</sub> out-gassed from the aquifer. It is a well-established fact that the δ<sup>13</sup>C of thermogenic methane depends on the maturity of the parent organic material (Hoefs, 1980). Paleozoic carbonate rocks underlying Yucca Mountain are known to have potential for natural gas (Grow et al., 1994). The Conodont color alteration index of these rocks (CAI = 3) corresponds to the vitrinite reflectance of 1.8 to 2.0 %, which indicates that the methane produced from these source-rocks may have δ<sup>13</sup>C ranging between -35 and -38 ‰ (Hoefs, 1980). Oxidation of such methane and subsequent mixing with the CO<sub>2</sub> of the underground atmosphere could produce the isotopically light CO<sub>2</sub> observed in the Yucca Mountain soils.

**Contribution of different sources into the isotopic composition of soil CO<sub>2</sub>.** Carbon from all four pools mixes in the soil environment and may become incorporated into the precipitating calcite. The ultimate isotope composition of carbon that will be incorporated in the calcite, however, depends not only on the isotopic values of the source terms, but also on the respective shares of these source terms ( $n_i c_i$ ), where  $n_i$  is volumetric or mass share of solution, containing dissolved CO<sub>2</sub> with δ<sup>13</sup>C<sub>*i*</sub>, and  $c_i$  is the concentration of CO<sub>2</sub>(aq) in the solution. The ultimate isotopic composition of carbon in the soil solution, from which calcite will form, may be expressed as:

$$\delta^{13}C_{\text{soilsolution}} = \frac{(\delta^{13}C_c \cdot c_c \cdot n_c + \delta^{13}C_a \cdot c_a \cdot n_a + \delta^{13}C_p \cdot c_p \cdot n_p + \delta^{13}C_{ds} \cdot c_{ds} \cdot n_{ds})}{(c_c \cdot n_c + c_a \cdot n_a + c_p \cdot n_p + c_{ds} \cdot n_{ds})} \quad (3-3-1)$$

and

$$n_c + n_a + n_p + n_{ds} = 1 \quad (3-3-2)$$

where lower indices  $c$ ,  $a$ ,  $p$ , and  $ds$  indicate carbonate, atmospheric, plant, and deep-seated sources of CO<sub>2</sub>, respectively. For example, the input from rainwater equilibrated with the atmospheric CO<sub>2</sub> ( $p\text{CO}_2 \cong 0.003$ ) may be roughly equal to the input from the ten times smaller amount of soil moisture equilibrated with the plant-derived CO<sub>2</sub> ( $p\text{CO}_2 \cong 0.03$ ) because concentration of the later in the soil air is about an order of magnitude greater than in the atmospheric air (i.e.,  $n_p \gg n_a$ ).

The plant CO<sub>2</sub> source term may further be expanded in the form:

$$\delta^{13}C_p = \frac{(\delta^{13}C_{C3} \cdot c_{C3} \cdot n_{C3} + \delta^{13}C_{C4} \cdot c_{C4} \cdot n_{C4} + \delta^{13}C_{CAM} \cdot c_{CAM} \cdot n_{CAM})}{(c_{C3} \cdot n_{C3} + c_{C4} \cdot n_{C4} + c_{CAM} \cdot n_{CAM})} \quad (3-3-3)$$

and

$$n_{C3} + n_{C4} + n_{CAM} = n_p \quad (3-3-4)$$

where lower indices *C3*, *C4*, and *CAM* indicate the metabolic pathways of plants respiring CO<sub>2</sub>. The term  $n_p c_p = (c_{C3} n_{C3} + c_{C4} n_{C4} + c_{CAM} n_{CAM})$  may be viewed as a proxy of the soil respiration rate.

The deep-seated source term may also be expanded in order to account for possible input from methane oxidation ("light" CO<sub>2</sub>), carbonate rocks decarbonation ("heavy" CO<sub>2</sub>), mantle CO<sub>2</sub>, CO<sub>2</sub> of the vadose zone (which, in turn may be a mixture of atmospheric and plant-derived CO<sub>2</sub> degassing from percolating meteoric waters), etc. This is not practical, however, because all of the sources are, in most instances, not quantifiable. The purpose of considering the expansion of the source terms is to demonstrate that a multitude of mixing scenarios involving input of CO<sub>2</sub> derived from very disparate sources may result in the identical isotopic compositions of soil CO<sub>2</sub>.

Whereas the atmospheric source-term may be viewed as largely constant, both, the plant CO<sub>2</sub> production rates and its isotopic properties may vary in time. The variations may be traced at the seasonal scale. For example, a two-fold difference in respiration rates and differences in δ<sup>13</sup>C ranging from 1 ‰ to as much as 11 ‰ were documented in soils in the Spring and Grapevine Mountains, Nevada, between spring and fall; Quade et al., 1989. Conceivably, similar variations may be expected to occur in association with the long-term climatic changes.

The rate of aquifer degassing is variably controlled by (a) the amount of CO<sub>2</sub> and CH<sub>4</sub> dissolved in the aquifer water at a given time and (b) the pneumatic conductivity of the rock between the water table and the Earth's surface. The first parameter may vary in concert with the tectonic development of the region, becoming greater during times of tectonic and/or magmatic activations. The second parameter may exert control by conducting changes in barometric pressure (e.g., changes related to the passage of atmospheric fronts) to the water table, thus changing the boundary conditions for degassing. (The role of changing atmospheric pressure in degassing of radon from subterranean waters and rocks is well documented in natural karst caves, e.g., Klimchuk and Nasedkin, 1992; Barnes et al., 1996). Generally, the role of the deep-seated source must be the greatest in the vicinity of the deep permeable fault zones. These are the transmissive structures, along which convective circulation of waters below the water table occurs readily (see Figures 1-24 and 1-31), and, thus, the appearance of waters carrying elevated amounts of dissolved CO<sub>2</sub> and CH<sub>4</sub> at the water table is most likely. Above the water table, the fault zones must have greater pneumatic conductivity than the rock far from faults.

Unfortunately, at Yucca Mountain, the number of boreholes for which gas data are available is limited in terms of both area coverage and depth. All instrumented boreholes from which data for the assessment of the migration of carbon gases were collected (UZ-1, SD-12, NRG-6, and NRG-7a) are located in the central part of the Yucca Mountain horst block, far from the major block-bounding faults (Solitario Canyon and Paintbrush fault zones). Thus, conclusions concerning the preferential downward

movement of gases in the vadose zone of Yucca Mountain via simple Fickian diffusion (e.g., Fabryka-Martin et al. 2000) may not be applicable to the more-fractured zones associated with the faults.

The isotopic character of soil CO<sub>2</sub> changes non-linearly across soil profiles (at a scale of 0.1 to 1.0 m) reflecting an interaction of two opposite CO<sub>2</sub> fluxes: the upward directed flux of isotopically "light" plant-produced CO<sub>2</sub> and the downward directed flux of isotopically "heavy" atmospheric CO<sub>2</sub>. The role of the latter decreases exponentially with depth, effectively vanishing at a depth of 10 to 50 cm, where, normally, plant-produced CO<sub>2</sub> prevails. Apparently, in some settings, the isotopically light deep-seated CO<sub>2</sub> may complement and reinforce the plant CO<sub>2</sub> source-term. The isotopic trend outlined above is recorded by carbonate depositing at different depths in the soil column. Quade et al. (1989) reported a decrease in the  $\delta^{13}\text{C}$  of soil calcite from +4 to +6 ‰ at the soil-air interface to -2 to -6 ‰ across the 100 cm-thick soil column. The role of atmospheric CO<sub>2</sub> must be recognizable at greater depths in the parts of the surface regolith that are devoid of or carry less vegetation (e.g., eolian sand deposits).

#### 3.3.3.1.2. Spring setting

**Carbonate rock-derived CO<sub>2</sub>** supplies isotopically heavy ( $\delta^{13}\text{C} = 0 \pm 4$  ‰) carbon for the travertine carbonates.

**Atmospheric CO<sub>2</sub>.** Precipitation of spring carbonate occurs in direct contact with the atmosphere. The leading mechanism of precipitation, however, is the escape of dissolved CO<sub>2</sub> into the gas phase, which makes the chances of any appreciable amounts of atmospheric CO<sub>2</sub> being incorporated into the depositing calcite, negligible. Craig (1953) first demonstrated that the deposition of travertine is so rapid that isotopic equilibration with the atmosphere does not take place.

**Plant (biota)-derived CO<sub>2</sub>.** Its role is largely dependent on (a) whether or not the spring orifice zone is colonized by biota, and (b) the water (plus dissolved CO<sub>2</sub>) discharge rate. The chemistry and the temperature of the discharging fluids, the combination of which may or may not create optimal habitat conditions, commonly control the first parameter. Another factor controlling it is the longevity of the spring activity, which must be substantial enough for the plants/biota community to establish itself. At Yucca Mountain, one location where these criteria were apparently met is the Busted Butte veins, which show abundant calcified root remnants (see Figure 3-3-3-c). Even if the biological activity at the orifice is present, the CO<sub>2</sub> carried by the discharging water may still dominate, thus controlling the isotopic values of the depositing carbonates.

**Deep-seated CO<sub>2</sub>.** This type of CO<sub>2</sub> is expected to predominate in the hot/warm spring setting. In this case, CO<sub>2</sub> is brought to the surface dissolved in water and its escape into the vapor phase effectively controls the precipitation of CaCO<sub>3</sub>. In addition, effervescence may occur as the fluid rises toward the

Earth's surface, which may lead to isotopic fractionation (i.e., enrichment of dissolved CO<sub>2</sub> with the "heavy" isotope <sup>13</sup>C).

The isotopic properties of carbon that become incorporated into the precipitating calcite are controlled by a number of mechanisms. Isotopic composition of carbon dissolved in hot water (mostly in form of the bicarbonate ion) serves as the starting point. Upon discharge at the topographic surface, CO<sub>2</sub> degassing occurs and calcite begins to precipitate. This precipitation, however, does not typically take place at isotopic equilibrium. If the rate of escape of CO<sub>2</sub> from the solution is not sufficiently slow, the isotopically lighter <sup>12</sup>CO<sub>2</sub> molecules will preferentially escape in the gas phase thus enriching the remaining solution and calcite depositing from it in the heavy <sup>13</sup>C isotope (Turi, 1986).

An important characteristic of this trend is its unidirectional character. As Gonfiantini et al. (1968) have established, "*The rate of escape of CO<sub>2</sub>, proportional to the CO<sub>2</sub> concentration in thermal waters, appears to be the controlling factor of disequilibrium. The system H<sub>2</sub>O-CO<sub>3</sub><sup>2-</sup>-HCO<sub>3</sub><sup>-</sup>-CO<sub>2</sub> is in isotopic equilibrium when the thermal waters reach the surface, and here the equilibrium is suddenly broken by fast outgassing of CO<sub>2</sub> at the orifices of springs. From this moment the system evolves towards the equilibrium corresponding to the surface conditions; the equilibrium is reestablished when the escape of CO<sub>2</sub> and the consequent deposition of CaCO<sub>3</sub> becomes very slow...*" (p. 57). The lateral δ<sup>13</sup>C enrichment trends have been reported from travertine depositing hot and ambient-temperature springs all around the world (e.g., Gonfiantini et al., 1968; Michaelis et al., 1985; Chafetz and Lawrence, 1994). It also has been demonstrated that under fast precipitation conditions the δ<sup>13</sup>C enrichment in the carbonate relative to HCO<sub>3</sub><sup>-</sup> is much lower than that at equilibrium (Turi, 1986). Studies of CO<sub>2</sub> and travertines collected at the orifices of 11 springs in Italy provided the following empirical relationship (Panichi and Tongiorgi, 1975):

$$\delta^{13}C_{CO_2} = 1.2\delta^{13}C_{travertine} - 10.5 \quad (3-3-5)$$

### 3.3.3.2. Oxygen

#### 3.3.3.2.1. Pedogenic setting

The oxygen isotopic composition of the soil water is primarily controlled by precipitation. Thus, for the pedogenic setting, there is only one "pool" of oxygen.

The variability of the δ<sup>18</sup>O in soil water and, subsequently, in pedogenic calcite may be caused by a number of factors.

1. The δ<sup>18</sup>O in atmospheric precipitation is largely controlled by climate, becoming greater during warm climatic periods (interglacials) and smaller during cooler (glacial or pluvial) periods. Similar

control may be exerted by orography, with oxygen in the precipitation process becoming "lighter" at greater altitudes.

2. The  $\delta^{18}\text{O}$  in atmospheric precipitation also varies through seasons of the year with winter precipitation containing isotopically lighter waters. This may play a role if carbonates form seasonally or if the depth and the velocity of water infiltration through soils change between different seasons (e.g., shallow percolation in summer and deep percolation during winter storm events).

3. When rainfall waters become soil solutions, their isotopic composition may be modified by evaporation. The latter shifts  $\delta^{18}\text{O}$  toward heavier values. This effect has been observed in many groundwaters in semi-arid regions (Fontes, 1980). The effect of evaporation is more pronounced immediately near the soil surface and decreases with depth. For example, Quade et al. (1989) reported an overall downward decrease in  $\delta^{18}\text{O}$  of 5 to 8 ‰ across a 1.0 to 1.2 m-thick soil profile. The mechanism is more efficient in hot and dry, arid settings.

#### 3.3.3.2.2. Spring setting

The source of oxygen in calcite depositing near a spring orifice is the spring's water. If precipitation occurs under equilibrium conditions, the  $^{18}\text{O}$  would distribute itself between the depositing calcite and the water in a manner that depends on the temperature of the water. The equilibrium isotope fractionation factor for the calcite-water system is defined as:

$$\Delta_{\text{CaCO}_3-\text{H}_2\text{O}} = 2.78 \cdot (10^6 T^{-2}) - 2.89 \quad (3-3-6)$$

where  $T$  is the temperature in K (by Friedman and O'Neil, 1977, as reported in Faure 1986, p. 462).

The  $\Delta$  value increases with decreasing temperature (e.g., from ~24 ‰ at 50 °C to ~31 ‰ at 15 °C). It has long been established, however, that many travertines have  $\delta^{18}\text{O}$  compositions, which do not correspond to the isotopic equilibrium with waters from which they are precipitated (Fritz, 1965). For the majority of the travertine systems, the values of isotopic fractionation were found to be greater than those corresponding to equilibrium (Turi, 1986). Friedman (1970) has demonstrated that the deviation from equilibrium increases with increasing rates of water movement and travertine deposition. The deviation from equilibrium decreases as the distance from the orifice increases (and thus, the temperature decreases). Since the fractionation factor increases with the decreasing temperature, the calcite depositing from such cooling water shows the progressively "heavier" values of the incorporated  $\delta^{18}\text{O}$ .

Another factor, leading to the systematic change in isotopic properties of the hot spring waters is evaporation, which leads to the progressive enrichment of waters in heavy  $^{18}\text{O}$  isotope. The rate of

evaporation depends strongly (exponentially) on the temperature, so the role of this factor decreases with distance away from the hot spring orifices, as the water cools down.

Due to the coupled action of the two factors described above, the isotopic values measured in carbonates, depositing from thermal waters discharging at the ground surface, commonly exhibit spectacular  $\delta^{18}\text{O}$  enrichment trends along the flow paths (Gonfiantini et al. 1968, Friedman, 1970; Chafetz and Lawrence, 1994). The effect is not typically observed in ambient-water springs. There, the water discharging on the topographic surface does not cool down, and evaporation is largely suppressed; the  $\delta^{18}\text{O}$  in the water and the depositing carbonate thus remains constant. Gonfiantini et al. (1968) concluded that "... large  $\delta^{18}\text{O}$  variations are possible only if the spring has a high temperature; cold springs produce travertines with practically constant oxygen isotopic composition " (p . 58).

### 3.3.3.3. Isotopic trends and correlations in pedogenic calcite and aquifer water

#### 3.3.3.3.1. Pedogenic carbonates

Pedogenic carbonates, sampled at individual locations are likely to exhibit a positive correlation between  $\delta^{13}\text{C}$  and  $\delta^{18}\text{O}$  values. This positive correlation stems from the fact that across the soil profile both isotopes change their values in a systematic manner. The controlling factors (i.e., mixing of light plant derived and heavy atmospheric  $\text{CO}_2$  for carbon and evaporation for oxygen), operating concurrently, tend to shift the isotopic values in the same direction (making both isotopic values heavier near the soil-air interface and lighter at deeper horizons within soils).

Another trend of concurrent decrease in the carbon and the oxygen isotope values with altitude was reported by a number of researchers of soil carbonates in the Great Basin. With increasing altitude, the  $\delta^{18}\text{O}$  of atmospheric precipitations becomes smaller. Concurrently, the  $\delta^{13}\text{C}$  in soils, analyzed along the elevation transects in the Great Basin increase at a rate of 4.6 to approximately 5 ‰ per 1000 m of altitude (Amundson et al. 1988; Quade et al. 1989). These authors held contrasting views as to what parameters control the observed systematic decrease in the soil  $\text{CO}_2$  isotopic composition.

Quade et al. (1989) were of the opinion that the variations result from differing soil-respiration rates, as well as from variations in the proportion of  $\text{C}_3$  to  $\text{C}_4$  and CAM plants in each site's surface biomass. By contrast, Amundson et al. (1988) concluded that in the arid regions (specifically, in the Mojave Desert) the  $\delta^{13}\text{C}$  of the pedogenic carbonates is primarily controlled by plant density, because the vegetation is, largely, isotopically homogeneous. In more humid regions, however, the  $\delta^{13}\text{C}$  of the carbonate is believed to be directly related to the isotopic composition of the vegetation (Cerling, 1984), although the control is sometimes variable (Talma and Netterberg, 1983). Quade et al (1989) concluded that when respiration rates are greater than about  $3 \text{ mmol m}^{-2} \text{ h}^{-1}$ , they are no longer a determining

factor in the  $\delta^{13}\text{C}$  content of soil carbonates, and the later is effectively controlled by the isotopic properties of the surface-plant biomass.

#### 3.3.3.3.2. Aquifer water

Carbonates deposited in connection with the discharge of regional aquifer in Devils Hole, Nevada display a strong negative correlation between carbon and oxygen isotopes (see Figure 2-16). The reason for this correlation remains unclear. It has been speculated that the feature is related to the change in the vegetation style, during the glacial periods, from subalpine to alpine in the upland recharge areas (Coplen et al. 1994). If recharge of aquifer were controlled primarily by uplands, this would lead to the increase in  $\delta^{13}\text{C}$  values of dissolved inorganic carbon in waters during glacial periods. The authors of this concept admit, however, that it is "seemingly contradicted by some paleohydrological evidence" (Coplen et al. 1994).

#### 3.3.3.4. Isotopic trends and correlations in travertine calcite

Gonfiantini et al. (1968) reported that a positive correlation exists between  $\delta^{18}\text{O}$  and  $\delta^{13}\text{C}$  in samples from the majority of the modern, fossil travertine deposits: *"The lowest  $\delta$  values are exhibited by  $\text{CaCO}_3$  deposited at the orifices of the springs; as the distance from the springs increases, the  $^{13}\text{C}$  and  $^{18}\text{O}$  contents of  $\text{CaCO}_3$  increase, because of the progressive  $^{13}\text{C}$  enrichment of the dissolved bicarbonate ... due to the preferential escape of isotopically light carbon dioxide, and because of the progressive cooling and  $\delta^{18}\text{O}$  enrichment by evaporation of the thermal waters."* (p. 57).

Travertine deposits with a nearly constant  $\delta^{18}\text{O}$  are also known. This happens when the cooling and the disequilibrium effects compensate each other. The  $\delta^{18}\text{O}$  values that do not change systematically with distance away from orifice were also reported for the ambient-temperature springs (Chafetz and Lawrence, 1994). Such a situation results in zero-correlation between  $\delta^{13}\text{C}$  and  $\delta^{18}\text{O}$ . Gonfiantini et al. (1968) also reported rare situations of weak negative correlation between  $\delta^{13}\text{C}$  and  $\delta^{18}\text{O}$ . This can occur in near-ambient springs, in which both cooling and evaporation are negligible.

#### 3.3.3.5. Discussion: The use of stable carbon and oxygen isotopes as environmental indicators

##### 3.3.3.5.1. Comparative approach

Establishing the mechanism of deposition of carbonates by a simple comparison of their isotopic values with the values of deposits with known (or presumably known) origin will not, in most instances, provide an unambiguous answer. As it is apparent from the Figure 3-3-15, the controversial Yucca Mountain surface calcretes and bedrock vein deposits are compatible with both pedogenic and travertine

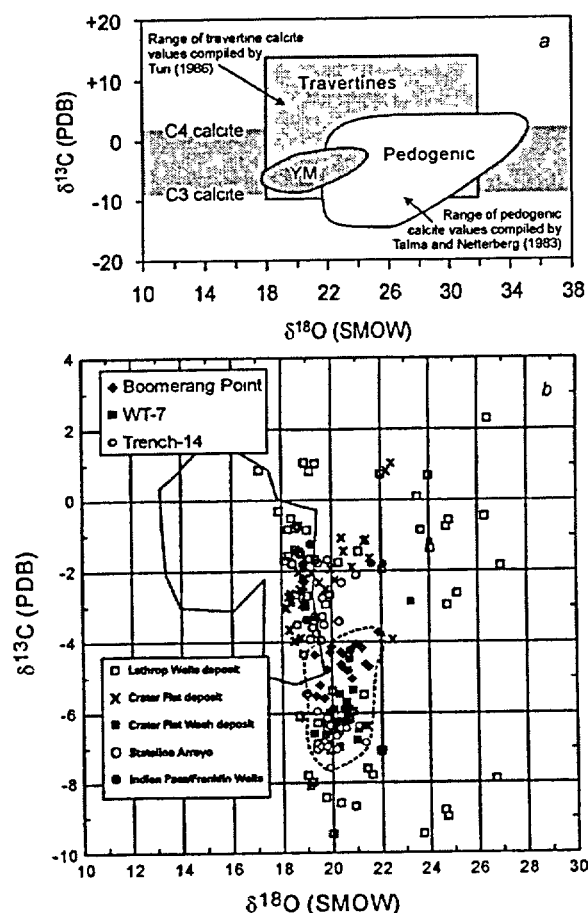


Figure 3-3-15. Comparative C-O isotope data for carbonate deposits formed at the Earth's surface. *a* -  $\delta^{18}\text{O}$  -  $\delta^{13}\text{C}$  plot of travertines, pedogenic calcites and the Yucca Mountain surface calcretes (YM). The field for travertines is constructed based on the data presented in Turi (1986); field for pedogenic carbonates is based on data compiled by Talma and Netterberg (1983). The field of the  $\delta^{13}\text{C}$  values of the C3- and C4-derived calcite is shown for comparison. *b* -  $\delta^{18}\text{O}$  -  $\delta^{13}\text{C}$  plot of carbonates from paleodischarge deposits near Yucca Mountain (from Forester et al. 1995) compared with the compositions of vein facies of the controversial carbonates from Boomerang Point near the Solitario Canyon mouth, WT-7, and Trench 14 (data from U.S. DOE, 1993 and Dublyansky, 2001-c). Polygon formed by solid line represents compositions of tufa and travertine deposits associated with sites of active discharge from regional Paleozoic aquifers (Grapevine Springs and Nevaes Springs in Death Valley, Devils Hole in Ash Meadows).

modes of deposition. A simple comparative analysis, thus, must be rejected as a methodology for determining the nature of deposition and an origin for the carbonates.

### 3.3.3.5.2. Trend analysis

One way of utilizing the  $\delta^{13}\text{C}$  and  $\delta^{18}\text{O}$  characteristics of carbonates would be to search for systematic variations (isotopic trends). For example, a systematic increase in  $\delta^{13}\text{C}$  toward the surface across the soil profile would be compatible with the pedogenic setting (although not entirely incompatible with the spring deposit one). A systematic increase of both  $\delta^{18}\text{O}$  and  $\delta^{13}\text{C}$  in the lateral direction and down slope (i.e., along the anticipated flow path) would serve as strong evidence of a hot spring setting. A cool spring setting may be indicated if only  $\delta^{13}\text{C}$  exhibits a systematic increase along the inferred flow path.

### 3.3.3.5.3. Correlation analysis

A positive correlation between  $\delta^{13}\text{C}$  and  $\delta^{18}\text{O}$  in individual locations (e.g., profiles across the massive carbonate deposits) are compatible with both pedogenic and spring settings. A consistent increase in the  $\delta^{18}\text{O}$  and  $\delta^{13}\text{C}$  values near the carbonate deposit-atmosphere interface would favor a pedogenic

setting, since in this setting the volumes of water involved are smaller than those in the springs, so that the effects of evaporation at the contact with the atmosphere and the incorporation of the "heavy" atmospheric CO<sub>2</sub> are expected to be more pronounced. Similar features, however, are possible in hot spring settings if the topography allows for pooling or slow seepage of thermal waters (e.g., a sienaga environment).

A complicating factor that must be recognized is the possible modification of calcite by late processes. Isotopic studies, thus, must be complementary to other ones, such as geological observations, textural features, mineralogy and geochemistry pertaining to the studied deposits.

#### 3.3.4. Isotopes of the <sup>238</sup>U Decay Series

To bolster their contention that the calcite-silica deposits at the topographic surface of Yucca Mountain must have been formed from infiltrating rainwater, the Yucca Mountain Project scientists have extensively used <sup>234</sup>U/<sup>238</sup>U ratios to link these deposits with rainwater. Their rationale apparently stems from the fact that infiltrating rainwater resides at the ground surface for short periods of time, so that the preferential <sup>234</sup>U-enrichment via the α-recoil mechanism and via the leaching from radiation damaged <sup>234</sup>U-sites is practically non-existent. This has the effect of keeping the <sup>234</sup>U/<sup>238</sup>U activity ratio for rainwater low. Atmospheric precipitations in the arid zone typically have activity ratios close to the secular equilibrium-value of one (Zverev et al., 1980; Gascoyne 1992). Deposits precipitated from such rainwater would inherit these low activity ratios, so that the latter may be taken as support for the pedogenic origin. Assuming this effect as given, the Yucca Mountain Project scientists then proceed to demonstrate two points, both of which are illustrated on Figure 3-3-16.

As to the first point, Stuckless et al. (1991) demonstrated that the present-day aquifer fluids at Yucca Mountain carry <sup>234</sup>U/<sup>238</sup>U values, which are higher than the inferred initial <sup>234</sup>U/<sup>238</sup>U ratio for parental fluids of the calcite-silica deposits. A similar incompatibility is also expressed by the <sup>87</sup>Sr/<sup>86</sup>Sr ratios, so that the authors regarded both of the incompatibilities as "*evidence against upwelling water.*"

Although this conclusion is narrowly permissible, the evidence is equivocal and allows for only ruling out the upwelling of those fluids whose U- and Sr-radiochemistry is similar to that of the present-day aquifer fluids. It is possible to rule out all "*upwelling water*" only by introducing the premise, which states that factors controlling U- and Sr-radiochemistry of aquifer fluids remain invariant with respect to time. This premise is valid only for a hydrologic system for which the state of boundary conditions along the base of the system does not change over time. The premise must be deemed inappropriate where seismic pumping and Rayleigh-Bernard instabilities are an intrinsic part of the dynamics of the system.

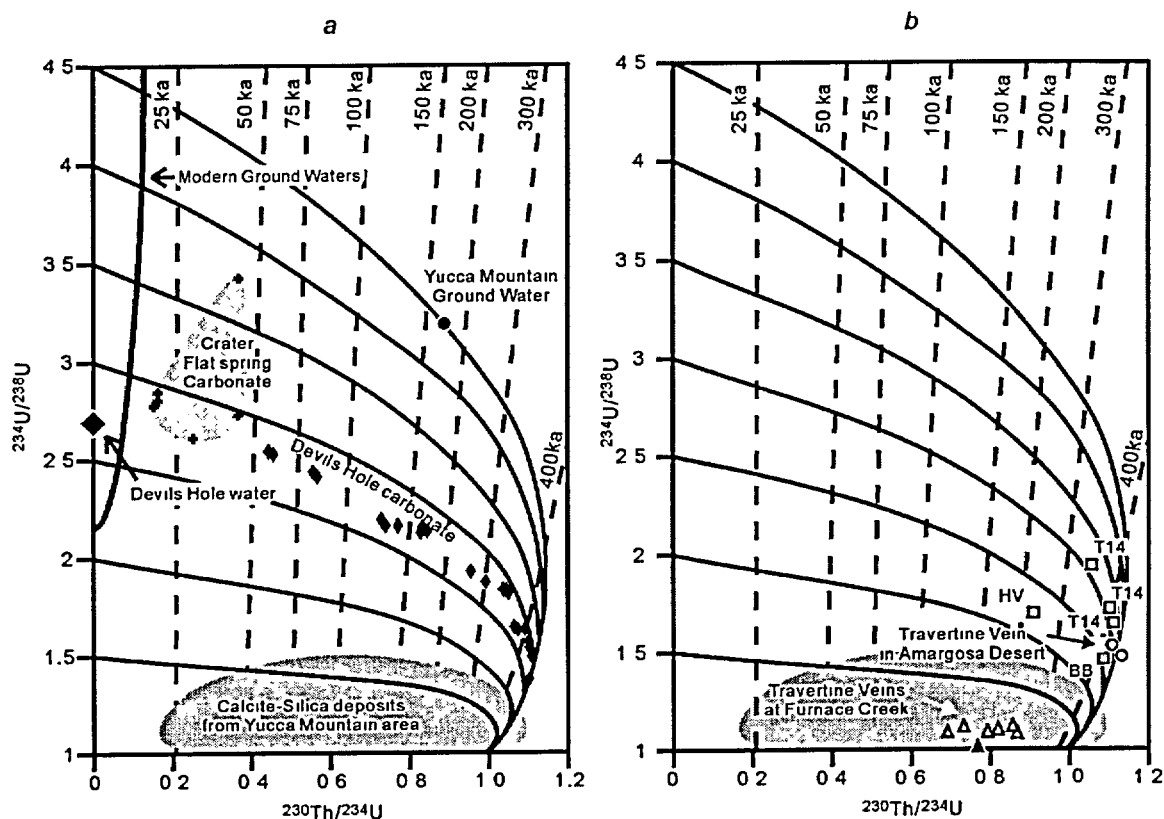


Figure 3-3-16. U-series isochron diagrams.

(a) Values of the calcite-silica surface deposits from the Yucca Mountain (gray area), as well as data for carbonate deposits, for which the spring origin is known with certainty (Devil's Hole carbonates and Crater Flat spring deposits). These U-series data are interpreted as "evidence" for pedogenic (i.e. from infiltrating rainwater) origin of the calcite-silica deposits. Modified from Paces et al. (1993).

(b) Data for spring deposits and some calcite-silica deposits from the Yucca Mountain area compared with the field of results for the Yucca Mountain surficial calcite-silica deposits (gray area, by Paces et al. 1993). *Triangles* - travertine veins at Furnace Creek (white - total dissolution, gray - carbonate leach, black - insoluble residue); *circles* - travertine vein from Amargosa Desert (by Szabo and O'Malley 1985); *squares* - deposits from Busted Butte, Trench 14 and Harper Valley (BB, T14, and HV; by Harmon 1993).

Because it is a *non sequitur* to investigate a changing water table by assuming it to be unchanged, the Stuckless's et al. (1991) conclusion lacks a logical foundation.

As to the second point, Paces et al. (1993) have shown that the present-day and, by inference, the initial  $^{234}\text{U}/^{238}\text{U}$  values from the controversial calcite-silica deposits are systematically lower than those from the local spring-deposits (see Figure 3-3-16-a). The latter deposits occur at Devil's Hole and at the Crater Flat (LWD and CFD groundwater discharge sites; see Figure 2-14 and the corresponding discussion). The authors regarded the differences in the initial  $^{234}\text{U}/^{238}\text{U}$  values, which were inferred by assuming a closed-system behavior, as evidence against a spring origin for the controversial calcite-silica deposits.

A close examination of the Paces et al. (1993) argument indicates that some of the relevant data are missing from the U-series isochron diagram shown on Figure 3-3-16-a. The missing data points, shown in Figure 3-3-16-b, represent travertine veins from the Furnace Creek and Amargosa Desert areas. Importantly, these clearly non-pedogenic travertine veins were found by the USGS scientists to carry  $^{234}\text{U}/^{238}\text{U}$  and  $^{230}\text{Th}/^{234}\text{U}$  values, identical to those from the controversial calcite-silica deposits from Yucca Mountain. Szabo and O'Malley (1985) reported that the Furnace Creek travertine veins (four samples) carry  $^{234}\text{U}/^{238}\text{U}$  activity ratios between  $1.07\pm 0.02$  and  $1.11\pm 0.02$  and  $^{230}\text{Th}/^{234}\text{U}$  activity ratios between  $0.793\pm 0.03$  and  $0.868\pm 0.035$ . For the Amargosa Desert travertine veins (two samples) the reported values are between  $1.486\pm 0.022$  and  $1.522\pm 0.022$  for  $^{234}\text{U}/^{238}\text{U}$  and between  $1.11\pm 0.03$  and  $1.13\pm 0.03$  for  $^{230}\text{Th}/^{234}\text{U}$ .

Harmon (1993) reported results of independent studies of the  $^{234}\text{U}/^{238}\text{U}$  ratios of the calcite-silica deposits. Out of nine samples, only four yielded  $^{230}\text{Th}/^{234}\text{U}$  activity ratios of less than 1.2, which made them suitable for inferring both the initial  $^{234}\text{U}/^{238}\text{U}$  ratio and the  $^{230}\text{Th}/\text{U}$  age determinations. Two of these samples, #36n from Trench 14 and #39a from Harper Valley, immediately to the west of the Busted Butte, yielded finite  $^{230}\text{Th}/\text{U}$  ages. The two additional samples, #30a from the Busted Butte and #36p2 from Trench 14, yielded  $^{234}\text{U}/^{238}\text{U}$  and  $^{230}\text{Th}/^{234}\text{U}$  values very close to secular equilibrium. For the remaining samples (two from the eastern Busted Butte and three from Trench 14)  $^{230}\text{Th}/^{234}\text{U}$  values are between  $1.37\pm 0.13$  and  $3.97\pm 0.79$ . These values are too high for a meaningful determination of the initial  $^{234}\text{U}/^{238}\text{U}$  ratio or for a meaningful  $^{230}\text{Th}/\text{U}$  age determination. They might indicate a post-depositional loss of  $^{234}\text{U}$  through the leaching of "hot" atoms by infiltrating rainwater or they could indicate contamination by detrital thorium.

Results presented in Szabo and O'Malley (1985) and those in Harmon (1993) complement each other in casting serious doubts on the validity of conclusions drawn by Paces et al. (1993) relative to the pedogenic origin of the calcite-silica deposits. Both sets of results are summarized on Figure 3-3-16-b. The figure shows that the present-day  $^{234}\text{U}/^{238}\text{U}$  and  $^{230}\text{Th}/^{234}\text{U}$  ratios from the travertine veins are identical to those measured in pedogenic deposits. These ratios, thus, are incapable of distinguishing the former from the latter. Furthermore, some of the deposits, which carry acceptably low  $^{230}\text{Th}/^{234}\text{U}$  values, also carry  $^{234}\text{U}/^{238}\text{U}$  values indicating the initial  $^{234}\text{U}/^{238}\text{U}$  ratios between 2.5 and 3.5. This initial value is identical to that from the spring-deposits (see Figure 3-3-16-a).

The analysis presented above demonstrates that spring deposits in the Yucca Mountain region may carry initial  $^{234}\text{U}/^{238}\text{U}$  ratios identical to those measured in the controversial calcite-silica deposits, and that these values range between 1 and 3.5. The latter high values in turn imply that the contention regarding the origination of solutions that deposited calcite and silica at the Yucca Mountain surface from

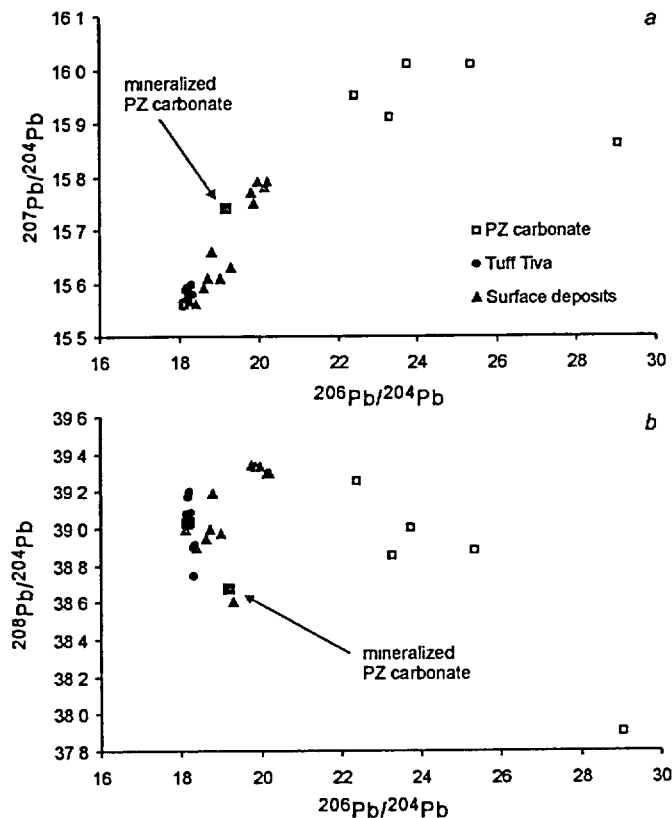


Figure 3-3-17. Pb isotope ratios in bedrock tuffs Tiva, mineralized and non-mineralized Paleozoic carbonates, and in surface vein and slope deposits from Trench 14 (data from Zartman and Kwak, 1993-a and -b).

a atmospheric precipitation, which would have characteristic  $^{234}\text{U}/^{238}\text{U}$  ratios close to unity, is not supported by the data.

### 3.3.5. Pb-Isotope Ratios

In considering the Pb-radiochemistry of a surface geologic material, such as a tuff or a calcite-silica deposit, it is important to keep in mind that Pb behaves as a very conservative element. For example, a granite melt (future tuff) has certain  $^{238}\text{U}/^{204}\text{Pb}$ ,  $^{235}\text{U}/^{204}\text{Pb}$  and  $^{232}\text{Th}/^{204}\text{Pb}$  ratios ( $^{206}\text{Pb}/^{204}\text{Pb}$ ,  $^{207}\text{Pb}/^{204}\text{Pb}$ , and  $^{208}\text{Pb}/^{204}\text{Pb}$  as well) at the time of its derivation, which the melt inherits from the melted crust. With an increasing age of the solidified tuff these three ratios decrease due to the decay of the U and Th isotopes, so that the ratios  $^{206}\text{Pb}/^{204}\text{Pb}$ ,  $^{207}\text{Pb}/^{204}\text{Pb}$ , and  $^{208}\text{Pb}/^{204}\text{Pb}$  increase accordingly. For a

young, late Tertiary tuff, however, these changes are very small, so that the tuff carries the Pb-isotope ratios, which are almost identical to those in the melt-source rocks.

Intermixing of the tuff-native (indigenous) lead with detrital lead, brought with material, which has been deflated from the outcrops of marine carbonates, and then, transported in the form of windblown dust would have the effect of enriching the mixture somewhat in the uranogenic isotopes ( $^{206}\text{Pb}$  and  $^{207}\text{Pb}$ ).

Similarly, deep-seated solutions, which have equilibrated with rocks that previously have acted as the melt-source, initially would carry dissolved lead with Pb-isotope ratios that would be almost identical to those in these melt-source rocks (and, therefore in the tuff). The passage of these solutions through the overlying marine carbonates (relatively high U/Th ratio) would have the effect of enriching the solutions somewhat in uranogenic Pb isotopes ( $^{206}\text{Pb}$  and  $^{207}\text{Pb}$ ). The result here is that the Pb-isotope ratios are intrinsically incapable of revealing whether lead, which is incorporated in the Trench 14 deposits, is a

mixture of lead transported by pyroclastic flows (tuff-native) and the detrital lead (transported in the form of the wind-blown dust), or whether this lead has been transported, in part, by hydrothermal solutions. It thus appears that the conclusion drawn by Zartman and Kwak (1993-a, p. 1), which states that "... *the remarkably similar lead isotopic properties of the veins to those of the slope calcretes support their interpretation as a surficial, pedogenic phenomenon.*" is clearly equivocal and is rejected by us.

An additional perspective for the subsequent considerations of Pb-radiochemistry of the calcite-silica deposits is provided by the Pb-radiochemistry of both the host tuffs and the underlying marine carbonates. Figure 3-3-17 shows the Pb-isotope ratios for the tuffs, for the Pb-unaltered Paleozoic carbonates (including one mineralized Pb-enriched sample, HD-541, of these carbonates), as well as ratios for the vein and slope carbonates from Trench 14 (data from Zartman and Kwak, 1993-a and -b).

Figure 3-3-17 shows that, relative to the Pb-unaltered carbonates, lower  $^{206}\text{Pb}/^{204}\text{Pb}$  and  $^{207}\text{Pb}/^{204}\text{Pb}$  values and similar  $^{208}\text{Pb}/^{204}\text{Pb}$  values characterize the tuffs. These values indicate that melting of rocks with low U/Th ratios, such as the ones comprising the crystalline basement or their detrital derivatives (phyllite, quartzite, and their non-metamorphic equivalents) produced the tuffs. This figure further shows that the Pb-isotope ratio from the sample of mineralized Pb-enriched Paleozoic carbonate plots in-between those of the tuffs and those of the Pb-unaltered carbonates (sample with the greatest Pb content of 37.6 ppm has the smallest  $^{206}\text{Pb}/^{204}\text{Pb}$  ratio of 19.2). This observation is important because it suggests that the altering, U-, Th-, Pb-bearing and reducing hydrothermal solutions have, most probably, ascended from the crystalline basement beneath the carbonates. The highly radiogenic strontium isotope value of the mineralized sample of Proterozoic carbonate rock ( $^{87}\text{Sr}/^{86}\text{Sr} = 0.72151$ ; Zartman and Kwak, 1993) strongly suggests that these solutions were responsible for the  $^{87}\text{Sr}$ -alteration at Bare Mountain (see Figure 2-19 and the corresponding discussion). The figure further shows that the Pb-isotope ratios of these Pb- and  $^{87}\text{Sr}$ - bearing solutions are quite similar to those of lead that has been found to be incorporated in the carbonate fraction of the veins and calcretes at Trench 14. The evident affinity, between the isotope ratios from the Pb-altered carbonates (marine) and from controversial Trench 14 deposits, allows for considering a possibility that the same  $^{87}\text{Sr}$ - and Pb-enriched fluids, which would have originated in the clastic parts of the basement, have been involved in both the alteration and mineralization of the marine carbonates and the deposition of the Trench 14 deposits.

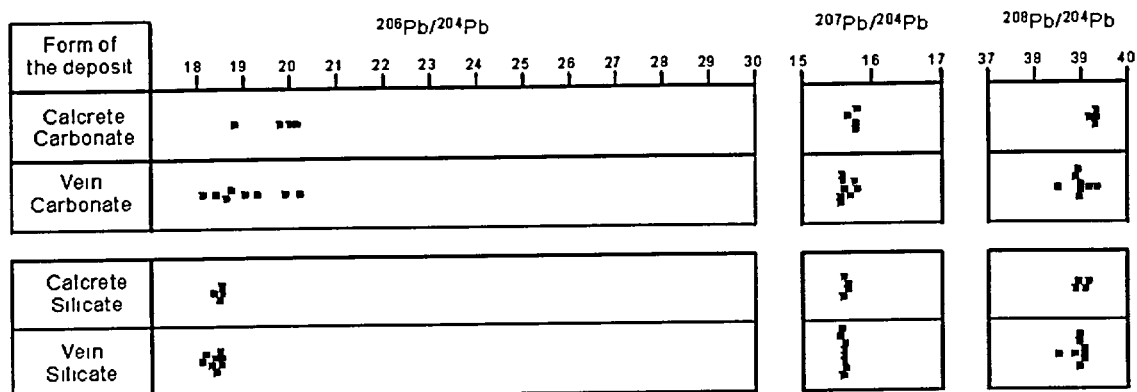


Figure 3-3-18. Pb-radiochemistry of calcite-silica deposits at Busted Butte and Trench 14. *Carbonate* refers to acid (0.8 N  $\text{CH}_3\text{COOH}$ , 2 hours) soluble fraction of sample, *silicate* – to the insoluble residue. *Calcrete*, and *vein* specify form of deposit, from which the sample was taken. Based on the data of Zartman and Kwak (1993-a).

The calcite-silica deposits in Trench 14 (Bow Ridge fault) and at the west side of Busted Butte (Paintbrush fault), are depicted in Figures 3-3-5 and 3-3-3, respectively. The Pb-isotope ratios for these deposits, plotted separately for leachate and for acid insoluble residue are shown on Figure 3-3-18. Figure shows that the isotopic characteristics of Pb, incorporated in the calcrete lithofacies, is for all practical purposes identical to that of the bedrock vein lithofacies. This isotopic similarity further confirms that both of the lithofacies share the same origin but does not provide any additional clues as to what this origin may be. The figure further shows that, as a whole, the incorporated Pb appears to be a mixture of two isotope species. One of these species is predominantly associated with the silicate fraction (acid-insoluble residue). This species is similar to the one, which is incorporated in the tuffs (see Figure 3-3-17). It is certain, therefore, that this species originates in the crystalline (Th-enriched) basement. It could have been transported to the ground surface by melt from which, upon volcanic eruption, tuffs have formed. The dissolution and re-precipitation of silica from these tuffs could have created opals bearing the "basement" Pb-signatures. Alternatively, upwelling hydrothermal solutions could have brought these signatures directly from the basement. The other species is associated with the carbonate fraction (leachate) and appears to be a mixture of two end-members, one of which is Pb from the crystalline basement and the other is Pb from the carbonate part of this basement (see Figure 3-3-17).

It thus appears that, based on the Pb-radiochemistry data alone, two equally plausible interpretations may be constructed (Figure 3-3-19). On the one hand, one may find that the interpretation developed by Zartman and Kwak (1993-a) is persuasive. In keeping with this interpretation, Pb incorporated in the calcite-silica deposits is a mixture of at least two end-members, one of which is Pb derived "... mainly from the chemical and mechanical breakdown of the adjacent...volcanic rocks." The other end-member has been introduced into the vein and calcretes "... by percolating surface water,

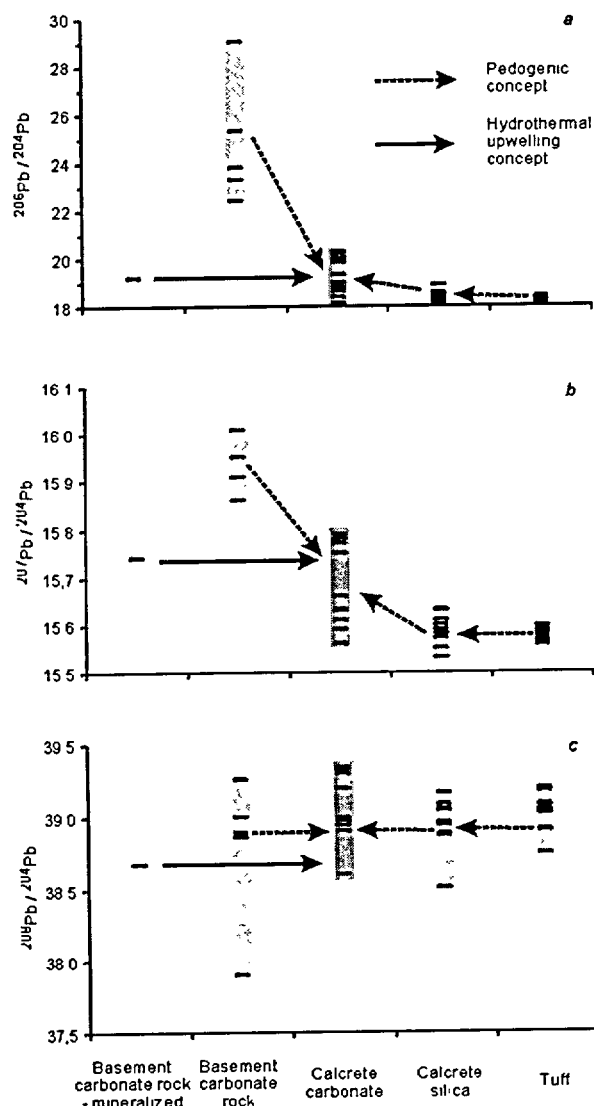


Figure 3-3-19. Conceptual models of the acquisition of lead by surficial calcite-silica deposits at Busted Butte and Trench 14. *Calccrete carbonate* refers to acid (0.8 N  $\text{CH}_3\text{COOH}$ , 2 hours) soluble fraction of sample, *Calccrete silica* – to the insoluble residue (data for both *calcrettes* and *veins* appear under this category). Category *Basement carbonate rock – mineralized* refers to the sample of mineralized marble from Bare Mountain with  $^{87}\text{Sr}/^{86}\text{Sr} = 0.72151$ . Based on the data of Zartman and Kwak (1993-a and -b).

which alternately dissolved and precipitated the hosting calcium carbonate. The ultimate source of the secondary carbonate lead was not conclusively demonstrated... but it was speculated that an eolian contribution to the soils...provided the best explanation for both the pedogenic carbonate and its contained lead." (p. 1953).

On the other hand, one may choose to recognize the radiogenic isotope (Sr and Pb) similarities between hydrothermal fluids, which were, most likely, responsible for the Pb-enrichment of the Paleozoic carbonate rock sample (see Figure 3-3-17), and fluids from which the near-surface calcite and silica were

precipitated. This similarity suggests that the same or similar fluids were involved in the Pb-enrichment of the Paleozoic carbonates and in the formation of the calcite-silica deposits. We know with confidence that both the hydrothermal fluids and the tuffs have originated in the crystalline basement, so that their Sr- and Pb-isotope properties would be similar. We also know with confidence that these  $^{87}\text{Sr}$ -enriched hydrothermal solutions have passed through the marine carbonates, so that they could have acquired, thereby, both the calcium and the more uraniumic Pb.

It thus becomes apparent that both interpretations share the same ultimate sources of Pb, which is incorporated in the calcite-silica deposits. Only the mode of Pb-transport, an eolian and magmatic-pyroclastic transport in case of the pedogenic hypothesis, or a hydrothermal transport in case of the competing upwelling water hypothesis, distinguishes these hypotheses. Because the Pb-isotope ratios only

provide information about the ultimate sources of Pb, but do not contain any information about the mode of transport, it is impossible to resolve the issue by considering these ratios alone.

### 3.3.6. Redox Potential

Oxidation means an increase in positive valence of an ion or a decrease in negative valence, and reduction means a change in the opposite direction. Alternatively, the oxidation may be described as a loss of electrons and the reduction as a gain, so that ionic radii decrease with the increasing positive valence. This is important because ionic radius is the chief parameter, which governs whether an ion is preferentially accommodated or excluded from the crystalline structure of a mineral phase.

The ability of a natural environment to bring about any oxidation or reduction process is expressed by its redox potential (Eh). The redox potential in many ways is analogous to pH. It expresses the ability of an environment to supply electrons to an oxidizing agent, or to take up electrons from a reducing agent, just as the pH of an environment expresses its ability to supply protons to a base or to take up protons from an acid. In a complex solution, the redox potential is determined by a number of reactions. The particular reactions are difficult to identify, and they are less important than the overall ability of the environment to maintain its redox potential and pH constant when small amounts of foreign material are added.

By controlling the valence of ions, the redox potential also controls the stability of mineral phases, in addition to controlling the ionic radii and solubility of various elements. To understand and constrain the redox potential is therefore essential for interpreting the observed abundances of trace elements, such as iron (Fe), uranium (U), cerium (Ce), and europium (Eu) in particular. The abundances of these trace elements are well known for the calcite-silica deposits at Yucca Mountain, and they may be used to further the understanding of circumstances under which these deposits were formed.

The proposed conceptual model (see Chapter 2-4) implies that the calcite-silica deposits have been formed, in part, from solutions that equilibrated with a low-Eh (reducing) environment. However, the strongest oxidizing agent found in nature is atmospheric oxygen. A stronger oxidizing agent than this cannot persist, because it would react with H<sub>2</sub>O to liberate oxygen. If it were presumed that a reducing fluid was brought up to the ground surface then, it follows that this fluid will eventually change its redox potential from reducing to oxidizing. It is this switch that now deserves attention.

Iron is a particularly sensitive indicator of the redox potential in the depositional environment. In a high-Eh (oxidizing) environment, it assumes the ferric form (Fe<sup>3+</sup>), whereas in a low-Eh (reducing)

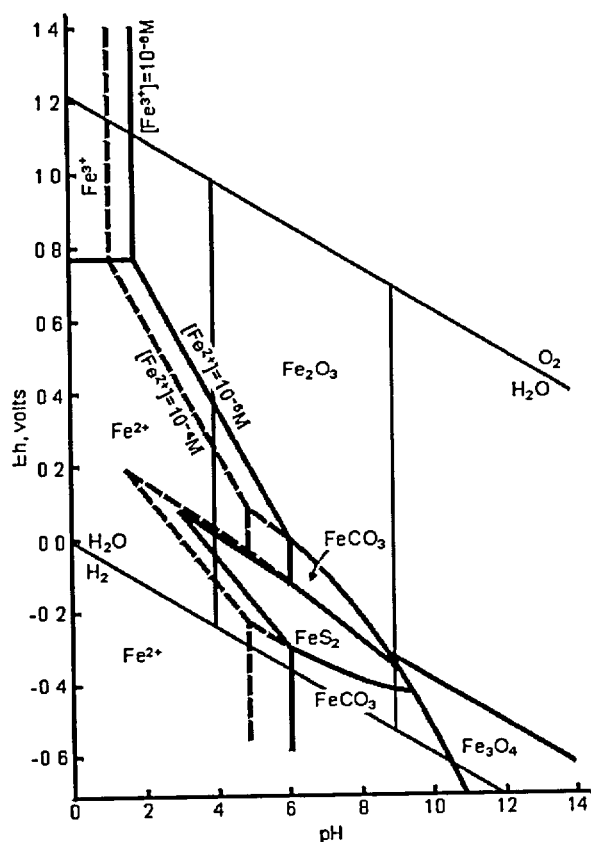


Figure 3-3-20. Eh-pH diagram showing stability fields of common iron minerals. Total activity of dissolved carbonate is 1 mole, of dissolved sulfur  $10^{-6}$  moles. Solid field boundaries are for total dissolved iron =  $10^{-6}$  moles, dashed lines for  $10^{-4}$  moles. After Garrels and Christ (1965).

environment it takes the ferric form ( $\text{Fe}^{2+}$  or rarely Fe). In the ferric form iron forms pyrite ( $\text{FeS}_2$ ) and magnetite  $[(\text{Fe}, \text{Mg})\text{Fe}_2\text{O}_4]$ , both of which have very narrow Eh-pH stability fields, as shown on Figure 3-3-20.

Figure 3-3-20 shows that hematite ( $\text{Fe}_2\text{O}_3$ ) is the stable mineral of iron in all moderately and strongly oxidizing environments. In a reducing environment, however, the stable minerals are siderite ( $\text{FeCO}_3$ ), pyrite ( $\text{FeS}_2$ ), and magnetite ( $\text{Fe}_3\text{O}_4$ ), depending upon concentrations of sulfur and carbonate in the solution. For conditions with a high abundance of carbonate but low abundance of sulfur, which are shown in the figure, siderite has two stability fields separated by the field of pyrite. However, magnetite is stable only in contact with strongly basic solutions. If the dissolved carbonate is less and the dissolved sulfur is more, the field of pyrite expands until it fills nearly all the lower part of the diagram. If the dissolved carbonate and sulfur both have low abundances, the stability field of magnetite

extends into the near environment where the Eh is equal to zero.

The Eh-pH stability fields for both pyrite and magnetite are important because they assist us in understanding the significance of trace minerals, which sometimes are associated with the calcite-silica deposits occurring at the ground surface of Yucca Mountain. In this regard, samples #5h (calcium carbonate and quartz from the WT-7 exposure) and #19e (opal-calcite-quartz from the Wailing Wall exposure) of Harmon (1993) are particularly relevant. According to Harmon, sample #5h "... does contain relatively abundant very small grains and microveinlets of pyrite and chalcocopyrite. The pyrite tends to occur as small, discrete grains scattered throughout the sample, whereas the chalcocopyrite occurs either as solitary grains or as microveinlets. All of the sulfides occur as particles on the order of a few microns diameter. Some of the microveinlets exhibit a clear association with zones of brecciation in the carbonate host." (pp. 20-21). As far as the #19e sample is concerned, Harmon noted, "... pyrite grains

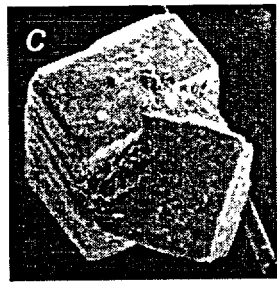
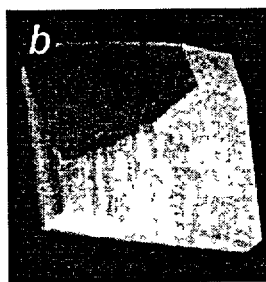
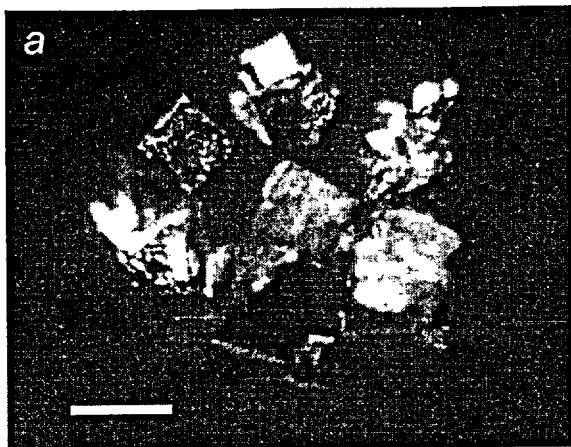


Figure 3-3-21. Pyrite from breccias associated with faults at Yucca Mountain. *a* – pyrite-quartz aggregate from breccia from the Stagecoach Road fault zone (sample SCR#2B); *b* – octahedral pyrite crystal from WT-7 breccia (Solitario Canyon fault zone, see Figure 3-3-6; sample WT#7B); *c* – intergrowth of two cubic pyrite crystals from trench intersecting the Stagecoach Road fault (sample SCE#3). Scale bar is 0.5 mm. Sizes of crystals shown on SEM microphotographs (*b* and *c*) are approximately 0.3 mm.

are also present in this sample, scattered throughout the host carbonate, and microveinlets consisting of chalcopyrite are observed to crosscut some of the euhedral-subhedral quartz crystals." (p. 21).

The crosscutting relationships described by Harmon indicate that the authigenic (i.e., non-detrital) pyrite and chalcopyrite ( $\text{CuFeS}_2$ ) are epigenetic relative to the host quartz and the host carbonate. It is also possible that some of the sulfides might be co-genetic with the host minerals. Both of the sulfides contain ferric iron, which indicates that the host quartz and carbonate must have been formed in a low-Eh (reducing) environment.

Ferric, iron-bearing, mineral phases, apparently grown *in situ*, was confirmed by Chepizhko and Dublyansky (1998) in their studies of accessory minerals associated with the calcite-silica deposits at the surface of Yucca Mountain. Crystals of magnetite, apparently grown *in situ*, have been separated from the AMC breccia, which has been exposed in a trench excavated across the Solitario Canyon fault (see Figure 3-3-8-c). Samples of this breccia (SCE#1 through SCE#3) were found to contain an elevated abundance of magnetite, between 116.5 and 911.4 ppm. A calcite vein exposed in the same trench contained up to 0.01 ppm of chalcopyrite.

Aggregates composed of pyrite intergrown with quartz have been found in samples SCR#1B and #2B, which represent the AMC breccia along a trace of the Stagecoach Road fault (see Figure 3-3-1). These samples yielded abundances of pyrite and magnetite, 0.15 to 0.44 and 15.7 to 122.6 ppm, respectively. Three examples of the separated pyrite intergrown with quartz are shown in Figure 3-3-21.

Two features of the crystals, which are shown in the figures, suggest an epigenetic hydrothermal origin, on one hand, and an *in situ* growth, on the other. First, the pyrite crystals have cubic and

octahedral habits, which are typical crystallographic forms of pyrite associated with hydrothermal ore deposits (Chepizhko et al. 1998). Second, the compositional fragility, the undamaged (scratch-free) flat faces (quartz), and the sharp edges of the pyrite crystals all indicate the absence of transport-induced abrasion, and thus suggest *in situ* growth.

The presence of the ferric minerals, suggesting reducing conditions that existed at some stages of formation of the near-surface calcite-silica deposits is perfectly compatible with the proposed conceptual model (see Chapter 2-4). Further confirmation of such anoxic environment is provided by the analysis of gases trapped in fluid inclusions in carbonate minerals.

### 3.3.7. Gases trapped in fluid inclusions

Three replicate analyses of gases trapped in inclusions in one sample of the bedrock vein calcite were reported in the literature (Levy et al. 1995). The sample was described as "*Pedogenic calcite from a fracture within the Bow Ridge fault in densely welded Tiva Canyon Tuff near the surface of Exile Hill*". According to Levy (2001, pers. com.), the analyzed material represented loose oolitic calcite. The contents of H<sub>2</sub>O, CH<sub>4</sub>, N<sub>2</sub>, O<sub>2</sub>, Ar, and CO<sub>2</sub> trapped in inclusions were determined by means of qualitative Quadrupole mass-spectrometry. Below we present a short summary of the results.\* Figure 3-3-22 compares the Yucca Mountain data with the data from the vadose-zone pedogenic calcites, deposited in fractures of the near-surface Bandelier tuff on the Pajarito Plateau at Los Alamos, New Mexico USA – a reasonably similar setting in terms of the bedrock geology (Newman et al., 1997).

Figure 3-3-22 demonstrates that, compared to the pedogenic calcites from New Mexico, samples from Yucca Mountain contain somewhat elevated amounts of argon (Figure 3-3-22-a). The contents of nitrogen in the Yucca Mountain calcite are similar to or slightly greater than in the typical travertine deposits, showing N<sub>2</sub>/Ar ratios only slightly greater than those, characteristic of the air. This feature might be related to the input of nitrogen related to biological activity, or from the deep-seated sources.

What clearly sets the Yucca Mountain apart from the New Mexico pedogenic calcites is the content of water. The former contains ≥ 99.2 mol % H<sub>2</sub>O, whereas all 32 reported analyses of the later contain 0 mol % (Newman et al., 1997). Pedogenic samples from other locations were found to contain somewhat greater amounts of H<sub>2</sub>O, with the maximum content recorded at 98 mol %. According to Newman et al. (1997) "... calcites with gas dominant inclusions have a vadose origin, while those with inclusions that contain over 98 mol% water form under saturated conditions." (p. 1790).

---

\* A somewhat more detailed analysis of the data is presented in Chapter 3-6 dealing with fluid inclusions.

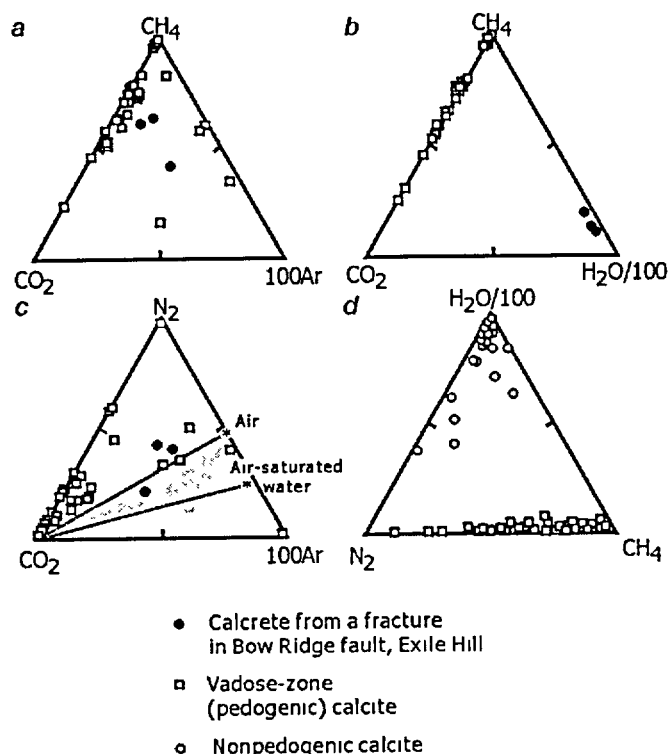


Figure 3-3-22. Comparison of the results of the Quadrupole mass spectrometric analysis of the Yucca Mountain calcrites and calcites (Levy et al. 1995) and of the vadose-zone calcite fracture fillings from Los Alamos, New Mexico (Newman et al. 1997). Diagram *c* also shows typical values of gases trapped in inclusions in ancient and modern travertines (gray field; by Newman et al. 1997). Diagram *d* shows characteristic H<sub>2</sub>O contents that distinguish, according to Newman et al. (1996), pedogenic and nonpedogenic (travertine and hydrothermal) calcites. Note, for the Yucca Mountain samples, generally greater contents of argon, somewhat greater contents of nitrogen (with ratios, identical or close to the travertine carbonates), and high contents of H<sub>2</sub>O, characteristic for the spring carbonates and atypical of the pedogenic deposits.

Sample of the Yucca Mountain surface calcrite (identified in the original paper by Levy et al. (1995) as "pedogenic calcite"; filled circles) is from a fracture within the Bow Ridge fault at Exile Hill.

Levy et al. (1995) admitted that the contents of H<sub>2</sub>O determined in the Yucca Mountain calcrites are "typical of saturated-zone calcite and much higher than the maximum of 86 % in pedogenic calcites from New Mexico...". In order to account for this observation, the authors had to invoke calcite precipitation and recrystallization in the "locally saturated environment", caused by "major meteoric recharge events". Two objections can be raised against such an interpretation. First, it is difficult to envisage a natural setting in which a local saturated environment persists for hundreds of thousands of years (reported duration of formation of calcrites at Yucca Mountain) within 1 to 3 m from the topographic surface (the depth of sample collection), underlain by a few hundred meter-thick vadose zone. Second, the proposed model fails to explain the composition of trapped gases predominantly consisting of methane, lesser amounts of carbon dioxide, and tiny amounts of oxygen (about 4.2 to 8.3·10<sup>-3</sup> mol %; Levy, pers. com. 2001). Hypothetical quantities of water supplied by a "major recharge event" would have to carry "atmospheric" gasses dominated by N<sub>2</sub> and O<sub>2</sub>.

The contents of oxygen also seem to be diagnostic. Figure 3-3-23 compares the Yucca Mountain results with those obtained from samples of travertines and pedogenic calcites of New Mexico (Newman et al., 1996). It is apparent from the figure that the Yucca Mountain surface calcrites have the O<sub>2</sub> contents

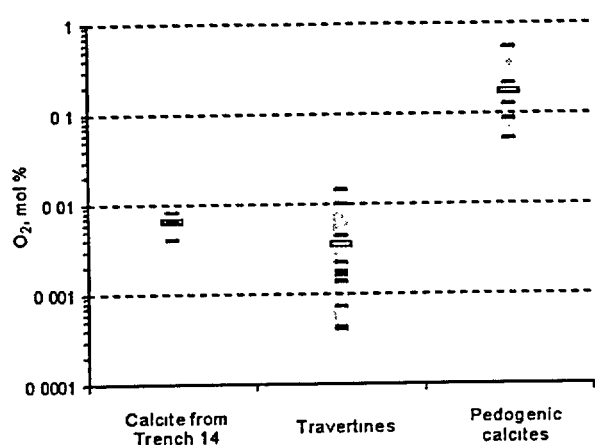


Figure 3-3-23. Contents of oxygen in sample of the Yucca Mountain surface calcite, Trench 14, Exile Hill compared with those in travertines and pedogenic calcites from New Mexico.

Calcrete from Trench 14 (sample TR14-10-SSL): average  $O_2 = 0.0064$ ,  $\sigma = 0.0021$  ( $n = 3$ ) (by Levy 2001, pers. com.). Travertines: average  $O_2 = 0.0035$ ,  $\sigma = 0.0045$  ( $n = 11$ ) and pedogenic calcite: average  $O_2 = 0.18$ ,  $\sigma = 0.18$  ( $n = 6$ ) (by Newman et al. 1996; all numbers are in mol %). Horizontal bar indicates average values. Quadrupole mass spectrometric data.

typical of travertines, and more than one order of magnitude smaller than the typical values of the pedogenic calcites.

The results of studies involving gases trapped in inclusions is summarized in the following discussion. The high contents of  $H_2O$  in inclusions (about 99.7 mol %) indicate that the Yucca Mountain surface carbonates have formed in the phreatic environments (see Newman et al., 1996 and 1997). The low contents of  $O_2$  ( $n \cdot 10^{-3}$  mol %) are compatible with a travertine origin and are too low for vadose-zone pedogenic carbonates (typically,  $n \cdot 10^{-2}$  to  $n \cdot 10^{-1}$  mol %). The high concentrations of  $CH_4$ , in conjunction with the low concentrations of  $O_2$ , indicate that the calcites were precipitated under reducing conditions (see e.g., Newman et al., 1996). Such

gas compositions are not expected to be present in desert soils. For example, the present-day soils in the Yucca Mountain area contain between 0.05 and 1.17 ppmv  $CH_4$ , which is less than the atmospheric values (Thorstenson et al. 1989). The chemistry of gases trapped in fluid inclusions, therefore, seems to be incompatible with the postulated rainwater origin of solutions that deposited the near-surface calcite and silica minerals.

It is important to note that the analysis above is based on only three fluid inclusion analyses from one Yucca Mountain sample reported in the literature. It must be realized, therefore, that the conclusions presented above are based on a small data set. The method of the Quadrupole mass spectrometric analysis of gases trapped in fluid inclusion has been evaluated for the purpose of discriminating between the origins of different types of calcites. For instance, Newman et al. (1996) stated: "*The origin of calcite fracture fillings at Yucca Mountain, Nevada, USA, has been contentious ... and a diagnostic technique such as quadrupole fluid inclusion analysis would be very useful in resolving this problem.*" (p. 206). They further concluded: "*Our results show that quadrupole analysis of fluid inclusion volatiles can be used as a diagnostic technique to identify whether calcites formed under saturated or unsaturated conditions, and also can be used to gain more information about the environmental conditions of the calcite precipitation process*" (p. 213, emphasis added). The preliminary quadrupole results, reported as

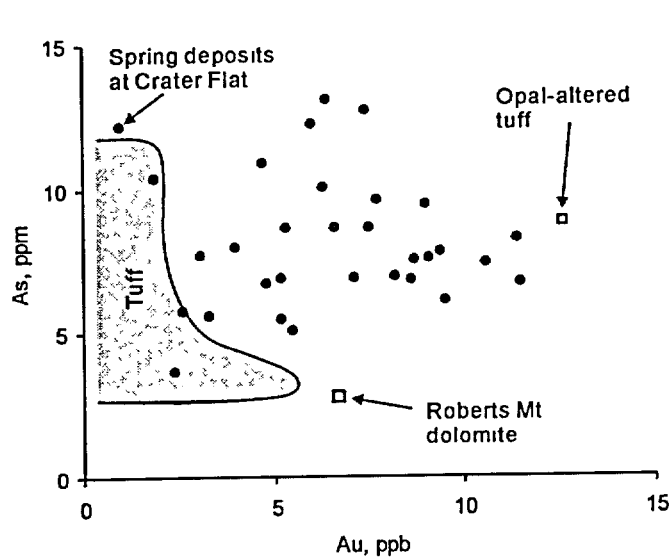


Figure 3-3-24. Au vs As cross-plot showing values measured in vein (*red circles*) and slope (*blue circles*) lithofacies of surface carbonates. Values for the Roberts Mt. dolomite (underlying the Yucca Mountain tuffs; sample from drill hole UE25 p#1), spring discharge deposit at southern Crater Flat, as well as field of the Yucca Mountain tuffs are shown for comparison. Based on the data from Vaniman et al. (1995).

early as 1995 by the Los Alamos researchers (Levy et al. 1995) and used in our analysis above, appear to be potentially informative with respect to the origin of the controversial surface deposits at Yucca Mountain. It is thus extremely disappointing that this line of inquiry was not pursued by the Yucca Mountain Project scientists any further and that no additional studies were carried out between 1995 and the time of publication of this book.

### 3.3.8. Trace-element geochemistry of surface deposits

Trace element analyses of samples from Trench 14 were reported in a U.S. DOE report (U.S. DOE, 1993) as well as in a Los Alamos National Laboratory's report (Vaniman et al., 1995). Additional analyses of carbonate-silica, surface deposits from various sites in the Yucca Mountain area were reported by Castor et al. (1999). Samples of calcite-silica veins and bedded slope carbonates were found to contain up to 218 ppb Hg (with one occurrence of >700 ppb), 30.4 ppm As, and 9-15 ppb Au (with highest Au contents being associated with the carbonate-silica veins; NBMG/UNR, 1999). For comparison, the Tiva Canyon tuffs at Yucca Mountain contain, on an average, from 0 to 35 ppb Hg (NBMG/UNR 1999), <0.5 to 3.5 ppm As, and <2 to 4 ppb Au (Marshall et al., 1995). Some data on the Au and As contents reported by Vaniman et al. (1995) are shown in Figure 3-3-24.

The "clearly anomalous" abundances of gold were asserted to be due to the introduction into the calcretes of windblown particles, "*possibly from the Bare Mountain area*" (Castor et al., 1999). No serious discussion of the alternatives was offered. For example, the nature of gold anomalies in the carbonate silica veins and slope calcretes was dealt with in the following manner in the report by

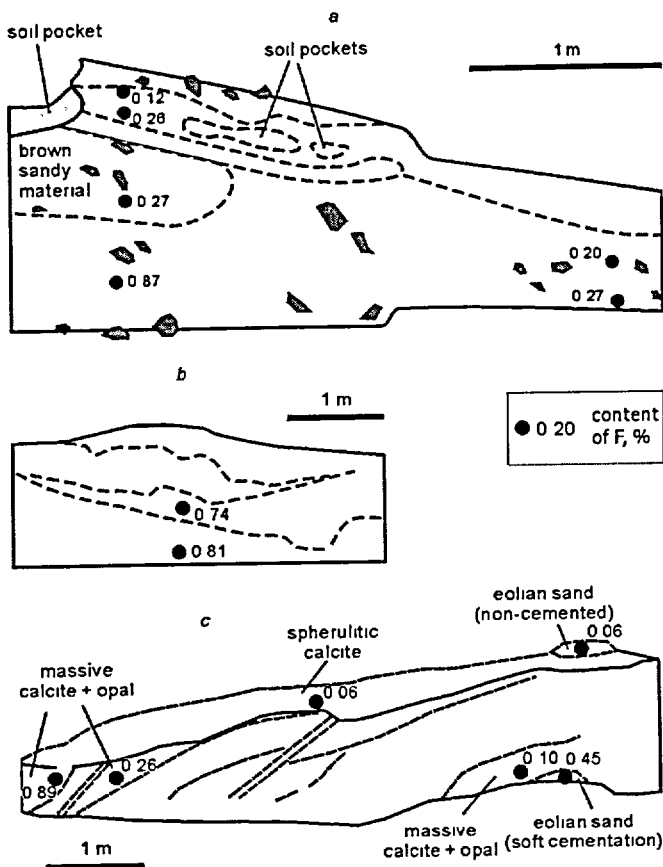


Figure 3-3-25. Schematic presentation of the trench walls showing contents of fluorine in the calcite-opal surface deposits at Boomerang Point (a, b) and the WT-7 drill pad (c) near the mouth of the Solitario canyon. Samples were taken from the walls of trenches excavated near the suspected spring orifices. Note conspicuous decrease in the F-contents toward the land surface. X-ray fluorescence data (Dublyansky, 2001-c).

Sample with the greatest F abundance (0.87 %), in figure a, is composed of the calcite (75.5 %) and C-opal, quartz and feldspar (24.5 %; the later two minerals are most probably detrital); sample with the highest F-abundance in figure c (0.89 %) contains calcite (72.3 %) and C-opal (27.7 %) with no discernible detrital minerals (XRD data).

NBMG/UNR (1999, p. 29): "Although the presence of slightly elevated gold in these rocks is interesting from an academic standpoint, it is purely academic because many lines of evidence indicate that the calcrete is pedogenic (Taylor and Huskins 1995) "

In addition to Hg, As, and Au anomalies, carbonate-silica deposits in the vicinity of the Solitario Canyon fault were found to contain up to 0.87-0.89 % F (Dublyansky, 2001-c). Abundances are greater in the deeper facies of the deposits and tend to diminish toward land surface (Figure 3-3-25). Fluorine enrichment is clearly related to the authigenic mineralization. For example, for a sample that has shown the highest F-abundance (WT#7N-1z, 0.89 % F) the whole sample and its insoluble residue were studied by means of XRD. The residue (27.7 wt.%) consisted of pure C-opal, without any discernible signals from detrital minerals (e.g. quartz and feldspar). Also, two samples of eolian sand were analyzed from the WT-7 location. Non-cemented sand from the top part of the deposit contained only 0.06 wt. % F, whereas carbonate-cemented sand from the lower part of the deposits was found to contain 0.45 wt. % F. The F-abundances in the authigenic carbonate-silica deposits are clearly anomalous, because the content of F in the unaltered Yucca Mountain tuffs is generally low, between <0.01 and 0.2 wt. %. It might be greater, however, in altered zones that also show elevated contents of Ba, Sb, Pb, and Sn (NBMG/UNR, 1999).

Our analyses of the typical unaltered tuffs from the ESF yielded F-abundances ranging from 0.01 to 0.032 wt. % (analysis done by the photometric method at the Analytical Center of the United Institute of Geology, Geophysics and Mineralogy, SB RAS, Novosibirsk, Russia; Dublyansky, 2001-c).

Fluorine is not an element which associates with carbonate minerals, such as calcite. In typical carbonate sediments, the content of fluorine does not typically exceed 0.0n wt. %. Similarly, pure spherulitic calcite (see Figure 3-3-25-c) contains some 0.06 wt. % of F. Pristine (non-cemented) eolian material does not seem to contain much fluorine, either (0.06 wt. %, see Figure 3-3-25-c). By contrast, cemented eolian sand contains an order of magnitude more F (0.45 wt. %). The greater percentage indicates that fluorine was transported by fluids that deposited carbonate-silica deposits at and on the surface of Yucca Mountain. Fluorine may be present in the carbonate-opal sediments in the form of fluorite. Our attempts to identify this mineral by means of the XRD analysis, however, have failed. This may indicate that fluorine does not form a separate mineral phase but, rather, occurs as an admixture in the silica (C-opal). Alternatively, fluorite may form crystals that are too small to be distinguishable by the XRD method.

Brief discussion presented above suggests that carbonate deposits that occur at the topographic surface of Yucca Mountain seem to be enriched in some elements that cannot be readily attributed to the potential sources rocks (i.e., Paleozoic carbonate deposits and bedrock tuffs), as would be required by the "rainwater" model. The trace element composition, however, does carry substantial resemblance to the hydrothermal alteration and mineralization known to occur in the Yucca Mountain vicinity from ca. 24 Ma to ca. 8 Ma (see Chapter 3-8 for discussion), which includes gold, fluorspar, and mercury deposits and occurrences (e.g., Weiss et al. 1994). Although the surface deposits are clearly younger than this mineralization, the specific trace element composition does suggest strongly a hydrothermal affinity for these deposits.

### *3.3.9. Rare Earth Elements*

The lanthanide, or rare earth elements (REE) typically occur in rocks and minerals in the form of trivalent ions, although europium occurs also as a divalent ion ( $\text{Eu}^{2+}$ ) and cerium as a tetravalent ion ( $\text{Ce}^{4+}$ ). The ionic radii of these reduced ( $\text{Eu}^{2+}$ ) and oxidized ( $\text{Ce}^{4+}$ ) ions differ substantially from their trivalent counterparts, which makes these elements useful as tracers with respect to the Eh conditions. Table 3-3-1 reproduced from Denniston et al. (1997) shows the ionic radii and valences for some of the six-fold coordinated lanthanide elements. The table also shows the "optimal site characteristics" for  $\text{Ca}^{2+}$  ions, which are six-fold coordinated with the O of the  $\text{CO}_3$  groups forming a slightly distorted octahedron.

Table 3-3-1

Ionic radii and valences for Ca ions in sixfold coordination with the O of the CO<sub>3</sub> groups and for some of the sixfold coordinated lanthanide elements. From Denniston et al. (1997)

Element	Valence	VI-coordinated ionic radius, Å
Ca	2 <sup>+</sup>	1 00
OSC	1.99 <sup>+</sup>	0 96
La	3 <sup>+</sup>	1.016
Ce	3 <sup>+</sup>	1 034
Nd	3 <sup>+</sup>	0 995
Sm	3 <sup>+</sup>	0 964
Eu	3 <sup>+</sup>	0 950
Dy	3 <sup>+</sup>	0 908
Er	3 <sup>+</sup>	0 881
Yb	3 <sup>+</sup>	0 858
Ce	4 <sup>+</sup>	0 880
Eu	2 <sup>+</sup>	1.170

Note: OSC – optimal site characteristic (by Smyth and Bish, 1988; reproduced from Denniston et al. 1997)

Table 3-3-1 shows that the divalent (reduced) Eu<sup>2+</sup> ion has an ionic radius equal 1.17 Å, whereas the radius is only 0.95 Å for the trivalent ion. These differences are important because the lanthanide elements having the valence and ionic radius closest to the "optimal site characteristics" will be preferentially incorporated in the crystalline structure of a six-fold coordinated calcite. The optimal radius for this calcite is 0.96 Å, so that the divalent (reduced) Eu ions with the 1.17 Å radius and tetravalent (oxidized) Ce ions with the 0.88 Å radius will tend to be excluded from the calcite structure. Ce<sup>3+</sup> and Ca<sup>2+</sup> in the six-fold coordination have ionic radii of 1.034 Å and 1.00 Å respectively (Shannon and Prewit, 1969). Due to that, in reducing environment Ce<sup>3+</sup> readily substitutes Ca in calcite (Rimstidt et al., 1998). By contrast, because of its smaller ionic radius (0.80 Å), Ce<sup>4+</sup> does not substitute Ca; it is thus being excluded from the calcite lattice.

Exclusion of the elements produces "troughs" on the graphs, showing the chondrite-normalized contents of the rare earth elements (REE-patterns). These troughs are referred to as negative Ce or Eu anomalies. Generally speaking, the calcite REE patterns showing the pronounced negative Eu anomaly could be interpreted as indicative of the reducing environment, whereas those exhibiting negative Ce anomaly would be indicative of the oxidizing environment. Importantly, however, besides being related to

the oxidation state-dependent uptake of the elements by calcite, both Ce and Eu anomalies may also be inherited from the mineral-depositing fluid (and, more generally, from the source-rocks, with which these fluids have equilibrated). In the relatively low-temperature conditions (ca. 25-100 °C), Eu invariably maintains the 3+ state (Sverjensky, 1984), which means that any Eu-anomalies found in calcite deposited in such environment, would likely reflect inheritance from the source-rock rather than the result of Eu exclusion during crystal growth.

Keeping the preceding remarks in mind, let us examine the chondrite-normalized REE patterns from the calcite-silica deposits at the topographic surface of Yucca Mountain. These patterns for Trench 14 and Busted Butte were reported in U.S. DOE (1993) and are reproduced in Figure 3-3-26-*a*.

Figure 3-3-26-*a* shows that the AMC breccias (identified on the graph as fault-breccia tuff), the bedrock veins, and the calcrete lithofacies all share the same REE pattern, which is characterized by the presence of a single negative Eu anomaly and absence of Ce anomaly. Although the REE-abundances vary by a factor of ten or more, the shapes of the chondrite-normalized patterns remain internally consistent. This internal consistency suggests that neither the deposition environment nor the REE incorporation mechanisms have changed appreciably over the deposition period for these lithofacies.

It is important to note that the REE patterns depicted in Figure 3-3-26-*a* closely resemble the REE patterns of the host and underlying tuffs, as well as those of Paleozoic carbonates and aquifer fluids, residing in the carbonate aquifer (Figure 3-3-26-*b* through -*d*). The similarity may be interpreted as suggesting that the calcite-silica deposits have inherited the REE pattern from the host tuffs and Paleozoic carbonates (supplied as wind-blown particles) via *in situ* dissolution, re-crystallization and other processes ("rainwater concept"). Alternatively, it might indicate that the deposits have acquired their REE pattern independently but from the deep-seated waters, equilibrated with the Paleozoic carbonate rocks, and/or with crustal rocks, from which the tuffs were derived ("hydrothermal upwelling" concept).

The hydrothermal or upwelling water transport of the REE is also supported by the similarity between the Yucca Mountain REE patterns and those from the locally known spring and hydrothermal-ore deposits. The comparisons of Trench 14, Busted Butte, and WT-7 calcite-silica deposits with the spring and hydrothermal-ore deposits are shown on Figure 3-3-27.

Figure 3-3-27-*a* shows that the calcite-silica deposits from Trench 14, Busted Butte, and WT-7 exposures exhibit REE patterns that are practically identical to those from the LWD and CFW discharge site (denoted on the figure as "Site 199"; see Figure 2-7). Furthermore, Figure 3-3-27-*b* shows that both the REE-abundances and REE patterns of the near-surface calcite-opal deposits are similar to those from

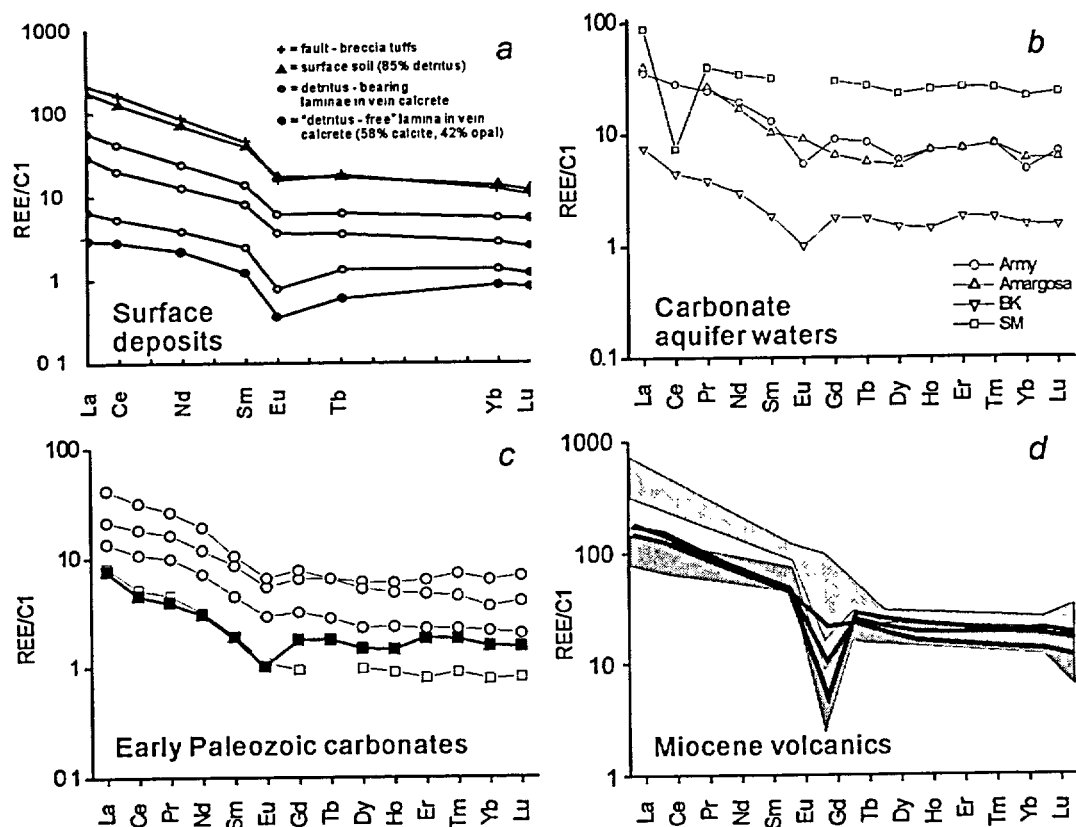


Figure 3-3-26. REE patterns for calcite-silica deposits at Trench 14 and Busted Butte (a) compared with patterns from carbonate aquifers (b), Early Paleozoic carbonate rocks (c) and Miocene volcanic rocks (d).

a – Surface deposits (by U.S. DOE, 1993). b – Carbonate aquifer waters: *Army* – South Nevada Test Site, *Amargosa* – Amargosa wells south and north of Bare Mountain, *BK* – Bonanza King, and *SM* – Spring Mountain (compiled from Johannesson et al. 2000). c – Early Paleozoic carbonates: *Open circles* – Frenchman Mountain, *open squares* – Fossil Ridge, *filled squares* – Bonanza King limestone (Early Cambrian); d – Volcanic rocks: upper (*light shading*; quartz latites) and lower (*heavy shading*, rhyolites) portions of the Topopah Spring Tuff (after Schuraytz et al., 1989 and Broxton et al., 1989 as reported in Denniston et al., 1997), and average values (of four samples each) of the Tram, Bullfrog and Crater Flat ignimbries (*solid lines*; from Scott and Castellanos, 1984).

epithermal fluorite deposits, which have been mined at Bare Mountain in the Diamond Queen open-pit mine.

The near-surface oxidizing environment is commonly inferred from the presence of the negative Ce anomaly in the REE pattern of carbonates. Thus, the conspicuous absence of such anomaly from both "controversial" surface deposits from Busted Butte, Trench 14, and WT-7, as well as from carbonate deposits for which spring discharge origin is established with certainty, is noteworthy. Two inferences can

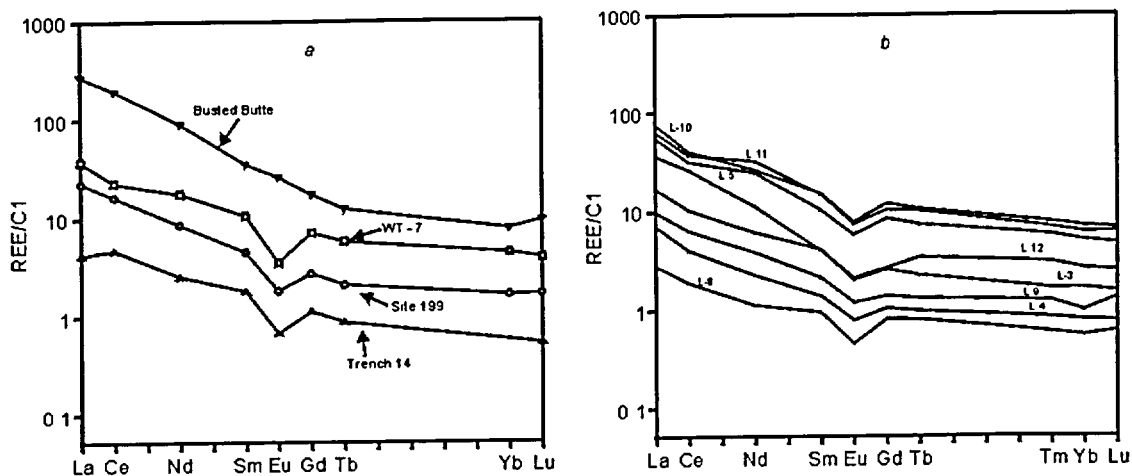


Figure 3-3-27. Comparison of REE patterns for known spring deposits (Site 199 = LWD and CFW discharge sites; see Figure 2-7) and surface calcite samples (a) and REE patterns for hydrothermal fluorite from the flourspar Diamond Queen mine, Bare Mountain (b). Data for surface and spring deposits are from Shmitt (1993); data for the hydrothermal fluorite are from this study.

be made in this regard. First, waters discharging at the topographic surface in the past were such, that calcite, depositing from these waters, did not acquire Ce-anomaly, characteristic of the near-surface oxidizing environment. Second, the "controversial" carbonate deposits carry REE patterns virtually indistinguishable from those of the spring discharge deposits in the vicinity of Yucca Mountain.

### 3.3.10. Concluding Remarks

A vast set of field observations and petrologic, mineralogical, and geochemical analyses has been assembled to form a coherent picture of hydrothermal-fluid discharges at the topographic surface of Yucca Mountain, at times assisted by CO<sub>2</sub> pressure. All lines of evidence, which have been used by the Yucca Mountain Project scientists in support of their contention that the calcite-silica deposits are products of infiltrating rainwater, have been examined. None of them has scientific merit as demonstrated by the analyses contained herein. To the contrary, every one of the official lines of evidence is equivocal and could alternatively be used in support of the opposite conclusion that the calcite-silica deposits are products of hydrothermal fluids transporting dissolved matter from the basement.

In this regard the progressive and concurrent changes in slope carbonates as a function of distance away from fault zones hosting the Paintbrush and Solitario Canyon geothermal anomalies are persuasive. These changes involve the macroscopic textures and the SiO<sub>2</sub>-abundance. These lines of evidence alone are sufficient, in our opinion, to validate the proposed conceptual model, as set forth in Part II of this monograph. Several independent lines of evidence suggest that, at least in part, the calcite-silica deposits

have been formed under reducing conditions. These are the presence of iron sulfides ( $\text{FeS}_2$  and  $\text{CuFeS}_2$ ), the absence of the negative Ce anomaly, and the predominantly  $\text{CH}_4$  composition of gases trapped in water-rich fluid inclusions in calcite. In view of these lines of evidence, it is our opinion that attributing the origin of these deposits to the infiltrating rainwater is untenable.